Universidad CEU San Pablo
CEINDO – CEU Escuela Internacional de Doctorado

DOCTORATE IN TRANSLATIONAL MEDICINE

An exploration of the bioenergetics and therapeutic efficacy of a pharmacologically induced metabolic therapy in glioblastoma.

DISSERTATION

Tomás Duraj

Director and Co-Director:

Ángel Ayuso Sacido, PhD

Noemí García Romero, PhD

MADRID

2022

DOCTORAL

DISSERTATION

TOMÁS DURAJ

2022

The work presented in this Doctoral Dissertation has been carried out by Tomás Duraj, under the direction of Dr. Ángel Ayuso Sacido and Dr. Noemí García-Romero, at the Institute for Applied Molecular Medicine (CEU San Pablo University).

This research project has been supported by grants from the "Fondo de Investigaciones Sanitarias" (FIS) (PI17-01489), the Miguel Servet Program from the Instituto de Salud Carlos III (CP11/00147), Ministry of Economy and Competitiveness-FEDER (RTC-2016-4990-1), as well as the Spanish program for university teacher training (Programa de Formación del Profesorado Universitario, FPU) from the Ministry of Education, Culture and Sports (FPU16/03198).

Applying for a Ph. D. Degree	Approval of Director	Approval of Co-Director
Tomás Duraj	Ángel Ayuso Sacido	Noemí García-Romero

Life as it is.

When life itself seems lunatic, who knows where madness lies?

Perhaps to be too practical is madness.

To surrender dreams, this may be madness.

Too much sanity may be madness!

And maddest of all:

to see life as it is and not ***as it should be!***

Dale Wasserman

Acknowledgements

There is an art to science poets find very troublesome, and I have yet to master.

How could *observations*, in all their imperfection, translate into *reality*? If death is the equalizer of all the living, science is, in its innermost essence, the equalizer of uncertainty.

A purely reductionist view of the Universe is both a comforting and unsettling proposition. Legends and tales, opinions and possibilities, all reduced to biophysical fundamental truths. If we are correct (and we aim to be), there is no room for more. This is a noble, albeit bittersweet, endeavor.

And yet, science is as human as poetry itself. The message is a matter of interpretation. The letters are meaningless outside the syntaxis of their singular language; such is the nature of communication. Words are minced in the Tower of Babel: many languages, many interpretations.

Richard Feynman once wrote: *"The first principle is that you must not fool yourself — and you are the easiest person to fool."*

This is the reason why science must be a *collective collaboration* (the hardest one there is). Navigating the maze of alluring words our brains dream past the unknown requires the help of others: we all need a guiding thread from Ariadne to find the truth. I would go as far as to declare this must be one of the axioms knowledge itself is constructed upon.

Thus, I am grateful. I am grateful to my mentors for teaching me how to think critically and ask the right questions. I am grateful to my colleagues for tolerating my inner struggles and helping me find my way. I am grateful to my family and friends for being by my side when I needed it the most.

I feel the gift of consciousness has this empty background noise we humans have a proclivity to surrender to. I am the first one to be drawn to futility. To abandon higher aspirations and be swept by the fickle yearnings of chaos. And yet, somewhere deep down, we foster this intuition: *this must not be so, or all is lost*. And so, we fight, we struggle. I am grateful to all who were ready to fall with me… just to raise and start all over again.

To strive, to seek, to find, and not to yield.

Thank you.

Abstract

Glioblastoma (GBM) is the most aggressive primary brain tumor, with an overall median survival at diagnosis of 16-20 months despite surgery and chemoradiotherapy. Pathogenesis is complex, with involvement of mitochondrial dysfunction, oncogenic signaling and metabolic rewiring. Targeting the intrinsic metabolic vulnerabilities of GBM remains challenging due to high intratumoral heterogeneity.

We characterized the bioenergetic phenotypes of 3 distinct glioma stem cells (GSCs), as well as non-stem U87MG, testing the antiproliferative potential of metformin (MF), dichloroacetate (DCA), sodium oxamate (SOD) and diazo-5-oxo-L-norleucine (DON).

We found that GBM27, highly oxygen-dependent, was the most resistant to all treatments except DON. GBM18 and GBM38, Warburg-like GSCs, were sensitive to MF and DCA, respectively. GBM18 was resistant to DON, without a clear correlation with basal metabolic dependencies. U87MG exhibited a typically glycolytic behavior with intermediate susceptibility against all tested inhibitors. MF and DCA shifted energy production towards glycolysis or oxygen consumption, respectively. DON decreased total ATP production, but demonstrated a more heterogeneous metabolic response, suggesting a multidimensional role of glutamine in cellular bioenergetics.

Radiomimetic drug bleomycin was toxic to rapidly proliferating non-tumoral cells (HBMEC), sparing normal stem cells (hMSCs). Effective targeting of GBM27 (oxygen-dependent GSC) would be toxic to normal cells. Circumventing toxicity entails dose-reduction strategies. Bleomycin exhibited therapeutically relevant synergistic effects with MF, DCA and DON in GBM27, and DON in all other cell lines.

Additionally, we explored ketolysis, a compensatory metabolic pathway for protection against nutrient deprivation. Archetypal of non-stem populations, U87MG was not able to adapt to long-term glucose and glutamine depletion despite the presence of ketone bodies. Cyclical ketone-compensated glucose depletion induced growth arrest, morphological changes, and a quiescent metabolic phenotype.

Our study highlights the need for better characterization of GBM from a metabolic perspective. Metabolic therapy should focus on both glycolytic and oxidative populations. Exploiting cancer addiction to fermentative energy sources, be it through microenvironment regulation, nutrient depletion or specific metabolic inhibitors, warrants further exploration.

Resumen

El glioblastoma (GBM) es el tumor cerebral primario más agresivo, con una mediana de supervivencia global de 16 a 20 meses a pesar de tratamiento quirúrgico y quimioradioterapia. La patogenia es compleja, con participación de disfunción mitocondrial, señalización oncogénica y reprogramación metabólica. Aprovechar las vulnerabilidades metabólicas intrínsecas del GBM es un desafío debido a la alta heterogeneidad intratumoral.

En este trabajo caracterizamos el fenotipo bioenergético de 3 líneas de células madre de glioma (GSC), así como U87MG, comprobando el potencial antiproliferativo de metformina (MF), dicloroacetato (DCA), oxamato de sodio (SOD) y diazo-5-oxo-L-norleucina (DON).

Describimos que GBM27 —una línea dependiente de oxígeno— fue la más resistente a todos los tratamientos, excepto DON. GBM18 y GBM38, GSCs de fenotipo Warburg, fueron sensibles a MF y DCA, respectivamente. GBM18 mostró la mayor resistencia a DON, sin una clara correlación con las dependencias metabólicas basales. U87MG presentó un comportamiento típicamente glucolítico con susceptibilidad intermedia contra todos los inhibidores. El tratamiento con MF y DCA redirigió la producción de energía hacia glucólisis y consumo de oxígeno, respectivamente. La aplicación de DON disminuyó la producción total de ATP, pero demostró una respuesta metabólica más heterogénea, lo que sugiere un papel multidimensional de la glutamina.

El radiomimético bleomicina fue tóxico para células no tumorales proliferativas (HBMEC), pero no afectó a células madre normales (hMSCs). La inhibición efectiva de GBM27 (metabolismo dependiente de oxígeno) sería tóxica para células normales. Esta toxicidad podría evitarse mediante reducción de dosis. La bleomicina exhibió efectos sinérgicos en combinación con MF, DCA y DON en GBM27, y con DON en todas las líneas celulares.

Seguidamente, exploramos el procesamiento de cuerpos cetónicos, una vía de protección frente a depleción de nutrientes. U87MG no fue capaz de adaptarse a la restricción de glucosa y glutamina, a pesar de la presencia cuerpos cetónicos. La depleción cíclica provocó una interrupción de proliferación, cambios morfológicos y un fenotipo quiescente.

Nuestra investigación subraya la necesidad de una mejor caracterización del GBM desde una perspectiva metabólica. Las terapias metabólicas deben centrarse en poblaciones tanto glucolíticas como oxidativas. Revertir la adicción del cáncer a fuentes de energía fermentables, a través de regulación del microambiente, restricción de nutrientes o inhibidores metabólicos específicos merece futuras investigaciones.

INDEX

Table of Contents

Abbreviations 1

1. Introduction 5

1.1. Brain cancer in the molecular era: origin, hallmarks and statistics 6

1.1.2. High grade gliomas: histopathological and molecular characteristics. 8

1.2. Molecular subtypes of GBM: deciphering heterogeneity 10

1.2.1. Cell of origin 10

1.2.2. Mutational landscape of GBM 10

1.3. GBM: clinical presentation, diagnosis, and standard of care 12

1.3.1. Localization and clinical presentation 12

1.3.2. Diagnosis: anatomical and metabolic imaging 12

1.3.3. Standard of care of GBM patients 13

1.4. Metabolic reprogramming in the origin and progression of cancer 16

1.4.1. Key chemical reactions for energy production in mammalian cells .. 16

1.4.2. Bioenergetics in normal cells: Embden–Meyerhof–Parnas pathway and mitochondrial respiration 16

1.4.3. Somatic mutation theory and mitochondrial metabolic theory of cancer: different culprits, different tactics 18

1.4.4. Somatic model for ATP synthesis: metabolism under genetic control. 18

1.4.5. Metabolic model for ATP production: mitochondrial dysfunction, the Warburg effect, and Q-effect 20

1.4.6. The role of mitochondria in the origin and progression of cancer ... 22

1.4.7. Advancements in the study of metabolic pathway flux 25

1.5. Metabolic profiles in GBM: overcoming intratumoral heterogeneity 26

1.5.1. Deciphering clonal heterogeneity: a biological perspective 26

1.5.2. Metabolic properties of glioma stem cells (GSCs): a living, evolving model 29

1.6. Metabolism as a potential therapeutic target: successes and pitfalls of metabolic therapy..... 30

1.6.1. Challenges for translational medicine: bringing metabolic therapy to the clinic 30

1.6.2. Mitochondrial activity and metformin: a therapeutic opportunity against oxygen-dependent cancer phenotypes..... 32

1.6.3. Pyruvate, lactate, and anti-glycolytic targeting..... 34

1.6.4. Lactate or acetyl-CoA: a tumor's dilemma 35

1.6.5. Glutamine addiction, glutaminolysis and mSLP: the missing link fueling ATP-synthesis in cancer?..... 37

1.7. Ketogenic metabolic therapy: a selective pressure against Warburg-like cancer cells 39

1.7.1. Ketone body metabolism as a physiological protection against glucose depletion 41

1.8. Metabolic therapy: cutting the supply lines of a hungry beast. Where do we stand? 43

2. Central hypothesis and aims 45

2.1 Central hypothesis 45

2.2. General objectives and specific objectives 46

3. Materials and methods 48

3.2.1. Culture of GSCs from human GBM samples, U87MG, HBMEC and human mesenchymal stem cells (hMSCs) 48

3.2.2. *In vitro* protocol for cyclic metabolic treatment 50

3.2.3. Reagents and metabolic inhibitors 52

3.2.4. Single-drug MTS assays and combination studies using the Chou-Talalay method. 52

3.2.5. Trypan Blue exclusion assay 53

3.2.6. Transduction of tumor cells 53

3.2.7. Bioluminescent imaging 54

3.2.8. Cell morphometry by light microscopy 54

3.2.9. Quantitative Real-Time PCR (qRT-PCR) analysis 55

3.2.10. Antibodies 56

3.2.11. Protein isolation/quantification and Western blotting 56

3.2.12. Seahorse XFp protocol for real-time metabolic evaluation of U87MG adherent cells and GSCs neurospheres 57

3.2.13. Gene-Set Variation Analysis and Glioblastoma Bio Discovery Portal. 61

3.2.14. Statistical analysis 62

4. Results 64

4.1. GBM can be stratified into glycolytic and oxidative phenotypes 64

4.1.1. Gene expression analysis of metabolic pathways and clustering of samples according to Verhaak subtypes 64

4.1.2. Heterogeneity in basal bioenergetic phenotypes of *in vitro* models of GBM 67

4.2. GSCs display a heterogeneous pattern of resistance to metabolic inhibitors 69

4.2.1. Differences of target enzymes across cell lines predicts responses to metabolic inhibitors 72

4.3. Doses of metabolic inhibitors and radiomimetic bleomycin corresponding to Warburg-like phenotypes spare viability of non-tumoral hMSCs and HBMEC cells. 77

4.3.1. Human mesenchymal stem cells (hMSCs) tolerate low to intermediate doses of MF, DCA, DON and bleomycin 79

4.3.2. Rapidly proliferating non-tumoral endothelial cells tolerate intermediate doses of MF and DCA, but not bleomycin..... 80

4.4. Synergy between bleomycin and metabolic inhibitors helps to overcome dose-limiting toxicity, predominantly in oxidative-like metabolic phenotypes 82

4.5. Bioenergetic profiling after metabolic treatment reveals opportunities for metabolic priming in surviving cell populations..... 89

4.6. Evaluating the *in vitro* effects of a ketogenically-compensated glucose-deprived cell culture media formation..... 95

4.6.1. GSCs and U87MG express detectable levels of the 3-oxoacid CoA-transferase enzyme at the protein level, regardless of the presence of BHB 96

4.6.2. Cyclical culturing of U87MG in LG-BHB medium permanently modified their morphological and metabolic phenotype..... 100

4.7. Genes involved in metabolic regulation are associated with patient survival. 102

4.7.1. A Prognostic Index for GBM survival, based on metabolic genes. 105

4.7.2. GBM stratification based on protein expression 107

5. Discussion..... 111

6. Closing remarks..... 126

7. Conclusions 129

8. Appendix 131

8.1. Scientific production relative to the present work: 131

8.2. Oral presentations relative to the present work: 131

8.3. Supplementary Material..... 132

8.3.1. Supplementary Figure S1. Genomic aberrations in GBM. 132

8.3.2. Supplementary Figure S2. Metabolic alterations in GBM..... 133

8.3.3. Supplementary Figure S3. Carcinogenesis and heterogeneity. 134

8.3.4. Supplementary Figures S4-S7. Viability curves of inhibitors. 136

8.3.5. Supplementary Figure S8. TMZ viability curves. 140

8.3.6. Supplementary Figure S9. Viability curves for radiomimetic bleomycin sulfate. 141

8.3.7. Supplementary Figure S10. MF dose-response curve with HBMEC.. 142

8.3.8. Supplementary Figure S11. Expression of OXCT1 in GSCs and U87MG. 143

8.3.9. Supplementary Figure S12. Differences in ATP production of U87MG after normal subculturing and chronic exposure to BHB. 144

8.3.10. Supplementary Figure S13. Changes of U87MG growing in intermediate glucose, BHB-compensated media. 145

8.3.11. Supplementary Figure S14. Cyclical LG-BHB exposure..... 146

8.3.12. Supplementary Figure S15. Progression of LG-BHB cells after finalizing the cyclical glucose-deprivation, BHB-compensated metabolic treatment. 147

8.3.13. Supplementary Figure S16. Representative images of LG-BHB adapted cells compared to controls. 148

8.3.14. Supplementary Table S1. Manually curated list of metabolic target-genes. 149

8.3.15. Supplementary Figure S17. RNA-Seq next-generation sequencing data of GSCs 150

8.3.16. Supplementary Figure S18. CGH analysis of selected genes. 151

8.3.17. Supplementary Figure S19. Oxygraphy and the OCR paradox. 152

9. References..... 156

List of Figures

Figure 1. Hallmarks of cancer..... 6
Figure 2. Standard of care for GBM and novel treatments under active development 15
Figure 3. Energy metabolism in normal oxidative cells. 17
Figure 4. Somatic mutation theory, metabolic reprogramming as a secondary hallmark. 19
Figure 5. Metabolic theory of cancer 21
Figure 6. Summarized overview of the clonal, stem cell, plasticity and mitochondrial models of cancer 28
Figure 7. Mechanisms of action of MF 33
Figure 8. Mechanism of action of dichloroacetate (DCA) and sodium oxamate (SOD)..... 36
Figure 9. Mechanism of action of DON 38
Figure 10. Ketone body metabolism at a glance 40
Figure 11. Design and application of our *in vitro* metabolic treatment 51
Figure 12. Experimental design of Seahorse XF Real-Time ATP Assay 59
Figure 13. Heatmap of the scaled ES obtained by GSVA with the samples grouped by their gene expression subtype (proneural, classical or mesenchymal) including those with high content of non-tumor tissue (low cellularity)..... 65
Figure 14. GSVA sample clustering according to subtype and gene expression .. 65
Figure 15. Clinically, standard imaging techniques such as 18F-FDG PET coupled with anatomical MRI can classify tumors according to glucose uptake 66
Figure 16. Representative optical microscopy images of cellular morphology 67
Figure 17. Seahorse XF Energetic Map 68
Figure 18. Cancer metabolism at a glance, with experimental in vitro IC50 values for selected metabolic inhibitors 70
Figure 19. Expression profiles of target enzymes for our selection of metabolic drugs under basal conditions determined by qRT-PCR..... 72

Figure 20. Western Blot analysis at 30 min, 60 min, 2 h, 6 h after MF 72 h-IC50 treatment for AMPKα and phospho-Thr172 AMPKα 74

Figure 21. Western Blot analysis after 6 h of treatment with respective DCA 72 h-IC50 doses for phospho-Ser293 PDH-E1 and total PDH-E1 75

Figure 22. (a) Expression profiles of SOD target enzymes under basal conditions determined by qRT-PCR (b) Relative mRNA expression compared to control after 72 h of SOD-72h IC50 treatment. 76

Figure 23. IC50 values at 72 h and mechanism of action of radiomimetic drug bleomycin (BM) 78

Figure 24. Representative optical microscopy images of hMSCs cellular morphology, in unaltered, basal conditions 79

Figure 25. Representative optical microscopy images of HBMEC cellular morphology 81

Figure 26. Combinatory drug studies between MF and bleomycin (BM) 84

Figure 27. Combinatory drug studies between DCA and bleomycin (BM) 86

Figure 28. Combinatory drug studies between DON and bleomycin (BM) 88

Figure 29. (a) Changes in metabolic phenotypes after IC50 treatment for 72 h with metformin (MF), dichloroacetate (DCA) and 6-Diazo-5-oxo-L-norleucine (DON) (b) XF ATP Rate Index for GSCs 91

Figure 30. Seahorse XF real-time kinetic graphs for MF 92

Figure 31. Seahorse XF real-time kinetic graphs for DCA 93

Figure 32. Seahorse XF real-time kinetic graphs for DON 94

Figure 33. Simplified diagram of ketone body metabolism 97

Figure 34. (a) Western Blot analysis and volume quantification of OXCT1 expression in GSCs and U87MG cell lines (b) MTS assays to evaluate U87MG growth under standard media and LG-BHB custom media. 98

Figure 35. ATP-linked bioluminescence of U87MG growing in several conditions of modified DMEM for up to 7 days 99

Figure 36. (a) Stable morphological changes in U87MG after 4 cycles of LG-BHB (b) MTS assays to evaluate U87MG growth under standard media and LG-BHB custom media. (c) Seahorse XF real-time kinetic graphs 101

Figure 37. Manually curated list of metabolic genes for expression analysis 103
Figure 38. Survival analysis based on the impact of a multi-gene prognostic index 106
Figure 39. Kaplan-Maier analysis of prognostic index (PI) for the full cohort and Verhaak subtypes compared to overall survival 107
Figure 40. Survival analysis based on the impact of a multi-gene prognostic index 108
Figure 41. Kaplan-Maier analysis of prognostic index (PI) for the full cohort compared to overall survival 109
Figure 42. Heatmap of the correlation between mRNA expression and protein-level evidence for the selected genes 109
Figure S1. Primary sequence alterations and significant copy number changes for components of the RTK/RAS/PI3K, TP53 and RB signaling pathways. 132
Figure S2. Common metabolic alterations in GBM 133
Figure S3. A comprehensive comparison between the clonal evolution, cancer stem cell (CSC) and mitochondrial metabolic models of cancer 134
Figure S4: Inhibitory curves for metabolic inhibitor MF at 24h, 48h, 72h 136
Figure S5: Inhibitory curves for metabolic inhibitor DCA at 24h, 48h, 72h..... 137
Figure S6: Inhibitory curves for metabolic inhibitor SOD at 24h, 48h, 72h 138
Figure S7: Inhibitory curves for metabolic inhibitor MF at 24h, 48h, 72h 139
Figure S8. Viability profiles of cells treated with TMZ for 72 h relative to DMSO-controls 140
Figure S9: Inhibitory curves for bleomycin at 72h 141
Figure S10: HBMEC inhibitory dose-response curve for MF at 72h 142
Figure S11. (a) Western Blot images of OXCT1 expression in GSCs and U87MG cell lines at 24 h. (b) Representative microscopy images of each cell line in normal media and LG-BHB media at 48h 143
Figure S12. Comparison of ATP-linked bioluminescence of U87MG growing in standard subculturing conditions and 10 days exposure to intermediate concentrations of BHB 144

Figure S13. High magnification optical microscopy of U87MG growing in a medium equivalent to LG-BHB, with a glucose concentration of 2.5 mM..... 145

Figure S14. Summary of morphological changes during LG-BHB and HG-FBS cycles..... 146

Figure S15. Representative morphological changes of U87MG after completing all LG-BHB cycles..... 147

Figure S16. Representative morphological changes of U87MG after more than 90 days upon completion of LG-BHB cycles..... 148

Figure S17. Correlations of RNA-Seq expression analysis in our GSCs to TCGA survival predictive genes..... 150

Figure S18. CGH analysis of the selected metabolic genes in GSCs 151

Figure S19. Interpretation of real-time oxygraphic measurements (Seahorse XF technology) 152

List of Tables

Table 1. WHO 2016 histopathological grading associated to the most frequent molecular alterations in astrocytic, oligodendroglial and oligoastrocytic gliomas 9

Table 2. Summary of molecular alterations in Verhaak TCGA GBM subtypes . 11

Table 3. Description and clinical evidence of standard and metabolic drugs. 32

Table 4. Cell culture media composition 50

Table 5. Forward (FW) and reverse (RV) primers for qRT-PCR 55

Table 6. Summary of synergy/antagonism at an optimal fraction of affected cells cutoff of 0.6 83

Table 7. TCGA *IDH* wild-type survival analysis of metabolic genes 104

Table S1. Genes involved in the targetable pathways of glycolysis, glutaminolysis and mitochondrial metabolism, based on KEGG pathways 149

ABBREVIATIONS

Abbreviations

13C-MFA: 13C-metabolic flux analysis
18F-FDG-PET: [18F]fluoro-deoxyglucose positron emission tomography
2-DG: 2-deoxy-D-glucose
3-BP: 3-bromopyruvate
3D CRT: three-dimensional conformal radiation therapy
3DT1: three-dimensional T1-weighted imaging
AACS: acetoacetyl-CoA synthetase
AAT: aspartate aminotransferase
AcAc: acetoacetate
ACAT1: acetyl-CoA acetyltransferase
ASNS: asparagine synthetase
ATP: adenosine triphosphate
AV-1: ardisianone
BBB: blood brain barrier
***Bcl-2*:** B-cell lymphoma protein-2
BDH: D-beta-hydroxybutyrate dehydrogenase
BHB: β-hydroxybutyrate
BM: bleomycin
BMPs: bone morphogenetic proteins
bFGF: basic fibroblast growth factor
BPTES: bis-2-[5-phenylacetamido-1,2,4-thiadiazol-2-yl]ethylsulfide
BSA: Bovine Serum Albumin
***CDKN2A*:** cyclin-dependent kinase inhibitor 2A
CGH: Comparative Genomic Hybridization
CI: Combination Index
CISNE: Code for the identification of synergism numerically efficient
CNS: Central Nervous System
CNVs: Copy Number Variations
CPS-II: carbamoyl phosphate synthetase
CR: caloric restriction
CSCs: Cancer Stem Cells
CT: computed tomography
CTPS: cytidine triphosphate synthetase
CV: coefficient of variation
DCA: dichloroacetate
DLAT, or E2 component: dihydrolipoamide S-acetyltransferase of PDH
DLD, or E3 component: dihydrolipoamide dehydrogenase of PDH
DON: 6-diazo-5-oxo-L-norleucine
DRI: Dose-Reduction Index
E3BP: E3 binding protein of PDH
ECAR: extracellular acidification rate
EGF: epidermal growth factor
***EGFR*:** epidermal growth factor receptor
EMT: epithelial-to-mesenchymal transition

ETC: electron transport chain
Fa: fraction of affected cells
FAO: fatty acid oxidation
FBA: flux balance analysis
FBS: fetal bovine serum
FCCP: carbonyl cyanide 4-trifluoromethoxyphenylhydrazone
FDA: US Food and Drug Administration
FGAR: formylglycinamide ribonucleotide amidotransferase
FH: fumarate hydratase
G6PD: phosphate dehydrogenase
GBM: glioblastoma
GFAT: glutamine:fructose-6-phosphate amidotransferase
GKI: glucose-ketone index
GLS: glutaminase (LGA/KGA)
GLUT1: glucose transporter 1
GMPS: guanosine monophosphate synthetase
GRAS: Generally Recognized as Safe
GS: glutamine synthase
GSCs: glioma stem cells
GSH: glutathione
GSVA: Gene Set Variation Analysis
HBMEC: Human Brain Microvascular Endothelial Cells
HBOT: hyperbaric oxygen therapy
HC: hierarchical cluster
***HDAC*:** histone deacetylases
HG-FBS: high glucose, FBS supplemented media
HIF: hypoxia-inducible factor
HK1: hexokinase 1
HK2: hexokinase 2
hMSCs: human Mesenchymal Stem Cells
HR: Hazard Ratio
HRE: hypoxia responsive element
IC50: half maximal inhibitory concentration
***IDH*:** isocitrate dehydrogenase 1
IMRT: intensity-modulated radiation therapy
iPSC: induced pluripotent stem cells
KD: ketogenic diet
KMT: Ketogenic metabolic therapy
LDH: lactate dehydrogenase
LG-BHB: low glucose, BHB supplemented media
***LKB1/AMPK*:** liver kinase B1/AMP-activated protein kinase
MCT: monocarboxylate transporter
MF: metformin hydrochloride
mGPDH: mitochondrial glycerophosphate dehydrogenase
MixLow: mixed-effects by Loewe additivity index
MPC: mitochondrial pyruvate carrier
MRI: magnetic resonance imaging
MRS: magnetic resonance spectroscopy

MTOR: mammalian target of rapamycin
MTS: [3-4,5-dimethylthiazol-2-yl-5-3-carboxymethoxyphenyl-2-4-sulfophenyl-2H-tetrazolium, inner salt
NADSYN: NAD synthetase
***NES*:** neural precursor and stem cell marker
***NF1*:** neurofibromin 1
NF-κB: nuclear factor kappa beta
NSCs: neural stem cells
NR: IC50 not reached.
O6-MeG: O6-methylguanine
OCR: oxygen consumption rate
OPCs: oligodendrocyte precursor cells
OXCT1: enzyme 3-oxoacid CoA-transferase 1
OXPHOS: oxidative phosphorylation
PBS: phosphate buffered saline
***PDGFRA*:** platelet-derived growth factor receptor α
PDH: pyruvate dehydrogenase
PDHX: component X of PDH
PDK: pyruvate dehydrogenase kinase
PDPs: pyruvate dehydrogenase phosphatases
PEP: phosphoenolpyruvate
PER: Proton Efflux Rate
PFK: phosphofructokinase
PI: Prognostic Index
PK: pyruvate kinase
PKG: phosphoglycerate kinase
PKM2: pyruvate kinase isoform M2
PPP: pentose phosphate pathway
PRPP: 5-phosphoribosyl pyrophosphate amidotransferase
***PTEN*:** mutated phosphatase and tensin homolog
***Rb*:** retinoblastoma
***REDD1*:** DNA damage responses 1
RTG: retrograde mitochondria-nucleus signaling
qRT-PCR: Quantitative Real-Time PCR
S.D.A.: Sequential Deletion Analysis
SDH: succinate dehydrogenase
SLP: substrate level phosphorylation
SOD: sodium oxamate
SREBPs: sterol regulatory element binding proteins
SUCL: succinyl-CoA ligase
TCGA: The Cancer Genome Atlas Research Network
TIC: tumor initiating cell
TMZ: temozolomide
***TNF*:** tumor necrosis factor
TTF: tumor treating fields therapy
WHO: World Health Organization

I. INTRODUCTION

1. Introduction

1.1. Brain cancer in the molecular era: origin, hallmarks and statistics

Cancer is one of the leading causes of morbimortality worldwide, with an estimated 19.3 million new cases and almost 10.0 million deaths in 2020 [1]. In reality, the generic designation of "cancer" encompasses a multitude of diseases, all characterized by unrestrained proliferation of abnormal cells as well as a cumulative number of hallmark capabilities, summarized in Figure 1 [2; 3].

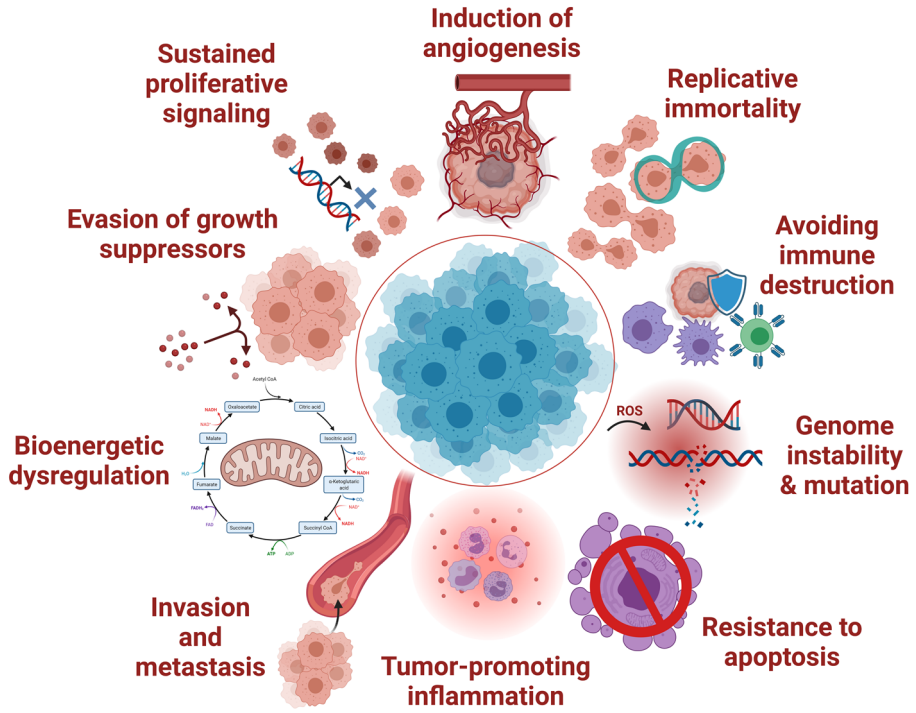

Figure 1. Hallmarks of cancer. The hallmarks of cancer encompass ten characteristics that are observed during tumor pathogenesis, enabling cancer cells to become tumorigenic and ultimately malignant and invasive. Classical descriptions include self-sufficiency in growth signals, insensitivity to anti-growth signals, evasion of programmed cell death, limitless replicative potential, sustained angiogenesis and tissue invasion/metastasis. Emerging hallmarks comprise deregulated metabolism, evasion of the immune system, genome instability and tumor-promoting inflammation.

The biophysical changes and mechanisms that underlie the origin of cancer are a controversial topic [4]. In a substantivalist perspective, cancer can be defined as uncontrolled growth and abnormal stromal interactions (spatial perspective), or dissonance in tissue organization (temporal perspective). In the relationist approach,

cancer is a systemic multi-level failure of cell control and/or escape from immune recognition.

Within this devastating disease, tumors of the central nervous system (CNS) emerge in the normal population with a global incidence of less 10 per 100,000 person-years, making them a relatively rare form of cancer. Gliomas are the most common (81% of all cases), and can be classified according to their presumed cell of origin: astrocytic tumors (astrocytoma, anaplastic astrocytoma and glioblastoma [GBM]), oligodendrogliomas, ependymomas, and mixed gliomas with morphological features of both astrocytes and oligodendrocytes, labeled oligoastrocytomas [5].

Historically, the World Health Organization (WHO) categorized gliomas based exclusively on histopathological criteria, but, with the advent of molecular subtyping and machine-learning technologies, a major restructuring took place in 2016 by incorporating molecular features [6]. The 2022 WHO classification is set to reinforce molecular subtyping as a diagnostic tool, achieving slightly greater prognostic separation [7].

Routinely, a minimum of four histopathological parameters defined WHO grading: nuclear atypia, proliferative (mitotic) activity, microvascular proliferation, and necrosis. In this classification, grade 1 neoplasms (pilocytic astrocytomas) are generally considered biologically benign and curable by surgical resection [8]. If there is only nuclear atypia, the tumor will be defined as grade 2 (diffuse astrocytoma, oligoastrocytoma or oligodendroglioma), whereas nuclear atypia and mitotic activity categorizes as grade 3 (anaplastic astrocytoma or oligodendroglioma). Diffuse infiltration into surrounding parenchyma renders grade 2 incurable by surgery, but they may have long-term clinical progression, whereas grade 3 is rapidly proliferating and swiftly fatal. Grade 4 gliomas are defined as highly infiltrating glial neoplasms with nuclear atypia, mitotic activity and, at least, one of the following: necrosis and/or micro-vascular proliferation.

As detailed below, current guidelines recommend subdivision of high-grade gliomas by molecular profiling, especially in isocitrate dehydrogenase 1 *(IDH)* 1/2 and 1p19q status [9]. The *IDH1 R132H* mutation is the most useful prognostic factor, inducing a neomorphic gain-of-function by disrupting functionally relevant codon Arg132, with epigenetic and metabolic reprogramming. It has been described in 5-10%

primary GBMs and more than 85% secondary GBMs. Most notably, *IDH1 R132H* confers a two to three times longer median overall survival than *IDH1* wild-type [10].

1.1.2. High grade gliomas: histopathological and molecular characteristics

GBM represents the most common and aggressive malignant primary brain tumor in adults, with an age-adjusted incidence rate ranging from 0.59 to 5 per 100,000 population, encompassing approximately 54-57% of all gliomas and 48% of all malignant brain tumors [11-13]. Incidence of GBM is on the rise, presumably owing to an aging population, better diagnostic capabilities, exposure to ionizing radiation, environment pollution and other lifestyle associated factors [14]. Given its fairly low incidence in comparison with other cancers, GBM is often regarded as an "orphan disease".

Histologically, GBM is described as a highly heterogeneous subtype of grade 4 glioma, distinguished by anaplastic cells that resemble immature astrocytes, oligodendrocytes, or a mixture of both. GBM demonstrates pleomorphic cell populations which range from small, poorly differentiated cells, to large multinucleate cells with multifocal necrosis, pseudopalisading nuclei and prevalent mitotic activity [15]. Due to almost an invariable recurrence even after therapy, patients with GBM typically die within 12-18 months after initial diagnosis.

The 2016 WHO system classified GBM into five groups [6]:

1. GBM, *IDH* wild-type (no mutation)
2. GBM, *IDH* mutation; diffuse or anaplastic astrocytoma,
3. *IDH* wild-type (no mutation); diffuse or anaplastic astrocytoma,
4. *IDH* mutation; oligodendroglioma or anaplastic oligodendroglioma,
5. *IDH* mutation with 1p19q co-deletion.

1p19q codeletion and *IDH* mutation are favorable prognostic markers for overall survival [16]. Of note, in our work, we focused exclusively on *IDH* wild-type cell lines and tissue samples.

Table 1. WHO 2016 histopathological grading associated to the most frequent molecular alterations in astrocytic, oligodendroglial and oligoastrocytic gliomas. Primary GBM show a complex chromosomal, genetic and epigenetic background.

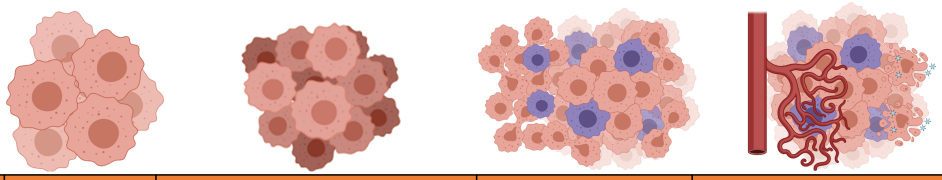

TYPE/GRADE	WHO GRADE I	WHO GRADE II		WHO GRADE III	WHO GRADE IV
	Good prognosis Typical in children	Hypercellularity 5-8 years median survival		Hypercellularity, nuclear atypia, mitotic activity 3-year median survival	Nuclear atypia, mitotic activity and necrosis or microvascular proliferation (angiogenesis) 12-18 months median survival
		Frequent IDH1/IDH2 mutation			10% IDH mutant, 90% IDH wild-type
ASTROCYTOMA	**Pilocytic astrocytoma** BRAF duplication, fusion or point mutation on chromosome 5 and 7	TP53 mutation; PDGFA/PDGFRA overexpression; 7q gain	**Diffuse low-grade astrocytoma** Progression with: 9p loss; CDKN2A/B, p14ARF deletion/methylation; RB1 mutation/deletion; 19q loss	**Anaplastic astrocytoma** Progression with: 10q loss Loss of DCC expression Other aberrations	**Primary GBM** **Amplifications**: EGFR, MET, PDGFRA, MDM2, MDM4, CDKN2A/B, CDK6 **Mutations**: ERBB2, NF1, PTEN, PIK3R1, PIK3CA, TP53 (<25%), RB1 **CTMP methylation** **Deletions**: p14 ^{ARF},CDKN2A/B, RB1 Monosomy 10; Trisomy 7; 19q gain; 20q gain
OLIGOASTROCYTOMA		TP53 mutation; PDGFA/PDGFRA overexpression; 7q gain; t(1:19)(q10:p10); 1p and 19q loss	**Low grade oligoastrocytoma** Progression with: 9p loss CDKN2A/B, p14ARF deletion/methylation	**Anaplastic oligoastrocytoma** (can progress to secondary GBM)	**Secondary GBM** (progression from previous grades)
OLIGODENDROGLIOMA		t(1:19)(q10:p10); 1p and 19q loss	**Low grade oligodendroglioma** Progression with: 9q loss; CDKN2A/B, p14ARF deletion/methylation; RB1 methylation; 10q loss	**Anaplastic oligodendroglioma** (rarely progresses to secondary GBM)	

Currently, molecular testing for *IDH* status is highly recommended in all patients, and grade 3–4 gliomas should undergo testing for *MGMT* promoter methylation, since patients with methylated *MGMT* typically respond better to alkylating chemotherapy [17].

As most notable changes, the 2022 edition includes updated taxonomy, nomenclature and grading, key diagnostic genes/pathways and embraces novel diagnostic techniques, such as methylome and molecular profiling. In the revised nomenclature, all *IDH*-mutant adult diffuse gliomas are defined as astrocytoma/oligodendroglioma with an assigned grade of 2, 3, 4, but should no longer be termed GBM. Thus, "GBM, *IDH* wild-type" is consolidated as a separate category.

Importantly, molecular characteristics can be used to predict outcomes and identify biopsies as *de facto* GBM even if they do not fulfill all the histological criteria [18]. Detection of at least one diagnostic molecular feature (*TERT* promoter mutation, *EGFR* gene amplification, combined gain of entire chromosome 7 and loss of entire chromosome 10 [+7/–10]) is sufficient to assign the entity of "GBM, *IDH* wild-type", assuming *IDH*-mutations have not been detected.

1.2. Molecular subtypes of GBM: deciphering heterogeneity

1.2.1. Cell of origin

The exact cellular origin of GBM is unknown, albeit neural stem cells (NSCs), NSC-derived astrocytes and oligodendrocyte precursor cells (OPCs) have been proposed as candidates. Whether these highly aggressive tumors initiate from stem cell populations or progenitors that, through accumulation of DNA damage, mitochondrial dysfunction or metabolic reprogramming, acquire stem-like potential, is not fully understood [19; 20].

1.2.2. Mutational landscape of GBM

Mutations and altered gene expression profiles are common in GBM, including the activation of oncogenes and silencing of tumor-suppressor genes. Based on copy number variation, gene expression and sequencing, three major signaling cascades are significantly altered in GBM: pathways related to receptor tyrosine kinase *RTK/RAS/PI3K* (comprising, in total, 88% of all cases), *TP53* (87%) and retinoblastoma (*Rb*) tumor suppressor pathways (78%). The genomic aberrations of GBM are summarized in Supplementary Figure S1.

Dating back to 2010, seminal work from Verhaak *et al.* took insights from The Cancer Genome Atlas Research Network (TCGA) and proposed four molecular subtypes of GBM, based on the analysis of surgical samples: proneural, mesenchymal, classical and neural [21]. Table 2 recapitulates the gene expression signatures of each subtype. It is important to note that Verhaak molecular subtypes had only been validated in tissue

samples, with a variable, heterogeneous contribution from both tumoral and normal cells; cell culture models might recapitulate some of the characteristics of molecular subtyping at the genomic level, but they are not directly translatable.

Table 2. Summary of molecular alterations in Verhaak TCGA GBM subtypes.

Verhaak subtype	Gene expression signature
Classical	*EGFR* amplification; *Ras* activation; loss of *PTEN* and *CDKN2A*; absence of *TP53* mutations
Mesenchymal	*NF1* mutation; loss of *TP53* and *PTEN*; activation of *TNF* and NF-κB; *CHI3L1/YKL40, MET, CD44* and *MERTK* amplification
Proneural	*IDH-1* mutation; *PDGFRA* amplification; loss of *TP53*, *PTEN*, and *CDKN2A*
Neural	Expression profiles similar to normal brain (*NEFL*, *GABRA1*, *SYT1*, *SLC12A5*, as well as *EGFR* amplification)

In the classical subtype, response to chemoradiotherapy is marginally improved, likely by functional p53 DNA-damage sensing. The mesenchymal subtype is characterized by increased angiogenesis, necrosis, inflammation and hypoxia, with higher activation of glycolytic metabolism and poor prognosis [22]. Thus, *RAS/PI3K* and anti-angiogenic agents, as well as metabolic therapies, may be especially well suited for this signature [23]. Tumors of the proneural subtype, on the contrary, are less pathological and carry a better prognosis. Interestingly, 90% of *IDH1* mutations are found here, suggesting that the proneural subclass may actually be a form of secondary GBM; despite poor response to TMZ, patients are younger, survive longer and might be good candidates for inhibitors *HIF*, *PI3K* and *PDGFRA* pathways. The survival advantage is thought to be primarily linked to *IDH* status [24]. Finally, neural malignancies have a lower degree of infiltration in the brain parenchyma and express gene signatures reminiscent of differentiated, non-tumoral cells [25]. Indeed, it was suggested that, in reality, this category defines samples with a high content of healthy brain tissue, rather than describing a tumor of lesser malignancy [26; 27].

The classification by molecular subtypes continued to evolve since its publication, further outlined with new genetic alterations and molecular features, such as *TERT* and *ATRX* mutations involved in telomere maintenance, tumor methylation profiles

(methylation of the *MGMT* promoter), *CDKN2A* and/or *CDKN2B* deletions as well as *H3 K27M* mutations [28; 29]. Importantly, *IDH* wild-type and *IDH* mutant gliomas have settled as two distinct and immiscible categories [30; 31].

1.3. GBM: clinical presentation, diagnosis, and standard of care

1.3.1. Localization and clinical presentation

The initial presentation of a patient with GBM is highly variable, contingent on the size, location and affected anatomical structures [32]. Among the most frequent anatomical enclaves we find the cerebral hemispheres, as 95% of tumors arise in supratentorial regions, whereas cerebellum, brainstem and spinal cord localizations are relatively unusual [33]. The tumor mass is usually formed by a single, large, irregularly shaped lesion which infiltrates white matter [15].

Clinical history is usually short, spanning 3-6 months in cases of newly formed, primary GBM. It can also develop over the span of multiple years if the tumor is an evolution of a low-grade precursor. Patients present with symptoms of increased intracranial pressure, including headaches and focal or progressive neurologic deficits. Direct brain damage/necrosis produces focal neural deficits in 40-60% of cases, as well as cognitive impairment that is contingent on the affected lobe (visual or hearing problems, personality changes, altered gait), whereas secondary intracranial pressure/edema leads to headaches, a hallmark sign in 30-50% [34]. Rapid apparition of neurological symptoms could be mistaken for a stroke in older patients. Seizures are expected in 25% of newly diagnosed patients, developing in as many as 50% at later stages [35].

1.3.2. Diagnosis: anatomical and metabolic imaging

Initial diagnosis is preferentially completed via magnetic resonance imaging (MRI) or computed tomography (CT). High-grade gliomas infiltrate surrounding tissues and cross the midline to involve the contralateral brain. CT scans show hypointense areas in comparison to adjacent brain and a midline shift because of the moderate to severe edema.

In MRI studies, GBMs can be marked with gadolinium to reveal an irregularly shaped mass with a dense ring of enhancement and hypointense center of necrosis. Tumors are mostly unifocal, although, in about 10-15% of cases, can appear as multifocal, distant or diffuse [36].

Additionally, [18F] fluoro-deoxyglucose positron emission tomography (18F-FDG-PET) has become part of the routine imaging protocol to evaluate glucose uptake (a marker of metabolic activity) and monitor progression/recurrence [37]. While specific partitioning of glucose destined for ATP or macromolecule synthesis cannot be determined using this method, PET allows for tracking of recurrence and metastatic disease with a high degree of accuracy, indicating a close relationship between metabolic alterations and invasiveness [38]. Recently, novel imaging techniques opened the possibility to examine *in vivo* uptake of other metabolites, including glutamine/glutamate (glutaminolysis), choline (cellular membrane turnover), N-acetyl aspartate (neuronal viability), fatty acids and ketone bodies (oxidation and biosynthesis), but they are still reserved for research settings [39; 40].

Metabolic imaging of GBM shows regional microenvironment metabolic heterogeneity, with histological analysis revealing regions of hypercellularity (pseudopalisades) surrounded by necrotic foci under hypoxia (pO2=2.5-5%) and infiltrating tumor cells under normal oxygen conditions (pO2=10%) [41]. In a clinical context, the lactate to pyruvate ratio increases up to three times in tumoral tissues over normal brain, suggesting glycolytic metabolism is retained *in vivo*, not merely an *in vitro* artifact [42; 43]. In the future, studying heterogeneity by non-invasive metabolic imaging could streamline the diagnostic process and improve patient stratification and evaluation response to therapy [44].

1.3.3. Standard of care of GBM patients

GBM is a virtually incurable, terminal illness that requires a multidisciplinary approach and palliative care. Current standard of care consists of maximally safe surgical resection, followed by radiotherapy and concurrent chemotherapy with the oral alkylating agent temozolomide (TMZ) [45].

Surgery relieves intracranial pressure, which may recover previously lost CNS functions and decrease the need for corticosteroid medication (e.g., dexamethasone) to manage cerebral edema. Maximal survival benefit corresponds to resection volumes greater than 98%, eliminating all gadolinium enhancing areas, which can be accomplished by assistance of intraoperative MRI and fluorescent guides to label metabolically active tissue [46-48]. Nevertheless, complete elimination of the tumor is rendered impossible by its highly infiltrative nature [49].

Postoperative radiotherapy was considered the only fundamental pillar of GBM treatment before the early 1980s, extending median survival from 3-4 months to 7-12 months, while also providing local control in newly diagnosed high-grade gliomas [50; 51]. At present, TMZ is the first-line chemotherapeutic agent for GBM, administered concomitantly with radiotherapy in a dosing regimen known as the Stupp protocol, based on a landmark clinical trial from 2009 that demonstrated synergistic effects, increasing overall median survival by 2.5 months when compared to radiotherapy alone [52].

At the cellular level, radiation produces single and double-strand DNA breaks by direct action and free radicals by indirect action, instigating cell death and activating replication checkpoints in rapidly proliferating tissues. TMZ acts by inducing genetic aberrations through the addition of methyl groups to purine bases (O6 and N7 positions of guanine, and N3 positions of adenine). The principal cytotoxic lesion, O6-methylguanine (O6-MeG), can be corrected by *MGMT* enzymes, so therapeutic responses to TMZ can be partially predicted by determining the methylation status of the *MGMT* promoter and expression of this DNA-repair enzyme in the tumor biopsy [17]. Apoptotic signaling is mainly triggered by O-6-methyl G:T mispairs.

Recently, the addition of novel treatments for newly diagnosed GBM, such as tumor treating fields therapy (TTF), an FDA-approved portable device that applies low-intensity, intermediate-frequency alternating electric fields to stop mitosis/cell division, extended overall median survival to 20.9 months [53]. Upcoming therapies for GBM in research stages are summarized in Figure 2. Despite incremental progress, the 5-year

survival rate for patients treated with both TTF and maintenance TMZ is still only 12.8% [54].

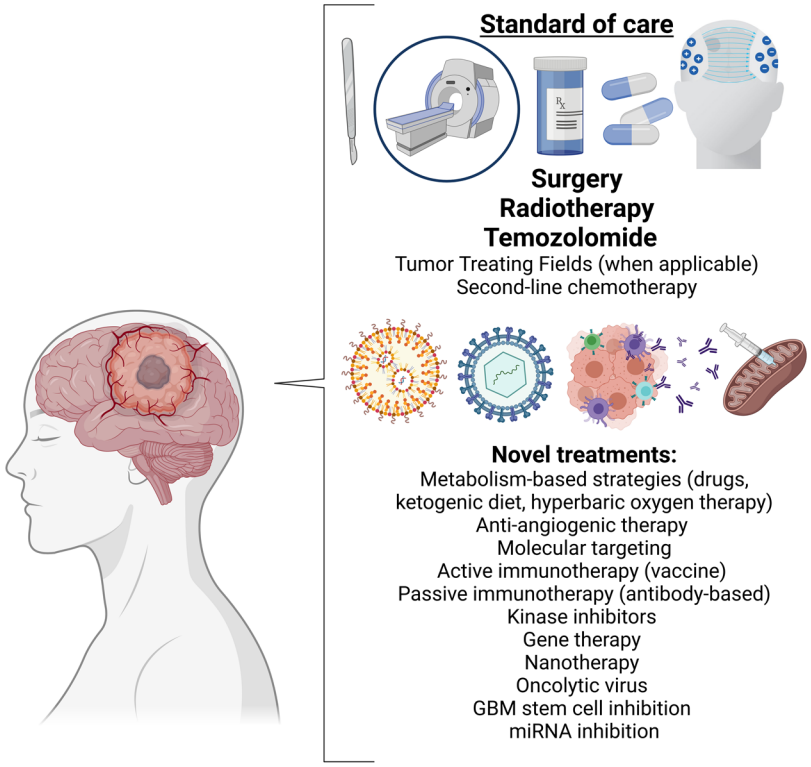

Figure 2. Standard of care for GBM and novel treatments under active development.

As standard of care is not a curative option, new therapies are sorely needed, with researchers worldwide trying to understand GBM from multiple points of view, mainly the "omics" sciences: genomics, proteomics and metabolomics. In view of these universal obstacles, new procedures are generally tested in the recurrent stage, where only a handful of approved rescue options compete for a practically non-existent survival benefit. Promising candidates then move to clinical trials of newly diagnosed GBM, to be combined with chemoradiotherapy.

Metabolism-based drugs reinforcing ketogenic metabolic therapy (KMT) have been proposed as attractive strategies at this juncture, with the possibility of non-toxic press-pulse management of highly glycolytic and glutaminolytic cancers [55].

Metabolic therapy is contingent on a series of assumptions about mitochondrial fitness of normal and cancer cells, as well as defective substrate flexibility. A near complete dependency upon fermentable fuels is a *sine qua non* condition for this approach, which has proven a controversial and divisive topic. The intersection between theories

attempting to explain the origin of cancer and how it should be treated based on causal biophysical mechanisms will be discussed in the following section.

1.4. Metabolic reprogramming in the origin and progression of cancer

Cellular metabolism encompasses a highly organized and integrated network of chemical reactions carried by a crossover of enzymatic pathways, which are regulated by activator/inhibitor metabolites and interconnected with signaling pathways closely related to proliferation and differentiation.

1.4.1. Key chemical reactions for energy production in mammalian cells

In eukaryotic animal cells, synthesis of ATP takes place in two distinct ways:

a) During enzyme-level reactions, called substrate level phosphorylation (SLP), that do not require oxygen.
b) During oxidative phosphorylation (OXPHOS), which generates NADH and $FADH_2$ hydrogen carriers, creating an electrochemical gradient in the mitochondrial electron transport chain (ETC) fueling ATP synthesis, a process with an absolute requirement of oxygen.

SLP can occur in the cytoplasm (as part of the glycolytic pathway) or in the mitochondria (at the succinyl-CoA ligase step of the TCA cycle). Multiple metabolites can act as substrates for SLP and/or OXPHOS, mainly glucose and glutamine [56]. When glutamine undergoes mitochondrial SLP (mSLP), it is termed "Q-effect". To understand the role of ATP synthesis in cancer, it is important to divorce the metabolite (monosaccharides, amino acids, fatty acids, ketone bodies and other sources) from the actual biochemical processes that generate energy (SLP/OXPHOS).

1.4.2. Bioenergetics in normal cells: Embden–Meyerhof–Parnas pathway and mitochondrial respiration

Under physiological conditions, glucose is converted into two molecules of pyruvate through a series of nine enzymatic reactions, collectively known as Embden–Meyerhof–

Parnas pathway or glycolysis. Two enzymatic reactions, phosphoglycerate kinase (PKG) and pyruvate kinase (PK), produce ATP by SLP.

In normal cells, the fate of pyruvate is determined by oxygen availability. In low oxygen conditions (e.g., exercising muscle), pyruvate is converted to lactate by the enzyme lactate dehydrogenase (LDH), a process known as anaerobic glycolysis or fermentation, replenishing NAD+ reduced during glycolysis. Under adequate oxygen levels, pyruvate will be preferentially oxidized, shuttled to the TCA cycle by the pyruvate dehydrogenase complex (PDH). In the mitochondria, acetyl-CoA from pyruvate undergoes complete oxidation, producing CO_2 and reducing two high-energy redox carriers, NAD+ to NADH and FAD to $FADH_2$. These hydrogen carriers uphold the proton motive force between the inner and outer membrane of the mitochondria, which synthetizes ATP in complex V (ATP-synthetase) of the ETC, yielding a theoretical of 30-32 ATP molecules per each glucose molecule. Aerobic respiration is responsible for the majority of ATP production in oxidative mammalian cells.

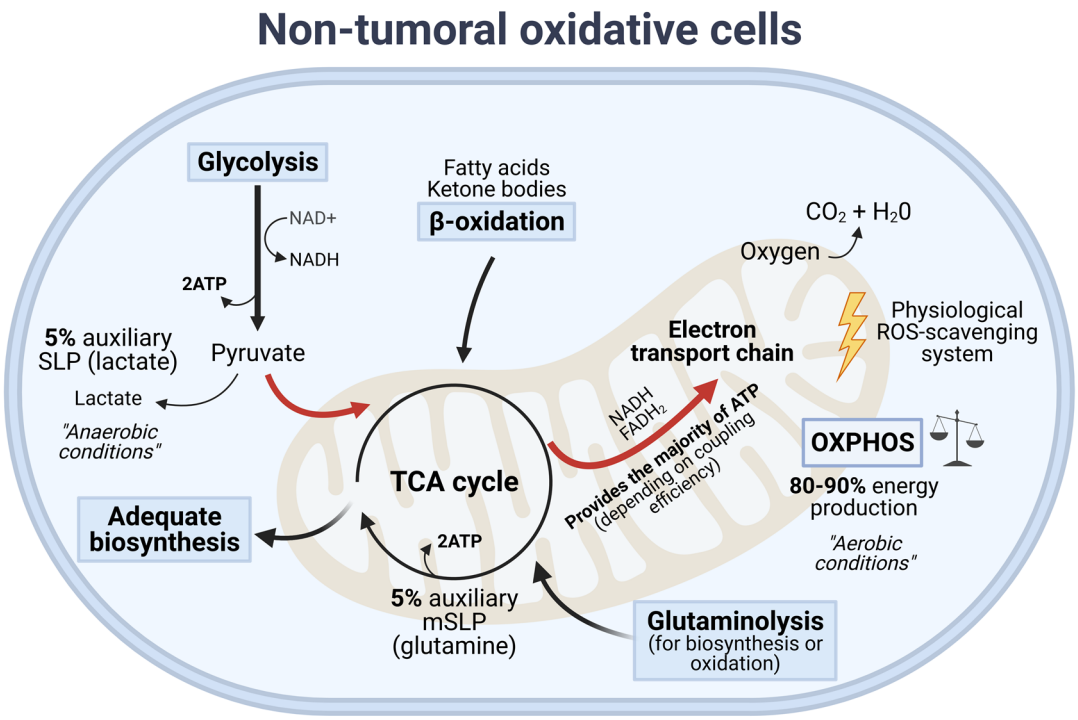

Figure 3. Energy metabolism in normal oxidative cells. Glycolysis generates a total of 4 ATP and 2 NADH per glucose molecule, utilizing 2 ATP in the process. Pyruvate grooming or the link reaction yields an additional 2 NADH. In the TCA cycle, 6 NADH and 2 $FADH_2$ molecules are generated for subsequent OXPHOS, as well as 2 ATP directly by SLP. The electron transport chain (ETC) then yields a theoretical 30 ATP from NADH and 4 ATP from $FADH_2$, depending on

stoichiometric efficiency. In normal cells, lactate production from pyruvate only takes place under hypoxic conditions (anaerobic glycolysis). OXPHOS is the main source of energy in mitochondrially healthy oxidative cells (up to 90% of ATP synthesis).

Rapidly proliferating cancer cells take up more nutrients than would be strictly needed to meet their energy demands, reprograming their metabolism to promote survival, invasion and treatment resistance.

1.4.3. Somatic mutation theory and mitochondrial metabolic theory of cancer: different culprits, different tactics

In both the somatic and mitochondrial theory, it is recognized that most cancer cells differ from normal cells in their use of glucose, amino acids (particularly glutamine), fatty acids and other oxidative fuels, irrespective of their oxygen status. SLP stands as the principal energy-generating pathway in cancer due to a rewired somatic program and/or partially or fully defective mitochondrial function [57; 58]. The difference between these two paradigms lies in the nuclear and mitochondrial control of tumorigenesis.

As a result, common metabolic alterations in cancer include upregulated aerobic glycolysis (the Warburg effect), increased glutaminolytic flux (for anaplerosis, oxidation and Q-effect) upregulated pentose phosphate pathway (PPP), lipid/amino acid metabolism, recycling of intermediates for biosynthesis and redox balance, defective mitochondrial biogenesis as well as oncometabolite production (such as lactate, succinate or 2-hydroxyglutarate) [59]. Notably, several metabolites have been recognized as oncogenic/tumor suppressor by virtue of their capacity to alter cell signaling and differentiation.

1.4.4. Somatic model for ATP synthesis: metabolism under genetic control

In the somatic mutation theory, the origin of malignant transformation resides in the combined effect of genetic alterations, with metabolic reprogramming as a downstream epiphenomenon. Figure 4 shows how different mutational landscapes contribute to the bioenergetic rewiring of cancer. In this interpretation, metabolic

flexibility of tumoral cells is maintained, with the ability to perform both SLP and OXPHOS to meet catabolic and anabolic demands.

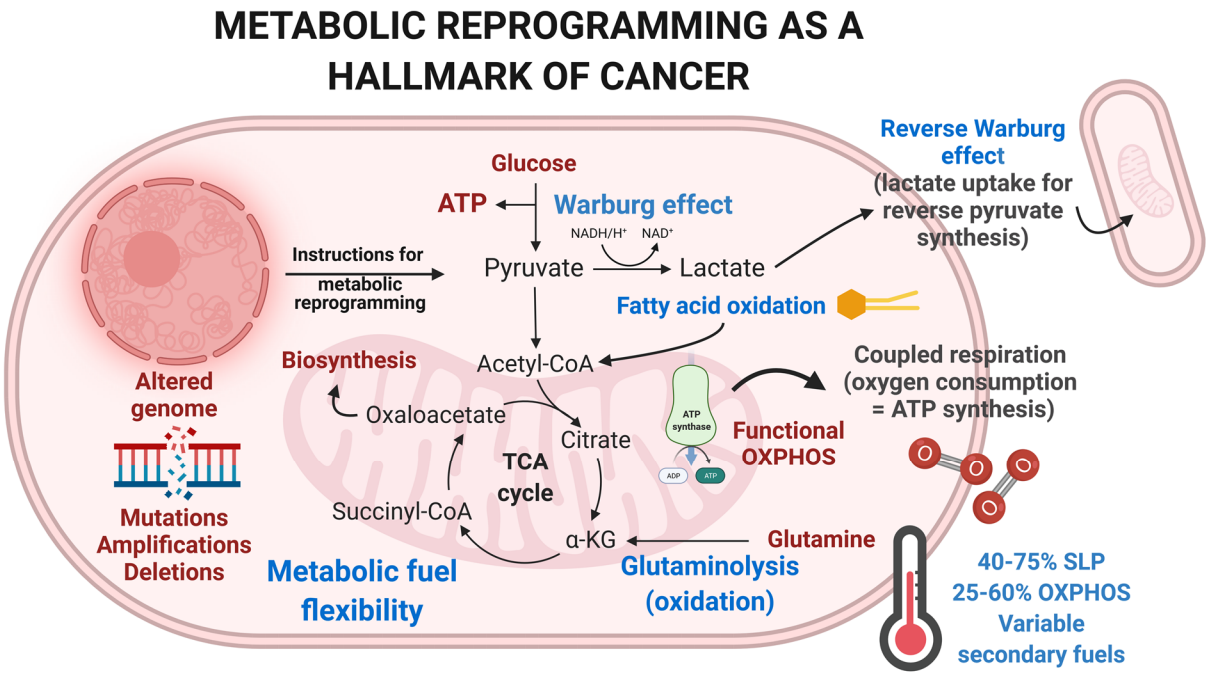

Figure 4. Somatic mutation theory, metabolic reprogramming as a secondary hallmark. Random mutations and/or DNA damage induce a proliferative program. Cancer cells adapt by increasing their demands for metabolic fuels, rewiring metabolism to produce ATP in a less efficient but more responsive manner (Warburg effect). Other fuels and biosynthetic precursors, such as glutamine and fatty acids, can be taken up and diverted to the TCA cycle to synthetize ATP and macromolecules. In the somatic mutation theory, OXPHOS is largely functional (oxygen consumption equals ATP synthesis), covering the remaining energetic demands; this is a metabolic advantage rather than a weakness. Lactate can be exported to the microenvironment by glycolytic cells and taken up by neighboring oxidative cells for energy and biosynthesis (reverse Warburg effect).

Consequently, metabolism and gene expression should not be viewed as independent categories [60]. However, given the basic assumption that each individual cancer cell could hold its own distinctive driver and passenger mutations, developing targeted therapies is proving arduous [61-63].

Despite bringing forth advancements in DNA sequencing techniques, with regards to cancer, the somatic explanation is faced with unresolved problems, such as the oncogenic paradox, tissue normalization and non-mutagenic carcinogens [64-67]. These open questions substantiate the exploration of alternative hypothesis to better understand

carcinogenesis, gathering of both molecular and metabolic experimental evidence and expanding therapeutic opportunities.

1.4.5. Metabolic model for ATP production: mitochondrial dysfunction, the Warburg effect, and Q-effect

The Warburg hypothesis establishes that all cancer cells arise from mitochondrial defects, making them avid consumers of glucose and other fermentable fuels through SLP, even in presence of oxygen. Warburg's initial observations have been readjusted to the modern molecular era, but cancer research shifted towards the search of a DNA-based primary cause, rather than a extranuclear origin [68].

It has been proposed that the root of cancer involves a cluster of metabolic alterations in a hierarchical evolutionary framework: specifically, defects in mitochondrial function, number and/or structure, with a varying degree of OXPHOS and ETC dysfunction [69].

Mitochondria stand at the center of the metabolic theory of cancer. These cytoplasmic organelles of suspected endosymbiotic origin serve bioenergetic, biosynthetic and signaling functions, with a vital role in adaptation to microenvironmental perturbations [70]. As previously stated, OXPHOS is the multi-step, cyclical mitochondrial pathway that allows cells to synthesize ATP from the oxidation of nutrients. During OXPHOS, electrons from NADH and $FADH_2$ are transferred to oxygen molecules, creating a proton electromotive gradient in the ETC that maintains ATP synthase in F1F0 mode, generating ATP via a proton-driven torque rotation [71].

The metabolic theory of cancer is conceptualized in Figure 5. In this paradigm, it is argued that mitochondrial defects, originating from any number of non-specific events that damage respiratory capacity, and the gradual shift towards SLP, ultimately initiate carcinogenesis. Even partial disruption of mitochondrial function over time leads to a shift towards SLP [58]. As gene expression is regulated by bioenergetics, it stands to reason that metabolic feedback loops will determine if a cell can execute genetic instructions [72]. Contrary to the somatic mutation theory, metabolic reprogramming and heterogenous mutational landscapes are downstream effects of mitochondrial failure [69].

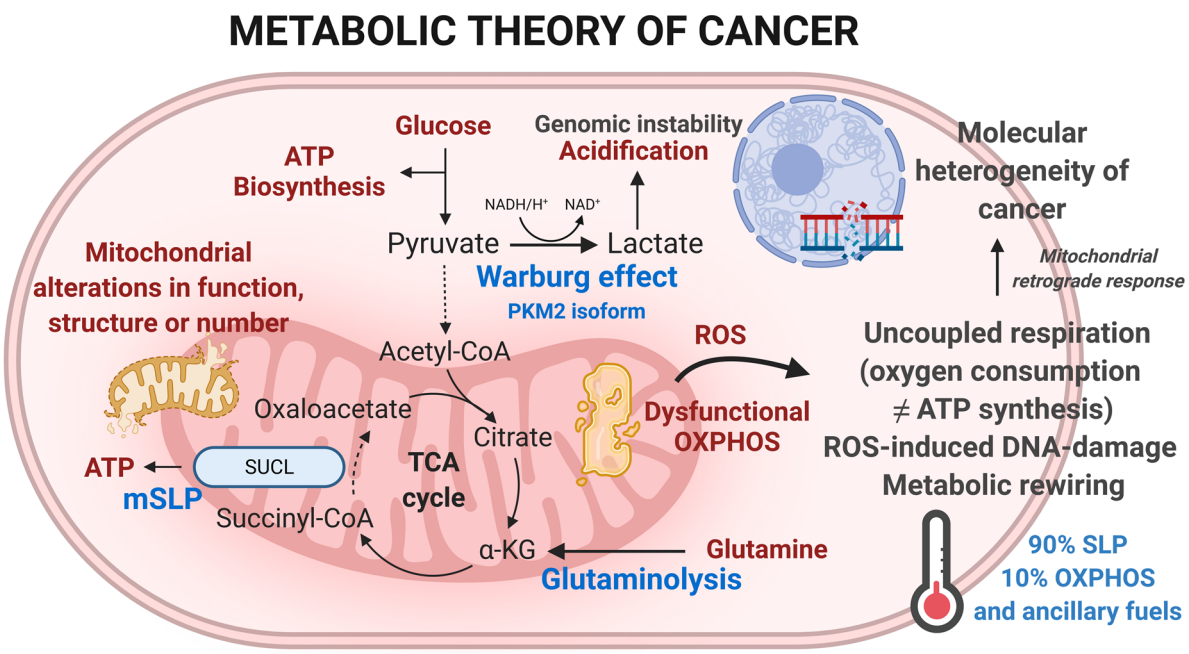

Figure 5. Metabolic theory of cancer. Mitochondrial dysfunction elicits a retrograde response in the nucleus, whereas molecular heterogeneity can be explained by ROS-induced mutations and genomic instability by acidification. The pyruvate kinase M2 (*PKM2*) isoform diverts glucose towards biosynthetic pathways, but a variable quantity of ATP is generated by the Warburg effect. Glutamine is not fully oxidized, but rather contributes to ATP synthesis at the succinyl-CoA ligase (SUCL) reaction of the tricarboxylic acid (TCA) cycle. Aerobic glycolysis and mitochondrial SLP (Q-effect) contribute to the majority of ATP synthesis in mitochondrially defective cancer cells. Mitochondrial energy-generation failure, beyond a threshold, is sufficient to induce a predominance of SLP metabolism.

Only cells capable of undergoing the SLP bioenergetic shift will ultimately become tumorigenic. Hypoxia, mitochondrial ROS and highly acidic microenvironments have been shown to induce genomic instability, in concert with disrupted inputs into primitive energy sensing pathways (e.g., *AMPK/MTOR* signaling networks) [73]. As the enzymatic machinery to repair the genome is dependent on energy flux (ATP-dependent nucleosome remodeling), bioenergetic reprogramming produces failure to repair DNA and enables progressive genomic instability [74-76]. Elevated levels of ROS and acidification of the tumor microenvironment induce DNA damage and genomic instability [77; 78]. Mitochondrial retrograde signaling is therefore responsible for dysregulated nuclear gene expression [79].

Theories linking the underlaying mechanisms of cancer to extranuclear causes remain controversial [80-82]. Even though cause and consequence are still up to debate,

one of the most well-defined characteristics of cancer cells, at a functional, bioenergetic level, is their preference and capacity to exploit SLP metabolism [3]. Pyruvate fermentation produces intermediaries and precursors for biosynthesis, regenerates NAD+ and creates an acidic extracellular and intracellular microenvironment that facilitates invasion and metastasis [83; 84]. The majority of solid tumors, including GBM, resort to aerobic glycolysis over OXPHOS, at least under cell culture conditions. Furthermore, glycolysis is connected to the PPP, generating NADPH and ribose-5-phosphate, essential for the biosynthesis of lipids and nucleic acids, as well as maintenance of redox balance by regeneration of glutathione (GSH). Glucose carbons are diverted to the PPP by glucose-6-phosphate dehydrogenase (G6PD), resulting in a provision of approximately 85% of pentose phosphates incorporated into newly synthesized DNA [85].

ATP production from aerobic glycolysis (Warburg effect) and mSLP glutaminolysis (Q-effect) exceeds OXPHOS to attain quotients sufficient to meet bioenergetic and proliferative demands, conferring what has been dubbed a “selective advantage”. Logically, this advantageous state only endures as long as we assume a constant supply of glucose and glutamine, or, in nutrient-deprived conditions, metabolic flexibility for other fuels, such as lactate, amino acids or fatty acids, even in presence of tumorigenic mutations and mitochondrial damage.

1.4.6. The role of mitochondria in the origin and progression of cancer

Mitochondrial function is a driving force of all energy-consuming cellular functions, associated with numerous pathophysiological conditions, including metabolic, cardiovascular, muscular and neurodegenerative disorders, as well as cancer [86].

In normal cells, the majority of ATP is produced by OXPHOS; this applies to healthy CNS tissues as well, where glucose-derived pyruvate and ketone bodies are taken up for oxidation under aerobic conditions [87; 88]. Despite its lower efficiency, SLP is almost 100 times faster, conferring an advantageous state of reactive plasticity to rapidly proliferating cells. In a framework of evolutionary pressure, cancer cells able to switch to SLP metabolism can survive in an everchanging microenvironment, disrupted by poor

angiogenesis, hypoxia and nutrient stress [89]. Metabolic therapy posits the simultaneous targeting of SLP, while maintaining viability of metabolically healthy cells via alternative fuels [90].

Warburg originally envisioned that dysfunctional mitochondrial ATP-synthesis forced cancer cells towards fermentative metabolism in order to preserve a constant energy flux. Modern revisions adapted this notion to encompass structural abnormalities, mitochondrial DNA (mtDNA) mutations, abnormal fission/fusion, cholesterol and phospholipid content (cardiolipin), mutations in enzymes of the TCA cycle and the ETC, as well as unstable mitochondrial membrane potential and uncoupled respiration [91; 92]. Supplementary Figure S2 recapitulates the mitochondrial alterations described in GBM.

Electron microscopy demonstrated alterations in mitochondrial number and structure in over a thousand tumoral samples, including GBM (typically, swelling and cristolysis of the inner membrane) [88; 93; 94]. Mitochondria conform into folding structures called cristae; abnormalities in morphology directly correlate with insufficient or defective respiration [95]. The ETC is a highly conserved set of protein complexes that allowed obligatory fermentative organisms to harness the energy contained in organic molecules through oxidation. Respiratory complexes are distributed in folding structures within mitochondrial membrane lipids (cardiolipin), indispensable to preserve ATP-synthesis [96]. Thus, when alterations in morphology and lipids accumulate, OXPHOS is impaired [58]. However, despite being ubiquitous in cancer cells, the functional relevance of structural alterations is yet to be fully unraveled [97].

Furthermore, a defective TCA cycle is a common feature in GBM. Mutations in aconitase, *IDH*, succinate dehydrogenase (*SDH*) and fumarate hydratase (*FH*) have been associated with CNS tumors, acute myeloid leukemia, paraganglioma, pheochromocytoma, ovarian, colorectal, gastrointestinal and other cancers [98]. As previously stated, *IDH1* and *IDH2* are particularly noteworthy in gliomas, identified in the majority of grade 2-3 gliomas and secondary GBM [99]. *IDH-R132H* mediated conversion of α-ketoglutarate to oncometabolite 2-hydroxyglutarate could contribute to tumor progression by driving DNA methylation; however, this phenomenon is also

paradoxically linked to reduced Warburg and Q-effect, providing a mechanistic explanation as to why *IDH1* mutations are a favorable prognostic factor [100]. This is a practical example of two paradigms leading to opposing therapeutic approaches: *IDH-R132H* mutations can be viewed either as a beneficial restrictor of SLP metabolism [101], or a targetable opportunity to avoid further genomic damage [102].

Mitochondrial contribution to tumorigenesis is further supported by mitochondrial transfer studies, where transplantation of normal mitochondria inhibits neoplastic phenotypes despite mutated genomes [103-108]. Taken together, these studies suggest that mitochondria play a significant role in cancer initiation and progression.

Despite this body of evidence, detection of oxygen consumption in cancer cells is commonly interpreted as functional OXPHOS. It is important to note that although structurally damaged mitochondria continue to consume oxygen, a gradual shift towards SLP has been initiated to ensure consistent power output [109]. This explains why the Warburg effect and OXPHOS often coexist in oxygraphic respirometry, as was the case in our study. The cell-specific threshold for tumorigenic SLP and metabolic reprogramming is unknown. Thus, oxygen consumption is not necessarily linked to ATP synthesis, especially under conditions of uncoupled respiration and reversed proton electrochemical gradient. Mitochondrial uncoupling refers to the dissipation of the proton motive force across the inner mitochondrial membrane, where electron flux does not synthetize ATP. Indeed, the tumorigenic potential has been correlated with oxygen consumption, but OXPHOS is not required for proliferation [110].

Beyond ATP, mitochondrial control of proliferation might be essential for regulation of biosynthetic and redox equilibrium [111]. Both aerobic glycolysis and TCA cycle anaplerosis provide intermediaries for macromolecular synthesis: glucose-derived carbons and glutamine-derived nitrogen are converted into precursors of nucleic acids, proteins, and lipids. Thus, a major function of glycolysis and OXPHOS might be to sustain biosynthesis [112].

The metabolic aberrations found in GBM offer multiple therapeutic avenues. Targeting SLP phenotypes by either metabolic drugs or nutrient deprivation is a promising way of selectively eradicating malignant cells while also sparing healthy cells.

Shifting energy production towards oxidation of ketone bodies and fatty acids forgoes glucose-dependency, which is an important concept to grasp, as glucose is often assumed "essential" for ATP-synthesis unless metabolic plasticity is well understood [113]. Effective targeting of glycolysis using inhibitors such as DCA, 2-deoxy-D-glucose (2-DG), 3-bromopyruvate (3-BP), or glucose depletion, is further enabled by adaptation to ketone body metabolism [114].

1.4.7. Advancements in the study of metabolic pathway flux

During the past decades, a deeper understanding of cancer metabolism has been boosted by refinement of techniques to evaluate *in vitro* and *in vivo* metabolic flux. Metabolomics, such as nuclear magnetic resonance (NMR), gas chromatography-mass spectrometry (GC-MS) and liquid chromatography-mass spectrometry (LC–MS), offer a bird-eye view of the presence of metabolites in a tissue or cell sample. Metabolic flux analysis (fluxomics), on the other hand, estimates the flow of metabolites in their natural pathways, including methods such as flux balance analysis (FBA), 13C-metabolic flux analysis (13C-MFA) and extracellular flux analysis (e.g., oxygraphy and flux analyzers).

In our study, we focused on real-time bioenergetics using the Seahorse XF flux analyzer. Formerly, assessing cellular bioenergetics comprised several independent measurements of oxygen consumption, lactate production, total ATP, glucose uptake and mitochondrial membrane integrity, by means of time-consuming protocols that did not provide real-time information. The Seahorse XF instrument, by contrast, provides a fully integrated solution that quantifies extracellular fluctuations in oxygen and proton extrusion (pH) during repeated sampling. This allows for simultaneous measurements of oxygen consumption rate (OCR) and extracellular acidification rate (ECAR), delivering an estimation of mitochondrial function and glycolysis.

It must not be forgotten, however, that oxygraphy is hindered by certain limitations, such as low throughput, low specificity/signal, susceptibility to changes in pH and difficulty for normalization. Most notably, the principal read-outs are simply extrapolations of metabolic flux, not direct measurements of ATP. Seahorse XF and other

oxygraphs such as the Oroboros Oxygraph-2k merely describe OCR/ECAR data, which needs to be interpreted with caution [115-118].

1.5. Metabolic profiles in GBM: overcoming intratumoral heterogeneity

Historically, aerobic glycolysis has been inferred as nearly universal; nevertheless, it has now been proposed that some subpopulations could adapt to both aerobic and anaerobic conditions [119]. Counterpoint evidence suggesting a more nuanced view can be encountered in oxygen-consuming phenotypes, especially in therapy-resistant and metastatic disease [120; 121]. *In vitro*, traditional GBM models have shown variability in experimental estimation of mitochondrial function (particularly, TCA cycle anaplerosis and OCR responses to mitochondrial inhibitors), while tissue-derived GBM stem cells exhibit glucose SLP dependency as well as reliance upon glutamine and fatty acid oxidation (FAO) [122-125]. *In vivo*, metabolic imaging can be used to evaluate substrate uptake, but differentiation between ATP and biosynthesis is methodologically challenging [126; 127]. Subpopulation heterogeneity renders the development of molecular targeting a complex problem.

1.5.1. Deciphering clonal heterogeneity: a biological perspective

A significant source of intratumoral heterogeneity emanates from a subpopulation within the tumor niche that is able to self-renew, differentiate, initiate tumorigenesis and phenocopy the original tumor *in vivo*: these are referred to as cancer stem cells (CSCs), tumor-propagating cells, tumor initiating cells or "persisters" [128]. CSCs are defined by their ability to give rise to differentiated progeny, sufficient to drive tumor maintenance, recurrence and therapeutic resistance [129]. CSCs have been detected in both low and high-grade malignancies, including GBM [130; 131].

In the somatic mutation theory, three major biological frameworks have been proposed to illustrate the mechanisms of heterogeneity, metastasis and therapy resistance.

The stochastic or clonal evolution model posits that all cancer cells are originally biologically equivalent, holding the same tumorigenic potential: any given cell could act as a tumor initiating cell by acquisition of genetic and epigenetic alterations. Therefore, a tumor is a hyperproliferative state caused by driver mutations and genomic instability. Aberrant microenvironmental conditions select the most aggressive, adaptable and resistant cells, thus increasing heterogeneity [132].

In contrast, the hierarchical CSC model posits that malignant transformation is initiated by a subset of cells with stem cell biological properties, or cells that underwent a dedifferentiation process ("stem-like"). CSCs can subsequently "persist" within the tumoral mass, responsible for unlimited growth, recurrence, clonal expansion and phenocopy capabilities. Each CSC subpopulation carries its own unique phenotype, hierarchy and differentiated progeny [133].

These two models place different weight on stemness and microenvironment as regulatory categories, but they are not mutually exclusive, crystalizing in the plasticity model [133]. Herein, the capacity of stemness that characterizes CSCs, rather than being a fixed entity, is a plastic quality that can be expressed to different degrees [134]. Thus, the plasticity model is defined by the interconversion between stem and differentiated states.

As previously discussed, an alternative hypothesis describes cancer as a bioenergetic disease, where mitochondrial damage and progressive loss of OXPHOS initiates compensatory SLP (unregulated growth). This signifies a regression to an ancient, evolutionarily conserved ATP-production system, which does not require oxygen, suitable for rapid proliferation at the cost of coordinated metazoan cell hierarchy [135]. The contention between eukaryotic quiescence and unicellular proliferation could be solved at the local level by this metabolic switch [136]. A significant injury to mitochondrial bioenergetics induces a glycolysis-driven, stem-like proliferative state [137]. CSCs share the same glycolytic behavior that exists in non-cancerous stem cells [138; 139]. In this model, genetic mutations are a downstream epiphenomenon of increased ROS production, microenvironmental acidification, and failure to repair DNA, which can explain tumoral heterogeneity as well as the paradoxical genetic backgrounds

by shifting the underlying mechanisms from somatic mutations (hereditary information) to ATP-synthesis (bioenergetic flux) [140; 141]. Furthermore, the Q-effect has been proposed as the missing link to explain residual viability of cancer cells upon simultaneous inhibition of glycolysis and OXPHOS [58].

Figure 6 provides a summarized explanation of the keystones of heterogeneity in GBM. Supplementary Figure S3 further explores the theoretical background of carcinogenesis.

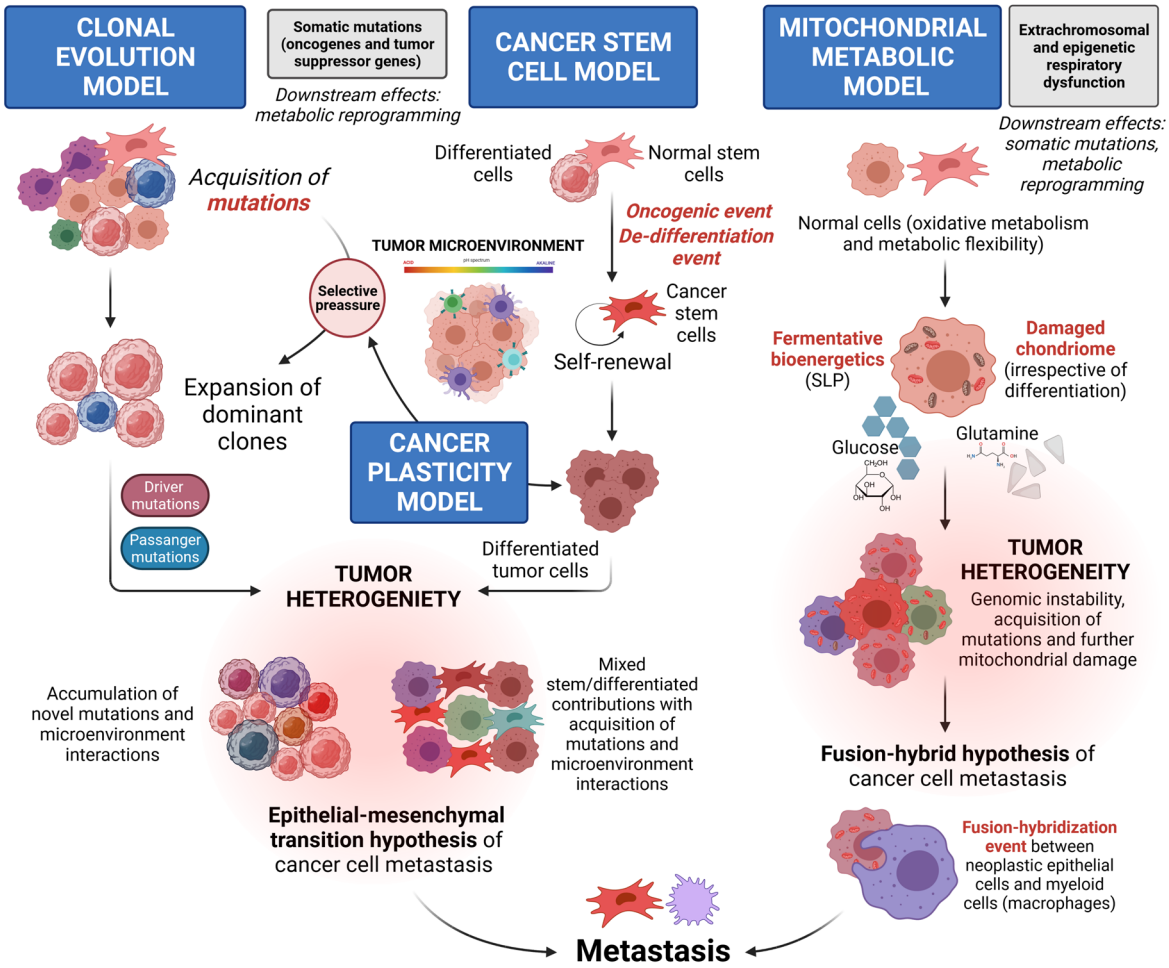

Figure 6. Summarized overview of the clonal, stem cell, plasticity and mitochondrial models of cancer. Own elaboration, based on [69; 142].

Metastasis, the leading cause of death in patients where tumor progression could not be contained, is also examined under two biological paradigms: the embryonic program known as the epithelial to mesenchymal transition (EMT), and the transformation/fusion with immune cells, most notably macrophages [143; 144]. While metastasis is relatively uncommon in primary CNS tumors due to containment by the

blood brain barrier (BBB), they are highly metastatic when given access to extraneural tissues [145-147]. Migration and colonization are worth understanding as metastases are hypothesized to arise from a pool of CSCs [148].

Even though the Warburg hypothesis is not fully compatible with the somatic mutation theory —a dichotomic matter of causality—, it can be easily integrated into molecular studies of genetic/metabolic reprogramming to enhance cancer therapies [149].

1.5.2. Metabolic properties of glioma stem cells (GSCs): a living, evolving model

In the search for representative and clinically translatable *in vitro* models of GBM, growing evidence points to GSCs as a more reliable and diverse preclinical model in comparison to traditional non-stem cell lines; consequently, significant strides have been taken to isolate and culture human GSCs to appraise their contribution to the tumorigenic process [128; 150]. Circumventing therapy resistance and recurrence will require a better understanding of the molecular and bioenergetic function of this subpopulation of cells, allowing for selective targeting.

Unfortunately, therapeutic success is hindered by the ability of GSCs to switch metabolic fuels (metabolic plasticity), with fermentation and oxygen consumption recognized as the driving ATP and biosynthetic pathways, often coexisting in the same tumor. A lesser degree of reliance upon Warburg metabolism has been shown in GSCs from surgical specimens [151]. Bulk tissue classifications of GSCs have been linked to specific metabolic features (e.g., mesenchymal subtypes tend to display higher glycolytic activity; inhibition of OXPHOS abolishes clonogenicity of proneural GSCs) [152; 153]. Additionally, GSCs were shown to proliferate in both perivascular aerobic and hypoxic regions [154; 155]. Glycolytic and oxidative phenotypes sustain the emergence of primary tumors, switching between respiration (as per oxygen consumption) and fermentation, indicative of a relative degree of metabolic flexibility [156; 157]. Notably, morphological alterations in mitochondrial structure have been previously reported by our group in the GSCs models used in this study, with loss of mitochondrial crest and double membrane

structures. It was consequently of interest to evaluate if architectural loss correlated with bioenergetics [158; 159].

Whether metabolic phenotypes are permanent and stable, independent or complementary, operating at a spectrum, is not completely understood [160]. In this puzzling context, recognizing the metabolic vulnerabilities of GSCs, as well as reducing tumorigenic potential by metabolic reprogramming, might be promising, non-toxic therapeutic strategies.

1.6. Metabolism as a potential therapeutic target: successes and pitfalls of metabolic therapy

Glycolytic and glutaminolytic dependencies can be targeted in multiple cancers, such as brain, pancreatic, breast, lung, gastric, skin and prostate, among others [161-163]. Currently, the "metabolic therapy" umbrella is wide-ranging, not strictly defined, including a variety of interventions, from dietary interventions to metabolic modulation, e.g., calorically restricted ketogenic diets (CR-KDs), fasting and fasting-mimicking diets, metabolic inhibitors (MF, DCA, DON), tumor microenvironment control (reversal of lactic acidosis), hyperbaric oxygen therapy (HBOT), inhibition of autophagy and regulation of oxidative stress [90; 164-167].

As a good candidate for metabolic therapy, clinical sampling of GBM reveals glycolytic phenotypes and partial mitochondrial defects [58; 168-170]. Therefore, once glycolysis has been targeted by dietary or pharmacological interventions, mitochondrial inhibitors symbolize an attractive opportunity to increase redox stress in weakened cancer cells [171; 172]. Compensatory ketogenic strategies effectively protect healthy neuronal tissues against glucose deprivation [173; 174].

1.6.1. Challenges for translational medicine: bringing metabolic therapy to the clinic

Development of metabolic therapies is hindered by a lack of standardization, as even similar studies cannot be compared due to differences in normalization,

randomization, dosing and timing [175]. Owing to its distinctive heterogeneity, GBM requires combinatory strategies for simultaneous targeting of multiple pathways [176]. Cell metabolism operates at a continuum, so it is expected that metabolic rewiring can rescue viability up to a cell-specific threshold (e.g., amino acids feed into the TCA cycle to provide ATP and nitrogen) [177]. Cancer cells able to withstand the initial metabolic stress might just be temporarily stunted and then proliferate again [121]. This is a core limitation of focusing on single molecular targets, as resistant cells are likely responsible for recurrence [178]. Focusing on multiple targets in a synergistical fashion yields more promising results, as exemplified by triple metabolic therapy and pilot clinical trials of metabolically-supported chemotherapy [179-181].

Mounting evidence shows that metabolic phenotypes are a determining factor of response to chemotherapy, but such concepts are often overlooked in clinical practice [182]. Routinely, outside FDG-PET staging, all tumors are considered "metabolically equal", managed with fixed protocols of chemoradiotherapy regardless of metabolic activity. Precise, accessible and easy-to-use techniques to study bioenergetics at the single-cell level, along with composite metabolic imaging, liquid biopsy and patient-derived models that accurately reflect the original tumor, are beginning clinical validation [183-186]. Metabolic stratification warrants further investigation, since revealing the global metabolic status is a way to by-pass the seemingly unlimited complexity of genetic landscapes [187]. Identification of Warburg/Q-effect/OXPHOS dependencies prior to treatment could be a predictor of response without the need for extensive gene expression screenings in search of individual genetic mutations [188].

As metabolic plasticity is being touted as a distinctive feature of GSCs, we wanted to explore the antiproliferative responses against metabolic inhibitors, considering the backdrop of basal bioenergetic states. To this effect, metabolic inhibitors such as MF, DCA, sodium oxamate (SOD) and 6-diazo-5-oxo-L-norleucine (DON) have a long-lasting history in metabolic therapy, with extensive evaluation in cell culture, animal models and clinical trials of diverse cancer subtypes [189-192]. Table 3 provides an overview of the metabolic inhibitors and DNA-damaging agents used throughout our study.

Table 3. Description and clinical evidence of standard and metabolic drugs.

Name	Description	Targeted pathway	Human clinical trials
Metformin hydrochloride (MF)	Inhibition of complex I of the ETC (AMPK pathway activation)	OXPHOS and glycolysis	Yes. FDA-approved drug for type II diabetes
Dichloroacetate (DCA)	Inhibitor of PDK	Glycolysis	Yes. Off-label therapy in cancer, approved as treatment for lactic acidosis
6-Diazo-5-oxo-L-norleucine (DON)	Inhibition of GLS	Glutaminolysis	Yes. GI toxicity at high intermittent doses. Orally bioavailable prodrugs in development
Sodium oxamate (SOD)	Inhibitor of LDH	Glycolysis	No, research chemical. High toxicity, low specificity. Novel lactate inhibitors in development
Bleomycin sulfate (BM)	DNA cleavage agent, induces DNA strand breaks by ROS-forming metallobleomycin complexes	Radiomimetic	Yes. FDA-approved antibiotic and chemotherapeutic, second-line for brain cancer management
Temozolomide (TMZ)	DNA alkylating agent prodrug, delivers methyl groups to purine bases of DNA	DNA damage and repair mechanisms	Yes. First-line GBM treatment (Stupp protocol)
Beta-hydroxybutyrate (BHB)	Alternative fat-derived oxidative fuel. Plasma concentrations increase with exercise, fasting, KDs and supplementation	Upregulation of ketone body metabolism	Yes. FDA GRAS status

1.6.2. Mitochondrial activity and metformin: a therapeutic opportunity against oxygen-dependent cancer phenotypes

Cancer cells contain alterations in mitochondrial morphology, lipid composition, polypeptide profiles, respiratory capacity, ETC and cytochrome c oxidase activity, as well as rates of electron/anion transport and calcium retention [193; 194]. It is unknown, however, if these abnormalities encompass all the chondriome.

As a central hub of metabolism, damaged mitochondria are particularly vulnerable to therapeutic interventions, exhibiting sensitivity to damage by ROS via decreased scavenging and unstable ETC and membrane potential [195-197]. Non-tumoral cells show a differentially higher tolerance to physiological ROS levels [198; 199].

Bearing in mind the potential synergy with chemoradiotherapy, mitochondria-targeting drugs are being explored in the full spectrum of clinical research (e.g., phenformin, lonidamine, imexon, idebenone, tigecycline, COL-3) [200]. In phase III clinical trials, MF and CPI-613 showed the greatest promise for rational metabolic therapy in cancer [201].

MF is an FDA approved first-line oral antidiabetic agent that acts as a mild ETC complex I inhibitor, increasing the AMP/ATP ratio, followed by downstream *AMPK* activation and *MTOR* inhibition. Its anti-diabetic action stems from reduced gluconeogenesis in the liver, but antitumoral effects extend beyond the reduction of blood glucose, enhancing chemoradiotherapy [202-204]. In epidemiological studies, MF appears to reduce cancer incidence and mortality [205; 206]. Encouragingly, concentrations corresponding to anti-diabetic treatment strengthened responses to chemotherapy [207-209]. Combinations with other inhibitors, such as DCA and 2-deoxyglucose, enhanced oxidative stress and cytotoxicity in a broad spectrum of cancers [210-214]. Additionally, effectiveness is superior in conditions of glucose-deprivation or pharmacologically impaired glycolysis [215].

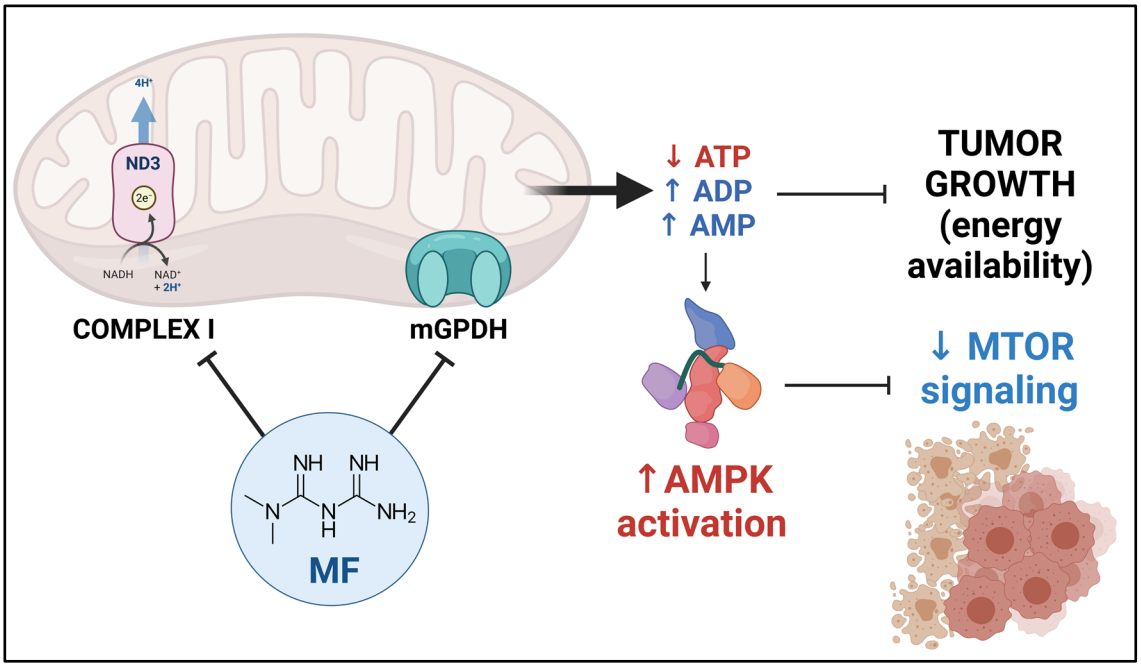

Figure 7. Mechanisms of action of MF. After cell membrane uptake through organic cation transporters (OCTs, such as SLC22A1/3), MF regulates energy production through inhibitory binding of the ND3 core subunit of the respiratory chain complex I and the mitochondrial glycerophosphate dehydrogenase (mGPDH). The mild inhibition of complex I decreases the rate of

NADH-propelled proton flux across the inner mitochondrial membrane and OCR in a dose-dependent manner, reducing the proton gradient (Δψ) and ultimately ATP synthesis at complex V. This leads to a global reduction of ATP availability and rise in AMP/ADP precursors, activating *AMPK* signaling, thus inhibiting *MTOR* and tumor growth. The inhibition of mGPDH modulates mitochondrial redox states and increases cytosolic NADH, reducing gluconeogenesis.

1.6.3. Pyruvate, lactate, and anti-glycolytic targeting

Pyruvate is a central metabolic junction, including the tail-end of glycolysis, malate oxidation, alanine synthesis, gluconeogenesis, and fatty acids synthesis. In terms of ATP-synthesis, pyruvate can be converted to lactic acid by LDH to recover cytosolic reducing equivalents and support the Warburg effect, or acetyl-CoA for TCA cycle oxidation through the PDH complex. Import of pyruvate into the mitochondria involves two distinct transport complexes: a voltage-gated porin complex, and the mitochondrial pyruvate carrier (MPC).

The LDH family of enzymes catalyzes the reversible redox reaction that allows malignant cells to preserve viability by keeping pyruvate concentrations low and regenerate oxidizing equivalents (NAD+). Cancer-specific LDH proteins are encoded by the *LDHA* and *LDHB* genes, which can be combined to generate five isoforms: LDH-1 (B4), LDH-2 (B3A1), LDH-3 (B2A2), LDH-4 (B1A3), and LDH-5 (A4) [216].

LDHA is a *HIF-1* (hypoxia inducible) target gene and a key glycolytic enzyme, whereas *LDHB* favors backwards conversion to pyruvate, which has been documented in lactate shuttling and the "reverse Warburg effect", but its contribution to overall tumor metabolism remains undetermined [217; 218].

Excess lactate is excreted by a family of passive proton-lactate membrane symporters, MCTs. Lactate extrusion and proton accumulation in the microenvironment leads to acidosis as well as genomic instability. At pH under 4.5, lactic acid has a neutral charge and is stabilized; at physiological pH, it exists primarily as dissociated, negatively charged lactate anions and protons. To prevent intracellular acidification, MCT overexpression is common in most cancers (especially MCT1 and MCT4) [219].

The role of lactate as a fuel in cancer is still open to interpretation. The reverse Warburg effect hypothesis posits that lactate and other high-energy metabolites (such as

ketone bodies and fatty acids) could be supplied to cancer cells by the stroma, which includes endothelial cells, pericytes, fibroblasts and leukocytes, collaborating in metabolite recycling. However, this symbiosis between glycolytic and oxidative cancer cells assumes ample metabolic flexibility and has only been documented in specific *in vitro* models with significant stromal contributions [220]. In the brain, the astrocyte–neuron shuttle could fulfill a similar purpose: glutamate increases glycolysis in astrocytes, which then release lactate to serve as an oxidative fuel for neurons [57]. While lactate alone is not sufficient to sustain neuronal viability, it could act as an "opportunistic", glucose-sparing substrate when supplied in high amounts [221]. The relevance of metabolite recycling in brain cancer is under active investigation [222; 223].

In the context of GBM, high expression of *LDHA* and increased plasma lactate are negatively correlated with survival [224]. Hypoxia, necrosis and *LDHA* expression are powerful promoters of the Warburg effect [225]. As many of the research chemicals targeting LDH lack specificity (e.g., SOD, oxalic acid, tartronic acid, gossypol), novel inhibitors such as GSK 2837808A, AZ-33, R-GNE-140 are being explored in clinical trials [226-229]. Additionally, a promising therapeutic strategy appears to be MCT-mediated transport (e.g., AZD3965) [230]. Upon inhibition, some cancer cells could rewire metabolism towards mSLP or OXPHOS, subsequently targeted by glutaminolytic or mitochondrial inhibitors [231].

1.6.4. Lactate or acetyl-CoA: a tumor's dilemma

PDH is a mitochondrial multi-enzyme complex that catalyzes the oxidative decarboxylation of pyruvate, regulated by a phosphorylation/dephosphorylation cycle via PDKs and pyruvate dehydrogenase phosphatases (PDPs) [232].

PDKs are serine/threonine kinases with four isoforms in humans (PDK1-4). Two PDP isoforms dephosphorylate the E1α subunit and restore catalytic activity. When the PDH E-1α subunit is phosphorylated by PDKs into its inactive form, the entry of pyruvate into the mitochondria is inhibited. Hypoxia, HIF-1 stabilization and increased Warburg metabolism through mitochondrial dysfunction keeps PDH in its inactive state [233]. Figure 8 illustrates the therapeutic modulation of LDH and PDH.

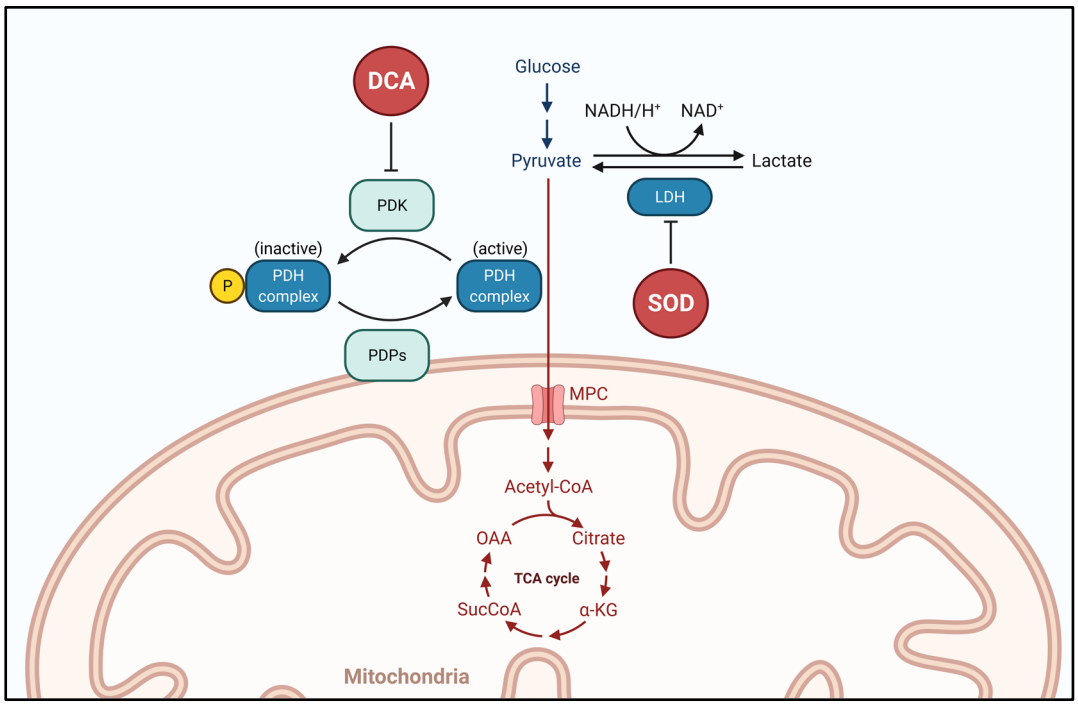

Figure 8. Mechanism of action of dichloroacetate (DCA) and sodium oxamate (SOD). DCA inhibits the mitochondrial enzyme PDK, maintaining the PDH complex in its unphosphorylated catalytically active state and shuttling pyruvate into the mitochondria, therefore increasing aerobic oxidation of glucose, oxygen consumption and mitochondrial ROS production. SOD is a competitive inhibitor of the LDH enzyme, inhibiting lactate buildup and extrusion, decreasing the Warburg effect.

DCA is a small molecule orphan drug that can activate PDH by inhibiting PDKs in a dose-dependent manner, with a variable affinity (inhibitory constant, K_i) towards different PDK subunits [234]. DCA is approved for clinical use and has been extensively studied for the treatment of mitochondrial diseases (e.g., inborn deficiency of PDH, Leigh syndrome, Kearns–Sayre syndrome, Friedreich ataxia), as well as lactic acidosis, by reconducting pyruvate into mitochondrial OXPHOS [235; 236]. Forcing OXPHOS in cancer cells with damaged mitochondria leads to depolarization of the MMP, release of cytochrome c and ensuing apoptosis, as well as increased ROS, upregulation of voltage-

dependent K+ channel and caspase activation [237]. Pilot clinical trials in cancer demonstrated feasibility and no adverse effects in alternating dosing regimens, including survival benefit as palliative care in GBM and advanced metastatic cancer [238-241]. To improve potency and reduce adverse effects, new prodrugs of DCA have been developed [242].

1.6.5. Glutamine addiction, glutaminolysis and mSLP: the missing link fueling ATP-synthesis in cancer?

Glutamine is a conditionally essential α-amino acid that is fundamental for tumor proliferation, redox balance and fatty acid/nucleotide biosynthesis [243; 244]. Importantly, glutamine is the most abundant amino acid in plasma (~500 to 800 μM), in sufficient quantities for a relatively faithful extrapolation from *in vitro* studies [245].

In concert with the Warburg effect, glutamine addiction is emerging as a reliable metabolic hallmark, documented across a wide range of cancers [246]. Glutamine is taken up by several families of amino acid transporters and converted to glutamate by GLS enzymes [247]. In humans, three isoforms of *GLS* are encoded by two genes: the kidney-type (*KGA/GLS*, also known as *GLS1*), accompanied by the glutaminase C splice variant (*GAC*), and the liver-type (*LGA/GLS2*) [248]. *KGA/GLS* is a known contributor to proliferation and malignancy, whereas the function of *LGA/GLS2* has not been fully characterized, with both growth-promoting and inhibitory effects [249].

It is unknown what proportion of glutamine substrate is directed towards mSLP at the succinyl-CoA ligase step (Q-effect), oxidation in the TCA cycle, or reverse processing through *IDH2* reductive carboxylation [250; 251]. Glutamine-derived glutamate is a precursor of glutathione, a critical component for redox homeostasis. Additionally, it has been shown that glutamine can support anaplerosis in both normoxia and hypoxia, as well as having a role in the regulation of ammonia (pH homeostasis), which is necessary to compensate for lactate production and involved in migration, invasion and metastasis [252; 253] Glutamine metabolism is under nuclear control via *MYC* oncogenes [254]. Glutamine has a powerful synergistic effect with glucose to support ATP production and tumor proliferation, yet to be replicated with other monosaccharides or amino acids across

a broad spectrum of cancer cell lines [255]. Thus, targeting glutaminolysis must be an integral part of any metabolism-based therapy.

To achieve this, GLS inhibitors such as bis-2-[5-phenylacetamido-1,2,4-thiadiazol-2-yl]ethylsulfide (BPTES), compound 968, acivicin, DON and azaserine are being evaluated in preclinical and clinical studies, demonstrating significant cytotoxic effects but also risk of multi-organ toxicity at high doses [161; 256].

DON has been selected due to promising antitumoral effects in human clinical trials, but its application is fraught by careful dosing and scheduling to avoid gastrointestinal toxicity (nausea and vomiting) and mild myelotoxicity (leucopenia and thrombocytopenia) [189]. Strictly glutamine-dependent tissues, such as the gut epithelium and immune system, are the most sensitive to off-target toxicity [257].

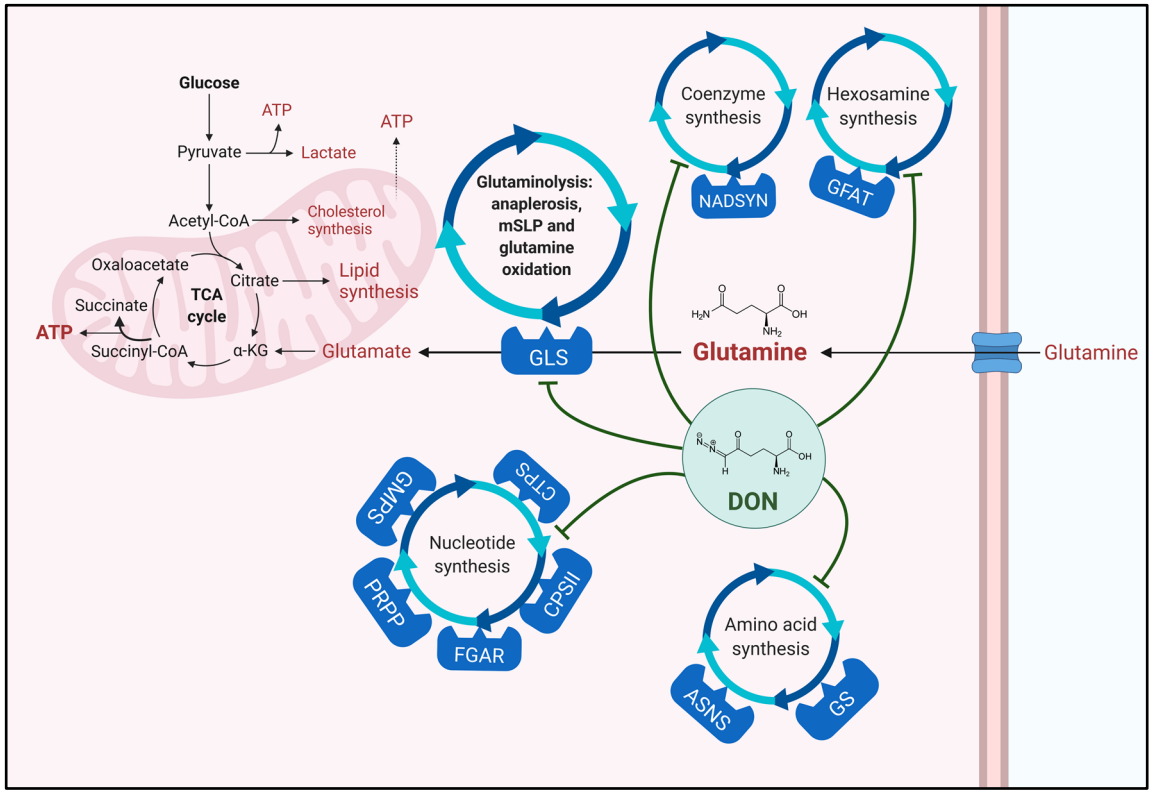

Figure 9. Mechanism of action of DON. Glutamine is imported across cell membranes via different amino acid transporters (e.g., ASCT2, BOAT2), frequently upregulated in cancer cells. It exerts essential functions in energy production (mSLP/oxidation) and anabolism (anaplerosis, nucleotide and amino acid synthesis). Cancer cells are largely dependent on glutamine to provide the nitrogen building blocks for proliferation. DON is an attractive metabolic modulator due to all-encompassing inhibition of glutamine-utilizing enzymes, ensuring expansive blockage of both the ATP and biosynthetic roles of glutamine. DON binds competitively and irreversibly to glutamine

active sites. Crucially, DON serves as a selective mechanism-based inhibitor of glutamine-utilizing reactions, rather than a non-specific reactive intermediate, due to conformational changes that occur only in proximity of the active site of enzymes.

A reduction of adverse effects can be achieved by first depleting the total amount of circulating glutamine (e.g., administration of PEGylated glutaminase) and then pulsing DON to selectively target tumoral tissues, as competition for glutamine is increased [258]. In animal models, intravenous administration of DON together with a calorically restricted KD and glycolytic inhibitors achieved long-term management of orthotopic GBM [259]. Moreover, it has been shown that glutaminolysis activates *MTOR* signaling and, indeed, inhibition of GLS by BPTES and DON also prevents growth induction via *MTOR*; thus, when desirable, glutamine inhibition could act in concert with mitochondrial inhibitors such as MF to prevent MTOR activity [260].

1.7. Ketogenic metabolic therapy: a selective pressure against Warburg-like cancer cells

Ketogenic metabolic therapy (KMT) is defined by the presence of ketone bodies (primarily BHB, the main energy-containing ketone body, which can be accompanied by acetoacetate and acetone), either produced by ketone-generating tissues such as liver, kidney epithelia, astrocytes and enterocytes, or via external supplementation [261].

Nutritional regimes resulting in ketogenesis have been evaluated as antiepileptic and antiproliferative [262-266]. The KMT is administered as a press intervention, with a micronutrient complete, calorically restricted, KD, a physiological stressor with a measurable impact on proliferation of glucose-addicted cells, reducing metabolite levels such as lactate [267; 268]. Complying with these principles, ketogenic-like cell culture media can be formulated *in vitro* [269].

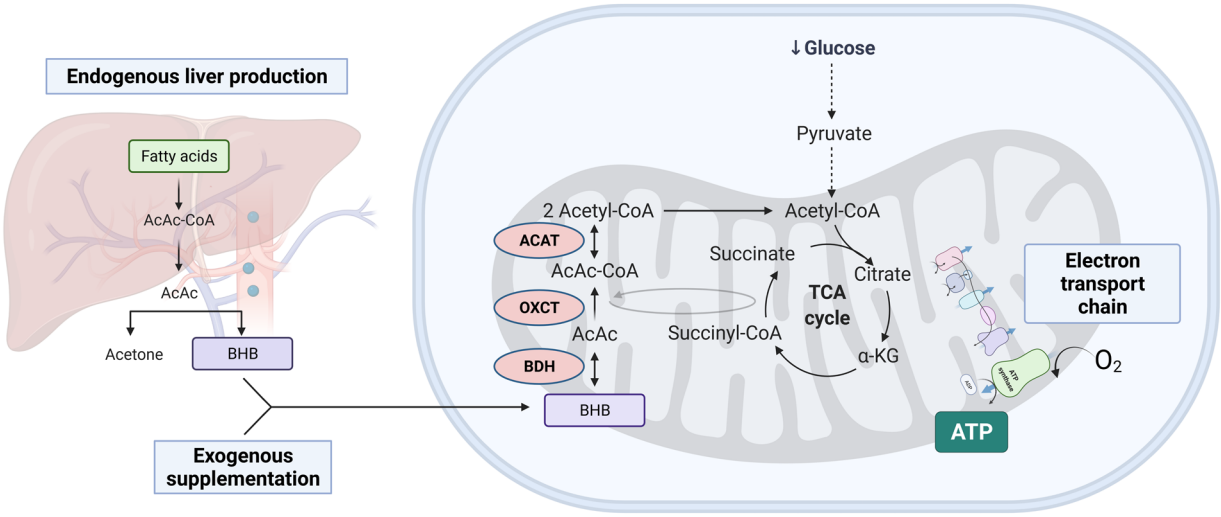

Figure 10. Ketone body metabolism at a glance. The three main ketone bodies, β-hydroxybutyrate (BHB), acetoacetate (AcAc) and acetone, are generated by the liver from fatty acids in physiological conditions of fasting, nutritional ketosis or exercise-induced ketogenesis. Albeit AcAc has been implicated in the anti-epileptic effects of the KD, the principal, energy-containing, signaling molecule is BHB. Uptake of BHB by extrahepatic tissues is mediated by MCT1/MCT2 transporters. BHB is converted into acetyl-CoA through catalysis via 3-hydroxybutyrate dehydrogenase 1 (BDH1), 3-oxoacid CoA-transferase 1 (OXCT1), and acetyl-CoA acetyltransferase 1 (ACAT1). OXCT1 is the rate-limiting step of ketolysis, converting AcAc into AcAc-CoA by the transfer of CoA from Succinyl-CoA. The products of ketolysis are integrated into the TCA cycle for energy or biosynthesis. One directional arrows indicate irreversible reactions, bidirectional arrows indicate reversible reactions.

KMT, fasting-induced ketogenesis and *in vitro* formulations of buffered, non-acidic ketogenic media, must not be confused with diabetic ketoacidosis. During nutritional ketosis, BHB ranges from 3-8 mM, with physiological levels reported during prolonged fasting as high as 10-12 mM, without metabolic acidosis. Thus, an upper limit of 10 mM was selected in our cell culture studies to ensure adequate uptake, while still providing a translational framework.

Differentiation and reprogramming protocols have been proposed as non-cytotoxic therapies with promising clinical applications [270-273]. In this study, we explored the potential of modulating the nutrient availability as a form of clonal selection, restricting the availability of essential SLP metabolites in cell culture (glucose, glutamine), while providing BHB, an obligatory mitochondrial fuel.

1.7.1. Ketone body metabolism as a physiological protection against glucose depletion

Ketogenesis is an effective way of whole-body metabolic priming, enhancing the efficacy of subsequent metabolic treatments [274]. Ketone bodies are readily transported across the BBB by passive diffusion and MCT transporters [275]. BHB is an obligatory oxidative fuel: it cannot generate ATP in hypoxia or cells with mitochondrial defects [276]. In non-tumoral cells, exposure to endogenous BHB as well as ketone ester supplementation reduces ROS, induces mitochondrial biogenesis and maintains ATP, assisting in DNA repair and genomic integrity [277; 278]. As an epigenetic regulator, BHB acts as an endogenous specific inhibitor of class I histone deacetylases (*HDAC*), integrating metabolic status and transcriptional regulation [279; 280].

Adjuvant KMT allows for dose reduction of chemotherapy and enhances penetration of metabolic inhibitors across the BBB [58; 180; 181; 281]. Therapeutic failure in monotherapy is partly due to highly variable clinical designs, unavoidable extrusions from the effective range and lack of glutaminolysis inhibition, which is currently limited [267; 282-284]. Glutamine targeting requires complex dosing and relatively toxic agents, but several clinical trials are underway [285]. In the case of *IDH1*-mutant GBM, a strict KD appears to provide benefit by synergy with oncometabolite 2-hydroxyglutarate to reduce mSLP, stabilize HIF-1 and reduce glycolysis, with a clearly defined mechanism of action [101].

In summary, ketone body metabolism is unable to rescue viability of GBM under severe glucose depletion, but intermediate metabolites could be diverted towards biosynthesis and potentiate fermentable fuels despite low energetic status (glucose, glutamine and other amino acids) [282; 286]. In physiological conditions, healthy neurons, astrocytes and oligodendrocytes can substitute nearly all glucose requirements by BHB [173; 174; 287]. As far as we know, there is no evidence of any cancer cell line, irrespective of origin, able to sustain long-term proliferation in glucose-depleted conditions despite compensation by ketone bodies or fatty acids, as measured by viability and OCR [288; 289]. It is worth noting that, at the protein level, the initially encouraging

hypothesis that cancer cell do not express ketolytic enzymes, making them incapable of BHB oxidation, has since been revisited [283; 290]. Uptake of ketone bodies has been observed in gliomas, with preferential distribution towards lipid synthesis, not ATP [291]. Detection of resilient, oxidative phenotypes would require targeting by mitochondrial inhibitors.

1.8. Metabolic therapy: cutting the supply lines of a hungry beast. Where do we stand?

Cancer metabolism has recently experienced a powerful resurgence, propelled by the rediscovered possibilities of targetable distinctions in tumoral cells. Despite open questions and unresolved challenges, there is no debate about the importance of aberrant metabolism in tumor progression and therapy resistance [58; 292]. Insufficient standardization and lack of precise metabolic analysis hinders the translational potential of metabolic therapy [175; 284]. Glycolytic and oxidative rewiring in GBM needs to be further investigated, particularly in light of clonal heterogeneity and stem-cell contributions to recurrence.

A better characterization of the metabolic profiles of GSCs could help us advance our understanding of GBM biology and propel the fight against cancer. In this work, we demonstrate that different GSCs subpopulations require tailor-made strategies for effective metabolic targeting. It is our hope that recognizing the metabolic plasticity of GBM will ensue the design of more successful therapeutic approaches.

II. HYPOTHESIS AND AIMS

2. Central hypothesis and aims

Metabolic therapy opens the door to both targeted pharmacological and systemic targeting of metabolic vulnerabilities in tumoral cells. Interventions are tested as co-adjuvant approaches with standard of care, when appropriate, or second-line palliative care in tumors with very poor prognosis, such as GBM and metastatic cancer. However, this area of research is held back by the absence of metabolic stratification. In view of the heterogeneity of GBM and increasingly recognized importance of GSCs in therapy resistance, we hypothesize that a careful categorization of metabolic phenotypes and inhibitor susceptibility should be a key component of metabolic targeting.

2.1 Central hypothesis

The molecular heterogeneity of GBM determines the efficacy of metabolic inhibitors according to three primary bioenergetic dependencies, namely, the Warburg effect, OXPHOS and glutaminolysis.

2.2. General objectives and specific objectives

i. Explore the effects of metabolic therapy in GBM.
   a) Define the metabolic clustering of clinical samples.
   b) Analyze basal bioenergetic states of GSCs in relation to traditional non-stem GBM lineages (U87MG) to uncover targetable differences.
   c) Examine the potency of inhibitors against glucose, glutamine, and oxidative metabolism.
   a) Study the mechanisms that regulate cellular adaptations by means of gene/protein expression and functional studies.
   a) Analyze differential toxicity of metabolic drugs in tumoral and non-tumoral cells.
   b) Evaluate synergism/antagonism between metabolic inhibitors and DNA-damaging agents.
   c) Inspect the metabolic priming of GBM cells after sustained modulation.

ii. Investigate metabolic flexibility in response to nutrient depletion and potential rescue by compensatory oxidative fuels (ketone bodies).
   a) Examine the ketolytic and ATP-synthesis capacity in long-term culturing under variable conditions of glucose, glutamine and BHB.
   b) Evaluate the morpho-metabolic adaptation to cyclical glucose deprivation and compensatory BHB.

iii. Develop an *in silico* prognostic factor based on the mRNA and protein expression of genes involved in the response to our selection of metabolic inhibitors.
   a) Examine RNA-seq and CGH data from GSCs models to discover potential metabolic vulnerabilities at the genome level.
   b) Develop a prognostic model based on TCGA gene and protein expression of metabolic enzymes.

III. MATERIALS AND METHODS

3. Materials and methods

3.2.1. Culture of GSCs from human GBM samples, U87MG, HBMEC and human mesenchymal stem cells (hMSCs)

GSCs (GBM18, GBM27 and GBM38) were originally isolated from surgical GBM specimens, as previously described in [158]. GSCs were cultured under a humidified atmosphere of 5% CO_2 at 37˚C, in a media containing, as a base, DMEM/F-12 (Gibco, 11039), further supplemented with: Non Essential Amino Acids (1% v/v; Gibco, 11140), HEPES (38 mM; Gibco, 15630), D-Glucose (0.54% v/v or 30.2 mM; Sigma, G8769), BSA-FV (0.01% v/v; Invitrogen), Sodium Pyruvate (1 mM; Invitrogen), L-Glutamine (4 mM; Gibco, 25030), Antibiotic-Antimycotic (0.4% v/v; Invitrogen), N1 Supplement (1% v/v; Invitrogen), Hydrocortisone (0.3 µg/ml; Sigma, H0135), Tri-iodothyronine (0.03 µg/ml; Sigma, T5516), EGF (10 ng/µl; Sigma, E9644), bFGF (20 ng/ml; Sigma, F0291) and Heparin (2 µg/ml; Sigma, H3393). This media is hereafter named “GSC medium”.

Cell culture media was replaced with fresh media every 3-5 days. Cells were subcultured after confluence (approximately every 1-2 weeks) with chemical dissociation using StemPro Accutase Cell Dissociation Reagent (A1110501, Gibco).

U87MG was purchased from ATCC, Rockville, MD, USA and cultured in DMEM/F-12 (Gibco, 11039) supplemented with 10% fetal bovine serum (FBS) and 2% penicillin-streptomycin (PS). Cells were maintained at 37˚C in humidified atmosphere air, CO_2 5%. The media formulation intended for U87MG cells was termed “high glucose, FBS supplemented media” (HG-FBS). Subculturing was performed every week, first washing with PBS w/o Ca2+ and Mg2+ and then dissociating with Trypsin-EDTA at 0.25% (25200056, Gibco). Medium was changed 2 to 3 times a week.

Human mesenchymal stem cells (hMSCs) (a gift from Dr. Carmen Escobedo Lucea) were cultured in DMEM, high glucose, GlutaMAX (Gibco, 10566016), supplemented with a final concentration of 20% FBS and 1% P/S. All hMSCs experiments were performed in the first 5 passages from isolation. Human Brain Microvascular Endothelial Cells (HBMEC, Catalog #1000) were purchased from

ScienCell Research Laboratories (Carlsbad, California) and grown in HG-FBS media. HBMEC are characterized by rapid proliferation and, upon confluence, had to be subcultured with Trypsin-EDTA once a week, similar to U87MG.

For experiments with very low glucose concentrations, we supplemented base DMEM, no glucose, no glutamine, no phenol red (A1443001, Gibco) with: D-Glucose (0.5 mM; Sigma, G8769), HEPES (15 mM; Gibco, 15630; at the same final concentration as DMEM/F-12), L-Glutamine (4 mM; Gibco, 25030), 3-hydroxybutyric acid (10 mM; 166898, Sigma-Aldrich). Acetoacetate is an unstable, volatile compound that is only available as a lithium salt; lithium itself is known to exert pleiotropic effects on diverse cell processes [293]. By contrast, 3-hydroxybutyric acid (BHB), the major ketone body, is chemically stable in cell culture; therefore, we focused on 3-hydroxybutyric acid in our experiments. This media was named "low glucose, BHB supplemented media" (LG-BHB). Phenol-Red was used to evaluate acidity in modified LG-BHB [294].

It is important to consider that the basal DMEM (A1443001) formulation, despite not being supplemented with D-glucose, L-glutamine nor sodium pyruvate, has a non-trivial amount of amino acids (Glycine 0.4 mM, L-Arginine hydrochloride 0.39 mM, L-Cystine-2HCl 0.2 mM, L-Histidine hydrochloride-H_2O 0.2 mM, L-Isoleucine 0.8 mM, L-Leucine 0.8 mM, L-Lysine hydrochloride 0.79 mM, L-Methionine 0.2 mM, L-Phenylalanine 0.4 mM, L-Serine 0.4 mM, L-Threonine 0.79 mM, L-Tryptophan 0.078 mM, L-Tyrosine disodium salt dihydrate 0.39 mM, L-Valine 0.8 mM), as well as vitamins and inorganic salts. Amino acids are present at supraphysiological concentrations and could feed into metabolic pathways such as pyruvate reconfiguration, mSLP and TCA cycle anaplerosis, known to sustain cell viability for limited periods of time in absence of glucose and glutamine [295].

All media formulations were prepared in sterile conditions and filtered with a vacuum filter, 0.22 μm PES Membrane (431118; Corning). All cell lines were regularly tested for *Mycoplasma* contamination.

For a comprehensive overview of the components in the cell culture media formulations, we provide the following summary table.

Table 4. Cell culture media composition.

Components added to basal DMEM	GSC medium (GBM18, GBM27, GBM38)	High glucose, FBS (HG-FBS), for U87MG and HBMEC	Human mesenchymal stem cells medium (hMSCs)	Low glucose, BHB (LG-BHB)	Seahorse XF DMEM, pH 7.4
Glucose	47.5 mM	17.5 mM	25 mM	0.5 mM	10 mM
Glutamine	6.5 mM	2.5 mM	4 mM	4 mM	2 mM
β-hydroxybutyrate (BHB)	-	-	-	10 mM	-
HEPES	18.8 mM	15 mM	25 mM	15 mM	5 mM
Sodium Pyruvate	1.5 mM	0.5 mM	-	-	1 mM
Fetal Bovine Serum (FBS)	-	10%	20%	-	-

3.2.2. *In vitro* protocol for cyclic metabolic treatment

Our ketogenically-compensated, glucose-restricted formulation was applied to U87MG as LG-BHB medium for 7-day cycles, allowing cells to recover in standard HG-10% FBS supplemented media for 7-days intervals in between. Control cells in HG-FBS were trypsinized each week and seeded at a density of $1x10^5$; after each cycle of LG-BHB, all surviving cells were transferred, and non-viable, detached cells were washed during trypsinization at the end of each cycle. LG-BHB adapted cells that completed all cycles could be frozen in liquid nitrogen, 10% DMSO, thawed and still maintained their distinct morphologic and metabolic phenotype. We also tested intermediate glucose concentrations (2.5 mM), which induced morphological changes towards neurosphere growth but did not halt proliferation, as shown in Supplementary Figure S13. A visual summary of our protocol is represented below.

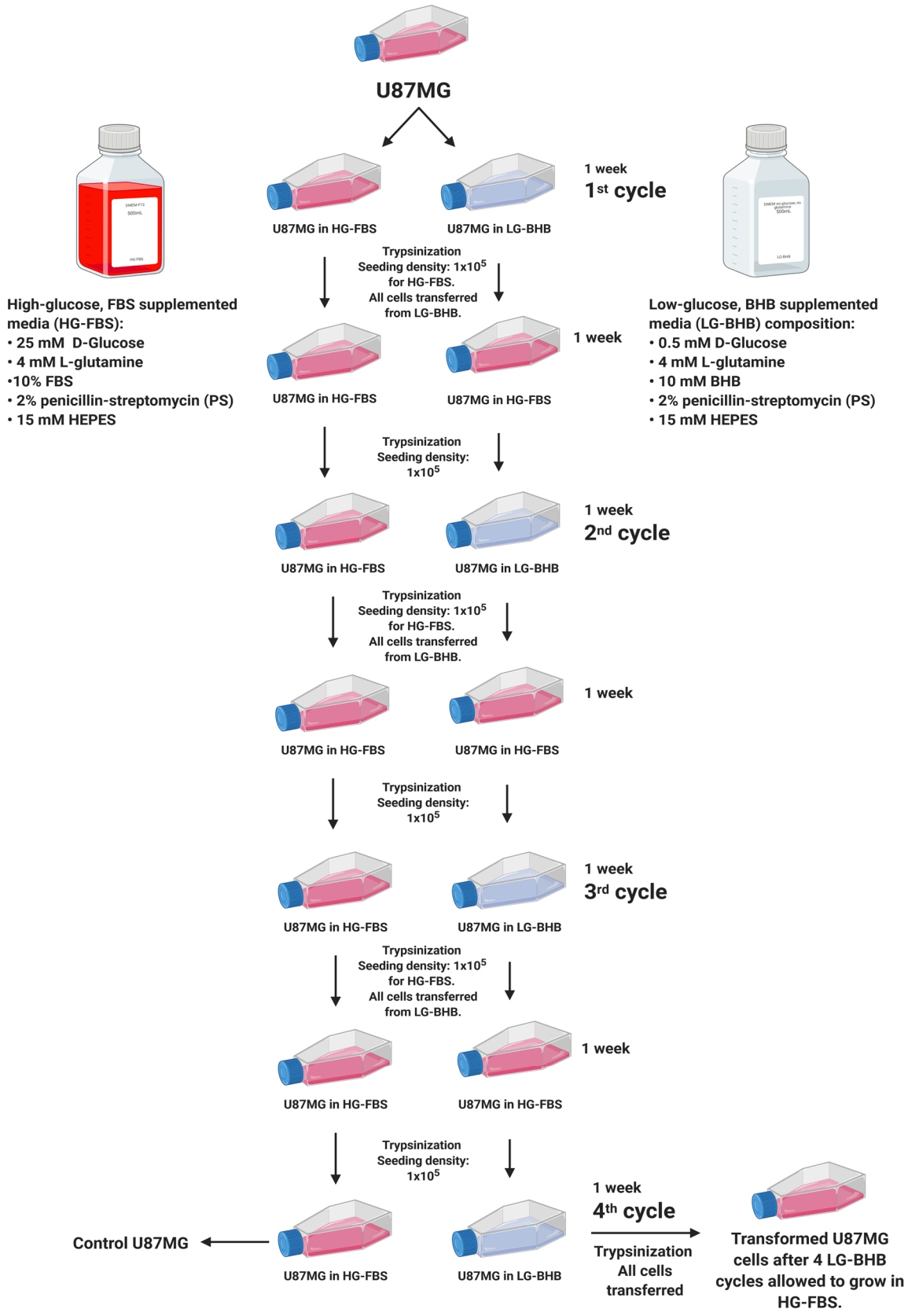

Figure 11. Design and application of our *in vitro* metabolic treatment.

3.2.3. Reagents and metabolic inhibitors

1,1-Dimethylbiguanide hydrochloride (D150959), sodium oxamate (O2751), sodium dichloroacetate (347795), 6-Diazo-5-oxo-L-norleucine (D2141) were purchased from Sigma-Aldrich. Temozolomide (Catalog No. S1237) was acquired from Selleck Chemicals LLC. Bleomycin sulfate (HY-17565) was acquired from MedChemExpress.

3.2.4. Single-drug MTS assays and combination studies using the Chou-Talalay method

The sensitivity to different metabolic drugs was assessed using [3-(4,5-dimethylthiazol-2-yl)-5-(3-carboxymethoxyphenyl)-2-(4-sulfophenyl)-2H-tetrazolium, inner salt (MTS) containing solution from Promega (CellTiter 96 AQueous One Solution, G3582). Briefly, single-cell suspensions of GSCs were plated in 96-well plates, 3000 cells/well, and allowed to grow and form spheres for 72 h. U87MG were seeded at 3000 cells/well and allowed to grow for 24 h. Cultures were then treated with their respective media (control cells) or increasing concentrations of each drug for 0, 24, 48 or 72 h. At each time point, MTS reactant was added, incubated at 37°C for 2 to 4 h, and absorbance was measured at 490 nm/630 nm using a Varioskan Flash (Thermo Scientific, 5250030) or a Sunrise Absorbance Reader (Tecan Trading AG). For half maximal inhibitory concentration (IC50) calculations, corrected absorbance was transformed, normalized, and extrapolated in GraphPad Prism version 8.0.1, using the logarithmic variable slope equation:

Y=100/(1+10^((LogIC50-X)*HillSlope)).

In specific dose experiments, hMSCs were seeded at 6000 cells/well and allowed to grow for 72 h. HBMEC were seeded at 3000 cells/well and allowed to grow for 24 h. Cells were exposed to treatments for 72 h before MTS read-out.

Combinatory studies were performed in the same manner as single-drug assays. After seeding and waiting the cell-line specific attachment intervals, combined treatments were added in the following final concentrations: IC50 for drug A alone; IC50 for drug B alone; full dose IC50 for drug A + drug B; IC50(A + B)/2; IC50(A + B)/8.

Experimentally, drug "A" was one of the metabolic inhibitors (MF, DCA or DON), while drug "B" was the radiomimetic bleomycin sulfate. CompuSyn software (version 1.0), based on the Chou–Talalay method, was employed to determine the interaction between drugs [296; 297]. This method utilizes a multiple drug-effect equation derived from enzyme kinetics, generating a "combination index" (CI) for each drug combination, at each fraction of affected cells (Fa) intensity. CompuSyn software defines synergy as a CI value lower than 1, CI = 1 equals to additive effects and CI > 1 indicates antagonistic effects. We have determined CI values for each metabolic inhibitor and bleomycin across tested cell lines using a constant ratio experimental design, as well as other valuable parameters such as the Dose-Reduction Index (DRI), which calculates how many folds of dose-reduction for each drug, at any given effect, would be allowed by the synergistic combination.

3.2.5. Trypan Blue exclusion assay

For Trypan Blue exclusion assays, we followed a previously described protocol for visual quantification of viable and dead cells [298]. Cells were counted three times from different aliquots under optical microscopy, in all quadrants of a Neubauer chamber (0640010; Paul Marienfeld GmbH & Co. KG).

3.2.6. Transduction of tumor cells

Experiments using the U87MG Fluc-IRES-EGFP transfected cells were performed in collaboration with Dr. Thomas N. Seyfried laboratory (Boston College, USA), as previously described [299]. The lentivirus vector CSCGW2-Fluc-IG was derived from CSCGW by deleting all promoter elements from the U3 region in the 3′LTR and inserting a firefly luciferase (Fluc)-IRES-EGFP cassette under control of the CMV promoter, a gift from Miguel Sena-Esteves [300]. Then, U87MG cells were transfected using lentivirus vector stocks produced with titers of 1×10^8 TU/ml. One day prior to infection, ~100,000 U87MG cells were plated in a 6-well plate in HG-FBS DMEM. Infection was performed with a multiplicity of infection (MOI) of 100 in a total volume of 1.5 ml. After 24 h of incubation, the vector media was substituted with fresh

medium. Upon confluence, cells were passaged to a 100mm Thermo Scientific™ BioLite Cell Culture Treated Dish for normal subculturing.

3.2.7. Bioluminescent imaging

Cell proliferation was monitored as a measure of bioluminescent signaling using the SPECTRAL Ami Instrument (Spectral Instruments Imaging, USA). Studying the transfected U87MG Fluc-IRES-EGFP, bioluminescence is directly correlated to production of ATP, viability, and cell number. Cells were plated in a 24-well plate at a density of 40.000 cells/well and left undisturbed overnight to attach to the surface of the plate. Then, standard cell culture media was carefully aspirated, substituted with the modified conditions of interest and bioluminescence was measured at the indicated time points after addition of 10 µl of D-Luciferin Potassium Salt (MB000102-R70170, Syd Labs), at a concentration of 10 mg/ml. Cells were grown in basal DMEM with 12 mM of glucose and 2 mM of glutamine (control), glucose only (12 mM), glutamine only (2 mM) and DMEM with no additional components, compared against the same conditions supplemented with 5 mM BHB. Data acquisition and analysis was performed using the Aura imaging software (version 3.2), with exposure time of 60 s, 2 × 2 binning, object height 1.5, FStop 1.2 and FOV 25. The first reading was acquired after changing the media and considered as baseline ATP production for the number of seeded cells prior to replication (U87MG have a mean population doubling time of approximately 34 h in HG-FBS supplemented DMEM) [301].

3.2.8. Cell morphometry by light microscopy

The number and length of morphology branching was counted in 6 images from random fields: U87MG were allowed to reach confluence before image acquisition (5-7 days), modified LG-BHB U87MG were evaluated after 90 days from seeding. For imaging, we used an optical light microscope Leica DFC345 FX® with a Leica DFC 425 camera. Number and length of branching was related to a total of 10 cells/group at 20X magnification for each cell line. The length of cell branching was measured using Image-J software, as described in [302; 303].

3.2.9. Quantitative Real-Time PCR (qRT-PCR) analysis

Primers were designed *in silico* and validated manually, as previously described [304]. For qRT-PCR, total RNA was isolated from cell pellets using NZYol (MB18501, NZYTech, Lda.), following the manufacturer's recommendations. For chronological parity with other experiments, GSCs were seeded in 6-well plates at a density of 90.000 cells/well, allowed to grow for 72 h, fresh cell culture media was added (1:1) and cell pellets were collected after 72 h; the same protocol was applicable to U87MG, but fresh cell culture media was added after 24 h from seeding. Purity of RNA was assessed based on 260/280 and 260/230 ratios using a Thermo Scientific NanoDrop 2000/2000c. RNA was retrotranscribed to cDNA (High-Capacity cDNA Reverse Transcription Kit; Applied BioSystems) using a Mastercycler (Eppendorf). Resulting samples were amplified with specific primers (Table 5) in a CFX Connect Real-Time PCR Detection System (Bio-Rad) and a LightCycler 480 Instrument (Roche). *β-actin* and *GAPDH* were used as housekeeping genes. For relativization and comparison with non-tumoral controls, we compared our samples with a pool of retrotranscribed RNA from brain tissues obtained from epileptic patients, provided courtesy of Hospital Universitario y Politécnico La Fe (Valencia).

Table 5. Forward (FW) and reverse (RV) primers for qRT-PCR.

Name	5' - Sequence – 3'
β-actin FW	TTCTACAATGAGCTGCGTGTG
β-actin RV	GGGGTGTTGAAGGTCTCAAA
GAPDH FW	TCCTCCACCTTTGACGCTG
GAPDH RV	ACCACCCTGTTGCTGTAGCC
GLS1 FW	GCCCGCTTTGTGTGACTAAA
GLS1 RV	CAGGGGTAAATAACGGCACA
GLS2 FW	GCACTAAAGGCCACTGGAC
GLS2 RV	CCAAGAGGCCACCACTACTG
MTOR FW	CTGACCGCTAGTAGGGAGGT
MTOR RV	AACATCCCAGAACCCTGCTG
LDHA FW	GTGGAGGTTGTGCATGTTGT
LDHA RV	CGTCAGAGGTGGCAGAACTA
LDHB FW	AGGACCTAAAAGACCTGTGACT
LDHB RV	GCTTTGATTCTGTGAGCCCA
PDK1 FW	ATCCTCCTGCCTGAGTCTCT
PDK1 RV	CAAATGCCAAGGACTGCTGT
PDK2 FW	TGCCTACGACATGGCTAAGCTC
PDK2 RV	GACGTAGACCATGTGAATCGGC

PDK3 FW	TGGAAGGAGTGGGTACTGATGC
PDK3 RV	GGATTGCTCCAATCATCGGCTTC
PDK4 FW	AACTCGGGATGTTGGGGATT
PDK4 RV	AGAGAAAAGCCCTTCCTACTGA
PRKAA1 FW	GTCCAGGGCTTGTTCTATTCA
PRKAA1 RV	ATGCTGCACTTAGAGACCCT
PRKAA2 FW	TGGAACATTGTTACAGCAGGC
PRKAA2 RV	AGCTCTTCTCCCGTGTCTTC

3.2.10. Antibodies

All primary and secondary antibodies are listed as follows: AMPKα Antibody (2532, Cell Signaling), phospho-AMPKα (Thr172) (2535, Cell Signaling), Anti-Pyruvate Dehydrogenase E1-α subunit antibody (ab110334, Abcam), Anti-PDH-E1α (phospho S293) antibody (ab177461, Abcam), antiOXCT1 (Sigma, HPA012047-100ML), β-Actin (A5441, Sigma-Aldrich), α-Tubulin (sc-8035, Santa Cruz Biotechnology). Secondary antibodies for horseradish peroxidase (HRP) detection were anti-rabbit IgG (sc-2004, Santa Cruz Biotechnology) and anti-Mouse IgG (PI-2000, Vector Laboratories).

3.2.11. Protein isolation/quantification and Western blotting

Centrifuged and pelleted U87MG and GSCs were resuspended in 100 µl of radioimmunoprecipitation buffer [RIPA; 100 mM Tris-HCl (pH 8.5), 200 mM NaCl, 5 mM EDTA and 0.2% SDS, with phosphatase and protease inhibitor cocktail] and stored at -80˚C for a minimum of 24 h. Samples were centrifuged at 13200 RPM for 20 min at 4˚C; protein-containing supernatant was preserved.

Total protein concentration was determined using Bio-Rad Protein Assay Kit II (Bio-Rad 5000002) according to the manufacturer's instructions and, after the corresponding incubation, absorbance was read at 595 nm.

In phosphorylation experiments, treatments were added 3-4 days after GSCs seeding, and 24 h in the case of U87MG. U87MG cells were washed twice with PBS and serum-deprived for 1 h prior to sample collection. Protein was subsequently recovered at the indicated time points (30 min, 60 min, 2 h, 6 h).

Western blotting experiments were performed adapting the protocol from Mahmood *et al.* [305]. Briefly, protein extracts were separated by 8-12% SDS-PAGE and transferred to nitrocellulose membranes. After blocking for 1 h with 5% Bovine Serum Albumin (BSA) in Tween-Tris Buffered Saline 1X [T-TBS; 10 mM Tris-HCl (pH 7.6), 150 mM NaCl, and 0.1% Tween-20], membranes were incubated with the corresponding primary antibody overnight at 4 ˚C. After washing 3 times for 10 minutes with T-TBS, membranes were incubated with HRP-linked secondary antibody for 1 h at room temperature. Detection was performed using ECL reagents (GE Healthcare) according to the manufacturer's guidelines and revealed in a BioRad ChemiDoc chemiluminescence system. The same membranes were then incubated with a housekeeping primary antibody overnight at 4 ˚C, washed the next day and incubated with an HRP-linked secondary antibody for 1 h room temperature before ECL detection. In some cases, band volume/intensity was quantified and compared using Image Lab Software (version 6.1), with the global volume background subtraction method (Bio-Rad, 110000076953).

3.2.12. Seahorse XFp protocol for real-time metabolic evaluation of U87MG adherent cells and GSCs neurospheres

Seahorse XF technology measures two key parameters of cellular bioenergetics: OCR (a proxy for mitochondrial ATP synthesis, assuming oxygen consumption is linked to normal mitochondrial function) and ECAR (quantification of glycolysis through changes in pH due to lactate/proton extrusion) [306; 307].

This methodology allows to study energy flux in label-free, live cells, providing researchers with unique insights into metabolic phenotypes and dynamic metabolic functions. Specific assays are available for this instrument depending on the desired application. We selected the Seahorse XF Real-Time ATP Assay as it offers a broad-spectrum estimation of metabolism (total ATP production, allocated to mitochondrial ATP and glycolytic ATP). This assay can be employed to quantify basal metabolic phenotypes and compare different cell types, or to evaluate pretreatments with

compounds, as in our case; on the other hand, to study acute effects, mitotoxicity, pathways liabilities and real-time metabolic switches, an "injection" strategy is offered.

It is important to note that while the Seahorse XF technology is a widespread tool to measure metabolic parameters, unless specific pathway inhibitors are administered in parallel (such as etomoxir, UK5099, BPTES), it cannot granularly allocate concrete contributions of metabolites (glucose, glutamine, long chain fatty acids, ketone bodies) feeding into "OCR", be it destined for mitochondrial ATP generation and/or other cellular processes [124; 306; 307]. Caution should be advised when interpreting Seahorse results, as OCR-linked ATP production could suggest a fully functional ETC, but it does not exclude obtaining energy from other sources, e.g., fermentation of glutamine though mSLP by succinyl-CoA ligase. Whenever possible, we opted for the term "OCR-linked ATP" when referring to "mitochondrial ATP" and "OXPHOS".

Seahorse XF technology requires full cellular attachment to the XFp PS Tissue Culture microplate, making evaluation of GSCs growing as floating neurospheres methodologically challenging. As detailed in Figure 12, we created a custom Seahorse workflow due to the low adhesion properties of our GSCs and the evaluated time points (72 h of active treatment, after which detachment of affected cells was noticeable).

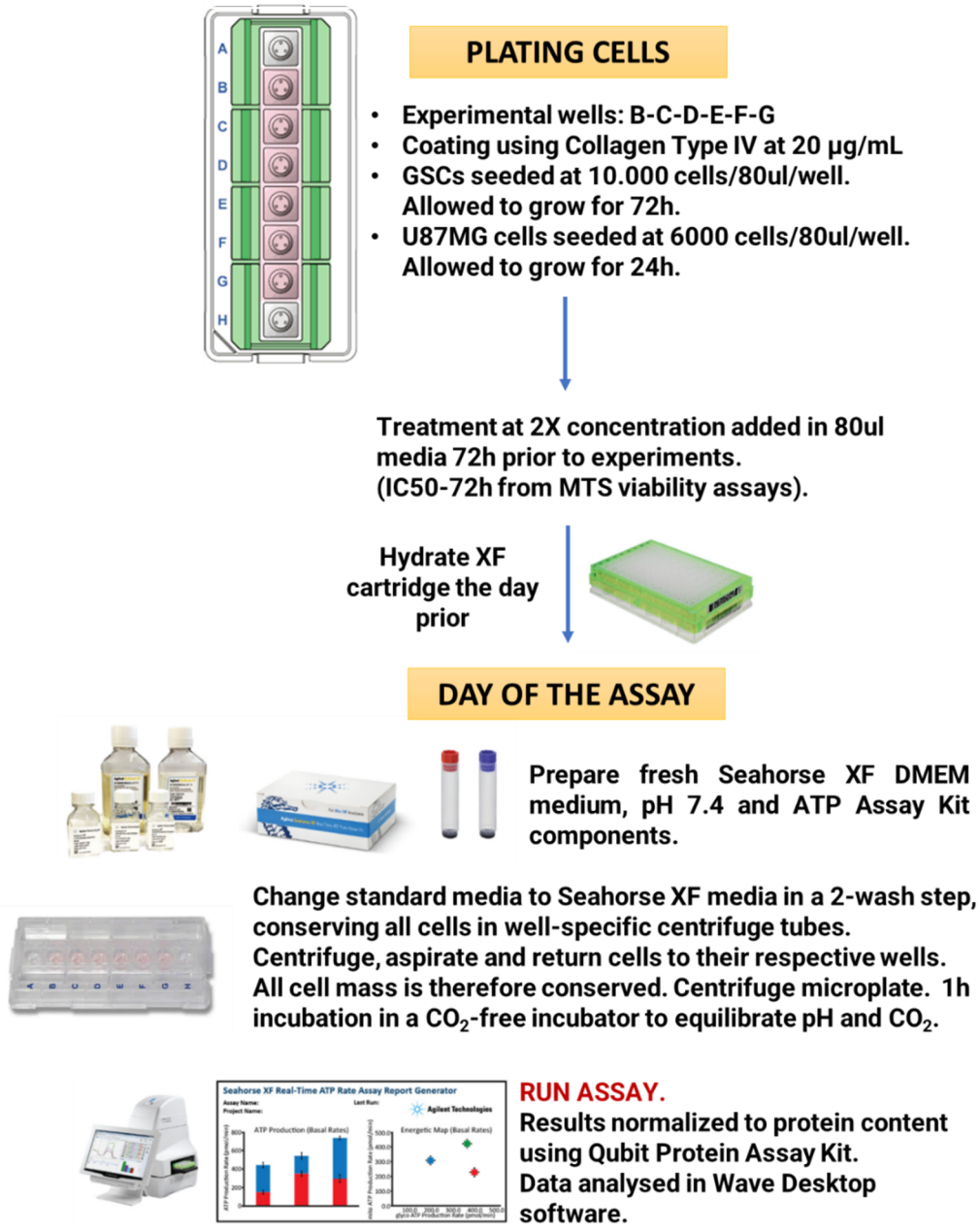

Figure 12. Experimental design of Seahorse XF Real-Time ATP Assay. Own work, based on [308; 309].

We coated the wells of a Seahorse XFp microplate with 20 µl of cell culture media supplemented with Collagen Type IV at 20 ug/mL (C6745-1ML, Sigma Aldrich). We allowed for layering with 1 h incubation at 37°C. After incubation, PBS was added to all wells and carefully aspirated without disturbing the collagen membrane.

For GSCs, cells were seeded at a density of 10.000 cells/well in standard media and allowed to grow for 72 h. U87MG cells were seeded at 6.000 cells/well and allowed to grow for 24 h. After seeding, plates were left undisturbed at room temperature for a

minimum of 1 h to promote uniform cell attachment. The day of treatment, metabolic drugs were added according to previous IC50-72 h MTS assays.

On the day of the experiment, cell culture media was carefully pipetted out of each experimental well without disturbing the attached cells, then placed into labeled centrifuge tubes. Seahorse XF DMEM medium (103575-100, Agilent) was added as a washing step, and pipetted out to the corresponding centrifuge tube. Seahorse XF media was then added to experimental wells. Tubes with original media and washing media were centrifuged at 1000RPM for 5 min at 25˚C. After centrifugation, all liquid was aspirated, the cell pellet resuspended and added back to respective wells. This cell recovery step was essential for consistent results, as treatment with metabolic inhibitors caused cell detachment even after collagen coating, and centrifugation allowed to conserve the complete cell mass in both control and treated wells. Without this recovery step we observed very low protein yields since many cells were removed in the unavoidable washing steps.

The Seahorse XF microplate was then centrifuged at 1000 RPM for 5 min for better cell attachment. Before measurement, cells were incubated for a minimum of 1 h in a CO_2-free incubator to equilibrate pH and CO_2 content of the wells, essential for accurate estimation of ECAR.

We then followed Seahorse XF Real-Time ATP Rate Assay User Guide (Kit 103592-100, Agilent). Briefly, after basal measurements of OCR/ECAR, a final concentration per well of 1.5 µM oligomycin and 0.5 µM Rotenone + Antimycin A was injected to calculate mitochondrial ATP, glycolytic ATP and total ATP production. The resulting data was analyzed in Seahorse Wave software (version 2.6.1). Analysis of OCR and ECAR was carried out using the Seahorse XF Real-Time ATP Rate Assay Report Generator (version 4.0.17). For normalization, Seahorse plates were frozen at -80˚C until quantification. Total protein was quantified using an Invitrogen Qubit 3 Fluorometer (Invitrogen, Q33216), or the Bio-Rad Protein Assay (5000002, Bio-Rad), based on the Bradford assay, measured at 595 nm. For the Qubit Protein Assay Kit (Q33211), content of each Seahorse XFp-8 well microplate was transferred to a 1.5 mL microcentrifuge tube, 30 µl of PBS was used to wash each well and then added to corresponding tubes. Wells

were incubated for 10 min at 37°C with 20 µl TrypLE™ Express Enzyme (12605010, Thermo Scientific). The content was transferred to previous microcentrifuge tubes, sonicated 2 times for 10 s at 20 kHz, centrifuged at 13200 rpm for 20 min at 4°C and supernatant was collected. After this step, we followed the manufacturer's protocol for protein quantification.

3.2.13. Gene-Set Variation Analysis and Glioblastoma Bio Discovery Portal

Affymetrix (HG-U133A) normalized gene expression datasets of GBM and non-tumor tissue samples from TCGA were downloaded from the GlioVis repository [310]. As *IDH* mutation status confers a characteristic metabolic rewiring of the TCA cycle, *IDH* mutant and *IDH* unknown samples were removed from the analysis [311]. The remaining 498 GBM *IDH* wild-type and 10 non-tumor samples were classified in proneural, classical, mesenchymal and those with a high content in non-tumoral tissue (low cellularity), as proposed elsewhere [312]. Four different canonical gene sets (two oxidative and two glycolytic) were obtained from the Molecular Signatures Database (MSigDB) [313]: KEGG (oxidative phosphorylation and TCA cycle), Hallmark (glycolysis, MTORC1 signaling). GSVA was performed on each sample to obtain an enrichment score (ES) using the GSVA R package [314].

Additionally, a manual exploration of the TCGA datasets was performed for metabolic genes predictive of patient survival (full list available in Supplementary Table S1). This list was constructed using canonical KEGG pathways for drug-target effectors [315]. Only *IDH* wild-type samples were included in this analysis. Genes were selected for statistically significant predictive capacity for patient survival (p value < 0.05) in the HG-U133A ($n = 186$) or Agilent-4502A ($n = 168$) microarray platforms, either for the global cohort or at least one molecular subtype. 15 survival predictive genes were found.

In the Glioblastoma Bio Discovery Portal (GBM-BioDP), mRNA expression values for these genes were used to create a Prognostic Index (PI) by weight averaging the genetic expression with the regression coefficients of a multi-gene Cox proportional hazards model. This PI was compared to overall survival using Kaplan-Maier analysis. *AKT3* was excluded from the final analysis to improve clustering due to outlier values

(narrow clustering would be valid, but only applies to a limited number of patients). The same methodology was then followed for the generation of a PI based on protein expression, utilizing the full list of metabolic genes due to low availability of protein-level evidence in the TCGA.

Comparative genomic hybridization (CGH) data was obtained as previously described [158]. In brief, after extraction of genomic DNA and quality control, labeled DNA was hybridized with Human Genome CGH Microarray 44K (Agilent G4426B-014950) containing 43,000+ coding and noncoding human sequences, compared to a pool female reference genomic DNA.

RNA-seq data from GSCs was obtained using an Illumina HiSeq 2500 sequencer across multiple passages (GBM18: p18, p27, p29; GBM27: p40, p42; GBM38: two samples from p32, p33, p37) and then averaged for each gene, as previously described [316]. In this study, metabolic genes were characterized by a high degree of biological coefficient of variation (CV).

3.2.14. Statistical analysis

Statistical analysis was performed using a 2-tailed Student t test (when comparing 2 groups) and One-Way ANOVA (3 or more groups). Data are presented as means ± standard deviation and calculated using the software package GraphPad Prism version 8.0.1 for Windows, GraphPad Software, San Diego, California USA. qRT-PCR expression data was graphed and analyzed directly in CFX Maestro 1.1 software (Bio-Rad Laboratories). P values < 0.05 were considered as statistically significant. For all figures, P values were expressed according to GraphPad 8 NEJM P-value style: $p > 0.05$ (ns); $p < 0.05$ (*); $p < 0.01$ (**); $p < 0.001$ (***).

IV. RESULTS

4. Results

4.1. GBM can be stratified into glycolytic and oxidative phenotypes

4.1.1. Gene expression analysis of metabolic pathways and clustering of samples according to Verhaak subtypes

Molecular heterogeneity is a key feature of GBM, with clinical and therapeutic repercussions. A better understanding of the differences in bioenergetic metabolism amongst different molecular and phenotypic subtypes of glioma is necessary to target altered metabolism with an increased degree of specificity. Reducing the vast molecular landscape of GBM into a limited number of metabolic categories would allow for such precise targeting, with patient-specific personalized treatments.

For this purpose, we explored TCGA expression databases using a GSVA approach. In the TCGA, Verhaak classification according to molecular characteristics differentiates four GBM-subtypes: mesenchymal, classical, proneural/neural [21; 317]. Importantly, the mesenchymal signature has been associated with increased inflammation, a higher degree of necrosis and the worst survival when restricting for samples with low transcriptional heterogeneity [21; 318].

As a control of normal metabolism, healthy brain tissue is available in the TCGA for comparison. In our analysis, filtering for canonical gene sets of glycolytic and oxidative pathways, Warburg-like phenotypes (signified by glycolysis and MTOR signaling) were enriched in the mesenchymal subgroup, whereas expression of mitochondrial enzymes predominated in healthy tissues (Figure 13). Between these two extremes, however, we still encounter ample genetic heterogeneity, owing to the mixed content of tumoral biopsies. To improve clustering, mesenchymal, classical, proneural and low cellularity samples can be differentiated into subgroups based on their oxidative or glycolytic nature (Figure 14).

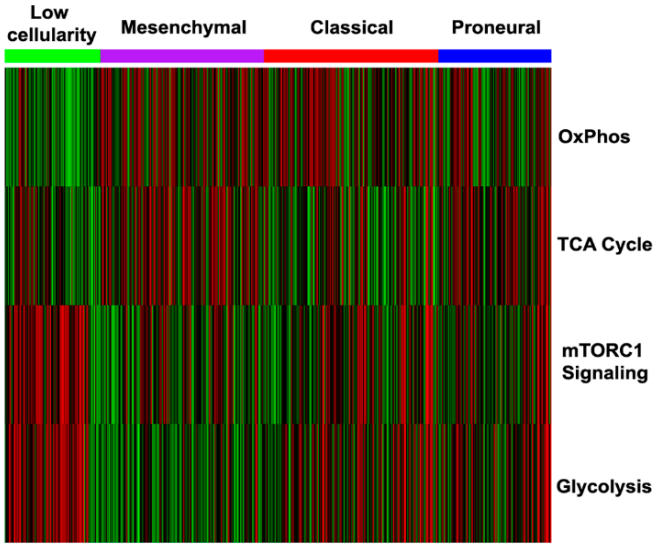

Figure 13. Heatmap of the scaled ES obtained by GSVA with the samples grouped by their gene expression subtype (proneural, classical or mesenchymal) including those with high content of non-tumor tissue (low cellularity).

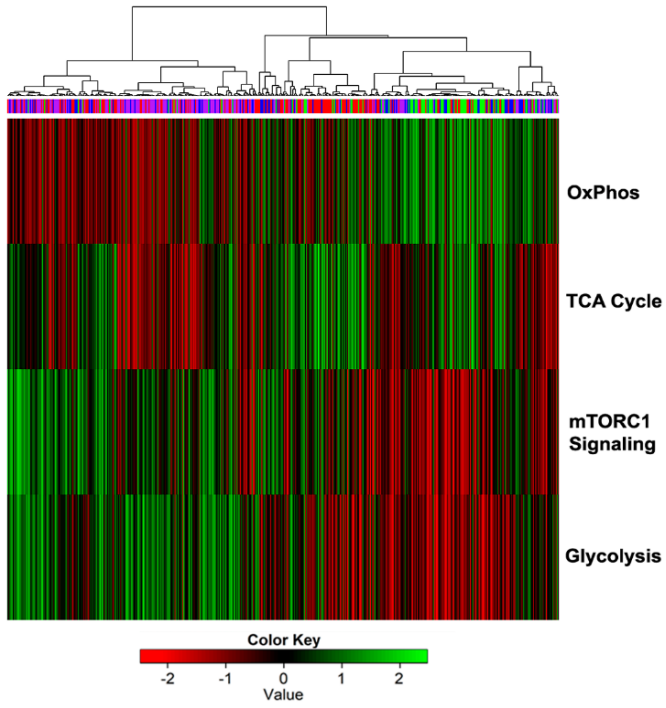

Figure 14. GSVA sample clustering according to subtype and gene expression. Normal tissue is characterized by enrichment in OXPHOS and TCA cycle, as well as downregulation in glycolysis and *MTOR* signaling. Mesenchymal and classical subtypes cluster under enriched glycolysis and *MTOR* signaling.

Differentiating between normal and transformed tissues is essential for the successful removal of the entire tumoral mass, thus avoiding recurrence, and trends in metabolic profiles could be factored to determine the status of dubious biopsies and to establish safe resection borders prior to surgery [319].

Continuing with this line of inquiry, we wanted to corroborate if heterogeneous metabolic dependencies could be detected in real-world clinical management of GBM. For this purpose, we examined 18F-FDG PET metabolic imaging from our own patient cohort. While most tumors were characterized by high glucose uptake (Figure 15a), others appeared as non-metabolically active despite tumoral progression (Figure 15b). 18F-FDG PET is a routine staging and recurrence prediction tool, but it cannot differentiate between SLP and glucose oxidation, nor identify the metabolites supporting growth despite absence of glucose uptake. Wider implementation and standardization of more advanced imaging techniques, such as glutamine-based PET and oxygen sensitive MRI, alongside other tracers, would be useful to complete the metabolic profile of any given tumor [320; 321].

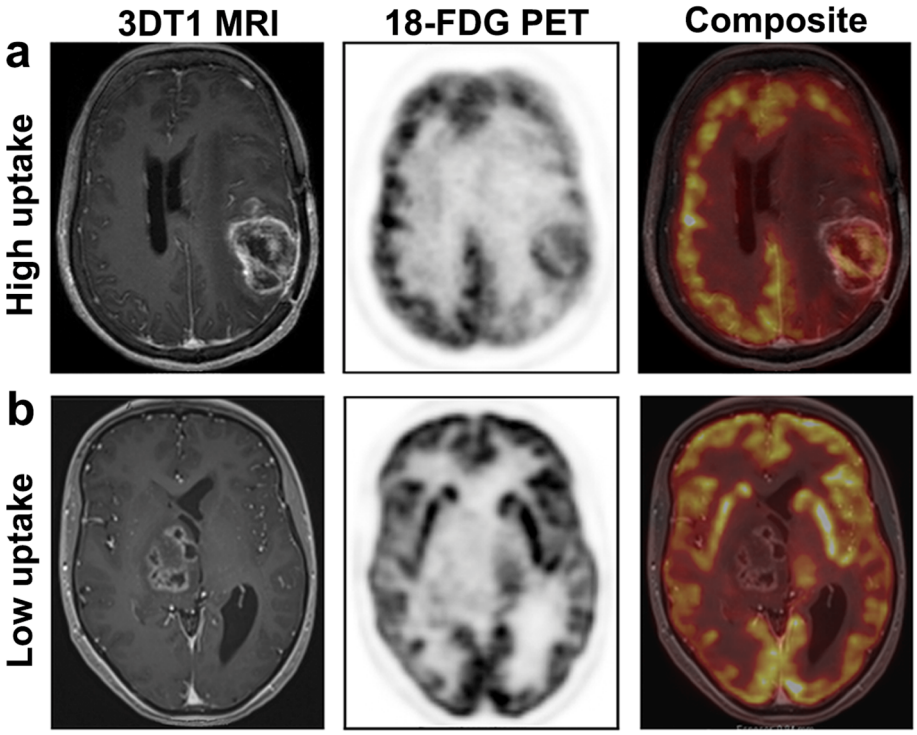

Figure 15. Clinically, standard imaging techniques such as 18F-FDG PET coupled with anatomical MRI can classify tumors according to glucose uptake. a) High glucose uptake. Parietal recurrent GBM in the left hemisphere shows heterogeneous enhancement on three-dimensional T1-weighted imaging (3DT1) and extensive uptake of 18F-FDG (right and medium side), even with high uptake in surrounding normal brain tissue. b) Low glucose uptake. Right thalamic GBM shows patchy contrast enhanced areas on axial 3DT1 and no uptake of 18F-FDG (medium and left side).

4.1.2. Heterogeneity in basal bioenergetic phenotypes of *in vitro* models of GBM

Once we examined tentative tissue-based metabolic stratification and common clinical findings, we carried out Real-Time ATP assays using the Seahorse XFp Analyzer to determine the *in vitro* bioenergetics of human GSCs.

Our GSCs are characterized by distinct molecular phenotypes, as previously described by our group [158]. OCR and ECAR were determined for each cell line, with subsequent calculation of total ATP Production Rate, glycolytic ATP Production Rate and mitochondrial ATP Production Rate (Figure 16).

We described basal metabolic rates and compared GSCs amongst themselves and non-stem U87MG We can observe that, in basal conditions, GBM27 and U87MG are close to a 1:1 ratio of ECAR/OCR-linked metabolism, whereas GBM18 and GBM38 have a strong preference towards a glycolytic phenotype. Furthermore, U87MG, a typically Warburg-like cell line, exhibited a relative elevation in OCR-linked ATP production.

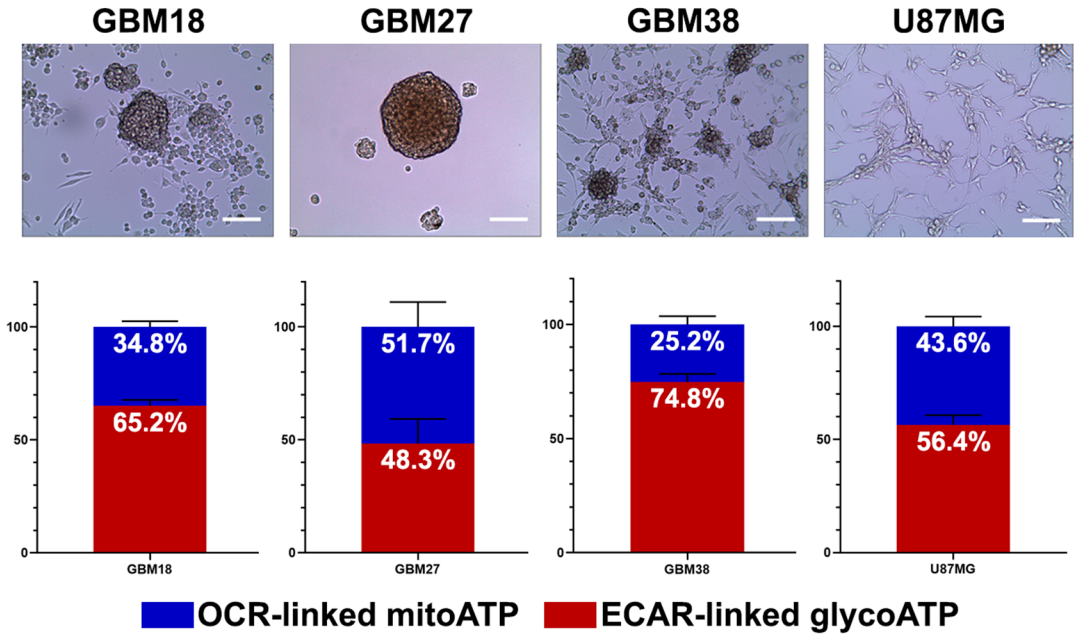

Figure 16. Representative optical microscopy images of cellular morphology. Under each cell line, average distribution of total ATP production from ECAR-linked ATP production and OCR-linked ATP production in basal (non-treated) conditions. Scale bar = 100 μm.

As shown in Figure 17, GBM27 demonstrated high mitochondrial ATP production as well as lower glycolytic ATP production when compared to GSCs GBM18 and GBM38: as much as 50% of its bioenergetic needs were met by OCR-linked ATP production. GBM18 and, especially, GBM38, relied predominantly on glycolytic metabolism (Warburg effect). In GBM27, OCR and ECAR fluctuated between sets of biological experiments, indicating a range of metabolic flexibility: further investigation into metabolite allocation for energy production would be necessary to fully characterize this adaptive capacity.

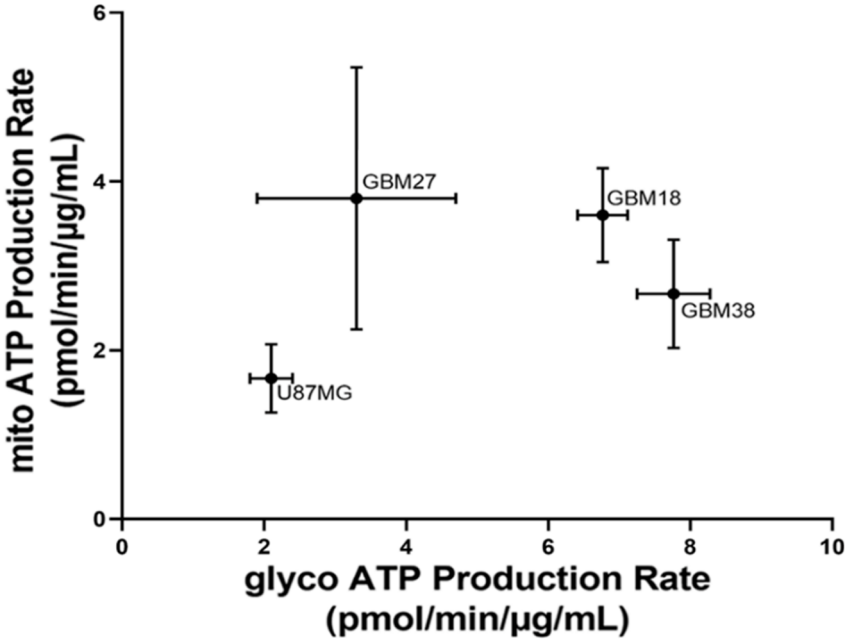

Figure 17. Seahorse XF Energetic Map. GBM18 and GBM38 clustered together as highly glycolytic-like cells. GBM27 displayed the highest variation in the metabolic profiles, with increased mitochondrial respiration, at a similar level to GBM18, but, in comparison, lower glycolysis. U87MG were not as metabolically active as GSCs. Data from 3 independent experiments, each with n=3, normalized to total protein concentration (µg/mL).

U87MG is a bona-fide, epithelial-like GBM cell line typically characterized by highly glycolytic phenotypes (lactate production and therefore ECAR) [151; 322; 323]. In our data, however, it showed a moderately elevated OCR-linked ATP production (up to 43.5 ± 4.2% of total ATP generation). Interestingly, the metabolic activity of U87MG cells, adjusted per protein content, is actually lower than GSCs. Thus, even if the ratio of ECAR/OCR-linked ATP generation is similar between U87MG and GBM27, the

normalized rates of ATP production are significantly higher in GBM27. Glycolytic activity is as much as six-fold higher in GBM18 and GBM38 than in U87MG.

Taken together, our results indicate that even under the same cell culture conditions, distinct molecular characteristics of GSCs produce unique metabolic phenotypes. We encountered a high degree of metabolic variability between our set of GSCs, and their ATP production rates per normalization unit were faster than U87MG. GSCs and U87MG maintain a basal metabolic profile and seem able to dynamically shift, to some extent, between ECAR-linked and OCR-linked ATP production to meet their bioenergetic needs.

4.2. GSCs display a heterogeneous pattern of resistance to metabolic inhibitors

At the outset, in order to determine the optimal doses to be administered in future experiments, we exposed our GSCs and U87MG to escalating concentrations of metabolic drugs.

Inhibitory curves for all time points are presented in Supplementary Figures S4-S7. Resistance against all metabolic inhibitors was observed at 24 h, except when using the highest doses, where effects at 24 h approximated those at 48 h and 72 h. GBM27 did not respond consistently to MF at 24 h nor 48 h, only at 72 h. Different temporal profiles indicate a protracted, non-immediate response to metabolic inhibitors. Of note, DON has a unique profile at all time points, showing a non-linear viability attenuation.

After conducting these experiments, we observed maximum inhibitory effects and reliable trends in viability data at 72 h; therefore, for every cell line, IC50 at 72 h was considered as the optimal inhibitory concentration (Figure 18). These are the selected working concentrations in all subsequent experiments. GBM27 had the highest resistance to all metabolic treatments, except for DON, where, in turn, GBM18 required the highest concentrations to achieve IC50 effects.

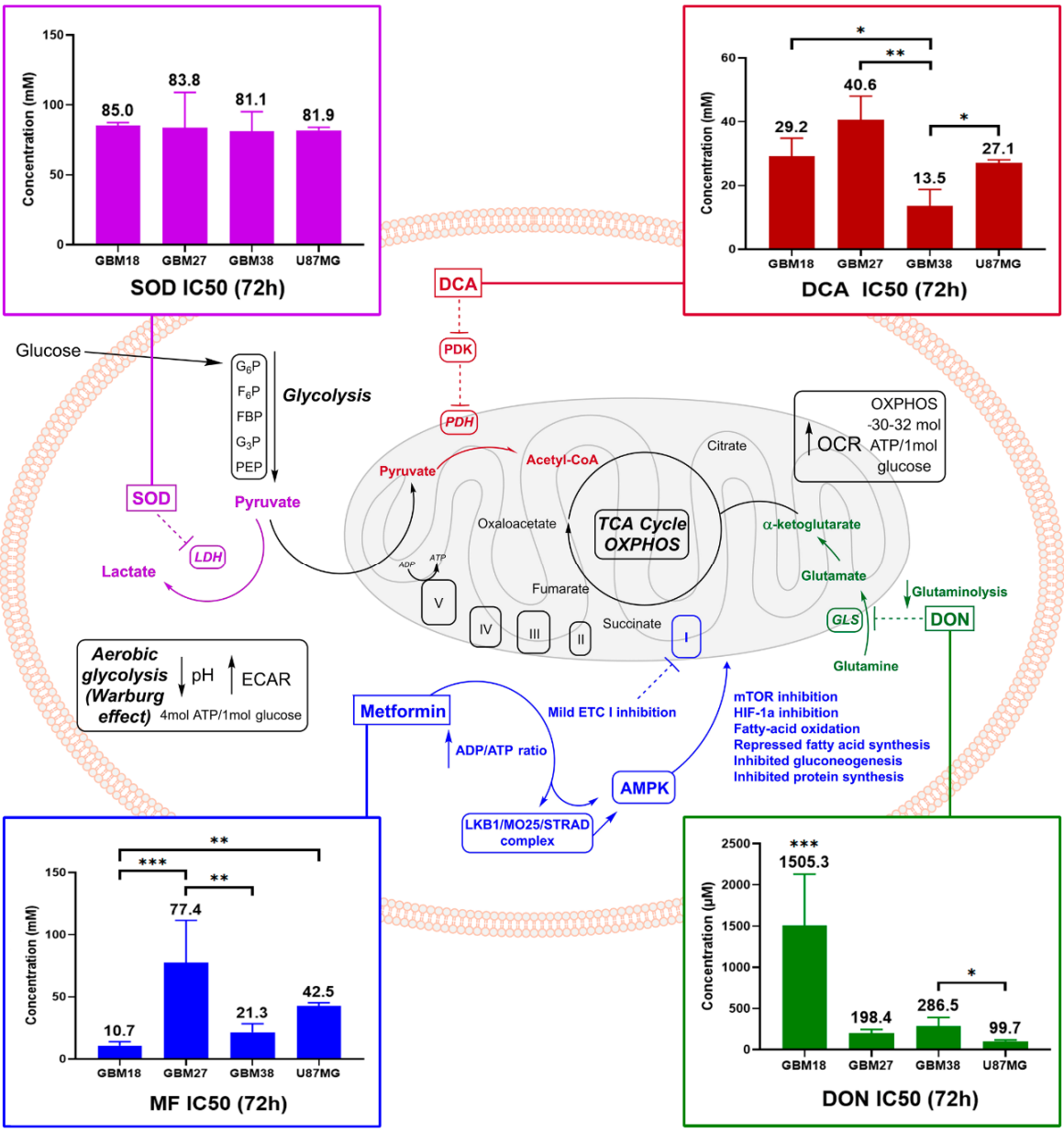

Figure 18. Cancer metabolism at a glance, with experimental in vitro IC50 values for selected metabolic inhibitors. Glucose enters cancer cells via GLUT1/GLUT4 transporters. Glucose then undergoes glycolysis in 9 enzymatic steps, converted into 2 molecules of pyruvate, generating 2 net ATP molecules and 2 reduced NADH. Pyruvate then arrives at the crossroads between oxidative and fermentative energy production [324]. If pyruvate is converted to lactate by LDH (in normal cells, only under anaerobic conditions), NADH is oxidized to NAD+, maintaining redox balance. Cancer cells divert up to 85% of pyruvate to lactate, regardless of the presence of oxygen (Warburg effect, yielding 2 net ATP); an estimated 10% goes towards biosynthesis and 5% to OXPHOS [325]. In normal, non-tumoral cells, the majority of pyruvate undergoes OXPHOS (30-32 ATP molecules). To decrease the Warburg effect and facilitate oxidative metabolic reprogramming, PDKs can be inhibited by DCA, supporting the entry of pyruvate into mitochondria, and LDH can be targeted via SOD. Glutamine addiction can be regulated by glutaminase inhibitors such as DON [326]. Lastly,

MF has pleiotropic effects: inhibition of ETC complex I leads to downstream signaling via *AMPK* and *MTOR* [327]. In color-matching boxes, we display average concentrations required for 50% viability inhibition (IC50) after 72 h of treatment. One-way ANOVA statistical significance of 3 biological experiments was calculated with normalized raw fluorometric data; $p < 0.05$ *; $p < 0.01$ **; $p < 0.001$ ***.

For MF, GBM18 and GBM38 were the most sensitive cell lines (10.66 ± 3.16 mM and 21.33 ± 7.08 mM, respectively) and GBM27 the most resistant (77.41 ± 34.02 mM). U87MG revealed an intermediate resistance (42.51 ± 2.74 mM).

For DCA, GBM38 required the lowest concentrations (13.52 ± 5.23 mM) and GBM27 the highest (40.61 ± 7.40 mM). In this case, GBM18 (29.20 ± 5.62 mM) and U87MG (27.10 ± 0.95 mM) showed no statistically significant differences in IC50 concentrations.

For SOD, all cell lines required relatively high *in vitro* concentrations to reach 50% growth inhibition; no statistical significance was reached between groups. Due to the low average variability, instead of different specific doses for each cell line, IC50-72 h was established as the arithmetic mean of all groups (82.9 mM) for a common dose in future experiments.

Lastly, examining glutaminolysis inhibition by DON, U87MG required the lowest IC50 DON dose (99.70 ± 14.82 μM), followed by GBM27 (198.4 ± 44.13 μM) and GBM38 (286.9 ± 103.2 μM), whereas GBM18 was the most resistant (1505 ± 625.4 μM). It should be noted, however, that a closer look at the growth inhibition curves for DON in GBM18 reveals a cytostatic "threshold" around the IC50 value, regardless of the dose, suggesting a non-linear inhibitory slope (Supplementary Figure S7). Therefore, IC50s are a statistical approximation caused by the relative resistance against DON, but we should not assume a linear correlation between dose and effect; this will become especially relevant in subsequent combinatory studies.

In summary, our selection of metabolic inhibitors exerted dose-dependent reductions of viability in a time-dependent manner. Extended activity allows for reduced dosing regimens. At 72 h, GBM18 was the most sensitive to MF, GBM38 to DCA, and U87MG to DON; on the other hand, GBM27 was the most resistant to MF and DCA, while GBM18 required the highest dose of DON. A very high resistance towards SOD,

as well as low variability in responses, was observed across all cell lines, including non-tumoral controls. SOD is known for low specificity and very poor cell-membrane permeability [192]. After investigating the possible reasons for this lack of response, without detecting any clear correlations with mRNA expression (*LDHA* and *LDHB*) (Figure 22), SOD was discarded from future combinatory studies due to low therapeutic efficacy.

4.2.1. Differences of target enzymes across cell lines predicts responses to metabolic inhibitors

To further investigate the relative sensitivity/resistance profiles of each cell line to our selection of metabolic drugs, we aimed to evaluate their basal genetic expression profiles (Figure 19). For comparison with non-tumoral brain tissue, gene expression was relativized to a pool of retrotranscribed mRNA from epileptic patients.

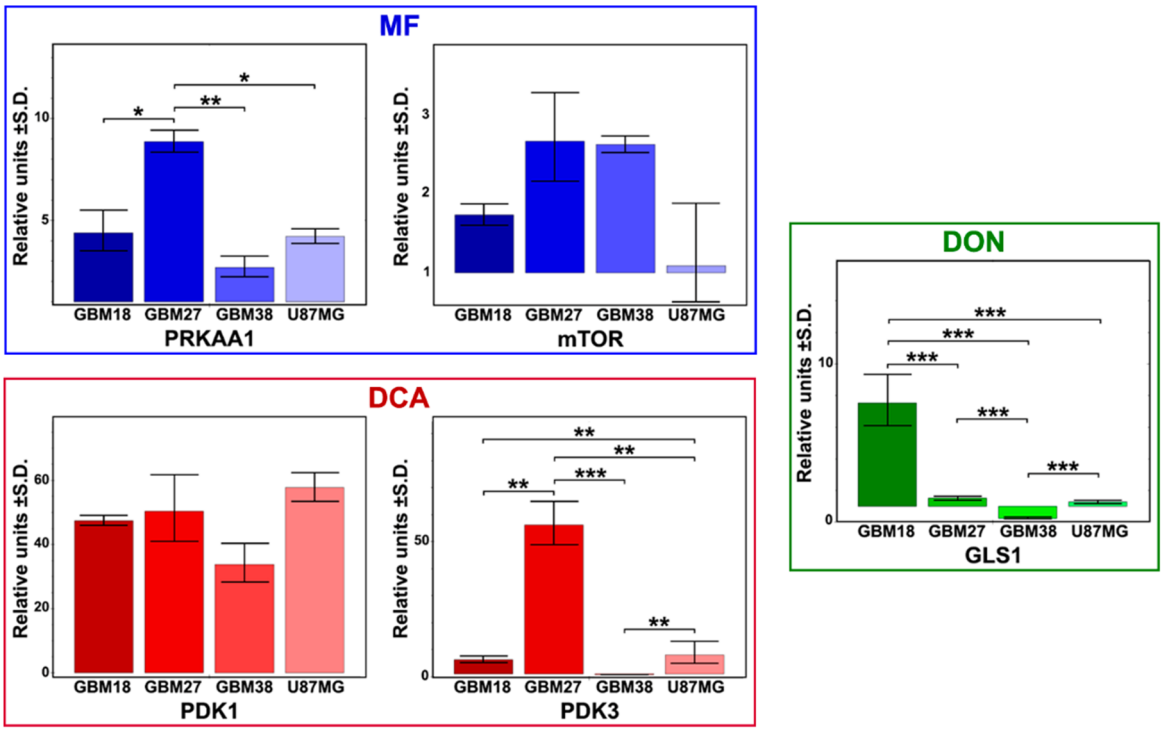

Figure 19. Expression profiles of target enzymes for our selection of metabolic drugs under basal conditions determined by qRT-PCR. Representative results from a minimum of two replicates (n=2). One-way ANOVA with Tukey correction. $p < 0.05$ *; $p < 0.01$ **; $p < 0.001$ ***.

MF acts through inhibition of the ETC complex I, increasing the ADP/ATP ratio, but its primary downstream target is the activation of *AMPK* (phosphorylation of Thr172 at AMPKα1), which ultimately leads to *MTOR* inhibition. We therefore evaluated basal

expression of *PRKAA1* and *PRKAA2* (together, the catalytic subunits comprising AMPKα1/2) and the *MTOR* gene. Although *PRKAA2* was not expressed in our samples, *PRKAA1* was significantly upregulated in GBM27 (9-fold relative to control), while also upregulated at similar levels (approximately 4-fold) in GBM18, GBM38 and U87MG. We also found the highest relative expression levels of *MTOR* in GBM27 and GBM38, but differences did not reach statistical significance.

DCA is a potent inhibitor of all 4 isoforms of PDKs (PDK1, PDK2, PDK3 and PDK4) [328; 329]. PDKs, known to be differentially expressed in GBM, are essential components in the regulation of the PDH complex (increasing or decreasing mitochondrial oxidation of pyruvate). Increased tumorigenicity correlates with higher *PDK* expression, lower PDH activity and reliance on glycolytic pathways [330]. Although we analyzed all *PDK* subunits, *PDK2* and *PDK4* were not expressed. Consistent with the biological function of DCA, *PDK3* expression was lowest in GBM38; in our proliferation studies, GBM38 required the lowest doses of DCA. Alternatively, GBM27 displayed a very marked upregulation of *PDK3* when compared to all other cell lines: as expected, GBM27 was the most resistant to DCA. While *PDK1* was upregulated with respect to non-tumoral epileptic controls, expression was similar across cell lines. These observations match previous reports where *PDK3* subunits were the most resistant to inhibition by DCA [331; 332]. *PDK2* subunits are the most sensitive to DCA treatment, while *PDK1* and *PDK4* display intermediate sensitivity. As *PDK2* and *PDK4* were not expressed in our samples, variances in dose-response profiles were most likely related to *PDK3* and *PDK1*.

Our analysis revealed no detectable amplification of *GLS2*; therefore, we focused on *GLS1* as a potential predictor for DON's antiproliferative effects. *GLS1* was significantly upregulated in GBM18, neutral in GBM27/U87MG, and downregulated in GBM38. Higher *GLS1* expression correlated with the relative resistance against DON in GBM18, but comparatively lower expression in GBM38 was not associated with lower doses.

Furthermore, we analyzed the phosphorylation of AMPKα to investigate the biological effects of MF (Figure 20). We observed strong phosphorylation of Thr172 AMPKα relative to control in GBM18 (60 min, 2 h, 6 h) and GBM38 (2 h). Cell lines GBM27 and U87MG did not phosphorylate AMPKα in the first 6 h, consistent with the need for higher concentrations of MF and slower responses against the drug.

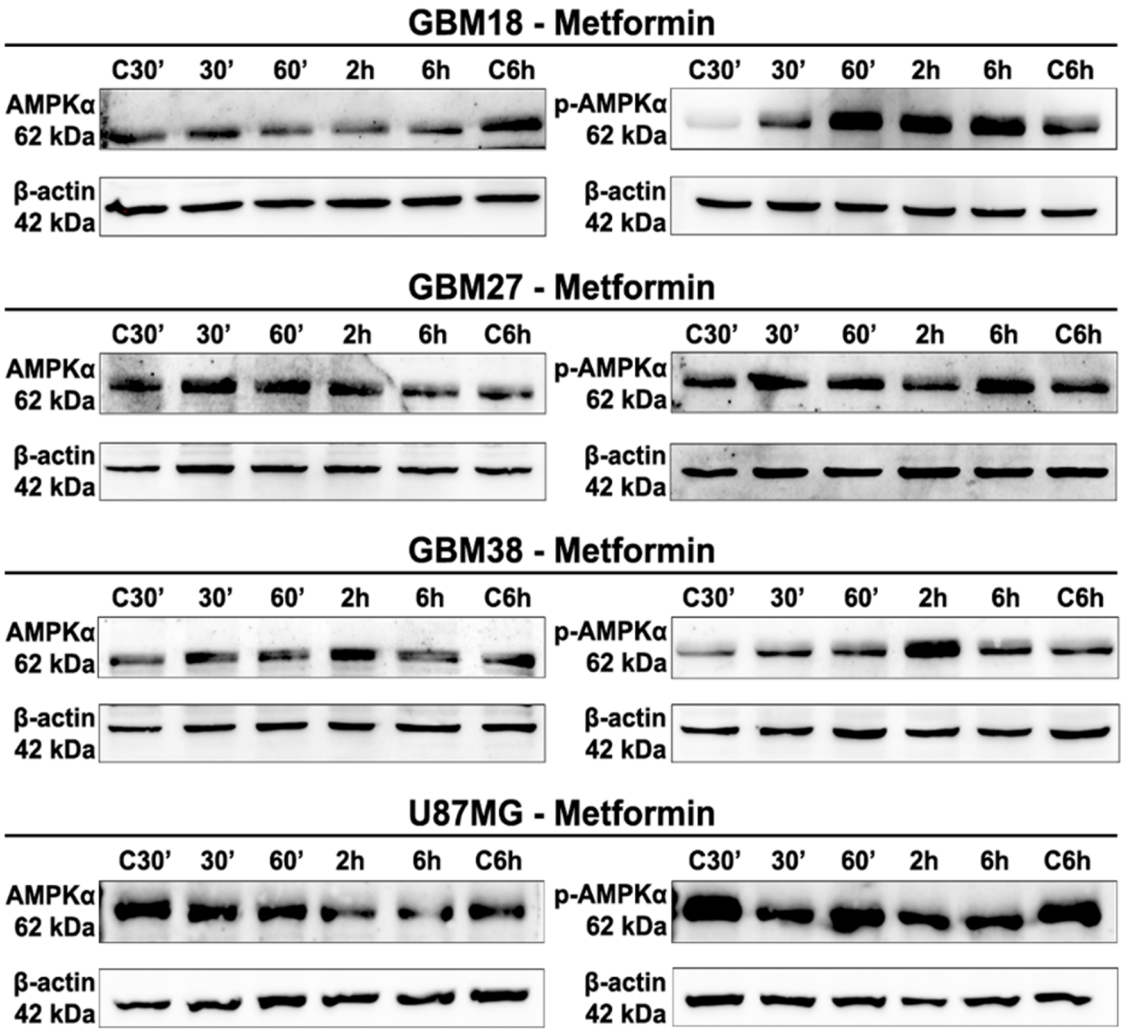

Figure 20. Western Blot analysis at 30 min, 60 min, 2 h, 6 h after MF 72 h-IC50 treatment for AMPKα and phospho-Thr172 AMPKα. All images are representative of a minimum of two biological replicates.

We continued our assessment of protein-level mechanism of action with DCA. The catalytic subunit PDH-E1α has three major phosphorylation sites, with site 1 (Ser-293) being the most frequent and powerful target, sufficient to completely inhibit PDH activity [333; 334]. With inhibition of PDKs by DCA, we detected rapid, visually discernable, de-phosphorylation of Ser-293 in all cell lines after 6 h of treatment with

IC50-72 h concentrations (Figure 21). In sum, the expression of PDKs in our dataset could provide a predictive biomarker to explain differential responses to DCA.

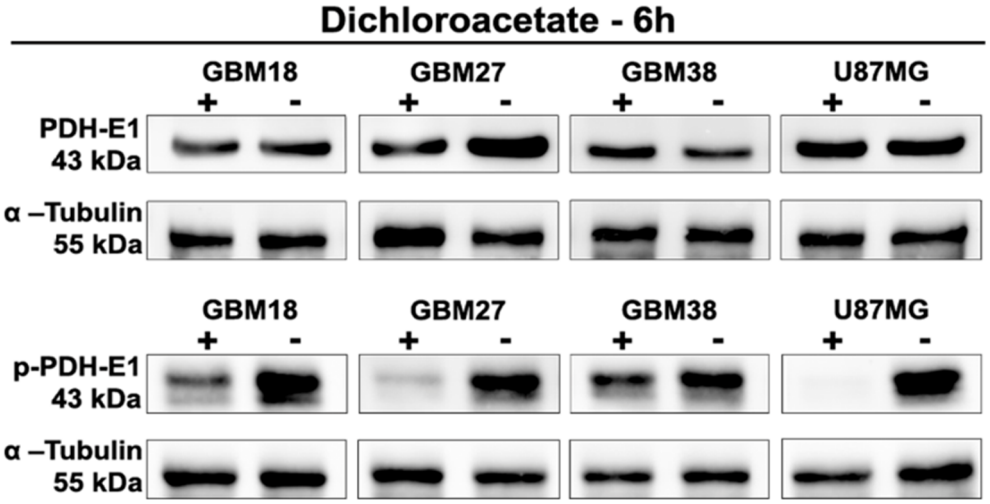

Figure 21. Western Blot analysis after 6 h of treatment with respective DCA 72 h-IC50 doses for phospho-Ser293 PDH-E1 and total PDH-E1. All images are representative of a minimum of two biological replicates.

Before abandoning SOD as a potential drug candidate, we decided to investigate whether the uniform lack of efficacy in antiproliferative responses could be derived from homogenous elevation of target-gene expression across cell lines. SOD inhibits the LDH enzyme, reducing the conversion of pyruvate to lactate. In humans, all LDH isoforms can be transcribed from *LDHA*, *LDHB* and *LDHC*. As *LDHC* is a testis specific enzyme, we only examined basal *LDHA* and *LDHB* expression [335].

Due to the low anti-proliferative effects of SOD, we first examined *LDHA* and *LDHB* expression (drug target) to discard low potency stemming from high basal expression. Figure 22a shows that both *LDHA* and *LDHB* were markedly upregulated in tumoral cells when relativized to epilepsy controls (non-Warburgian metabolic behavior). This implies enhanced expression of the enzymatic machinery required for cytosolic SLP in GSCs and U87MG (which has been previously replicated in real-time metabolic phenotypes by Seahorse XF). Remarkably, *LDHA* expression was almost 250-fold higher in U87MG than in control tissue, further supporting the pivotal role of aerobic glycolysis in this cell line. Despite this, neither upregulation nor differing expression levels (irrespective of statistical significance) were clearly correlated with SOD resistance.

Finally, as verification of the potential effects of SOD treatment on target gene expression, we evaluated *LDHA* and *LDHB* after exposing all cell lines to the specific IC50-72 h dose (Figure 22b).

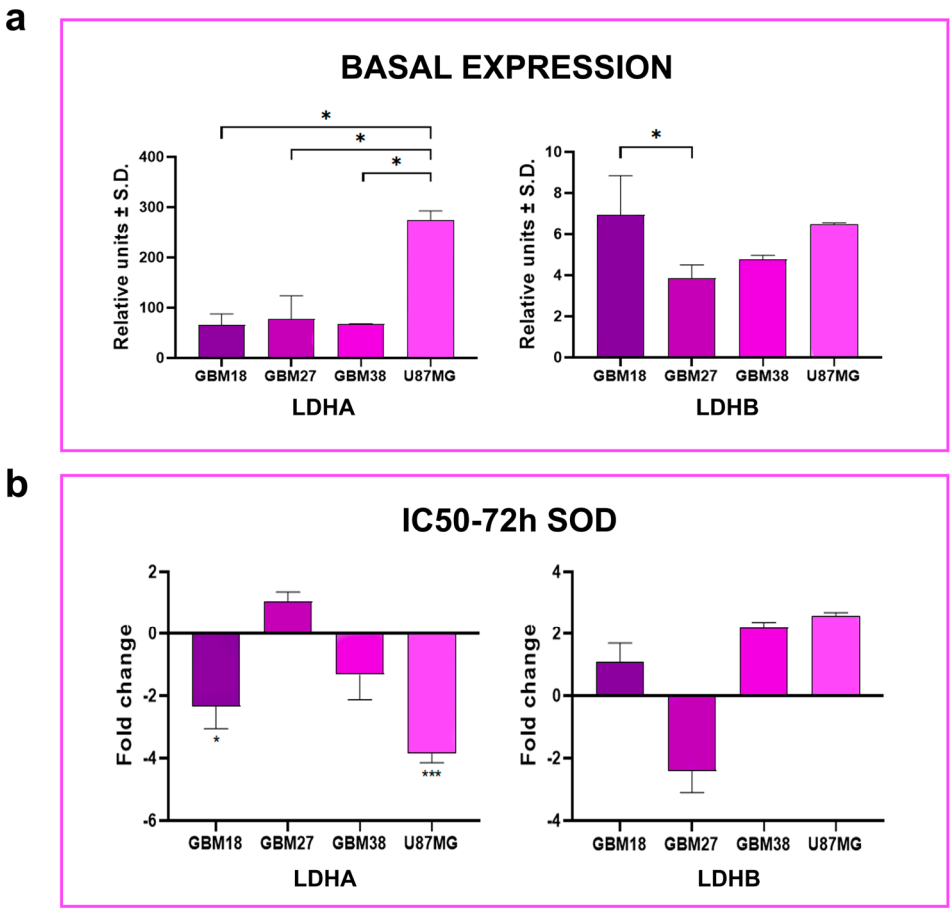

Figure 22. (a) Expression profiles of SOD target enzymes under basal conditions determined by qRT-PCR. Fold-differences relativized to retrotranscribed mRNA isolated from non-tumoral brain tissue. Data from 2 independent experiments. **(b) Relative mRNA expression compared to control after 72 h of SOD-72h IC50 treatment.** One-Way ANOVA with Sidak correction, $p < 0.05$ *; $p < 0.01$ **; $p < 0.001$ ***.

For *LDHA*, approximately 2-fold and 4-fold decreases in expression were observed in treated vs. control samples in GBM18 and U87MG, respectively. Differences in *LDHB* were minor and non-significant. The relative reduction in *LDHA* in U87MG could be explained by the exceptionally high basal levels. However, the biological relevance of these changes remains to be elucidated, as they cannot account for the homogeneity in dose-response profiles. As stated before, bearing in mind the low affinity

and poor cell membrane penetration of SOD, correlations between basal and induced mRNA expression and drug susceptibility cannot be easily drawn for this compound.

4.3. Doses of metabolic inhibitors and radiomimetic bleomycin corresponding to Warburg-like phenotypes spare viability of non-tumoral hMSCs and HBMEC cells

In preparation for synergistic studies, we questioned whether our cell lines would respond favorably to standard chemotherapeutic agents.

As our group previously published that GSCs are relatively resistant to TMZ ([158] and Supplementary Figure S8), we decided to use bleomycin sulfate, a water-soluble radiomimetic/DNA-targeting drug.

The mechanism of action and average IC50-72 h concentrations for bleomycin are represented in Figure 23. To substantiate combinatory studies, we first performed complete dose-response MTS assays to determine optimal concentrations for each cell line: we observed resistance in GBM18 and GBM27, whereas GBM38 and U87MG were equally sensitive to the drug (Supplementary Figure S9).

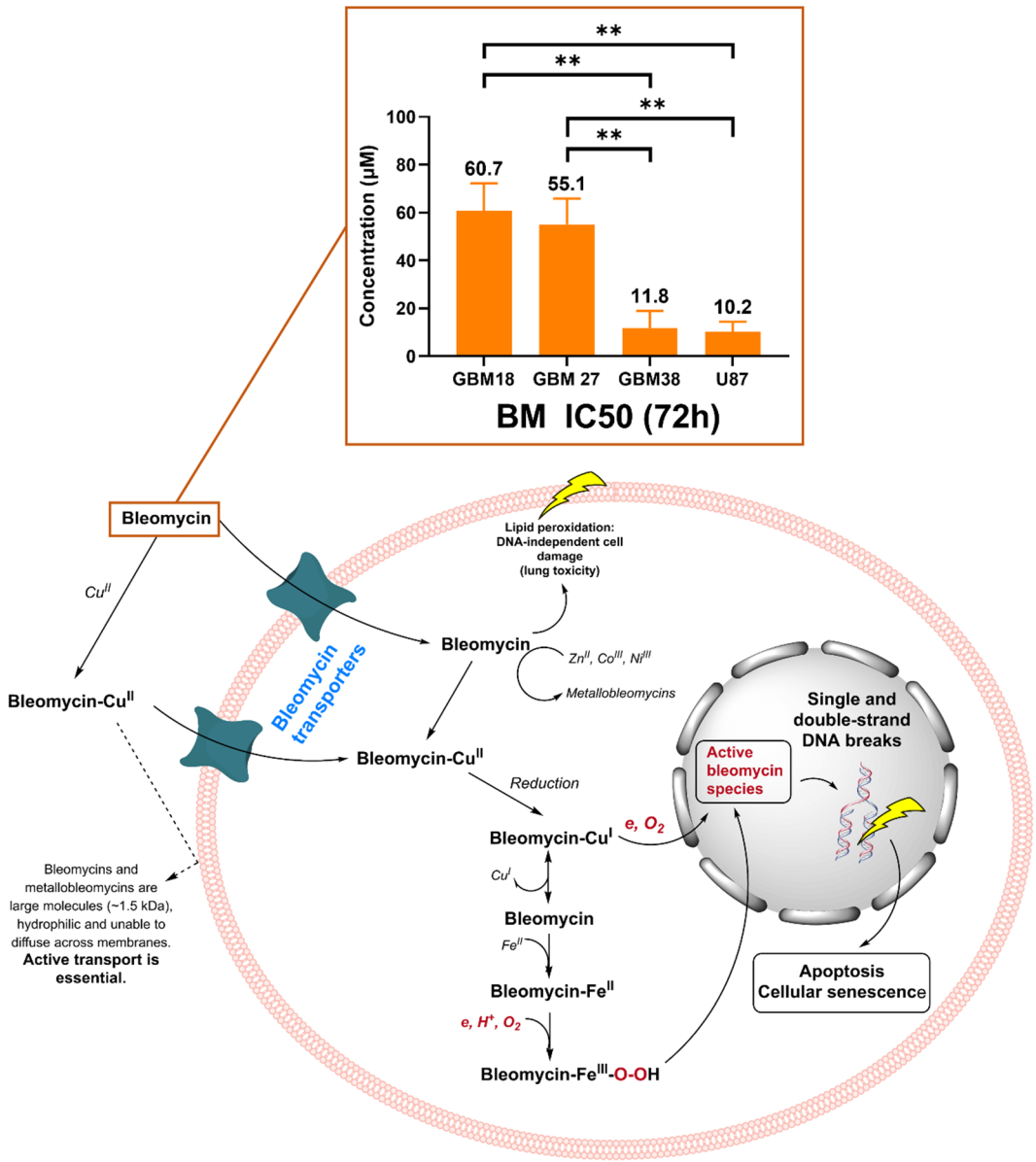

Figure 23. IC50 values at 72 h and mechanism of action of radiomimetic drug bleomycin (BM). Bleomycin is a large molecule (~ 1.5 kDa) and cannot freely diffuse cell membranes; it is transported into cells either alone or as a bleomycin–Cu(II) complex, then reduced to bleomycin–Cu(I), which reacts with oxygen leading to DNA strand breaks. Successful chemotherapy with bleomycin is dependent on active transport. Bleomycin–Cu(I) can also dissociate inside the cell to form bleomycin–Fe (II) complexes, transforming into «activated bleomycin species» resulting in DNA fragmentation and chromosomal aberrations. Complexes with zinc (II), iron (II), and cobalt (III) have also been characterized. Calculated IC50, as per MTS assay, with a minimum of 2 biological replicates. Average values are indicated above the bar chart. One-way ANOVA with Tukey correction, $p < 0.05$ *; $p < 0.01$ **; $p < 0.001$ ***.

4.3.1. Human mesenchymal stem cells (hMSCs) tolerate low to intermediate doses of MF, DCA, DON and bleomycin

As with any form of treatment, the clinical success of metabolic therapies will be limited by toxicity to healthy cells. Therefore, our first aim was to investigate whether all IC50-72 h concentrations determined thus far could be a realistic goal, exploring their effects on non-tumoral hMSCs (Figure 24).

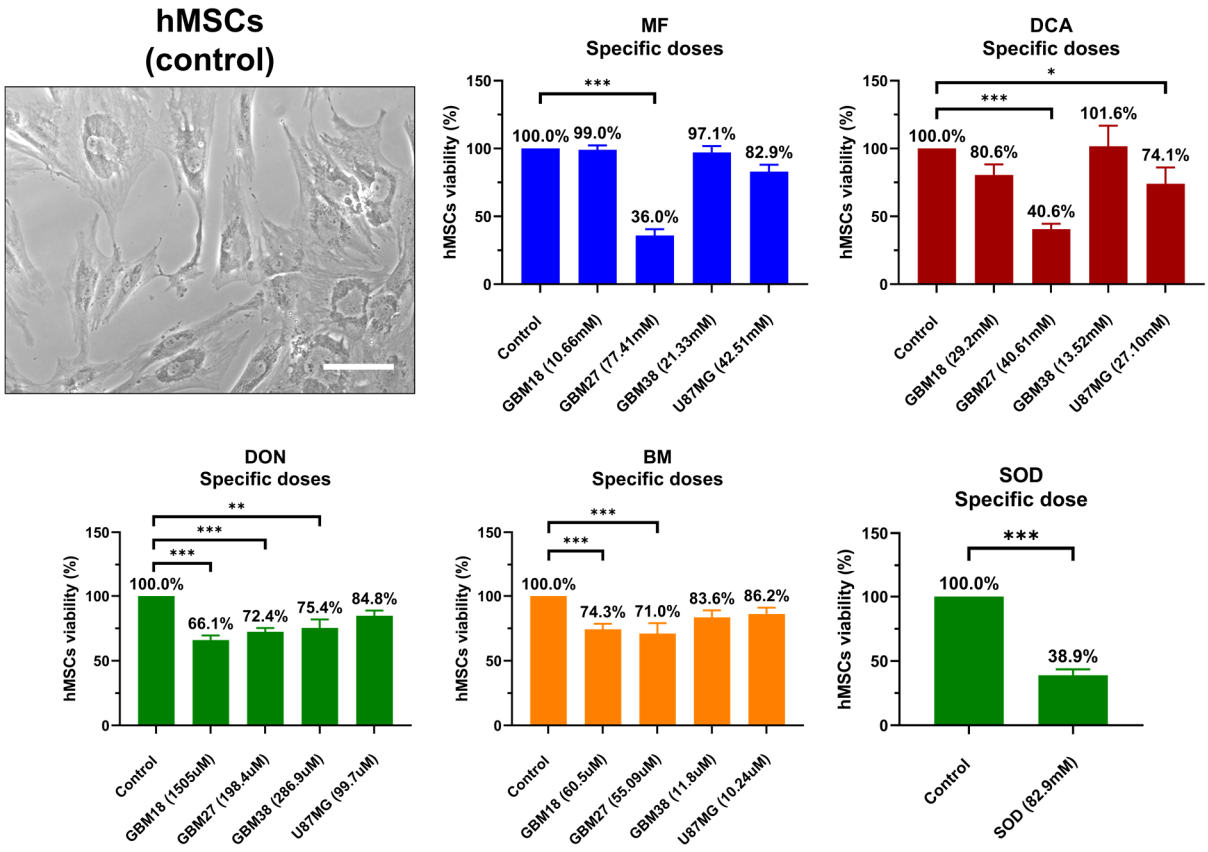

Figure 24. Representative optical microscopy images of hMSCs cellular morphology, in unaltered, basal conditions. Viability profiles relative to control hMSCs after treatment with all calculated 72 h-IC50 doses (n=2). Average percentage of viability values are indicated above the bar chart. One-way ANOVA with Dunn's correction, $p < 0.05$ *; $p < 0.01$ **; $p < 0.001$ ***. Scale bar = 100 µm.

MF/DCA affected more than 60% of cells when using GBM27 IC50s (corresponding to an "oxidative-like" metabolic phenotype), but all other doses were well tolerated (toxicity of less than 20%). In fact, DCA IC50-72 h concentrations from GBM38 slightly increased cell viability relative to control (as per metabolic activity

measured by the MTS assay), possibly due to normal upregulation of OXPHOS in cells with a functional chondriome after forced PDH activation and entry of pyruvate into the TCA cycle.

DON inhibited cell growth up to 35% at the highest dose (1505 μM), suggesting a saturation point after which increased dosages do not linearly correlate with antiproliferative effects (in contrast to GBM27, GBM38 and U87MG, lower glutamine dependence).

Unfortunately, the universal dose of SOD determined by previous MTS assays (IC50-72 h = 82.9 mM) also reduced proliferation of hMSCs. Low specificity against Warburg-like cells and toxicity in normal stem cells further supported our decision to reconsider SOD as a viable candidate for LDH inhibition.

Bleomycin, in contrast, only affected up to 30% of hMSCs at the highest IC50, correlating well with slower proliferation rates.

In summary, cell lines with predominantly Warburgian phenotypes could be targeted with metabolic inhibitors without affecting normal stem cells, but OCR-dependent phenotypes, such as GBM27, will require individualized, tailor-made approaches.

4.3.2. Rapidly proliferating non-tumoral endothelial cells tolerate intermediate doses of MF and DCA, but not bleomycin

We wanted to explore the potential effects of metabolic inhibitors against rapidly proliferating non-cancerous, non-stem cells, wherein lies a significant proportion of the undesired acute toxicity of standard chemoradiotherapeutics (e.g., damage to epithelial surfaces of skin and digestive tract, vascular endothelium, immune system, reproductive organs) [336; 337].

As we emphasized brain-related structures, we investigated the HBMEC cell line, a widely adopted BBB model. We sought to elucidate the impact of metabolic inhibitors on this population of cells, as they also embody the endothelial barrier of drug transport after systemic application [338]. HBMEC are rapidly proliferating and recapitulate the BBB enzymatic distribution and carrier-mediated transport systems [338].

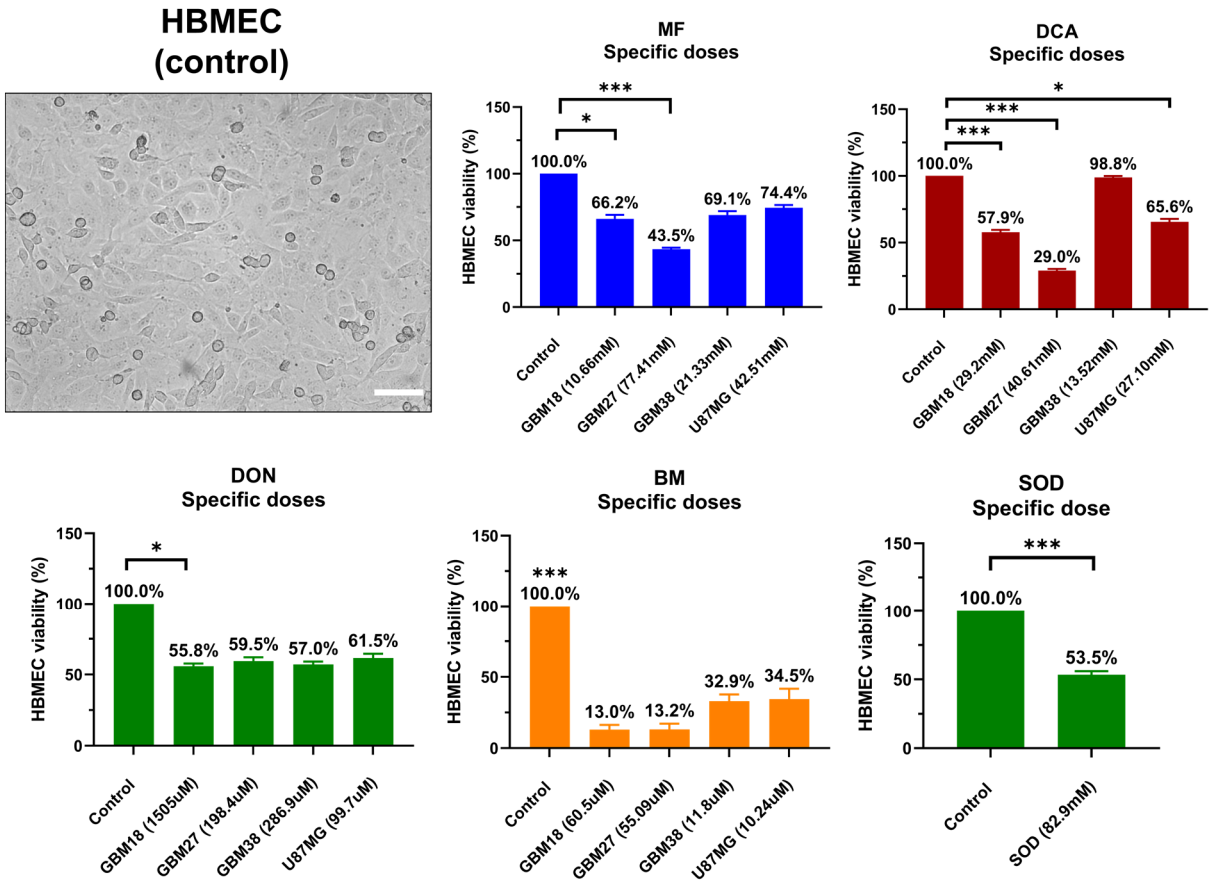

Figure 25. Representative optical microscopy images of HBMEC cellular morphology. Viability profiles relative to control of HBMEC treated with all calculated 72 h-IC50 doses (n=2). Average percentage values are indicated above the bar chart. One-way ANOVA with Dunn's correction, $p < 0.05$ *; $p < 0.01$ **; $p < 0.001$ ***. Scale bar = 100 µm.

We detected high tolerance towards intermediate doses of MF and DCA. As the outcomes with MF seemed counterintuitive (i.e., similar viability regardless of low to intermediate doses), we further confirmed this observation by applying an increasing dose-response curve, which showed a non-linear decrease in viability, illustrated in Supplementary Figure S10. In HBMEC cells, MF induced a significant decrease in viability at concentrations > 60 mM, but it was relatively well tolerated up to that point.

Comparable to hMSCs, DON reduced cell viability by approximately 50%, independent of concentration. For the radiomimetic bleomycin, as would be expected given the accelerated proliferation rates of this cell line, viability was significantly reduced, making a potential dose-reduction attributable to synergism a very appealing proposition to preserve normal rapidly proliferating tissues. The universal dose of SOD recapitulated the IC50 effects seen in all other cell lines, once again substantiating that SOD lacks differential effects as a single agent in our cell lines.

4.4. Synergy between bleomycin and metabolic inhibitors helps to overcome dose-limiting toxicity, predominantly in oxidative-like metabolic phenotypes

One way to solve the challenge of non-specific damage to healthy cells is to exploit coexisting weaknesses of tumoral cells in combinatory strategies. Since GBM27 doses of MF/DCA were affecting viability of hMSCs, and bleomycin at high doses had unacceptable "toxicity" in rapidly proliferating non-tumoral HBMEC cells, we explored the possibility of dose-reduction resulting from synergistic properties.

After individually confirming the validity of each previously calculated 72 h-IC50, we performed combinatory studies to determine the existence of synergy, additive or antagonistic effects. Using the Chou-Talalay theorem in a fixed drug ratio, which allows for a comprehensive analysis of synergism/antagonism of two or more drugs, CI and DRI were calculated for each combination [296; 297]. Of note, CI and DRI values are most important at high effect (Fa) levels, that is, when drug combinations are killing most of the malignant cells, since this is the primary objective of cancer therapy [339].

As shown in Table 6, drug mixtures with CI < 1 and DRI > 1 at Fa = 0.6 were considered as the optimal cutoff to identify promising therapeutic combinations. Nevertheless, in constant ratio experiments, close attention needs to be paid to the full range of Fa and CI/DRI to evaluate synergy of any given drug combination.

Table 6. Summary of synergy/antagonism at an optimal fraction of affected cells (Fa) cutoff of = 0.6. This value was selected as the most promising combinatory threshold, with therapeutically relevant antiproliferative effects (a viability reduction of 60%), synergism in most combinations and dose-reductions even in cases of theoretical antagonism. All combinatory experiments were performed in 2 biological replicates (n=2).

	MF + Bleomycin		DCA + Bleomycin		DON + Bleomycin	
Cell line	Effect at Fa = 0.6	DRI at Fa = 0.6	Effect at Fa = 0.6	DRI at Fa = 0.6	Effect at Fa = 0.6	DRI at Fa = 0.6
GBM18	Additive	DRI > 1 for both	Antagonism	DRI > 1 for both	Synergism	DRI > 1 for both
GBM27	Synergism	DRI > 1 for both	Synergism	DRI > 1 for both	Synergism	DRI > 1 for both
GBM38	Synergism	DRI > 1 for both	Antagonism	DRI > 1 for bleomycin	Synergism	DRI > 1 for both
U87MG	Synergism	DRI > 1 for both	Antagonism	DRI > 1 for both	Synergism	DRI > 1 for both

All final reports with complete datasets are presented in the accompanying publication [340].

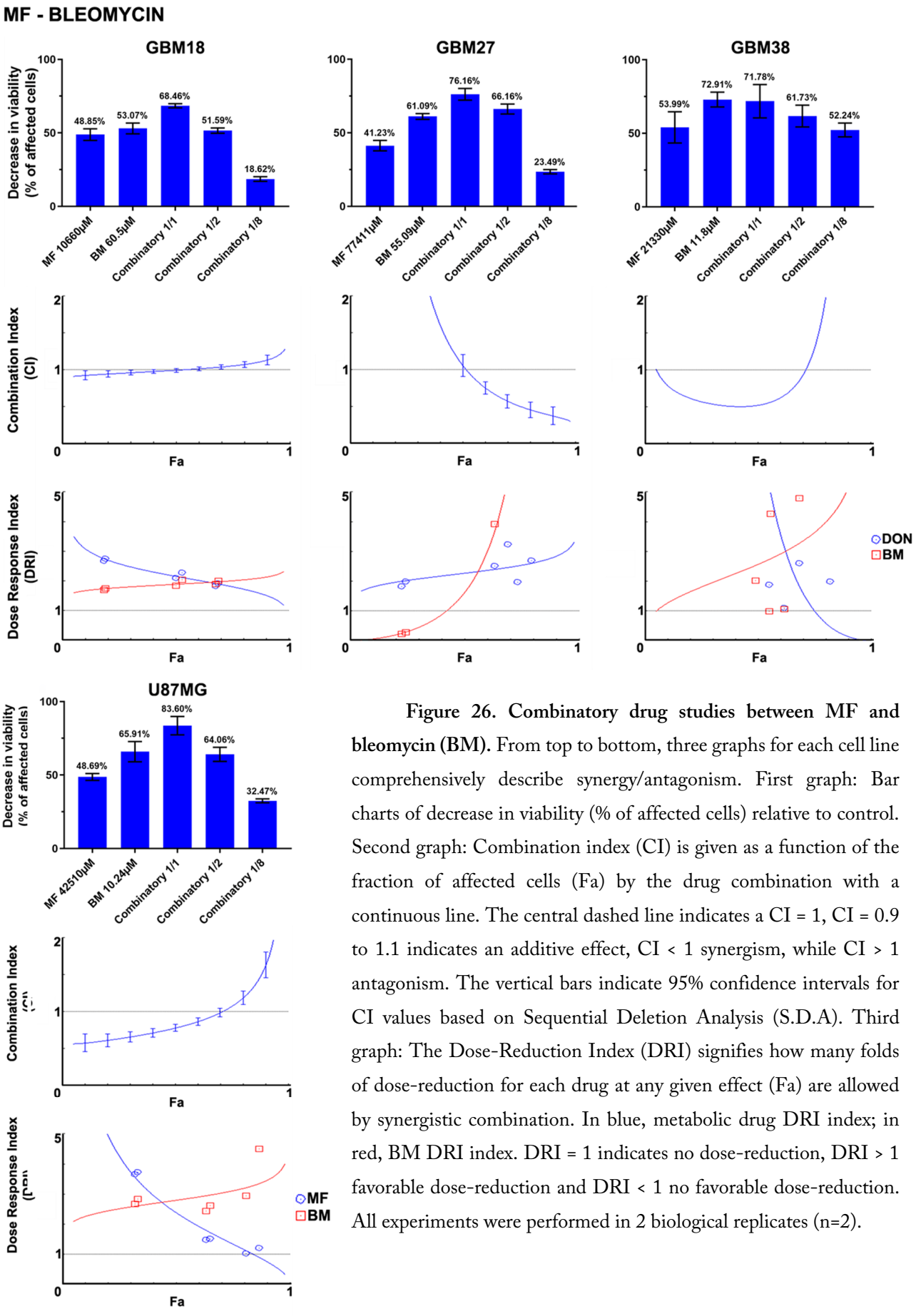

Figure 26. Combinatory drug studies between MF and bleomycin (BM). From top to bottom, three graphs for each cell line comprehensively describe synergy/antagonism. First graph: Bar charts of decrease in viability (% of affected cells) relative to control. Second graph: Combination index (CI) is given as a function of the fraction of affected cells (Fa) by the drug combination with a continuous line. The central dashed line indicates a CI = 1, CI = 0.9 to 1.1 indicates an additive effect, CI < 1 synergism, while CI > 1 antagonism. The vertical bars indicate 95% confidence intervals for CI values based on Sequential Deletion Analysis (S.D.A). Third graph: The Dose-Reduction Index (DRI) signifies how many folds of dose-reduction for each drug at any given effect (Fa) are allowed by synergistic combination. In blue, metabolic drug DRI index; in red, BM DRI index. DRI = 1 indicates no dose-reduction, DRI > 1 favorable dose-reduction and DRI < 1 no favorable dose-reduction. All experiments were performed in 2 biological replicates (n=2).

Our results describe a wide variety of combinatory effects depending on the cell subtype and Fa level. Figure 26 describes the combined effects of MF and bleomycin.

GBM18 exhibits mostly additive effects (no synergy), where combining theoretical IC50 values decreases viability up to 64%, but, more significantly, reducing doses by half still affects 46% of cells (similar to full IC50 doses for each drug independently). In the CI graph, we can observe that at Fa levels ≥ 0.75 the two drugs start to behave antagonistically. In the DRI plot, bleomycin has a DRI > 1 as Fa levels increase, whereas MF falls below DRI < 1 close to Fa = 1. This means that when we increase Fa, we can reach an optimal point, close to Fa = 0.7, where bleomycin doses could be decreased almost 1.5-fold and achieve an equal effect as with higher doses, thus reducing toxicity.

GBM27, on the other hand, is a prototypical example of synergistic effects at high Fa values: in the CI index, Fa ≥ 0.75 has a CI < 0.4, indicative of strong synergism. Consequently, DRI is > 1 for both MF and bleomycin, with significant dose reductions at Fa ≥ 0.6, potentially reducing the toxicity of both agents.

GBM38 is synergistic at Fa ≈ 0.5 but has a tendency towards antagonism at Fa ≥ 0.75. When we examine the DRI graph, bleomycin dosages could be decreased at high Fa levels, but MF would also need to be increased to achieve similar effects. GBM38 appears to have a threshold for both MF and bleomycin, where even small doses produce significant anti-proliferative effects, but further increases provide no additional benefits.

Finally, the CI in U87MG is close to synergistic/additive up to Fa = 0.75, then turning antagonistic.

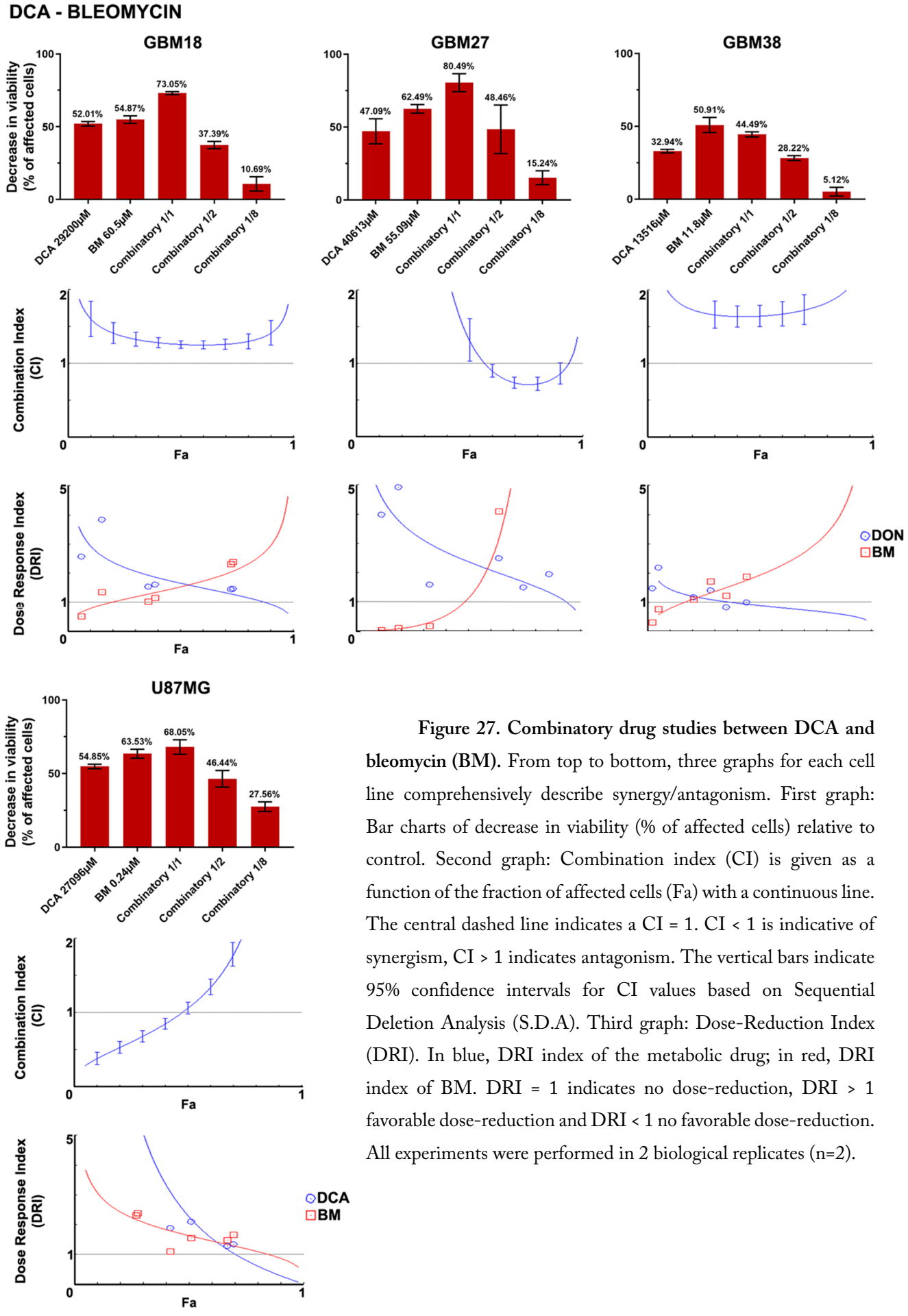

Figure 27. Combinatory drug studies between DCA and bleomycin (BM). From top to bottom, three graphs for each cell line comprehensively describe synergy/antagonism. First graph: Bar charts of decrease in viability (% of affected cells) relative to control. Second graph: Combination index (CI) is given as a function of the fraction of affected cells (Fa) with a continuous line. The central dashed line indicates a CI = 1. CI < 1 is indicative of synergism, CI > 1 indicates antagonism. The vertical bars indicate 95% confidence intervals for CI values based on Sequential Deletion Analysis (S.D.A). Third graph: Dose-Reduction Index (DRI). In blue, DRI index of the metabolic drug; in red, DRI index of BM. DRI = 1 indicates no dose-reduction, DRI > 1 favorable dose-reduction and DRI < 1 no favorable dose-reduction. All experiments were performed in 2 biological replicates (n=2).

Next, Figure 27 describes the combinatory effects of DCA and bleomycin.

For GBM18, the CI is > 1 (antagonistic) at any given Fa; despite this, DRI > 1 for bleomycin at high Fa levels indicates the possibility of dose-reduction. In GBM27, therapeutic effects are determined by the Fa cutoff: close to Fa ≈ 0.75, CI is < 1 (synergistic), with dose reduction predicted at this value. GBM38, on the other hand, represents a clear example of strong antagonism (CI values > 1.5 at any Fa level); consequently, the combination of drugs does not surpass the effects of bleomycin by itself. Even still, DRI suggests that bleomycin concentrations could be decreased at the expense of DCA. Lastly, up to Fa = 0.5, U87MG displays synergistic/additive effects, with antagonism prevailing thereafter; this translates to unfavorable dosing in the Chou-Martin plot at Fa > 0.8 (DRI < 1 for both drugs).

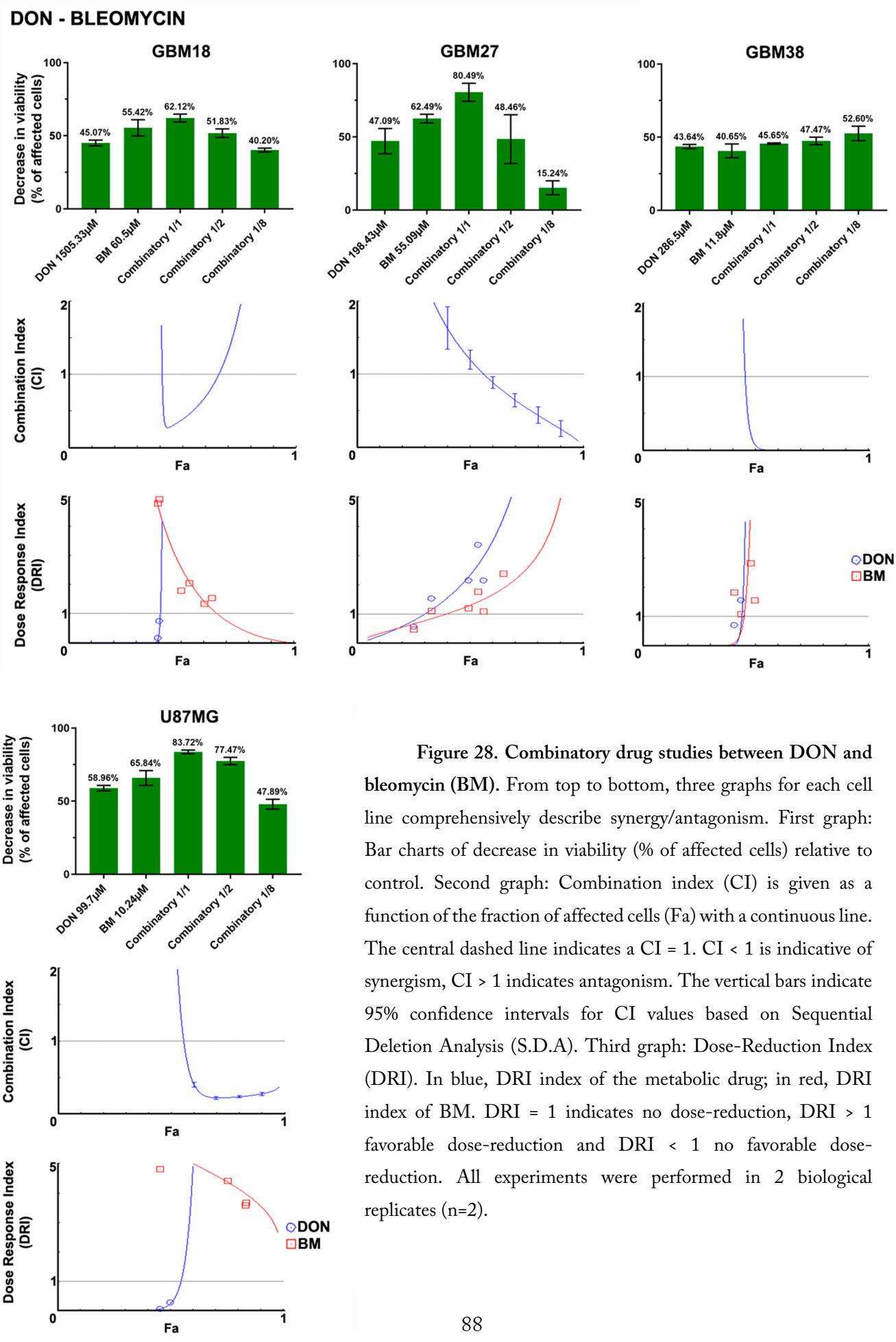

Figure 28. Combinatory drug studies between DON and bleomycin (BM). From top to bottom, three graphs for each cell line comprehensively describe synergy/antagonism. First graph: Bar charts of decrease in viability (% of affected cells) relative to control. Second graph: Combination index (CI) is given as a function of the fraction of affected cells (Fa) with a continuous line. The central dashed line indicates a CI = 1. CI < 1 is indicative of synergism, CI > 1 indicates antagonism. The vertical bars indicate 95% confidence intervals for CI values based on Sequential Deletion Analysis (S.D.A). Third graph: Dose-Reduction Index (DRI). In blue, DRI index of the metabolic drug; in red, DRI index of BM. DRI = 1 indicates no dose-reduction, DRI > 1 favorable dose-reduction and DRI < 1 no favorable dose-reduction. All experiments were performed in 2 biological replicates (n=2).

To conclude, Figure 28 details the interaction between DON and bleomycin.

As previously shown, growth inhibition curves for DON do not always follow a linear dose-effect relationship (Supplementary Figure S7). For GBM18, combining the compounds presents a strong synergistic relationship at Fa close to 0.5; however, at higher Fa, this synergy is lost. Ascending DRI for DON indicates the potential of important dose-reduction. GBM27 benefits from additive effects close to Fa ≈ 0.5, and, as we move closer to Fa = 1, the combination becomes strongly synergistic; this too would allow for dose reduction of both drugs. In GBM38, the combined treatment has a similar threshold as in U87MG, as even one eight of the concentration significantly decreases proliferation: in these 2 cell lines, CI is < 1 and DRI > 1 at Fa levels > 0.5, making DON and bleomycin a very promising therapeutic combination.

In summary, for GBM27, synergism with radiomimetic bleomycin was observed for all metabolic inhibitors at therapeutically relevant Fa ≥ 0.9. Combining inhibitors and bleomycin could be leveraged to reduce dosing requirements of oxygen consuming GSC subtypes. Additionally, DRI was > 1 for both drugs at Fa = 0.6 in GBM18 (MF, DCA, DON), GBM27 (MF, DCA, DON), GBM38 (MF, DON) and U87MG (MF, DCA, DON); thus, almost all cell lines could benefit from combined treatment, especially in the case of DON. Owing to synergism and additive effects, more realistic, non-toxic concentrations could be achieved.

4.5. Bioenergetic profiling after metabolic treatment reveals opportunities for metabolic priming in surviving cell populations

Using Seahorse XF technology, we determined total ATP production and ratio of mitoATP/glycoATP production under metabolically treated conditions. As previously shown, GSCs and U87MG maintain a basal, relatively stable, bioenergetic profile. After establishing IC50 values for each drug and cell line, we sought to determine how chronic treatment affected the metabolic profiles of the surviving fraction.

As shown in Figure 29, normalized total ATP production was decreased in all treated cells, with the exception of DCA-treated GBM27: here, rather than a significant drop in total ATP production, there was a shift from glycolytic to OCR-dependent metabolism, with total ATP rates remaining relatively stable.

Furthermore, consistent with the proposed biological action, we observed a reduction in OCR-linked mitoATP production and a shift toward glycolysis using MF. Even though IC50 values should have affected all cell lines proportionately, we noticed that the reduction in total ATP production was less pronounced with lower doses, e.g., in the case of GBM18, exposed to the lowest IC50 (MF = 10.66 mM), OCR-linked ATP was almost completely abolished, but total glycolytic ATP decreased only marginally, indicating a surviving population of almost exclusively glycolytic cells.

OCR-linked ATP production was increased after treatment with DCA, especially in GBM27, a GSC with a clear preference towards oxygen consumption under both basal and treated conditions. The XF Rate Index after exposure to DCA can provide an idea of the oxidative potential of each cell line: highest in GBM27, followed by GBM18 and lowest in GBM38/U87MG.

In the case of DON, we could appreciate a notable reduction of total ATP for each calculated IC50 value. As previously stated, DON is a glutamine analog that predominantly targets GLS (inhibition of TCA cycle intermediaries from glutamine would be expected to reduce mitoATP, unless glutamine derived α-ketoglutarate was diverted towards biosynthesis or mSLP, rather than oxidized). Examining the XF ATP Rate Index, GBM18 and, especially, GBM27, shifted towards oxygen consumption, whereas GBM38 and U87MG remained unaltered. In conclusion, DON did not consistently change the metabolic phenotypes of surviving cells; interestingly, however, in U87MG, a characteristically glutaminolytic cell line, even small concentrations of DON (99.7 μM) were enough to drastically reduce total ATP production.

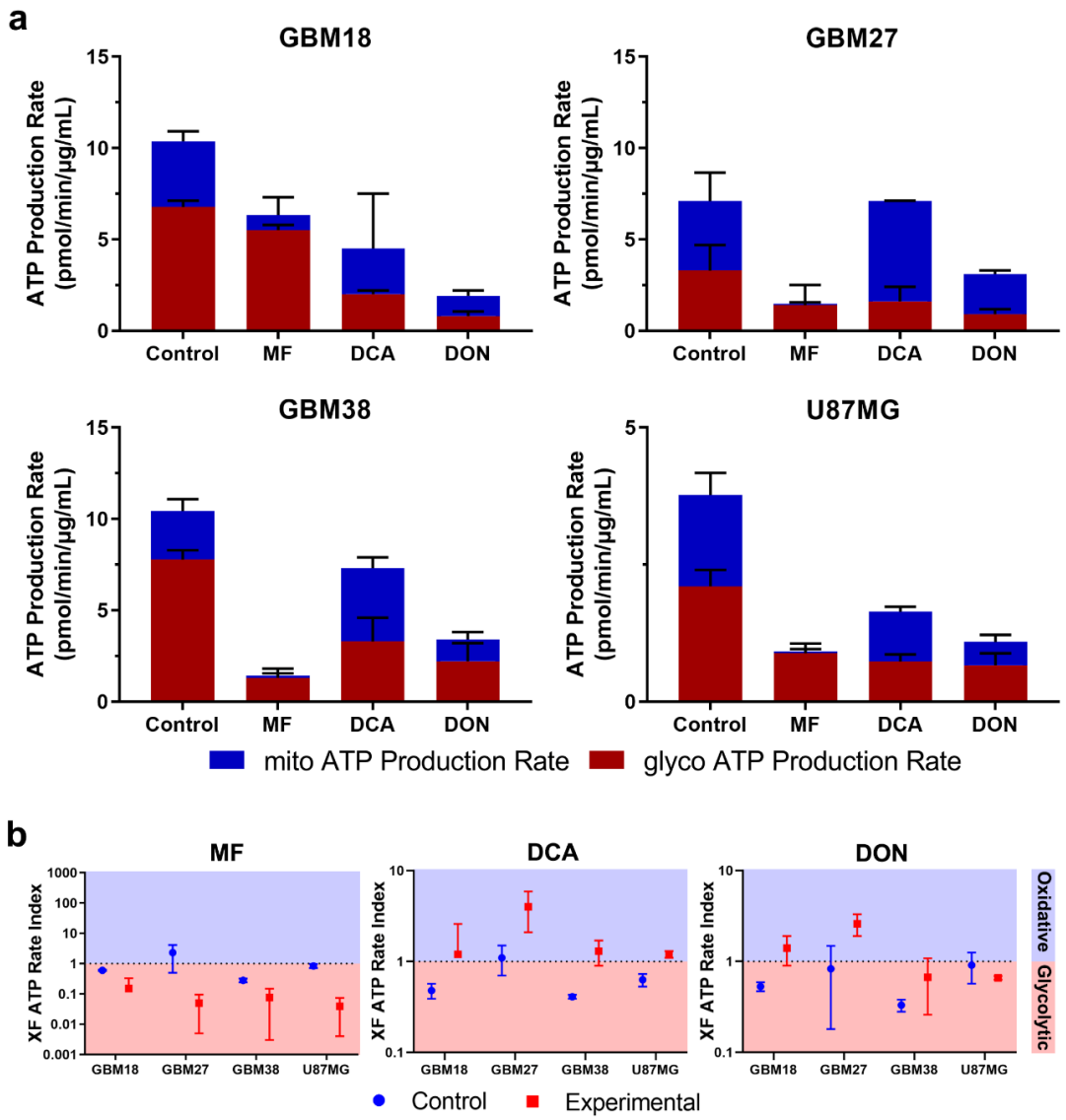

Figure 29. (a) Changes in metabolic phenotypes after IC50 treatment for 72 h with metformin (MF), dichloroacetate (DCA) and 6-Diazo-5-oxo-L-norleucine (DON). In all cell lines, with the exception of DCA in GBM27, treatment with metabolic inhibitors successfully inhibited total ATP production. Interestingly, DCA-treated GBM27 retained their metabolic activity but with a significant shift towards OCR-linked ATP. MF acts as a mitochondrial inhibitor, while also reducing total glycolytic ATP production in all cell lines except GBM18. In our results, the major characteristic of DCA is its ability to shift glycolytic cell lines to a more OCR reliant phenotype, rather than affecting total ATP production. Finally, DON reduces total ATP without consistent shifts in ATP distribution. **(b) XF ATP Rate Index for GSCs and U87MG.** The ATP Rate Index is the ratio of the mitoATP Production Rate divided by glycoATP Production Rate, indicating higher OCR-dependent or glycolytic bioenergetic profiles. In our results, each metabolic inhibitor shifted the ratio consistently with its biological action: MF decreased the index (surviving cells rely on glycolysis), DCA increased the index, especially in GBM27 (treated cells are more oxidative), and DON had a more variable effect, with slight increases in GBM18 and GBM27, and no significant changes in GBM38 and U87MG.

Normalized values of OCR/PER in real-time after each drug injection of the Seahorse XF protocol are provided in Figures 30-32. These kinetic graphs allow us to examine how previous metabolic treatments changed the basal metabolic state and the acute responses to mitochondrial inhibitors included in the assay: oligomycin (complex V inhibitor, i.e., mitochondrial ATP synthesis) and rotenone/antimycin A (total inhibition of mitochondrial respiration, complex I and complex III, respectively).

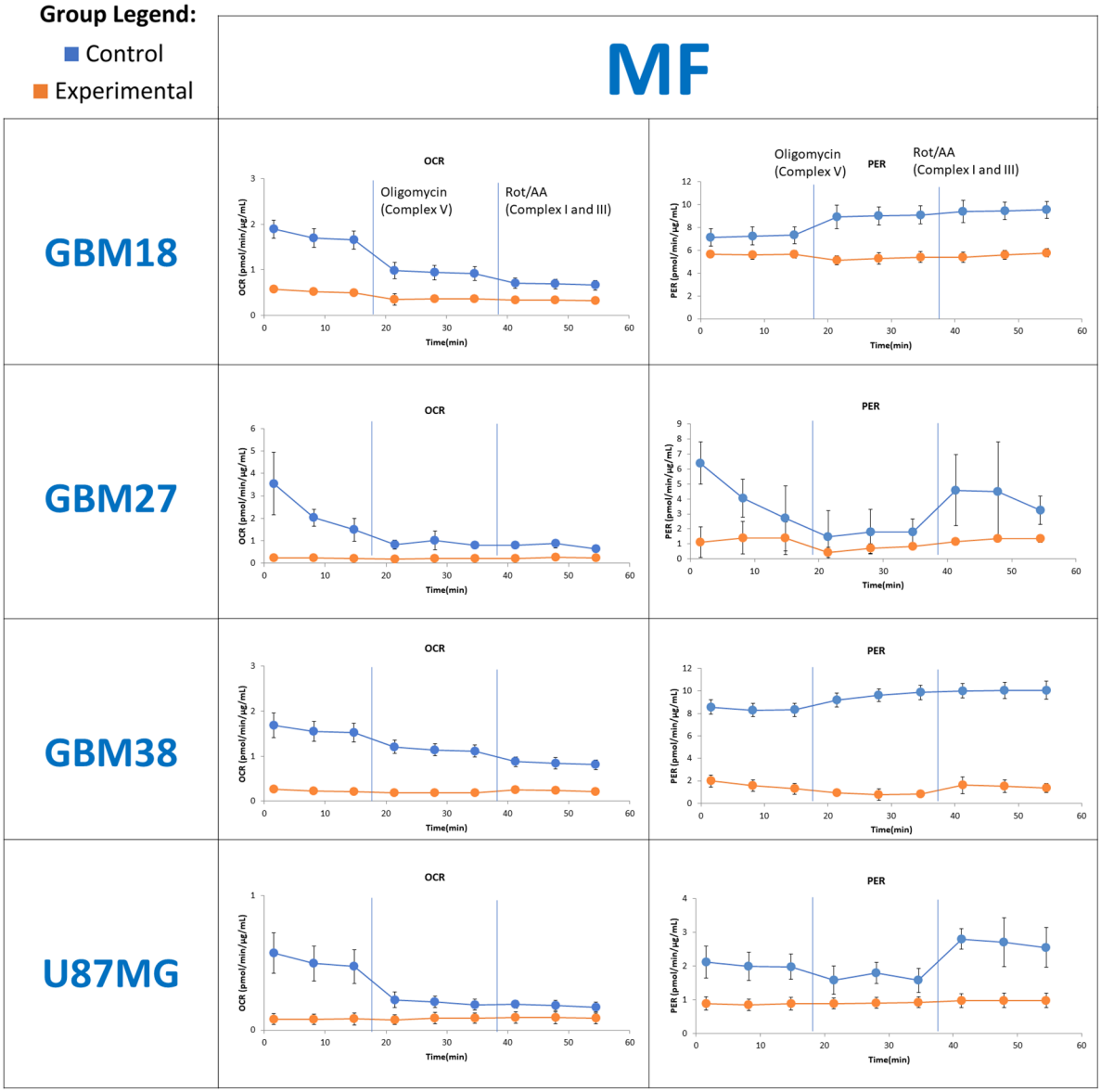

Figure 30. Seahorse XF real-time kinetic graphs for MF. Normalized OCR and PER (pmol/min/µg/mL) values. Control and treated cells are measured in basal conditions and then after sequential injection of oligomycin (inhibition of complex V) and rotenone/antimycin A (inhibition of complex I and III). Measurements are performed at 6 min intervals. Oligomycin is expected to rise PER to compensate for loss of mitochondrial ATP synthesis (ATP-linked OCR and glycolytic

capacity on PER), whereas complete inhibition of the ETC indicates residual OCR and maximal glycolytic reserve.

As MF significantly reduced basal OCR in GBM18, glycolysis levels (PER) did not increase after injection of oligomycin; however, PER levels were maintained in treated cells. In GBM27, GBM38 and U87MG, there was a significant reduction of OCR and PER, and, similarly, levels did not change after injection of inhibitors.

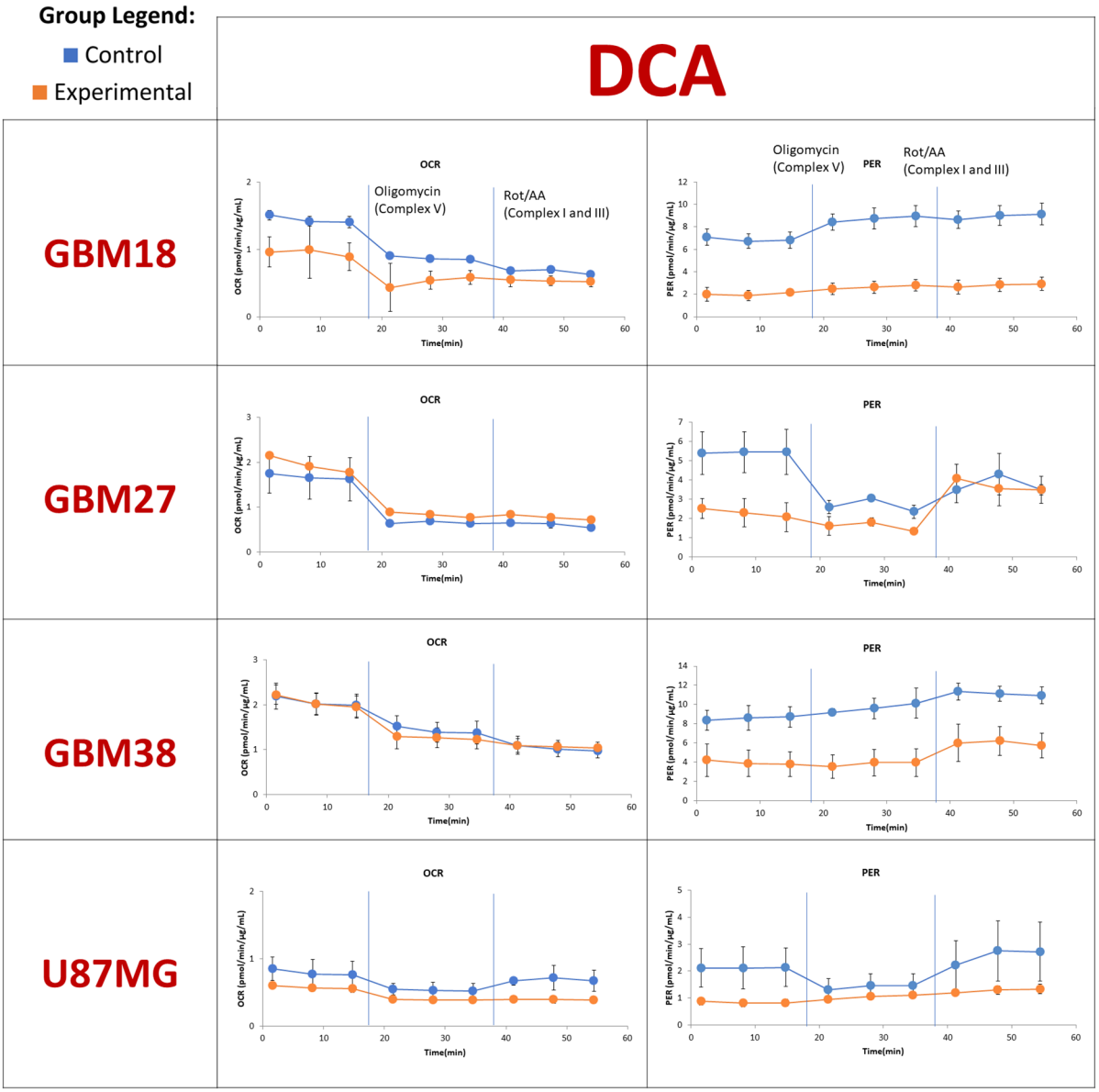

Figure 31. Seahorse XF real-time kinetic graphs for DCA. Normalized OCR and PER (pmol/min/µg/mL) values.

In terms of OCR changes, DCA treated and non-treated cells responded equally. GBM18, GBM38 and U87MG were not able to compensate total respiration inhibition (rotenone/antimycin A), but, interestingly, GBM27 was able to rescue inhibition by glycolysis, raising to equal levels as control cells, even though basal PER levels were initially lower.

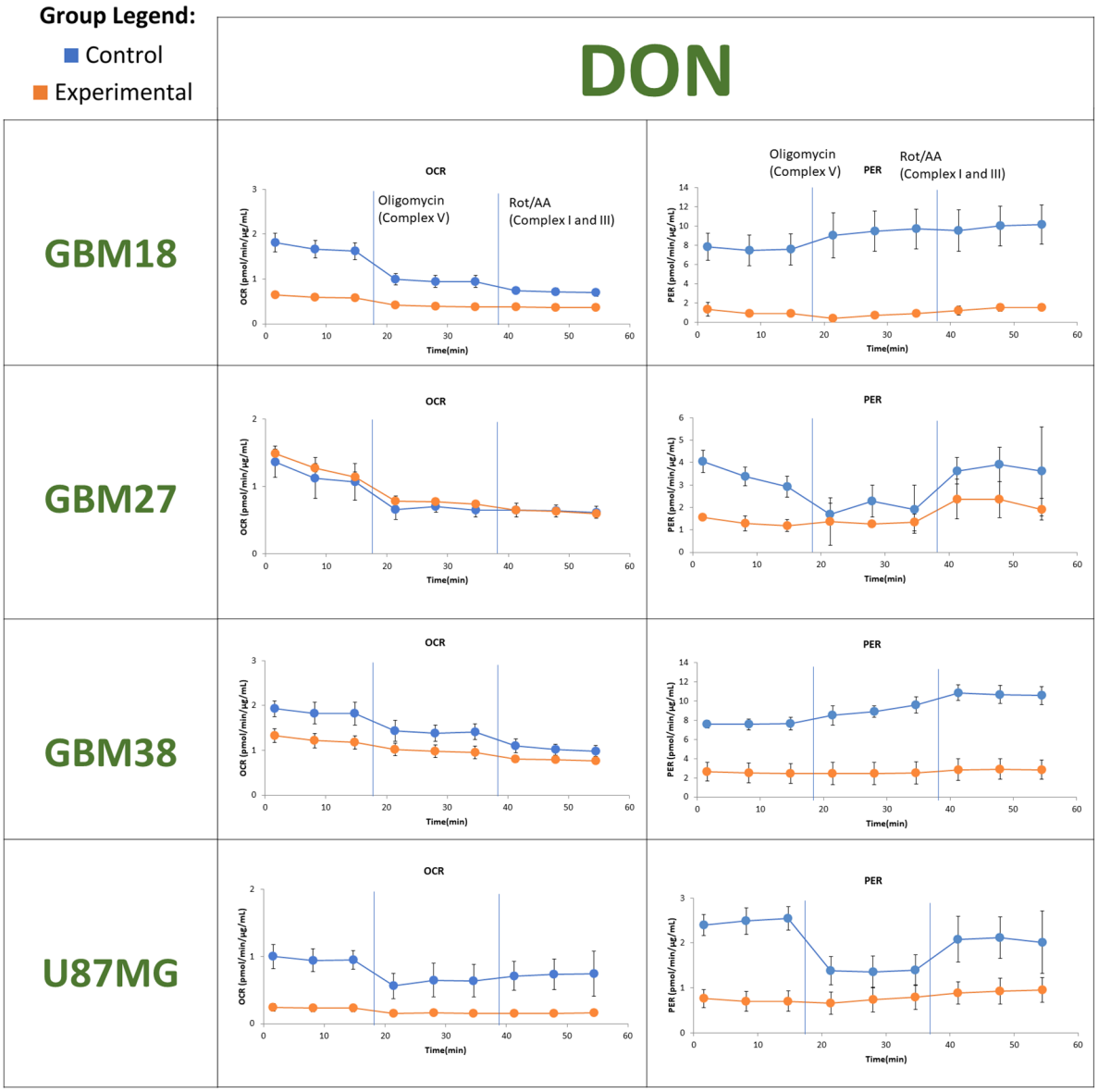

Figure 32. Seahorse XF real-time kinetic graphs for DON. Normalized OCR and PER (pmol/min/µg/mL) values.

DON reduced OCR in GBM18 and U87MG, and, in these cell lines, PER was already low and did not change after any injection of mitochondrial inhibitors. In GBM27 and GBM38, OCR fluctuations after inhibitors were similar in control and treated cells;

surprisingly, DON did not reduce OCR in GBM27 at all (inhibition of glutaminolysis had no effect on mitochondrial ATP production rates). However, PER increased in GBM27 in both control and treated cells after rotenone/antimycin A, whereas, in GBM38, PER was globally decreased and remained unaltered even after injection of inhibitors.

Kinetic profiles of OCR and ECAR allow for the identification of resistance to ETC inhibition and residual non-mitochondrial OCR (i.e., after injection of rotenone/antimycin A, OCR does not reach zero). In our study, cells in basal conditions often maintained residual OCR, whereas MF treated cells demonstrated nearly completely abolished OCR. Glycolytic upregulation in response to partial and complete mitochondrial inhibition (Warburg phenotype) and residual non-mitochondrial OCR should be highlighted in GBM18 and GBM38.

To review our principal findings, we can conclude that pre-treatment with metabolic drugs could become a valuable tool to characterize the bioenergetic phenotypes of surviving, resistant fraction of cells, priming them for further treatments. To the extent of our knowledge, our group was the first to characterize the bioenergetic effects of chronic metabolic treatments (>72 h) in GSCs with DCA and DON. Despite methodological differences, our results also confirm the responses observed after low-dose MF in other GSCs [341], and DCA in established glioma cell lines [342; 343]. Finally, oxygen consuming GSCs such as GBM27, an anomaly in the predominantly glycolytic dependencies of solid tumors, need to be fully recognized to improve metabolic therapies. Based on our results, sequential drug application, targeting previously weakened ATP-generating pathways, warrants further exploration.

4.6. Evaluating the *in vitro* effects of a ketogenically-compensated glucose-deprived cell culture media formation

Metabolic differences between healthy and malignant cells have led to the hypothesis that mitochondrial dysfunction may be cancer's "Achilles heel" [344]. As such, only cells with functional OXPHOS would be expected to withstand the nutrient stress of press-pulse interventions [269; 284; 345-348]. To date, diet/drug-induced

hypoglycemia with BHB adaptation has been studied as a form of systemic metabolic priming *in vitro* and animal models [113; 349-351]. The Warburg hypothesis needs to be fully tested to determine if restoring mitochondrial function and changing nutrient availability could kill, reverse or stabilize highly proliferative phenotypes [104].

4.6.1. GSCs and U87MG express detectable levels of the 3-oxoacid CoA-transferase enzyme at the protein level, regardless of the presence of BHB

At the outset, we wanted to complement therapeutic interventions with a characterization of GBM from a metabolic perspective. Congruent with this aim, we questioned whether our cell lines could benefit from ketone bodies (namely, BHB) as an alternative oxidative fuel.

A translational approach to determine ketolysis, as proposed in clinical trials, is to study the protein expression of the 3-oxoacid CoA-transferase 1 (OXCT1) [267; 352; 353]. As a reminder of ketolytic metabolism, Figure 33 provides a visual overview of the prerequisite oxidative processing of ketone bodies for ATP production [354]. OXCT1 is the primary enzyme for the catabolic processing of ketone bodies. OXCT1 is required to convert acetoacetate to acetoacetyl-CoA as part of mitochondrial ketolysis; without this reaction, ketone bodies cannot be turned into acetyl-CoA nor oxidized in the TCA cycle. Even though other enzymes cooperate in this pathway, such as D-beta-hydroxybutyrate dehydrogenase (BDH) and Acetyl-CoA acetyltransferase (ACAT1), OXCT1 is the rate-limiting enzyme.

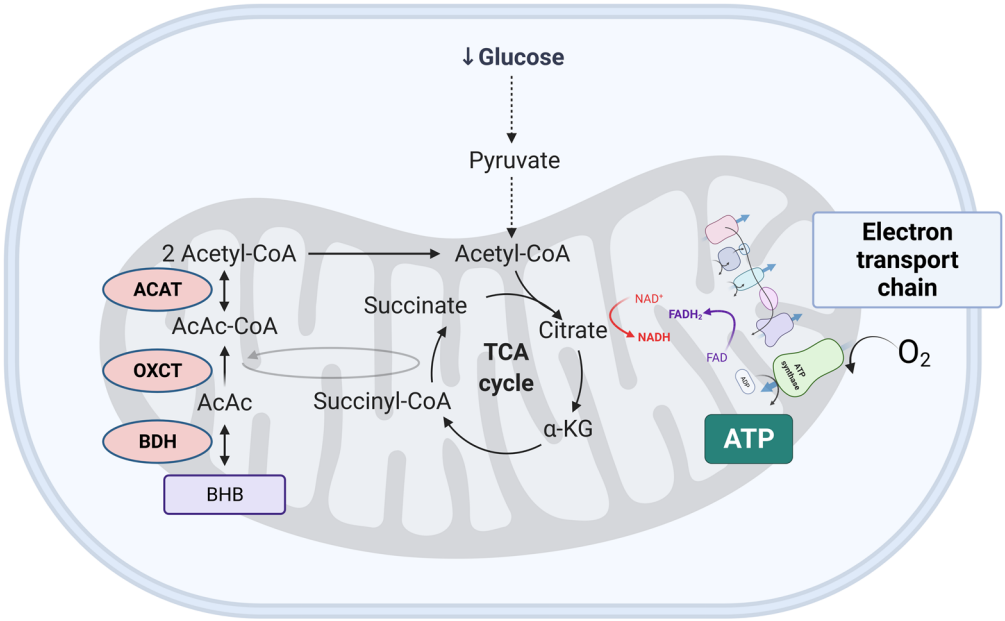

Figure 33. Simplified diagram of ketone body metabolism. At times of glucose shortage, such as prolonged fasting, ketone bodies are an important energetic source for the brain and extrahepatic tissues. The oxidoreductase 3-hydroxybutyrate dehydrogenase (BDH) mediates the first step of ketone body degradation, between 3-hydroxybutyrate and acetoacetate. 3-oxoacid-CoA transferase 1 (OXCT1) catalyzes the transfer of coenzyme A from succinyl-CoA to acetoacetate, generating acetoacetyl-CoA. Via acetyl-CoA acetyltransferase 1 (ACAT1), acetoacetyl-CoA is converted into two molecules of acetyl-CoA, which then enter the TCA cycle. Furthermore, ketone bodies provide substrates for the synthesis of various molecules, especially lipids, via action of acetoacetyl-CoA synthetase (AACS).

For Western Blot analysis of OXCT1, cells were grown in their standard media, as well as equivalent low glucose media (0.5 mM) supplemented with 10 mM BHB. First, protein was recovered at 24 h, but we were not able to detect visible changes in protein levels, as seen in Supplementary Figure S11a. Our results are concordant with previous reports which evaluated OXCT1 expression in U87MG at 24 h [283]. Representative changes of GSCs and U87MG under optical microscopy after 48 h in standard and low-glucose BHB supplemented media are shown in Supplementary Figure S11b.

We therefore asked if relative changes in protein expression due to cell culture media composition could have taken place before the 24 h point, as metabolic adaptation to severe glucose deprivation would need to be swift to ensure adequate survival. Rapid changes in protein expression in nutrient stress (glucose depletion) have been described for other enzymes [355-357]. Figure 34 shows that there was no differential expression of OXCT1 in GSCs and U87MG at 6h. Changes in glucose and BHB concentrations had no effect on OXCT1 at the protein level.

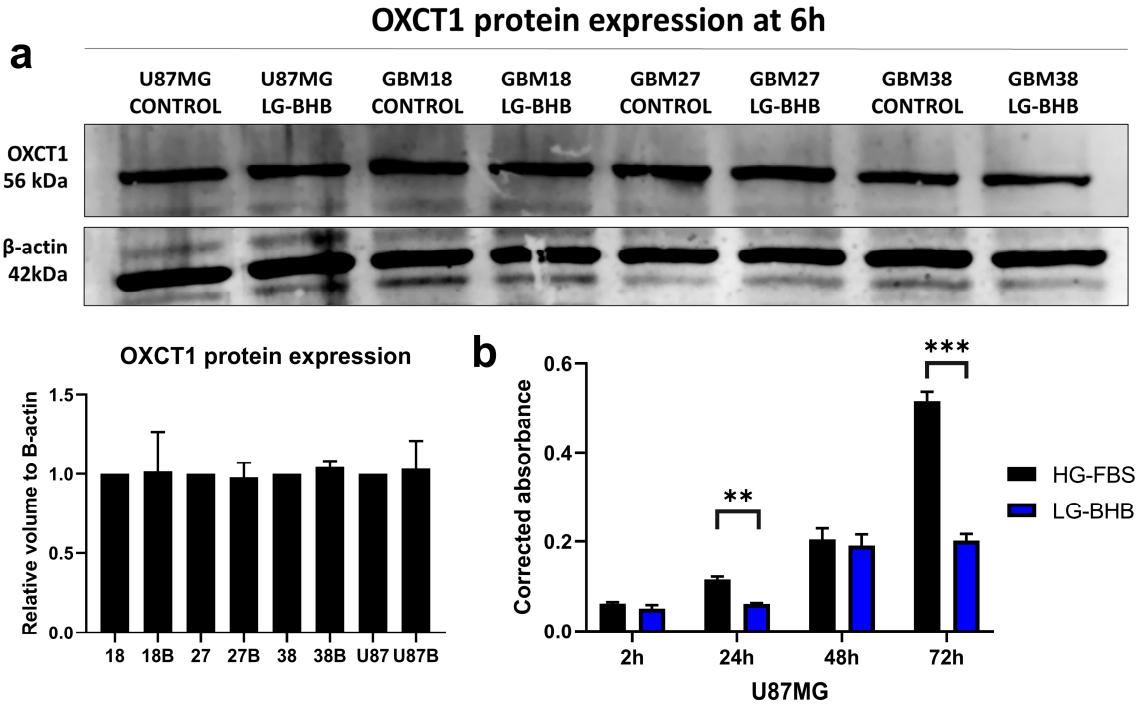

Figure 34. (a) Western Blot analysis and volume quantification of OXCT1 expression in GSCs and U87MG cell lines. Cells were exposed for 6 h to standard cell culture media and custom LG-BHB media (0.5 mM glucose and 10 mM BHB). Quantification data is representative of three independent experiments. **(b) MTS assays to evaluate U87MG growth under standard media and LG-BHB custom media.** Two-way ANOVA with Tukey correction, $p < 0.05$ *; $p < 0.01$ **; $p < 0.001$ ***, two biological replicates, each with n=4.

Owing to previous studies, U87MG is a well-characterized model for comparative evaluation of BHB-compensated glucose deprivation [283; 358; 359]. U87MG is recognized to harbor a highly aberrant genomic structure [360-362]. Working with a uniform genetic background provides a model to test whether metabolic changes could lead to stable, long-term changes in proliferation [323; 363]. As previously suggested by our data, the complete eradication of oxidative-like GSCs might require more targeted approaches. Hoping to better understand how classical Warburg-like phenotypes adapt

to nutrient stress, we decided to continue investigating the effects of metabolic modulation in U87MG.

Accordingly, we determined the long-term cell culture viability and ATP-synthesis capacity of U87MG in different nutrient conditions. We detected a slight potentiation of ATP production in the presence of BHB in the control and glucose-only groups, especially after 5 days of continuous growth. Interestingly, even though ATP production in the glutamine-only and basal DMEM conditions drastically decreased after 5 days, there was still a non-trivial amount of bioluminescent signal (i.e., viable cells).

Additionally, we tested if chronic exposure to BHB during normal cell subculturing could change the response to BHB-compensated restriction of glucose and glutamine, but ATP-synthesis remained unaltered, with cells unable to efficiently use BHB as a fuel (Supplementary Figure S12).

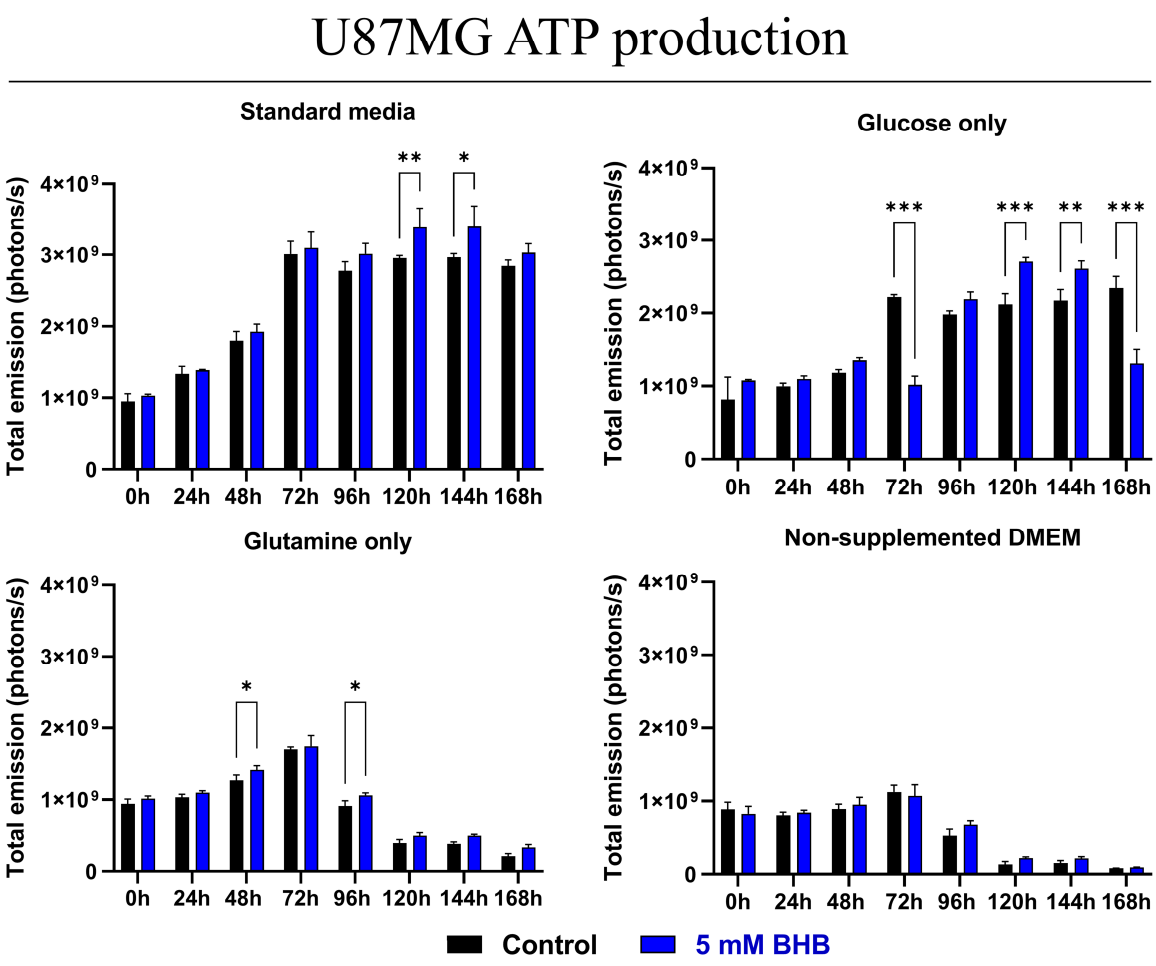

Figure 35. ATP-linked bioluminescence of U87MG growing in several conditions of modified DMEM for up to 7 days. Bioenergetic production of ATP is directly correlated with cell viability and

number. All experiments were performed in 2 biological replicates. Two-way ANOVA with Bonferroni correction. *** $p < 0.05$ *; $p < 0.01$ **; $p < 0.001$ ***.

4.6.2. Cyclical culturing of U87MG in LG-BHB medium permanently modified their morphological and metabolic phenotype

We selected cell culture conditions that mimic clinically-relevant, severe glucose deprivation compensated by a deep ketogenic state (glucose concentrations of 0.5 mM or 9 mg/dl) [350; 364]. Extremely low blood glucose levels are physiologically tolerable for brief periods upon ketogenic adaptation [365].

Our *in vitro* ketogenic treatment was applied in alternating 7-day cycles for a total of 8 weeks. Upon completion of the final LG-BHB cycle, we allowed cells to grow undisturbed for 15 days and observed significant changes in morphology (number of branches and branch-length) and much slower proliferation rates when compared to standard media controls.

During the cyclical nutrient modulation, we compared LG-BHB cell viability with HG-FBS controls (Supplementary Figure S14). Comparative optical microscopy images were acquired during all stages of subculturing. At the end of the glucose-deprivation sequence, we allowed cells to grow for 90 days in HG-FBS (Supplementary Figures S15 and S16).

As an endpoint, we examined the resulting modified morphology using branch length quantification and real-time metabolic profiles using Seahorse XF technology (Figure 36).

Control U87MG had a higher number of protrusions, but of much lower length than LG-BHB treated cells. After exposing cells to 4 cycles of metabolic treatment and an extended recovery period, the typical fusiform cell body of U87MG was substituted by a unipolar/bipolar/multipolar shape (resembling sensory neurons or interneurons). Branch length was 58.94 ±12.75 µm in control U87MG and 216.1 ± 53.32 µm in surviving LG-BHB cells.

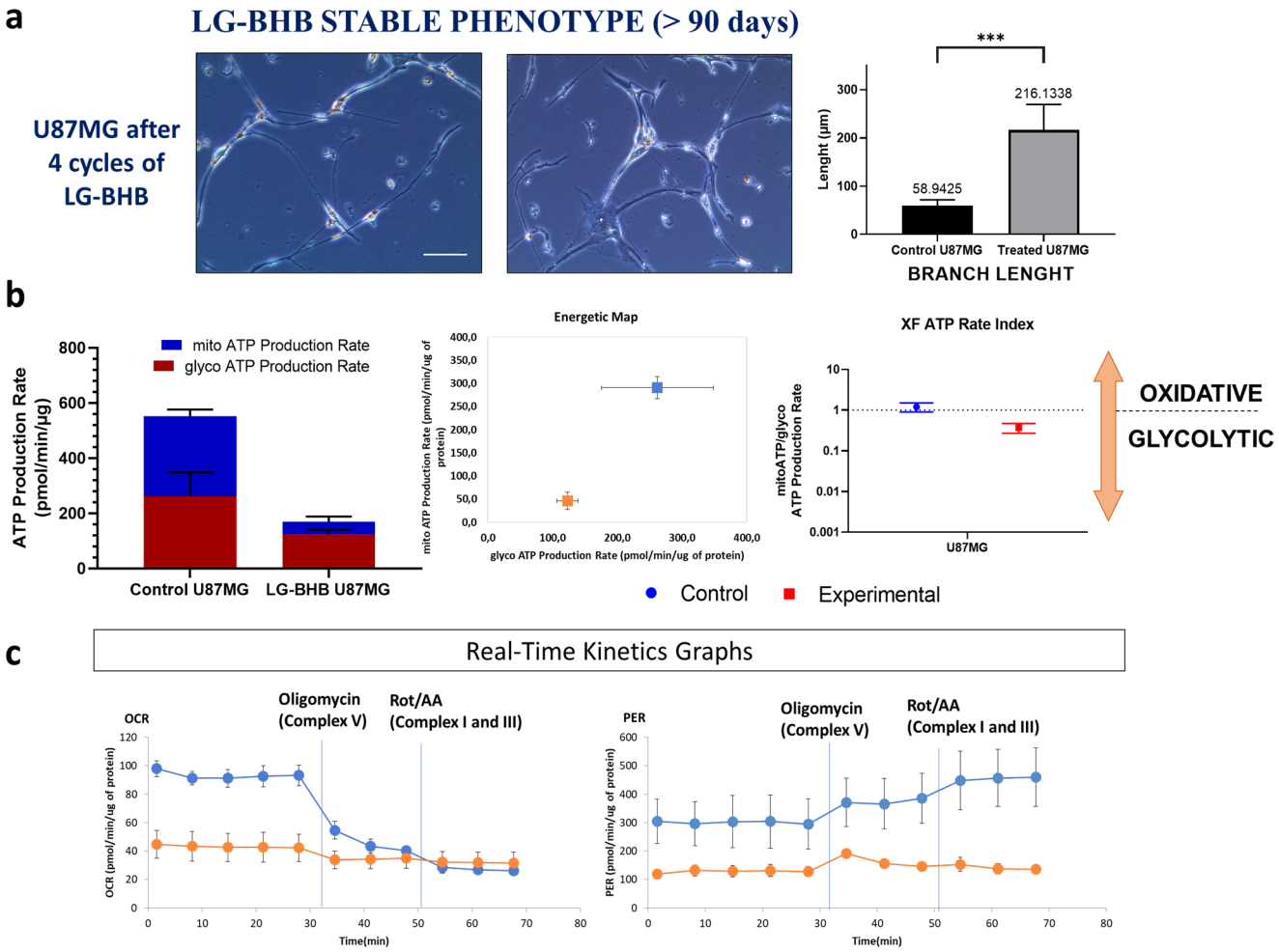

Figure 36. (a) Stable morphological changes in U87MG after 4 cycles of LG-BHB. Cell branch length was quantified in confluent control cells and modified U87MG after 90 days (n=6). Unpaired t test with Welch's correction, $p < 0.05$ *; $p < 0.01$ **; $p < 0.001$ ***. Scale bar = 100 um. **(b) Glycolytic and mitochondrial ATP production rates, Seahorse XF Energetic Map and XF ATP Rate Index comparing control U87MG and modified U87MG growing in HG-FBS for 90 days.** Modified U87MG have a low-energetic phenotype, with a relative shift towards aerobic glycolysis and lower OCR. **(c) Seahorse XF real-time kinetic graphs.** OCR and PER values are represented in basal conditions and after oligomycin (complex V) and rotenone/antimycin A (complex I and III) inhibition. Measurements are performed at 6 min intervals. Oligomycin injection is expected to rise PER to compensate for mitochondrial ATP synthesis (ATP-linked OCR and glycolytic capacity on PER), whereas complete inhibition of the electron transport chain (ETC) indicates residual OCR and maximal glycolytic reserve. We can observe that modified U87MG are unaffected by mitochondrial inhibition injection.

In the Seahorse XF Real-Time ATP assay, treated U87MG had a significantly reduced global energetic state, shifting towards glycolytic ATP production in the XF ATP Rate Index. This is concordant with a "quiescent" phenotype in the Seahorse XF

Metabolic Map. Control U87MG closely recapitulated the bioenergetic profile shown in our previous experiments, with an equal distribution between mito/glycoATP.

In LG-BHB treated cells, inhibition of complex V (oligomycin) only reduced OCR minimally, not being accompanied by the expected increase in ECAR/PER. Similarly, attempted inhibition of complex I and III (rotenone/antimycin A) did not affect metabolically treated cells at all.

In summary, cyclical glucose deprivation with BHB compensation in U87MG was able to produce stable, slowly-proliferating, and low-energetic metabolic phenotypes. This was achieved by performing a clonal selection using exclusively changes in nutrient availability. Further characterization will be required to understand the underlying metabolic rewiring.

4.7. Genes involved in metabolic regulation are associated with patient survival

To perform an in-depth examination of genetic expression profiles in our GSCs, we designed a custom list of genes implicated in the regulation of OXPHOS, glycolysis and glutaminolysis, modulated though *AMPK* signaling (MF), PDK-PDH complex (DCA), *LDH* targeting (SOD) and glutaminolytic enzymes (DON), based on canonical KEGG pathways [315]. We included well-known regulators of glycolysis and glutaminolysis, such as *TP53* and *MYC*, as well as TCA cycle enzymes and biologically relevant glucose and monocarboxylate transporters (complete list available in Supplementary Table S1).

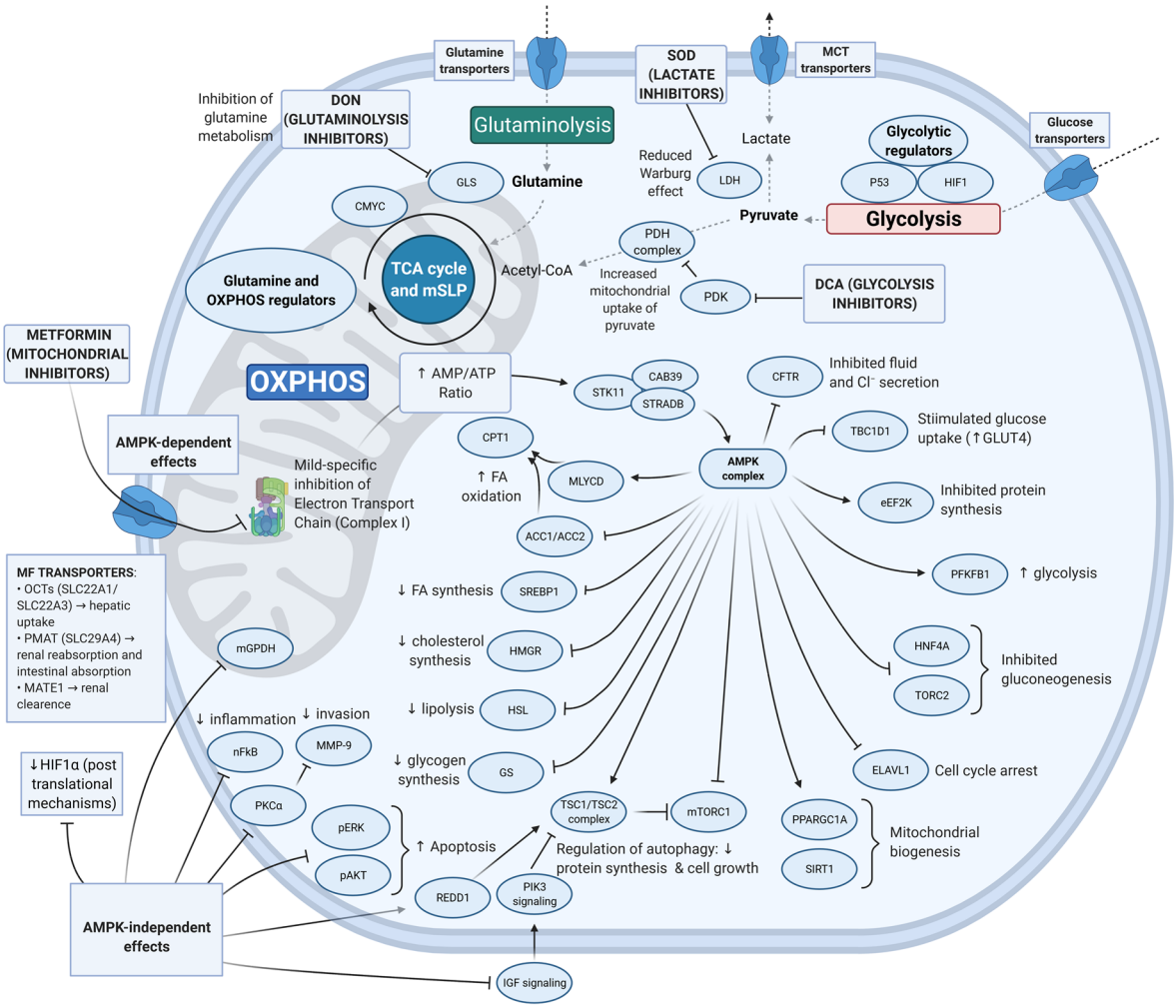

Figure 37. Manually curated list of metabolic genes for expression analysis. MF acts through AMPK dependent and independent mechanisms, with the primary effects focusing on AMPK activation via AMP/ATP ratio. Modulation of glycolytic metabolism is symbolized in the central pyruvate junction: PDH complex and LDH isoforms (targets of DCA and SOD). Glutaminolysis can be diverted to mSLP or oxidation, thus encompassing all the TCA cycle. GLS and other glutamine-utilizing enzymes are inhibited by DON.

We investigated the influence on patient survival of targetable metabolic genes in TCGA high-grade glioma databases using the GlioVis platform [310], subdividing predictive genes by Verhaak molecular subtypes [21]. Following the same methodology as in our GSVA approach, *IDH*-mutant samples were excluded from this analysis, as *IDH*-mutant GBM has been recognized as a separate molecular and metabolic category [366].

We subdivided *IDH* wild-type samples by subtype, comparing high and low expression using Kaplan-Meier survival analysis. We determined 15 genes with statistically significant ($p < 0.05$) survival predictive capacity.

Table 7. TCGA *IDH* wild-type survival analysis of metabolic genes. Hazard ratio (HR) for survival applies to specific Verhaak subtypes or the whole cohort (all subtypes). HR < 1: lower mRNA expression equals higher survival. HR > 1: higher expression, higher survival.

GENE	HAZARD RATIO	SUBTYPE
LDHA	HR < 1	ALL
LDHA	HR < 1	PRONEURAL
SIRT1	HR < 1	CLASSICAL
SLC16A3	HR < 1	ALL
SREBF1	HR < 1	ALL
SREBF1	HR < 1	CLASSICAL
TBCD	HR < 1	MESENCHYMAL
TSC2	HR < 1	MESENCHYMAL
ARNT	HR < 1	CLASSICAL
AKT3	HR < 1	CLASSICAL
FBP1	HR < 1	PRONEURAL
LDHB	HR > 1	ALL
LDHB	HR > 1	CLASSICAL
MAPK8	HR > 1	CLASSICAL
MYC	HR > 1	PRONEURAL
PDK3	HR > 1	CLASSICAL
TP53	HR > 1	PRONEURAL
PFKB1	HR > 1	ALL

In our own RNA-seq datasets, predictive genes were expressed heterogeneously across all three principal GSCs (Supplementary Figure S17). Unfortunately, statistical significance between different cell line HR-grouped average expression was not reached due to high data dispersion. Although our previous classification of GSCs identified mesenchymal-like (GBM18 and GBM38) and proneural-like (GBM27) characteristics, TCGA microarray gene expression from bulk samples and RNA-seq from cell lines are

not directly comparable [158]. To further explore the metabolic landscape of our GSCs, we studied their copy number variations via CGH analysis [367], revealing only one homozygous amplification in the *SDHA* gene in GBM38 (Supplementary Figure S18). Clear differences were observed in the copy number profiles between cell lines, which could correlate with basal metabolic states and patterns of resistance to metabolic inhibitors.

Despite methodological issues to translate cell-specific data to patient cohorts, expression of metabolism-involved genes in tissue samples could be applied to develop predictive models for patient stratification [368; 369].

4.7.1. A Prognostic Index for GBM survival, based on metabolic genes

The aforementioned list of survival-associated metabolic genes was evaluated in the GBM-BioDP platform, exploring TCGA GBM databases to determine if specific sample clustering of mRNA expression could be a predictor of survival in larger cohorts [370; 371].

As shown in the hierarchical cluster (HC) of Figure 38, 13 survival-associated metabolic enzymes were mapped to mRNA expression patterns in the TCGA, separating patients into two main clusters.

In the right patient cluster (upper cyan bar), we can observe a higher percentage of samples from the mesenchymal subtype (red in the subtype row), while the left cluster (upper red bar) contains a higher percentage of mixed samples (proneural, classical and neural, identified as purple, blue and green, respectively). In the survival analysis, patients with a PI in the first quartile (1Qt) demonstrated significantly longer survival than those in 4Qt (HR 3.01, p-value=0), even after adjusting for age and *MGMT* methylation status in the Cox covariate model. This observation was applicable to all Verhaak subgroups. Thus, a PI in 4Qt was universally associated with lower survival.

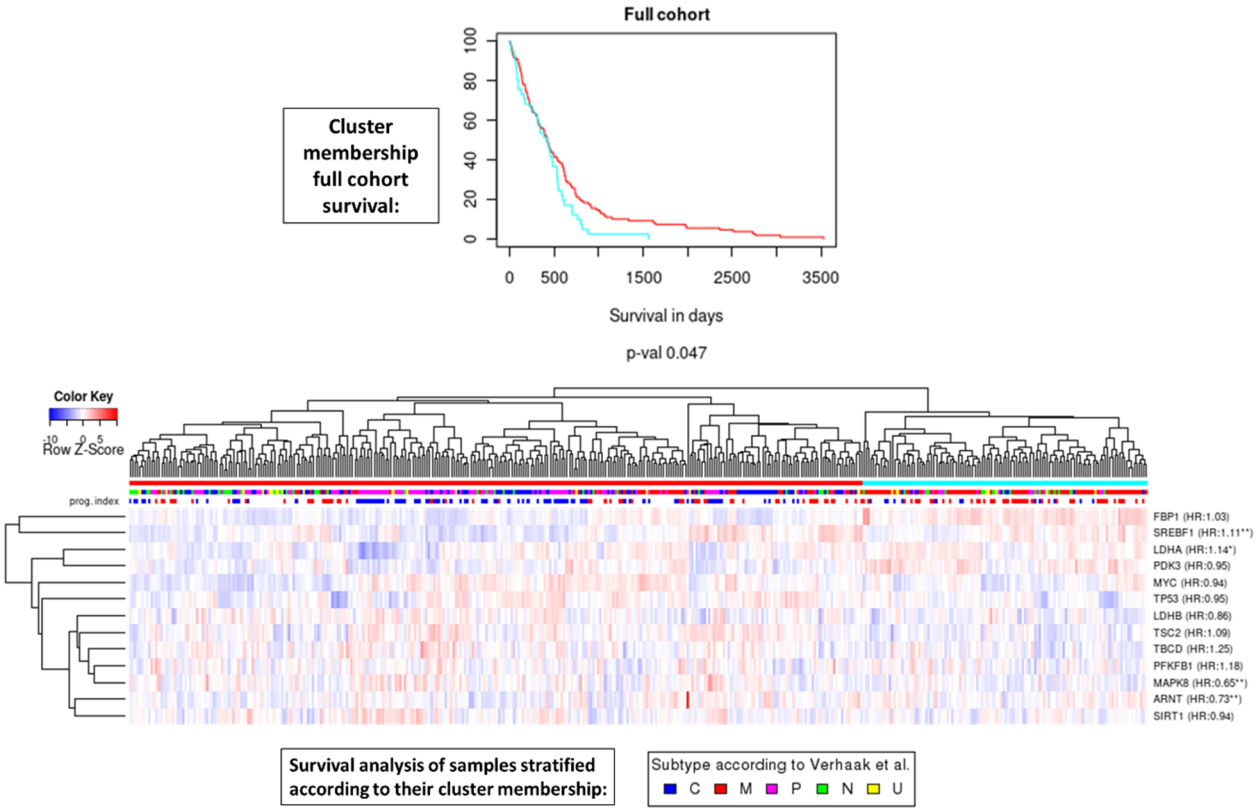

Figure 38. Survival analysis based on the impact of a multi-gene prognostic index. GBM-BioDP separated GBM patients into two main clusters by mRNA expression of 13 metabolic enzymes in the TCGA database. Molecule names are annotated with Hazard Ratios (HR) from Cox analysis; * indicates HRs with p-vals < 0.1; ** indicates HRs with p-vals <= 0.05. Verhaak subtypes: C (classical); M (mesenchymal); P (proneural); N (neural); U (undetermined).

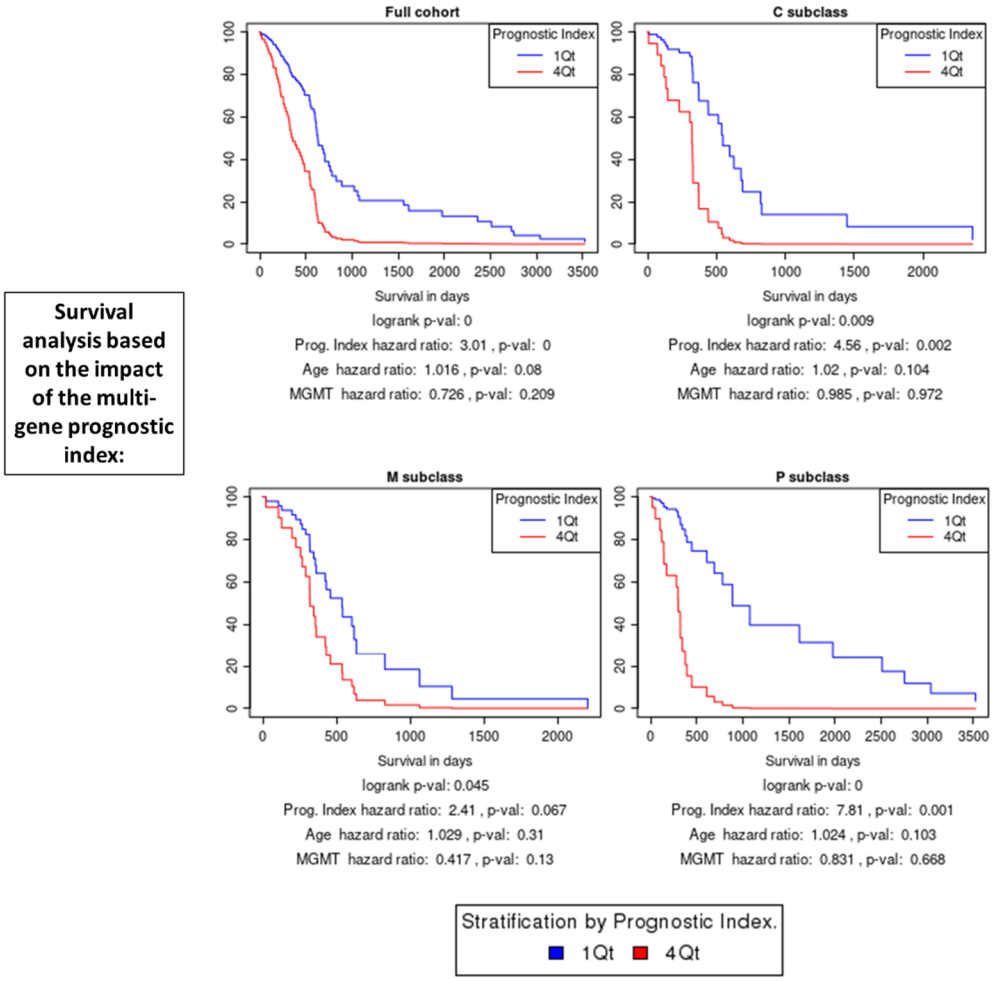

Figure 39. Kaplan-Maier analysis of prognostic index (PI) for the full cohort and Verhaak subtypes compared to overall survival. mRNA expression values for metabolic genes stratified patients by weight averaging the genetic expression with the regression coefficients of a multi-gene Cox proportional hazards model.

In summary, our results indicate that a statistical exploration of mRNA expression of genes involved in metabolic function could serve as a useful tool for patient stratification. Further clinical validation in individual samples and correlations with standard and metabolic treatment would be necessary to confirm this prognostic capacity.

4.7.2. GBM stratification based on protein expression

Transcript levels are not always sufficient to establish genotype-phenotype relationships, which often requires examining protein-level evidence [372]. It must be noted that protein quantification data is scarcer in the TCGA cohort. Therefore, we

evaluated the full list of metabolic genes to obtain a prognostic factor based on normalized and clinically relevant protein expression in surgical samples (Figures 41 and 42).

Relative protein expression of 17 enzymes involved in drug-target pathways generated an age/*MGMT* adjusted stratification model with a PI HR (1Qt vs 4Qt) of 19.63 (p=0.008). In the cluster membership, almost all patients in the high survival group (cyan bar) were of the proneural subtype. Unfortunately, subclassification according to Veerhak subtypes is not possible when analyzing protein expression due to the lower number of samples (models not convergent). Gene-to-protein correlation heatmaps by aggregated platforms are presented in Figure 40. There was a high degree of correlation between mRNA and protein expression within the same genes (e.g., IGF1R gene and IGF-1R-beta-R-C antibody).

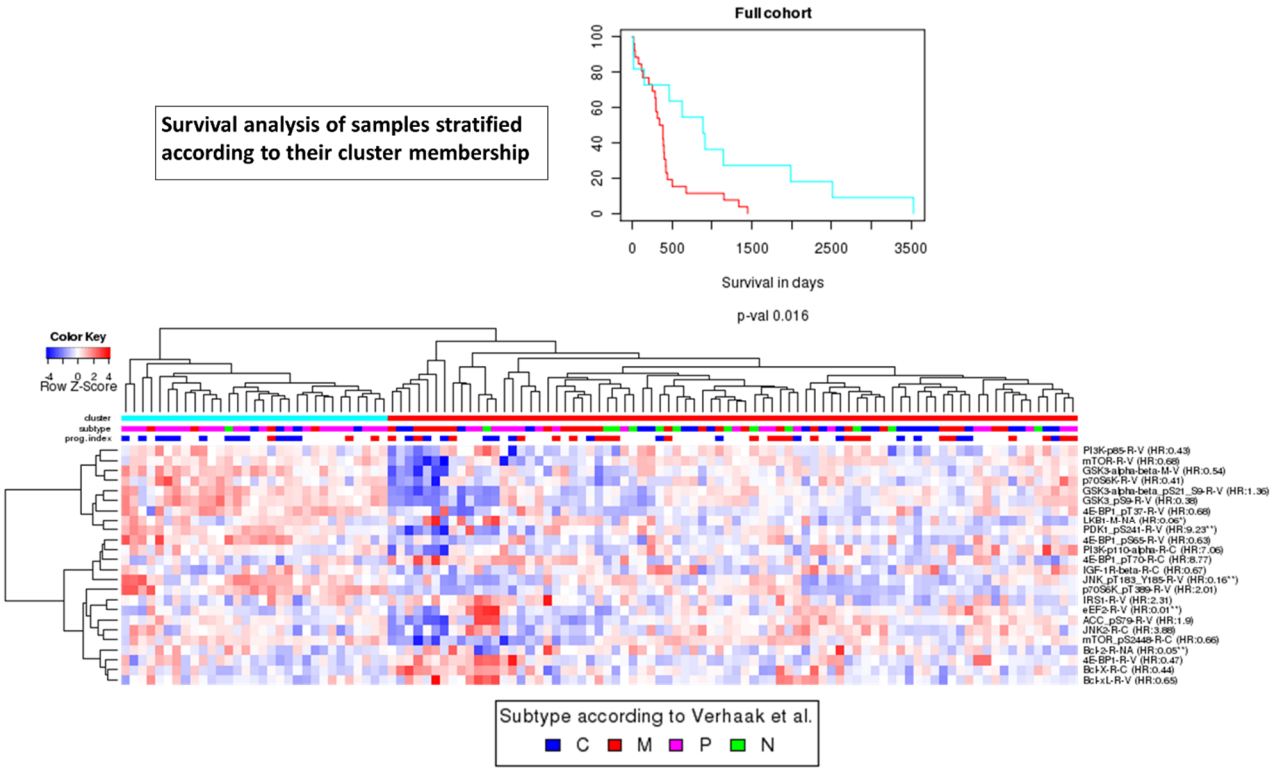

Figure 40. Survival analysis based on the impact of a multi-gene prognostic index. The Glioblastoma Bio Discovery Portal separated GBM patients into two main clusters by normalized reverse phase protein array (RPPA) expression. We can observe a higher percentage of proneural samples in the left cluster (cyan bar) while the right cluster (red bar) contains a higher percentage of classical, mesenchymal and proneural samples.

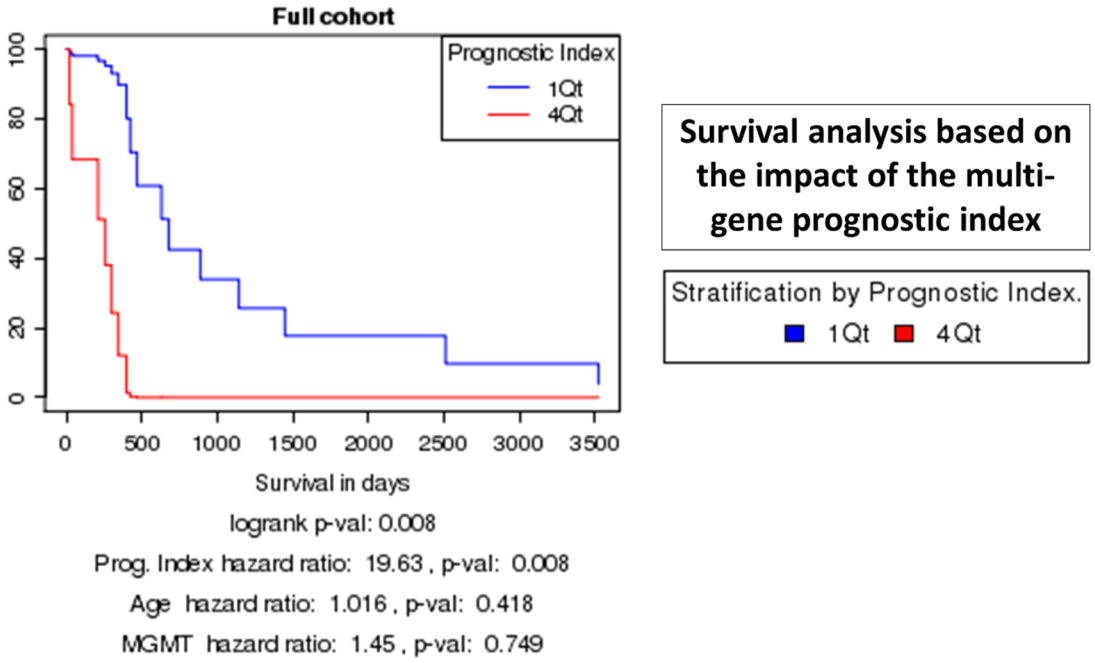

Figure 41. Kaplan-Maier analysis of prognostic index (PI) for the full cohort compared to overall survival. This graph shows that patients with a PI in the first quartile survived longer than those in the fourth (HR 19.63, p-value=0.008).

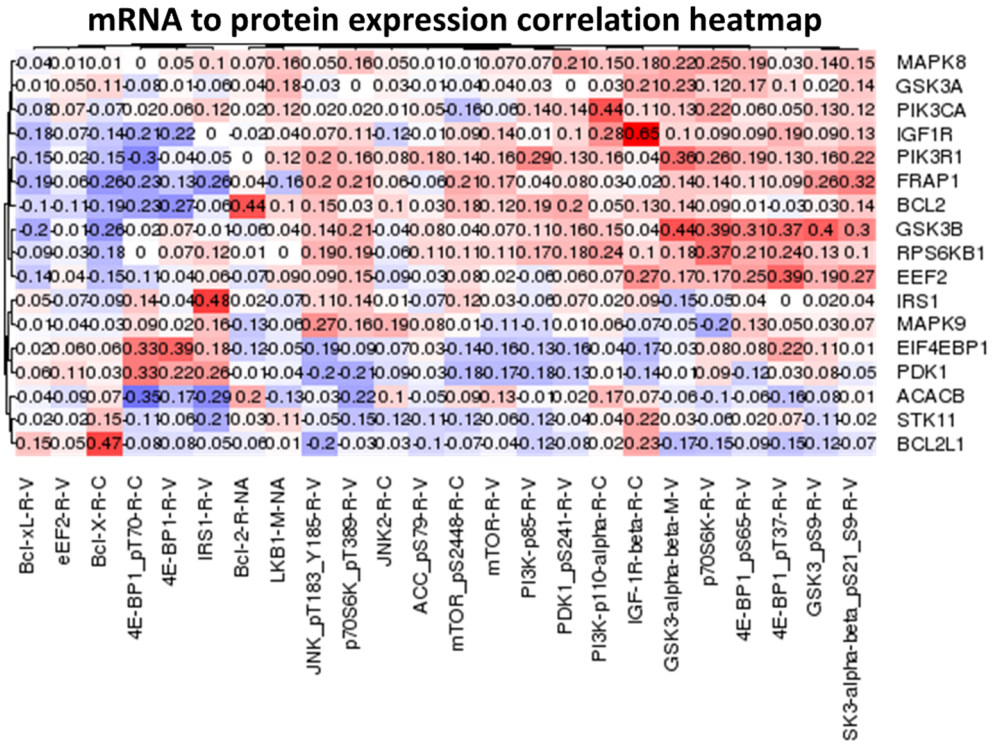

Figure 42. Heatmap of the correlation between mRNA expression and protein-level evidence for the selected genes. Values in red indicate a high level of correlation, values in blue a low level.

V. DISCUSSION

5. Discussion

During the last two decades, cancer metabolism has regained attention as a promising therapeutic target, coinciding with the development of new technologies for *in vitro* and clinical assessment of bioenergetics. As our understanding of metabolic reprogramming grows, two seemingly competing paradigms at the core of malignant transformation are slowly conquering improvements in patient survival and quality of life.

Despite uncertainty regarding oncogenesis, which, in turn, determines the underlying rationale of upcoming therapies (leveraging DNA or metabolic alterations), we believe that major advancements can be attained by integrating conflicting views into a single unified theory.

GBM is a unique model to study bioenergetic alterations due to profuse molecular heterogeneity, with a gamut of mitochondrial defects, SLP adaptations and oxygen consumption seemingly coexisting in cell culture, tissue samples and clinical metabolic imaging; more specifically, GSCs are the subpopulation with the uppermost metabolic flexibility [151; 157; 322; 373; 374]. Extremely discouraging survival rates are a compelling reason to explore new therapeutic options, predominantly in combination with standard of care [375].

Given the high intratumoral molecular and metabolic heterogeneity, it is becoming increasingly clear that designing a successful metabolic therapy will entail simultaneous targeting of glycolytic, glutaminolytic and, if present, oxidative phenotypes [376].

In this work, we described how metabolic modulation could be leveraged to inhibit GBM proliferation, both in GSCs and non-stem cell lines, demonstrating that distinct, stable, basal metabolic phenotypes contrast in their susceptibility to treatment. Synergistic strategies can potentiate DNA-damaging agents and reduce dosing requirements. We present a comparison between untreated and metabolically treated GSCs populations, leading us to hypothesize that inhibiting metabolic pathways might not only kill malignant cells, but also make them vulnerable against subsequent targeting ("metabolic priming") [340].

In the following sections, we discuss our results in chronological order, structuring our analysis around the most relevant, novel, and critical findings.

To begin from a clinical perspective, we highlight that tumor stratification based on single-cell and regional metabolic differences is not limited to the application of metabolic therapy but can have serious repercussions on the predicted response to chemoradiotherapy [182; 377; 378]. In line with this idea, we showed that standard 18F-FDG PET imaging and GSVA subtyping of metabolic dependencies could be useful for patient stratification (Figures 13 and 15). While glucose uptake (GLUT1/3 via 18F-FDG) is evaluated routinely in most solid tumors, novel PET-tracers and MRS techniques for additional metabolites lack standardization and clinical integration [379; 380]. The clinical relevance of substrate flux in light of heterogeneity and metabolic targeting is self-evident, but more research is needed to elucidate the impact on prognosis.

Warburgian dependencies in tumor samples and cell culture models are a well-recognized and wide-ranging feature of cancer, especially in GBM [119; 381]. Accordingly, we sought to understand how "bulk" tissue gene-expression profiles translated into our assortment of patient-derived stem and non-stem cells.

Previous inquiries into the bioenergetics of GSCs, as well as traditional cell lines, uncovered surprising metabolic heterogeneity [157; 322; 382]. Worth mentioning, isogenic mouse GSCs exhibited both a highly glycolytic/oxygen-dependent metabolism when compared to their own differentiated progeny, in concert with established cell lines such as U87MG and U251, suggesting higher metabolic plasticity of GSCs [151; 322]. It has been reported that human GSCs from surgical specimens have a considerably lower metabolic activity ("quiescent" phenotype), particularly when compared to U87MG and U251 (significantly more lactate and oxygen dependent per normalization unit) [322]. Contrary to our results, ECAR/OCR have been reported as higher in adherent cell lines than in stem-like neurospheres. This is no surprise given the ample oxygraphic heterogeneity induced by cell culture conditions and dynamic mitochondrial dysfunction [175]. Further characterization of the metabolic profiles of different GBM subtypes is warranted.

Even acknowledging the heterogeneity of GSCs, we were surprised by the high OCR of GBM27, at odds with Warburg's central hypothesis of damaged mitochondrial metabolism. Dynamic upregulation of OXPHOS in the functional portion of the chondriome might explain these differences, despite a global shift towards SLP. The presence of highly oxygen-dependent GSCs inside tumor will need to be addressed to prevent recurrence after metabolic therapy.

A potential limitation of oxygraphic studies is that the resulting ATP rates are based on mathematical extrapolations, calculated using general stoichiometries and phosphate/oxygen ratios that assume complete reduction of oxygen, as well as proton efflux rates directly translated into glycolytic ATP [309]. These conversions are still debated and might be influenced by mitochondrial integrity [383]. A detailed explanation of Seahorse XF raw data interpretation and the OCR paradox is provided in Supplementary Figure S19. We and others have reviewed the limitations of Clark polarography and oxygraphic tools such as Seahorse XF and Oroboros O2k for the partitioning of ATP [58; 175; 384]. Thus, throughout our work, we preferred the term "OCR/ECAR-linked ATP production" instead of "mito/glyco ATP" to avoid confusion.

Lastly, we were intrigued by the variability of OCR in U87MG. Bestowing to well-characterized and manifest lactate production, we expected a typically "Warburg-like" phenotype from U87MG. Preceding our experimental data, a bibliographic survey indicated that U87MG typically behaves as a highly glycolytic cell line (elevated basal ECAR); however, some experimental setups revealed a significant contribution from basal OCR [151; 172; 322; 385-387]. Even though rarely discussed, examining U87MG after FCCP (uncoupling) and rotenone/antimycin A (complete ETC shutdown) reveals a high proton leak and residual non-mitochondrial OCR [172; 386; 388; 389]. Maximal respiratory capacity of U87MG is also fairly inconsistent [151; 386; 387; 390]. Interestingly, maximal and spare respiratory capacity of normal astrocytes is significantly higher (up to 150% on average) than in U87MG cells [172; 343; 387; 391-402]. After injection of oligomycin (ATP-linked OXPHOS), we could observe a characteristic adaptation by upregulation of ECAR [322; 387; 388; 390; 403; 404]. This reveals partial mitochondrial dysfunction in U87MG, which could translate into susceptibility against simultaneous targeting of SLP and OXPHOS.

In dose response profiles, perhaps the most striking result was the high resistance of GBM27 against all tested drugs, with the exception of DON. This phenomenon might be owed to GBM27 slower proliferation rates and characteristically "oxidative" metabolism (up to 50% OCR-linked ATP). GBM18 and GBM38 were more sensitive to both MF and DCA, consistent with their basal metabolic phenotypes: lower basal OCR, more easily inhibited via MF, as well as higher lactate production and susceptibility to redirect pyruvate into the TCA cycle via DCA.

Gene and protein expression analysis has been carried out to confirm if dose-response profiles were associated with basal status of regulatory pathways. *PRKAA1* expression was highest in GBM27, correlating well with resistance to MF. *PRKAA2* was not expressed in our samples, and differences in *MTOR* did not reach statistical significance. Functional proteomic studies confirmed that phosphorylation at Thr-172 accounts for most AMPKα activation [405; 406]. We were unable to detect phospho-Thr172 activation at 24 h; based on previous reports, we hypothesized that activation of AMPKα at IC50 doses might have occurred prior to this point. We successfully detected phospho-Thr172 AMPKα activation in GBM18 and GBM38, with visible phosphorylation starting at 60 min. GBM27 did not phosphorylate AMPKα in the first 6 h, consistent with the need for higher concentrations and slower inhibitory responses. U87MG did not follow a clear trend for AMPKα activation, matching previous reports where 10 mM MF did not alter phospho-Thr172 at 6 h [407]. Our results indicate that treating U87MG with IC50-72 h doses of MF did not increase AMPKα phosphorylation above its basal threshold.

Sensitivity to DCA correlated with the intrinsic regulation of the PDH complex. GBM38, characterized by high ECAR and lowest *PDK3* expression, was the most sensitive to DCA. Conversely, GBM27, which demonstrated the highest *PDK3* expression, consistently required the highest concentrations, as would be expected by differential resistance against DCA by the target protein, PDK.

At a mechanistic level, subunits of PDK display variable sensitivity to inhibition by DCA: *PDK2* subunits are the most sensitive, *PDK1* and *PDK4* have intermediate binding affinity and *PDK3* are the most resistant (DCA *Ki PDK2* < *PDK1*≃ *PDK4* < *PDK3*) [331; 332]. As *PDK2* and *PDK4* were not expressed in our samples, and levels of *PDK1*

were similar across cell lines, differences in dose-response profiles were likely related to *PDK3*.

Regarding protein function, the catalytic subunit, PDH-E1α, has three phosphorylation sites: Ser293 (site 1), Ser300 (site 2), Ser232 (site 3). Phospho-Ser293 is the most common and potent activation site of the complex [408]. We quantified total PDH-E1α subunit and PDH-E1 phospho-Ser293, confirming de-phosphorylation (activation) at 6h of IC50-72 h treatment. This effect was most noticeable in GBM18, GBM27 and U87MG.

Continuing with the assessment of metabolic drugs, SOD was similarly inefficacious across all tested cell lines, including U87MG and GBM27, albeit with a higher degree of variability in the latter. Interestingly, *LDHA* and *LDHB* expression was up to 300 times higher in U87MG and 100 times higher in GSCs when compared to non-tumoral epileptic control, indicative of increased SLP metabolism though lactate production in all malignant cell lines (i.e., Warburg effect). Unable to detect clear correlations between qRT-PCR and drug resistance, we also compared expression between control and SOD IC50-72 h treated cells (Figure 22b). For the *LDHB* gene, mRNA expression analysis did not reveal statistically significant differences between groups. On the other hand, *LDHA* had almost 4 times lower expression in SOD-treated U87MG. We hypothesize that these relatively small expression changes might have been caused by normalization of the markedly upregulated basal expression of *LDHA* in U87MG, or by non-specific responses to reduction in viability. As a competitive pyruvate analog, at doses higher than 80 mM, as was our case, SOD likely disrupted other pathways beyond lactate production (e.g., alanine, fatty acid, insulin and gluconeogenesis metabolism) [409; 410].

Our GSCs appeared highly resistant to SOD, as evidenced when compared to much lower IC50s in other *in vitro* models, such as nasopharyngeal carcinoma and gastric cancer [411-413]. Nonetheless, more than 50% ECAR inhibition in real-time (after 5-min of incubation with SOD) has been reported with doses as low as 0.6 mM in H460 cells and 4.4 mM in A549 cells, suggesting that viability and changes in metabolic fluxes do not necessarily go hand in hand [414]. In studies where SOD was effective, it usually reached peak effects in the first 24 h [415]. Interestingly, as OXPHOS is considered the

main ATP source in healthy neuronal tissues, up to 20 mM oxamate was very well tolerated by normal neurons and astrocytes [416; 417]. Optimizing delivery and potency would be indispensable for successful clinical application of SOD.

To conclude, when we set out to develop a therapeutic strategy to induce metabolic lethality, we were looking for a readily available and thoroughly researched LDH inhibitor. As our primary focus is on translational medicine, we recognize that SOD, without prodrug modifications, is not a promising candidate, with only a limited number of animal studies [415; 418-420]. As far as we know, the efficacy of oxamate derivatives has not been evaluated in GSCs. Despite issues with potency, we were hoping to obtain distinct IC50 dose-response profiles, as hinted by basal metabolic dependencies. Resistance against SOD in our model should not discourage LDH targeting, which is biologically sound.

The last compound we examined in monotherapy is DON, a pan inhibitor of glutamine-utilizing enzymes. Glutaminolysis plays an essential role in cancer, contributing to biosynthesis of amino acids, nucleotides and fatty acids, regulation of oxidative stress and, upon conversion to α-ketoglutarate, serving as an mSLP fuel and anaplerotic carbon source to replenish TCA cycle intermediates [243; 421].

In our study, GBM18 was the most resistant to DON, while other GSCs appeared more vulnerable. In regards to viability, our results corroborate the inhibition profile in U87MG at 72 h recounted by Ohba *et al.*, with a similarly flattened inhibitory curve but a higher extrapolated IC50 [422]. DON exhibited a saturation point in terms of antiproliferative effects: rather than linear, dose-dependent cytotoxicity, we noted a cytostatic effect in GBM18, GBM38 and, to a lesser extent, GBM27.

In our experiments, *GLS1* expression was highest in GBM18 and lowest in GBM38, although the magnitude of these changes was low (Figure 19). Indeed, higher mRNA expression in GBM18 was accompanied with the need for higher doses of DON to reach the same inhibitory effect; correlations between doses and *GLS1* expression in other cell lines was not as self-evident. *GLS2* was not detectable in our samples. Differences in basal glutamine addiction could explain heterogeneous metabolic responses to glutaminase inhibitors, as described after DON treatment (Figure 32) [423].

Addressing the potential clinical relevance, we are aware that systemic application of MF at the IC50 values defined by our data would be impractical due to risk of lactic acidosis [424]. Even though direct transformations from *in vitro* to *in vivo* concentrations are unfeasible due to pharmacokinetic and pharmacodynamic differences, screening compounds for the highest potency and lowest toxicity is the first logical step to improve translational prospects [425; 426]. In this sense, clinical trials with DCA at doses sufficient for cancer treatment demonstrated safety and efficacy [237; 427]. Furthermore, DCA could be administered to prevent MF-induced lactic acidosis [428]. Our results largely agree with previously published data, highlighting that, *in vitro,* DCA concentrations ≥ 10 mM are required for consistent anti-proliferative responses [429-432]. Shen *et al.* demonstrated clear differential sensitivity to DCA between tumoral and healthy cells [433]. Lastly, DON binds to the active site of GLS in an irreversible manner, presenting a polar structure and reactive moiety that reduces its transport across the BBB [434; 435]. Even still, the KD significantly increases the delivery of DON to the CNS [259]. Toxicity can be further avoided by glutamine depletion strategies [189; 259]. Future *in vivo* studies could involve prodrugs with optimized BBB delivery and reduced gastrointestinal/immune toxicity [435-438].

To improve the translational outlook and tackle GBM heterogeneity, metabolic therapies could focus on multiple cellular pathways to achieve compounded effects. Potentiating standard of care opens the door to a variety of combinatorial approaches [439-446]. TMZ has already been evaluated with MF and DCA in all stages of clinical research: *in vitro* models, including GSCs, animal models and human trials, with moderate, dose-dependent antiproliferative effects [241; 442; 447-450]. On the other hand, combinatory experiments with radiotherapy/radiomimetics remain relatively unexplored. In traditional GBM cell lines, MF and DCA enhanced the effects of radiotherapy, but stem cells had not been evaluated in prior studies [341; 386]. To the extent of our knowledge, the accompanying publication was the first to report the combinatorial effects of the radiomimetic drug bleomycin with MF, DCA and DON (Table 6).

Examining our synergy results, we want to bring attention to the fact that GBM27, identified as distinctly oxygen consuming, benefited the most from pairing bleomycin

with metabolic modulators. Synergistic interactions would allow for substantial dose reduction, as individual IC50 concentrations for MF and DCA were higher than in other cell lines, thus reducing toxicity to normal cells. Notwithstanding, it is important to examine the full CI/Fa range for each drug, as additive and even "antagonistic" effects did not exclude dose-reduction at a specific Fa: for example, bleomycin-DCA combinations in GBM18 and GBM38 would allow for dose reduction of bleomycin at Fa ≥ 0.5 even though the combination was theoretically "antagonistic" in terms of CI values.

One of the strengths of our study is the design in a constant drug ratio: this allows for a data-driven, more accurate and comprehensive description of synergy/antagonism, without relying solely on computer simulations [451]. Conversely, a potential weakness is the limited *in vitro* validation, which would require performing a complete suite of viability experiments. Despite this, attending to parameters of variability, the accuracy of predictive models for synergy has been thoroughly established [452]. More recent mathematical models based on nonlinear mixed-effects using the Loewe additivity index (MixLow), response surface, or revisions of the Chou-Talalay theorem such as "code for the identification of synergism numerically efficient" (CISNE), have attempted to improve curve fitting, but they lack standardization and integration, reducing comparability and confidence in the results [453; 454].

From a clinical perspective, reducing the risk of toxicity associated with metabolic drugs is feasible, as even low "interconvertible" doses from *in vitro* experiments have already demonstrated improved outcomes in combination with standard of care [207; 424; 455; 456].

Beyond acute, immediate effects on viability, the lasting metabolic changes induced by MF, DCA and DON had not been properly illustrated until now. Preexisting literature evaluated the short-term OCR and ECAR responses to MF in traditional glioma cell lines [386], as well as pancreatic and colorectal CSCs [457; 458]. Oxygraphic data after DCA exposure has been reported in glioma, melanoma and pancreatic cancer [239; 342; 386; 459-461]. Bioenergetic measurements for DON have not been described at all.

In terms of OCR/ECAR, all metabolic modulators exerted biologically coherent responses, especially well-defined after IC50-72 h treatment with MF and DCA (Figure 29).

MF shifted surviving cells to a primarily glycolytic phenotype, with very low percentages of OCR-linked ATP generation. These results are consistent with Seahorse XF assays in traditional glioma cell lines and colon CSCs [407; 457]. Sesen *et al.* reported inhibition of OCR and increased ECAR in U87MG treated with 10 mM MF for 48 h, reaching almost 90–95% ECAR from basal 70–80%, while decreasing total ATP production by approximately 30% [341]. In our data, the metabolic effects of MF were determined by the sensitivity of each cell line.

DCA induced bioenergetic changes consistent with forced activation of PDH, in congruence with previous reports [386; 433]. Interestingly, when comparing total ATP production rates, DCA only reached maximal attenuation of approximately 50% relative to control. Indeed, DCA is believed to act more as a "metabolic modulator", not only reducing proliferation but also "shifting" the glycolysis/OXPHOS ratio via increased mitochondrial uptake of pyruvate [324; 462].

Lastly, DON yielded heterogeneous metabolic adaptations, but consistently inhibited total ATP production in all tested cell lines. In previous reports, changes in OCR could not be detected after exposing U7MG to low concentrations of DON [423]. Preclinical data shows that relatively high *in vitro* doses of DON might be required in some cancer models, which might explain the variability in antiproliferative and metabolic effects [463-468].

GLS inhibitors such as DON, EGCG and BPTES could be employed in concert with Seahorse XF technology to determine glutamine contribution to oxidative ATP synthesis, as OCR from glucose and glutamine cannot be distinguished without experimental removal of substrate or acute injection of glutamine inhibitors [469]. If we inhibit GLS activity, the reduction in total ATP production will be correlated with reduced TCA cycle entry of glutamine-derived intermediaries for oxidation [243].

After treatment with DON, a drop in total ATP could be accompanied by compensatory oxidation of glucose (ATP Rate Index increases, e.g., GBM18, GBM27),

lactate production (ATP Rate Index decreases; this shift was not detected with DON but was shown with MF in all cell lines) or constant glucose oxidation/fermentation (ATP Rate Index remains unchanged, e.g., GBM38, U87MG). We can conclude that increases in mitochondrial ATP cannot originate from enhanced glutamine oxidation, as GLS is being inhibited by DON: this was apparent in GBM27, where inhibition of glutaminolysis led to preferential oxidation of glucose (indicative of a degree of metabolic flexibility). GBM18 presented a similar trend, albeit less pronounced, whereas GBM38 and U87MG saw their total ATP production diminished without compensatory shifts in ECAR/OCR.

Continuing with our inquiry into nutrient-based metabolic modulation, we set out to investigate the response of U87MG to severe glucose deprivation and BHB supplementation. Safe, ketogenically compensated, medically induced hypoglycemia has been proposed as a form of anti-cancer therapy since the case reports published by Wilhelm Brünings more than eighty years ago [470]. It was not until rigorous clinical studies corroborated the remarkable human metabolic flexibility after prolonged fasting that this approach gained a viable outlook [113; 471]. Seminal work from Drenick *et al.* demonstrated that, after a 2-month fast in obese subjects, insulin failed to precipitate hypoglycemic reactions with plasma glucose as low as 0.5 mM (9 mg/dl) [364; 365]. During prolonged fasting, long-term maintenance of blood glucose levels below 30 mg/dL (1.70 mM) had been closely monitored without any adverse effects [472; 473].

Indeed, physiological inhibition of gluconeogenesis must be preceded by ketogenic adaptation to optimize utilization of fat-derived fuels. After this period, sustained glucose concentrations of approximately 0.5 to 2 mM are not outside the realm of physiology, given adequate levels of compensatory metabolites (e.g., ketone bodies) [474; 475]. Glucose deprivation could be further enhanced by the application of titerable hypoglycemic agents, such as SGLT2 inhibitors (kidney glucose reabsorption), CS-917 and MB07803 (second generation gluconeogenesis inhibitors), together with direct glucose perfusion to pertinent organs [113; 471; 476-478]. Given that cerebrospinal fluid/plasma glucose ratios are approximately 0.6-0.7, and brain extraction of serum glucose was determined as 40% in animal models, competition for glucose between the growing tumoral mass and normal brain would be highly potentiated [479].

While the straight-forward hypothesis that abrupt deprivation of glucose and glutamine reduces cell proliferation is part of routine cell culturing, prospective evaluation of BHB-compensated glucose restriction has not been well described [269; 480-487]. In pilot clinical trials, aiming towards a global reduction of circulating glucose facilitated by ketogenesis is a semi-standardized component of KMT, particularly in tumors with strong Warburgian dependencies [90; 274; 284]. Metabolically supported chemotherapy with insulin-induced hypoglycemia showed promising survival improvements in advanced and metastatic cancer [181; 456; 488; 489]. Unfortunately, metabolic stratification of patients is often overlooked, leading to mixed responses and confounding factors.

To explore the ketolytic capacity of our cell lines, we first determined the presence of the rate limiting enzyme of ketolysis, OXCT1 [490]. Glucose restriction strategies (such as the KD) or anti-glycolytic drugs are only fitting if ketone bodies provided to normal cells cannot be hijacked by cancer cells. In this framework, it has been suggested that tumor cells cannot utilize ketone bodies for ATP synthesis [283; 491; 492]. To date, OXCT1 was only evaluated in traditional glioma cell lines and tissue samples, not GSCs [283; 353]. In our experiments, we detected OXCT1 expression in both GSCs and U87MG, irrespective of timing, glucose depletion and presence of BHB in cell culture media.

As our point of comparison, previous studies indicated that U87MG can express OXCT1 at the protein level, with no apparent changes by addition of BHB [283]. In fact, secondary enzymes of ketolysis have been found at both the mRNA and protein level in U87MG, U251MG, LNT-229, T98G and A172; these findings are contrary to histopathological analysis where extrahepatic tumors did not express OXCT1 [493; 494]. However, the detection of OXCT1 was not correlated with survival in glucose depleted, BHB compensated conditions. Our data confirms previous publications where U87MG was not able to maintain viability under glucose deprived, BHB compensated conditions (as shown in Figure 35). We have not encountered reports of any cancer cell lines able to withstand long-term survival under glucose deprived, BHB supplemented conditions [283; 480; 491]. Maurer *et al.* described immediate loss of viability and apoptosis in U87MG cells undergoing BHB-compensated glucose deprivation, whereas primary rat

astrocytes could survive for up to 12 days [495]. *In vivo*, metabolic imaging reveals accumulation of ketone bodies in tumoral tissues in patients following a KD, but it remains unclear whether uptake equals utilization [282].

Given that glucose depletion eradicated most, but not all, U87MG cells after a 7-day period, we investigated how a cyclical *in vitro* formulation of glucose-depleted KMT could lead to stable, enduring changes in morphology and metabolic phenotypes. We propose that this could be defined as a clonal selection or metabolic reprogramming strategy. Targeted differentiation has proven remarkable clinical benefits in hematologic malignancies, especially acute promyelocytic leukemia, where remission rates exceed 90% after treatment with differentiation-inducing agents [270; 496]. In the metabolic theory of cancer, selecting mitochondrially healthy clones would be a way to reverse SLP without the need to decipher all the effectors of molecular rewiring, reducing heterogeneity into a manageable number of metabolic categories [60; 90; 120; 497].

We tested several combinations of glucose and BHB to determine the optimal degree of selective pressure (Supplementary Figure S13). After exposing U87MG to 2.5 mM glucose and 10 mM BHB, cells underwent morphological changes consistent with dedifferentiation and neurospheroidal growth, rather than diminished proliferation. Comparable changes have been reported by serum-free subculturing in this and other traditional GBM cell lines [498]. We determined that *in vitro* glucose concentrations ≤ 0.5 mM were required for effective eradication of highly proliferative U87MG clones (Supplementary Figure S14).

While we did not observe immediate changes in the HG-FBS recovery, as evidenced by viability assays, it was after the last LG-BHB cycle when surviving U87MG cells started to show morphological changes. After a prolonged recovery period (>90 days), LG-BHB adapted cells growing in HG-FBS displayed a predominantly multipolar shape with extended branch length.

Owing to its extremely slow proliferation and delicate nature, examining this modified cell line was challenging. Our main goal was to achieve growth regulation by nutrient modulation and to explore the resulting bioenergetic adaptations. LG-BHB adapted U87MG demonstrated a quiescent metabolic profile, with lower absolute ATP

production rates, sustained primarily via ECAR-linked ATP production, although the calculation of OCR was subject to high resistance against mitochondrial inhibitors (Figure 36c). Low basal OCR, higher than expected ECAR and marginal changes in response to mitochondrial inhibitors are likely caused by microenvironmental factors (Crabtree effect), typical of terminally differentiated, quiescent neurons, neural progenitor cells and neuronal tissues [306; 499-502]. Nevertheless, some researchers noted higher OCR in fully differentiated cortical neurons (DIV7), whereas undifferentiated neurons (DIV1) exhibited a more quiescent phenotype [503]. Further characterization would be required to demonstrate the mitochondrial fitness and molecular changes induced by our proposed metabolic approach.

In summary, we described how 4 cycles of BHB-compensated glucose deprivation changed the metabolic and cellular phenotype of U87MG [323; 504; 505]. This non-proliferative phenotype lasted even after provision of glucose and serum. Survival of cancer subpopulations in near absence of glucose involves metabolic reprogramming for quiescence (a lack of glucose carbons for biosynthesis), sufficient mSLP from glutamine, or OXPHOS from BHB, glutamine and other amino acids (neither lactate, pyruvate nor fatty acids were supplemented in this study).

Long-term clonal selection and nutrient modulation continues to be an unexplored avenue, possibly due to methodological constraints. Wappler *et al.* was able to select cholangiocarcinoma cells by escalating glutamine restriction over several months to produce comparatively less glutamine-addicted clones [506]. Sperry *et al.* evaluated U87MG and primary gliomaspheres under BHB-compensated glucose deprivation in cell culture and orthotopic xenograft mouse models [475]. Glucose deprivation caused significant loss of cell viability even after supplementation with fatty acids and BHB in both U87MG and primary patient-derived cell lines, discerning a nominal proliferation boost with BHB when glucose and glutamine were also abundant. We observed a similar trend in U87MG (Figure 35 and Supplementary Figure S12). As viability collapsed after glucose/glutamine deprivation, unable to be rescued by BHB, we hypothesize that the slight upregulation of ATP production after BHB supplementation was likely related to potentiation of SLP. This BHB-induced proliferation boost requires further investigation.

Low glucose media paired with 4 mM BHB reduced the proliferative potential of both stem and non-stem GBM cells [495]. Furthermore, patient derived GSCs cultured in a KD-mimicking medium (2.5 mM glucose, 10 mM BHB) demonstrated attenuated stemness and lower proliferation by increased ROS production [269]. Culture of non-enriched GBM cells from human tumors under glucose deprived conditions (2.5 mM) for 1-week (without BHB) increased markers of stemness, with more than two-fold increases in CD133+ cells [507]. Therefore, reexamining the plasticity of GBM cells, the influence of metabolic status along the differentiation hierarchy needs to be taken into account in future research.

Lastly, following the emphasis on translational medicine, our *in silico* analysis was focused on the clinical applications of metabolic subtyping. Statistical modeling of next-generation sequencing is revolutionizing early detection and diagnosis of cancer, but the contribution of metabolic pathways is difficult to capture [508; 509]. We set out to determine if a mechanism-based selection of metabolic genes, according to concrete therapeutic targets (mitochondrial metabolism, glycolysis and glutaminolysis), could be useful for patient stratification.

Previous genome-wide association studies identified genetic markers correlating with anticancer potential of MF, using an untargeted approach [510]. We developed a PI based on the expression of metabolic genes associated with survival (Figures 38 and 39). Our classification shows a comparable predictive capacity to gene signatures selected by a co-expression network construction software (i.e., without input of biological principles) [511].

To conclude, protein-level expression of metabolic enzymes could be useful to determine survival outcomes (Figure 40). This analysis aimed to evaluate if a subset of patients could benefit from specific metabolic drugs. Accordingly, the protein-level PI could be clinically relevant, with druggable therapeutic targets such as IRS1, IGF1R, PIK3CA, PIK3R1 (insulin signaling), LKB1, ACC, eEF2, MTOR (AMPK-MTOR signaling) and PDK1 (pyruvate metabolism), among others. The cohort of susceptible patients could be treated with tailor-made strategies, e.g., insulin suppressive therapy, PI3K inhibitors, glycolytic and low-dose mitochondrial inhibitors.

VI. CLOSING REMARKS

6. Closing remarks

Precision medicine will soon extend beyond enclosed clinical trials and out-of-reach laboratory settings. Patient stratification is a powerful diagnostic tool; unfortunately, actionable insights are currently limited to basic forms of metabolic imaging (glucose uptake) and established patterns of genetic aberration [512; 513]. While we firmly believe that precision oncology could eventually lead to impressive survival results, general applicability will require a meticulous single-cell classification of all tumoral and normal tissues: constructing such a massive library of molecular alterations is not "technically" unfeasible, but it might take time [514].

Conceptualizing cancer as a metabolic disease reduces the intimidating complexity of the cancer problem to a "simple" restriction of its most avidly expended fuels: glucose and glutamine. As Otto Warburg poignantly stated in response to Weinhouse critique of his seminal paper on respiratory dysfunction:

"It is something deeper when Weinhouse dislikes the statement that the shifting of the energy production from the aerobic to the anaerobic state is the cause of cancer. He feels that this is far too simple: How can cancer, as mysterious as life itself, be explained by such a simple physicochemical principle? Yet this feeling is not justified. The problem of cancer is not to explain life, but to discover the differences between cancer cells and normal growing cells. Fortunately, this can be done without knowing what life really is." [141].

The body of scientific knowledge is not constructed on unshakeable grounds and incontrovertible evidence: it is not possible to dissociate historical perspective and bias from the scientific method [515]. Biological sciences are based on model systems and indirect observations. Despite best efforts to ground biology in objective biophysical evidence, its inherent complexity forces us to work with estimates and conjectures [516]. The position of the Sun as the center of our Solar System is a physical phenomenon that can be elegantly explained by mathematical models, which, in turn, cannot accommodate Earth at the very same position. This revolutionary idea was also based on indirect observations (astronomical patterns and telescopic evidence). However, replacing the Ptolemaic model with the Copernican Revolution constitutes a demonstrable mathematical law, allowing us to make predictions about the future with an almost

absolute degree of certainty [517]. For better or for worse, this degree of precision has not been reached for the somatic mutation theory. Consequently, reexamining its strengths and weaknesses is not only appropriate, but a necessary step in the quest for truth (i.e., attaining a more accurate description of nature).

Dogma is the antithesis of science. Unfortunately, dogma is a crystalized evolutionary template, giving meaning and order to the unsettling chaos of opposing ideas, as inherently human as the emergent attribute of conscience itself [518]. Regrettably, we are currently experiencing a critical disconnect between preclinical and clinical research [63]. As a consequence, metabolic explanations of cancer are capturing the interest of researchers once again [519-521]. When the wheel of research is turning in one singular direction, building knowledge with no particular aim, it is very hard to steer [522].

A *détente* is necessary.

The pathogenesis of cancer is complex, with involvement of mitochondrial dysfunction, oncogenic signaling and metabolic reprogramming [119; 523]. Even though metabolic evaluation is becoming an essential tool to uncover malignancies that could benefit from targeted therapy [166; 524-527], we are just starting to unravel the optimal dosing and scheduling in clinical settings [446]. Therein lies the crossroads where uncertainty is confronted with real-world applications. If we want to develop novel therapies based on different fundamental principles, they must be fully understood. This cutting edge could be a comfortable place for metabolic therapy to occupy. We believe that, in the near future, cancer guidelines will offer chemo-radiotherapeutics, molecular targeting and/or metabolic therapy, depending on the characteristics of each tumor. Clinical studies, patient stratification and training in metabolic oncology will be key components of this puzzle. If a combination of these strategies improves the long-term management of this ominous disease, they are all welcome.

We will explain life later.

VII. CONCLUSIONS

7. Conclusions

The following conclusions can be drawn from our experimental results:

i. It is possible to detect metabolic differences in GBM at the tissue level and the cellular level. Bulk-tumor gene expression and metabolic imaging (18F-FDG PET) could be useful for patient stratification, especially by differentiating the mesenchymal subtype with upregulated glycolytic signaling.

ii. GBM exhibits heterogenous oxygraphic metabolic profiles in basal conditions. Higher baseline OCR-dependency (as highlighted by GBM27) involves the highest comparative doses of glycolytic and mitochondrial inhibitors.

iii. Targeting mitochondrial function (MF), the Warburg effect (DCA) and glutamine metabolism (DON) reveals differential anti-proliferative effects in consonance with the basal metabolic phenotypes of each cell line.

iv. Metabolic inhibitors generally spare non-tumoral cells, but doses corresponding to OCR-dependent subtypes are toxic to normal cells. The radiomimetic drug bleomycin is toxic to rapidly proliferating non-tumoral cells.

v. Metabolic drugs could benefit from synergistic combinations with bleomycin, leading to meaningful dose-reductions and antiproliferative effects in GBM27, as well as DON in all cell lines.

vi. Metabolic pre-treatment induces biologically coherent adaptations in bioenergetic phenotypes of surviving cell subpopulations, acting as a form of "metabolic priming" for prospective interventions.

vii. Enzymatic ketolytic capacity is present in GBM, but BHB cannot rescue viability in absence of glucose and glutamine. Cyclical exposure to glucose depletion with concurrent BHB compensation produces sustained growth arrest and morpho-metabolic changes, suggestive of metabolic quiescence.

viii. *In silico* analysis of the TCGA GBM cohort can stratify patients according to a survival prognostic index based on pathway-driven expression of metabolic genes and proteins.

VIII. APPENDIX

8. Appendix

8.1. Scientific production relative to the present work:

- Duraj, T., García-Romero, N., Carrión-Navarro, J., Madurga, R., Ortiz de Mendivil, A., Prat-Acin, R., Garcia-Cañamaque, L. & Ayuso-Sacido, A. (2021). Beyond the Warburg effect: Oxidative and glycolytic phenotypes coexist within the metabolic heterogeneity of glioblastoma. *Cells*, *10*(2), 202.

- Duraj, T., Carrión-Navarro, J., Seyfried, T. N., García-Romero, N., & Ayuso-Sacido, A. (2021). Metabolic therapy and bioenergetic analysis: The missing piece of the puzzle. *Molecular metabolism*, *54*, 101389.

8.2. Oral presentations relative to the present work:

- Duraj, T., Esteban Rubio, S., Rackov, G., Carrión Navarro, J., García Romero, N., Barbas Arribas, C. & Ayuso Sacido, A. (2018). Metabolic therapy in cancer: role of metabolism and nutrition in human glioma. NUTRIMAD 2018, IV World Congress of Public Health Nutrition XII. *Revista Española de Nutrición Comunitaria (RENC)*, Vol. 24, supplement 2. DOI: 10.14642/RENC.2018.24.sup2.5190.

8.3. Supplementary Material

8.3.1. Supplementary Figure S1. Genomic aberrations in GBM.

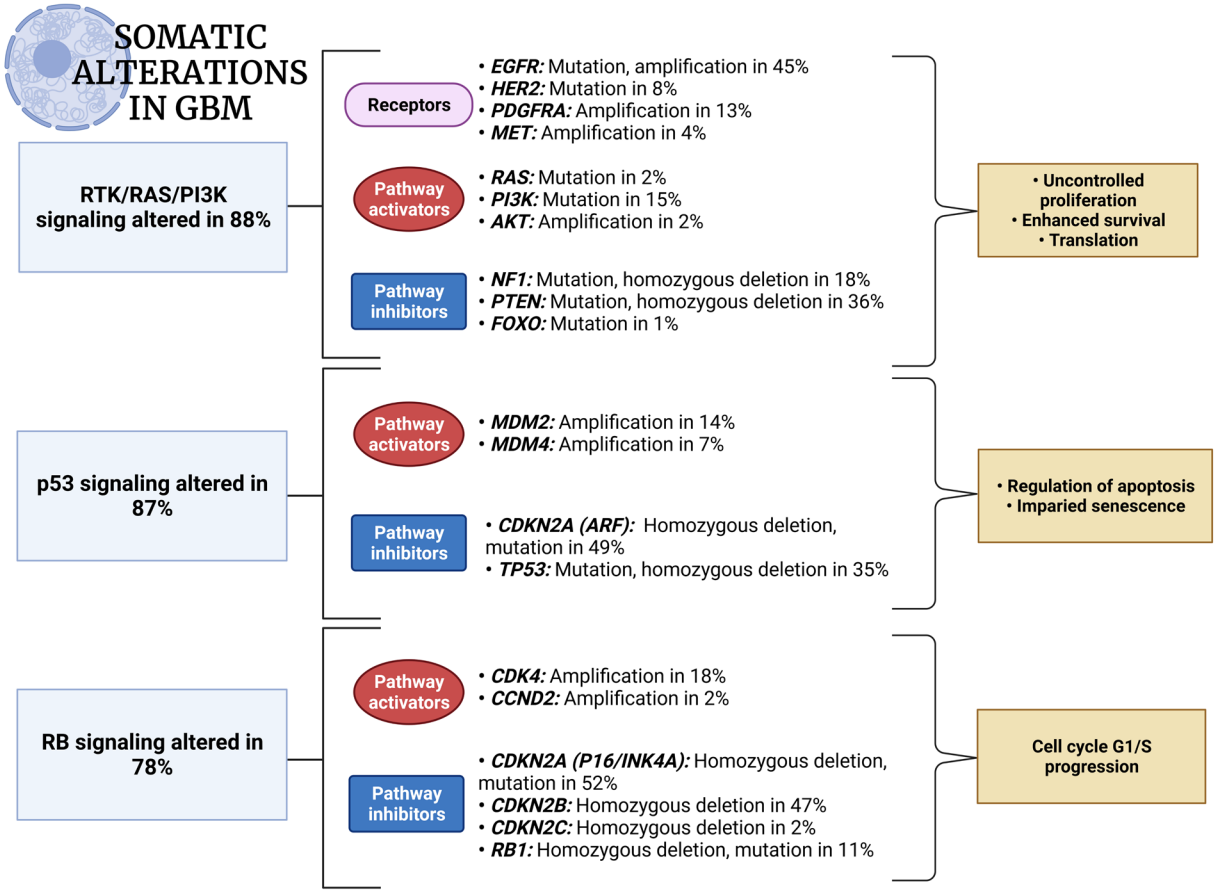

Figure S1. Primary sequence alterations and significant copy number changes for components of the RTK/RAS/PI3K, TP53 and RB signaling pathways. Based on [528].

8.3.2. Supplementary Figure S2. Metabolic alterations in GBM.

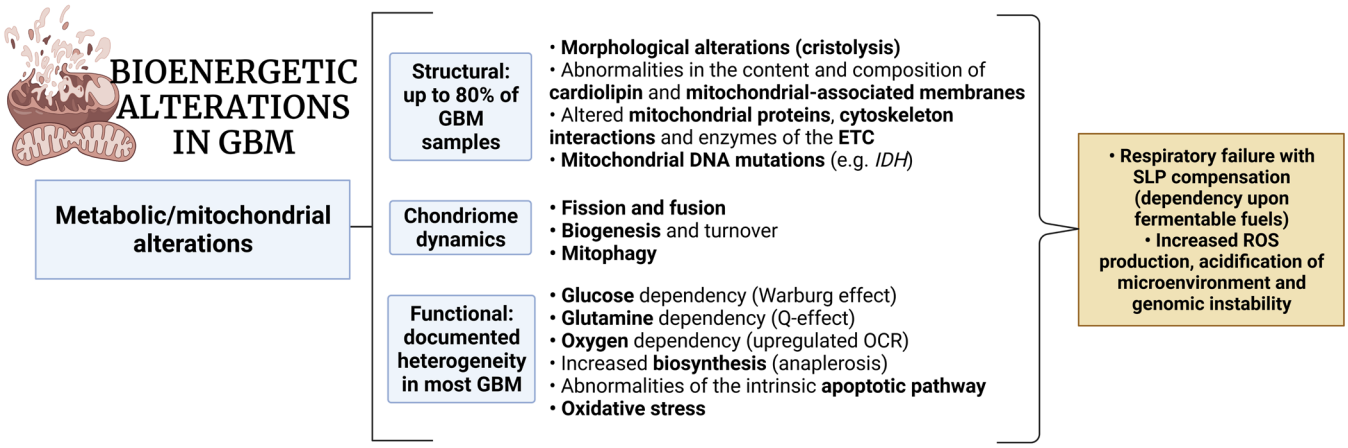

Figure S2. Common metabolic alterations in GBM. Own elaboration, based on [170; 529-531].

8.3.3. Supplementary Figure S3. Carcinogenesis and heterogeneity.

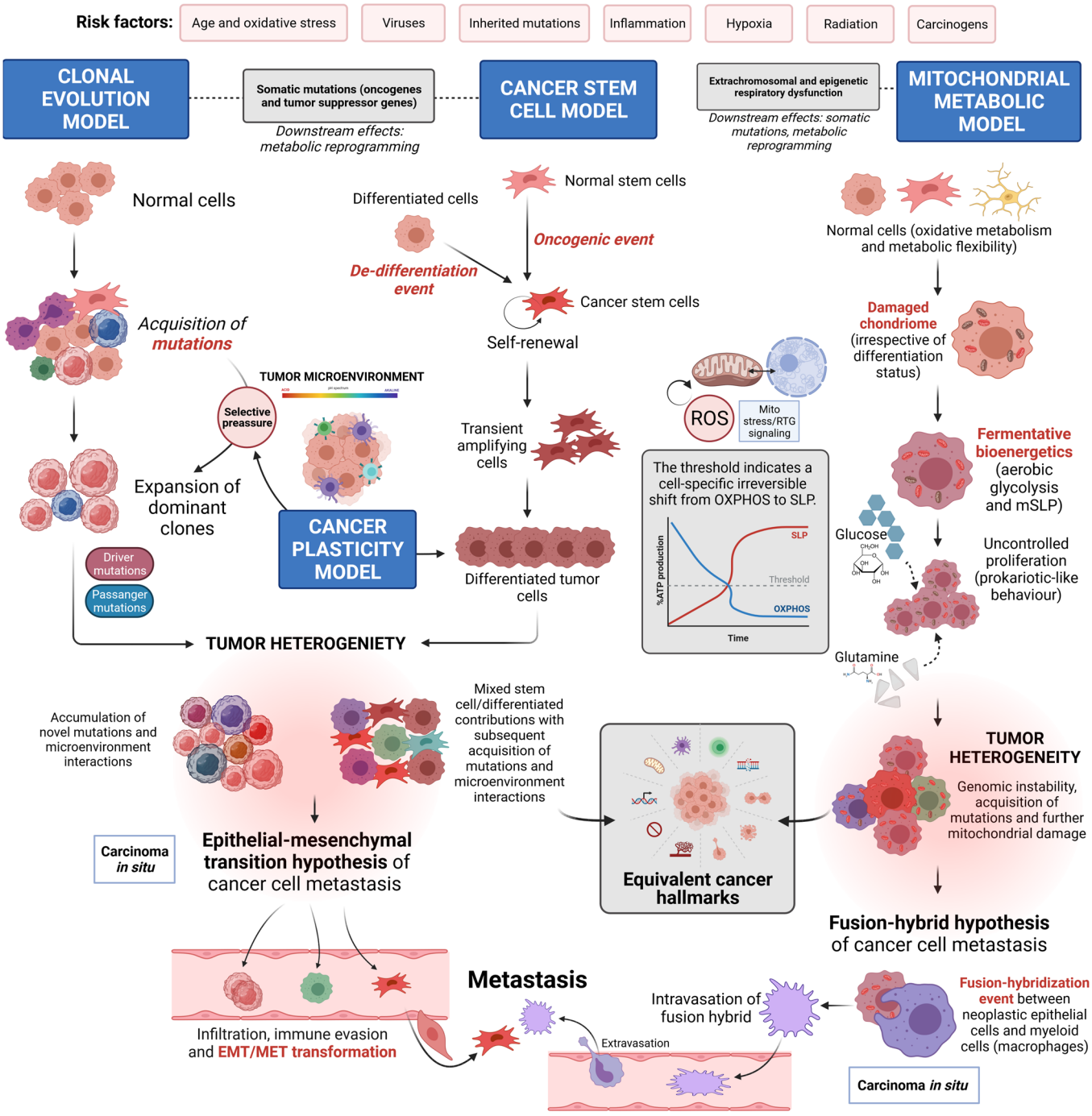

Figure S3. A comprehensive comparison between the clonal evolution, cancer stem cell (CSC) and mitochondrial metabolic models of cancer. Own elaboration, based on [69; 142].

In all conceptual models of carcinogenesis, cancer development is influenced by genotoxic and unspecific risk factors that could alter either the nuclear genome (somatic mutation theory) or mitochondrial bioenergetics (mitochondrial metabolic theory). In the **clonal evolution model**, tumorigenic random mutations are selected by

microenvironmental pressure, giving rise to uncontrolled expansion of dominant clones that can subsequently accumulate new driver and passenger mutations. In the **hierarchical cancer stem cell model**, normal stem cells or de-differentiated cells can be transmuted into CSCs, that, upon amplification, give origin to tumoral heterogeneity. A **mixed plasticity model** with contributions of selective pressure from the microenvironment (immune interactions, angiogenesis, pH and oxygen gradients, metabolic reprogramming) is equally applicable to CSCs. Tumoral heterogeneity converges in the epithelial-mesenchymal transition, a phenomenon where cascading genetic changes transform epithelial cells into mesenchymal cells (EMT), capable of immune evasion, and these changes are then suppressed or reverted to recover the original epithelial characteristics at secondary micro-metastatic growth sites (MET).

In the **mitochondrial metabolic model**, non-genotoxic risk factors such as oxidative stress, hypoxia or inflammation cause chronic damage to OXPHOS by altering the number, structure, and function of the mitochondria. Dysfunctional OXPHOS leads to adaptive fermentation (cytoplasmic SLP in the Warburg effect and mitochondrial SLP in the Q-effect), mitochondrial stress and retrograde mitochondria-nucleus signaling (RTG). This is followed by metabolic reprogramming (e.g., activation of oncogenes such as *HIF-1* and *MYC*, that upregulate glycolysis and glutaminolysis). Excessive ROS, extracellular acidification and inflammation are carcinogenic and mutagenic, driving genomic instability (random somatic mutations and aneuploidy). Despite the shift from respiration to SLP, ATP generation is kept constant by upregulated SLP. Tumoral heterogeneity is explained by the protracted mitochondrial stress and disturbances in intracellular and extracellular environments, in concert with accumulating genomic instability. In the fusion-hybrid model, rather than requiring a vague EMT/MET reconfiguration, metastasis arises from respiratory damage in cells of myeloid/macrophage origin, either directly or after fusion-hybridization with epithelial-derived tumor cells [532].

Thus, all major hallmarks of cancer are linked to extrachromosomal and epigenetic respiratory dysfunction, providing an answer to the oncogenic paradoxes of the somatic mutation theory (i.e., presence of driver mutations in normal tissues, non-genotoxic carcinogens, foreign-body carcinogenesis, differential cancer resistance across species, etc.) [64; 533].

8.3.4. Supplementary Figures S4-S7. Viability curves of inhibitors.

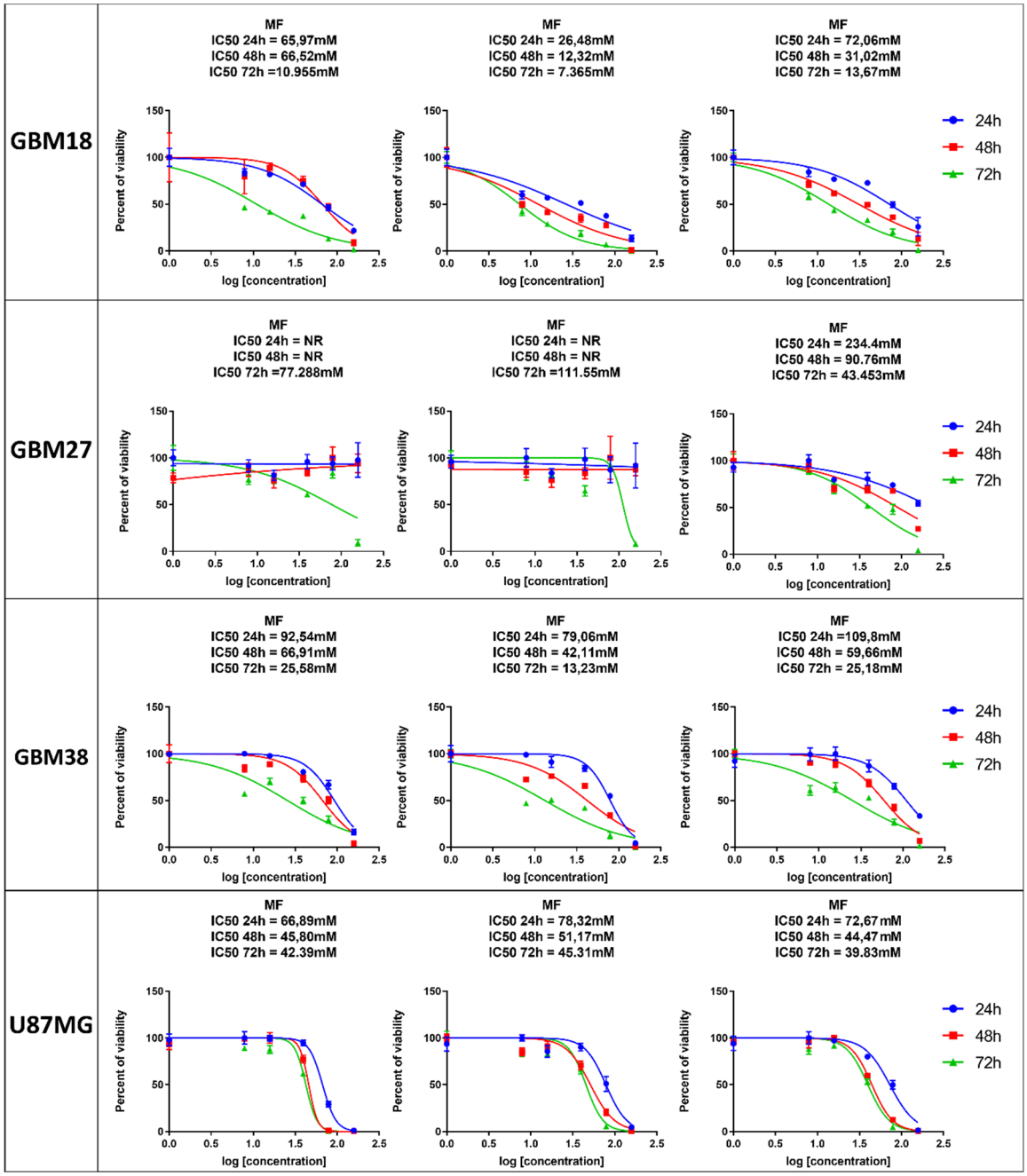

Figure S4: Inhibitory curves for metabolic inhibitor MF at 24h, 48h, 72h. Calculated IC50s for each cell line and time-point are included. In GBM18, MF shows rapid action at high doses, even at 24h. GBM27, by contrast, is highly resistant to MF, only reaching significant viability inhibition at 72h. GBM38 has a similar profile to GBM18 but reaching IC50 at higher doses. U87MG, on the other hand, shows a similar viability decrease at 24-72h, shifted to the left at 72h, but higher doses of MF induce loss of viability even at 24h.

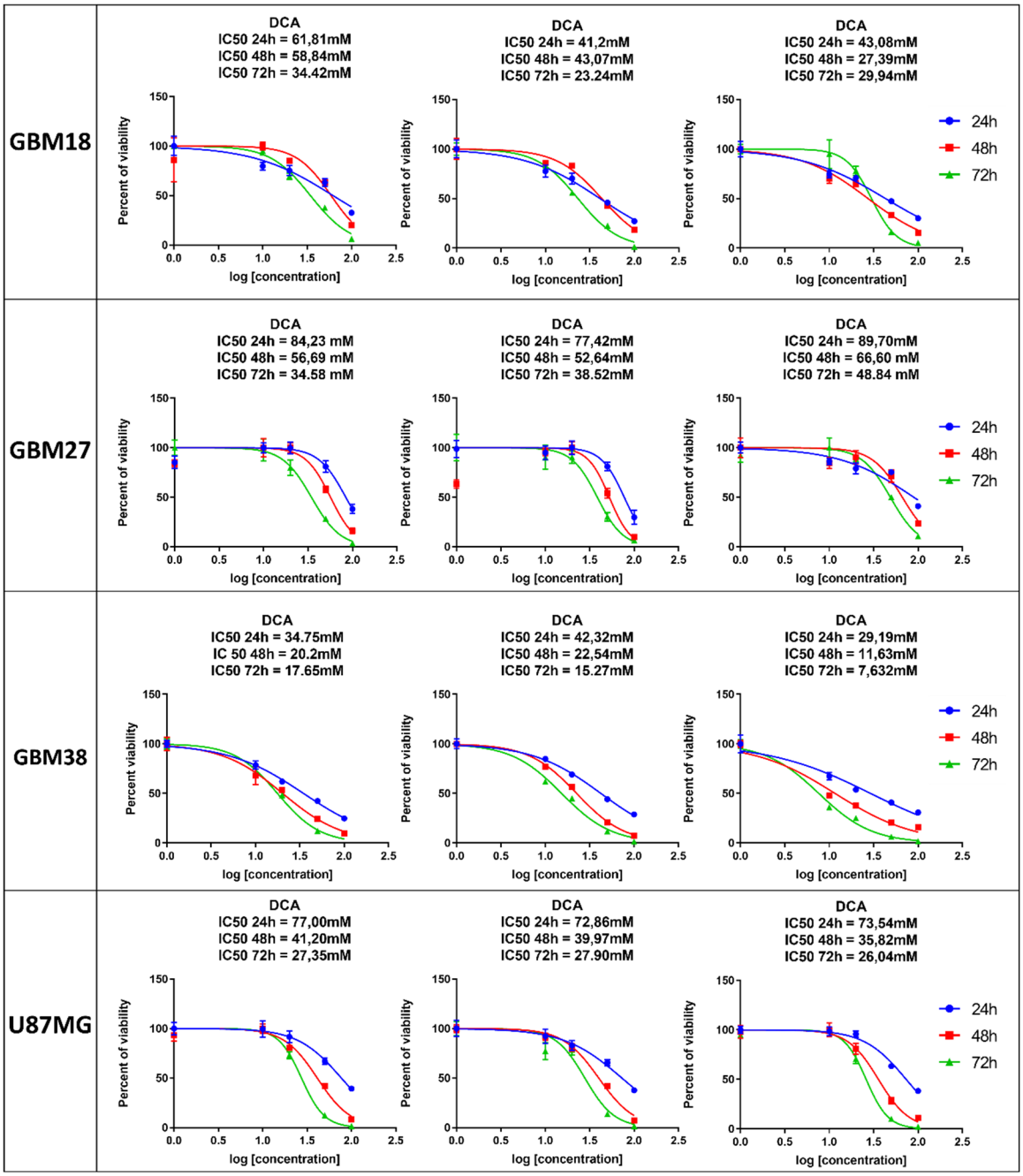

Figure S5: Inhibitory curves for metabolic inhibitor DCA at 24h, 48h, 72h. Calculated IC50s for each cell line and time-point are included. GBM18, GBM38 and U87MG display similar inhibition profiles, with rapid action of DCA at intermediate doses. GBM27 shows increased resistance to DCA, where the initial fall of viability is not observed until relatively high doses of the compound (>50 mM) are reached.

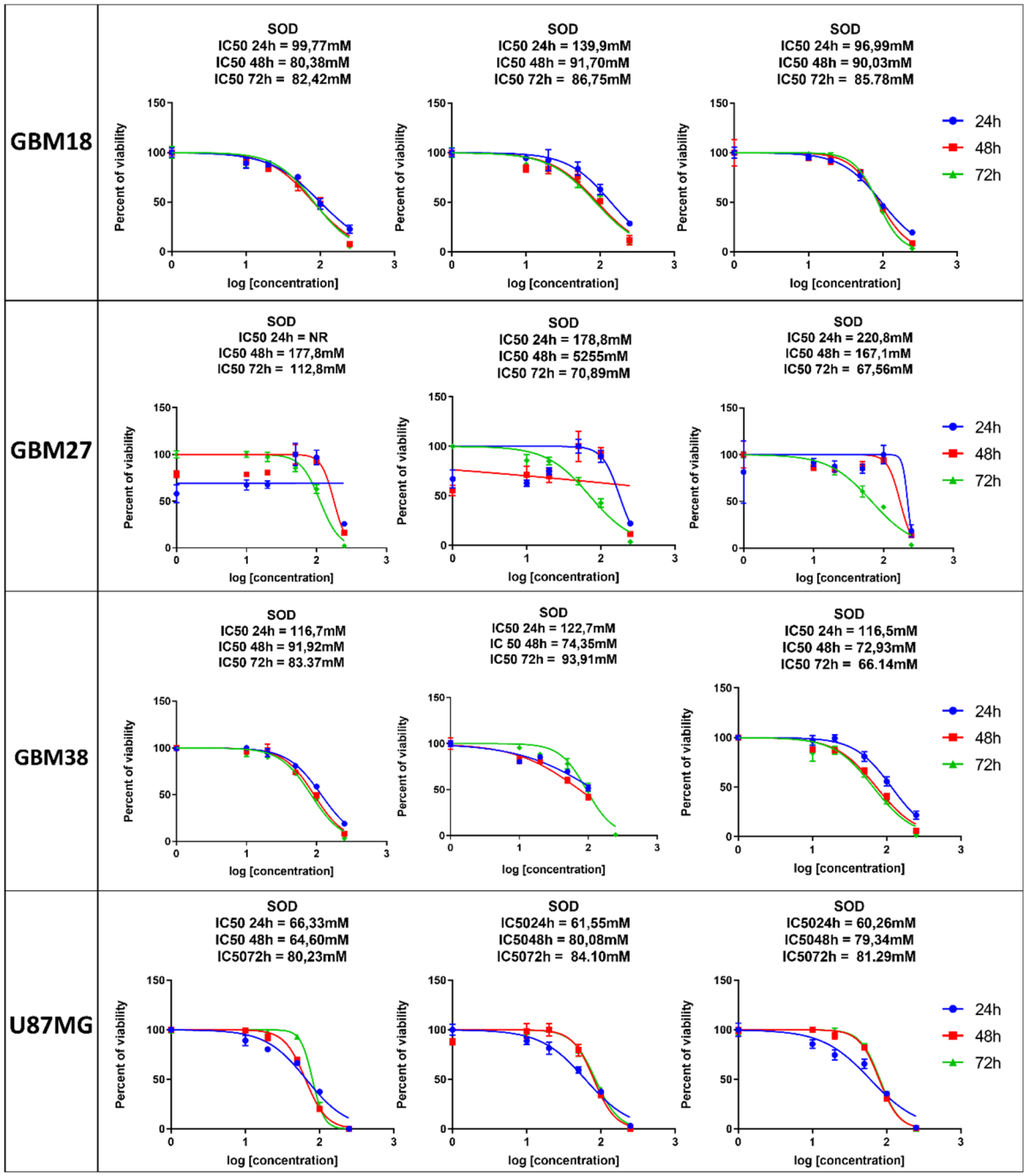

Figure S6: Inhibitory curves for metabolic inhibitor SOD at 24h, 48h, 72h. Calculated IC50s for each cell line and time-point are included. SOD requires high doses (>100 mM) across all cell lines, and full inhibition of viability was usually attained only at 250 mM. Interestingly, in GBM18 and GBM27, there were no discernible differences in the linear dose-dependent trends between 24h, 48h and 72h, whereas U87MG presented with a paradoxical effect where IC50 was lower at 24h than at 48/72h, possibly due to better cell penetration and enhanced LDH inhibition, consistent with previous reports [534]. In GBM27, we only saw consistent results at 72h, where the logarithmic variable slope equation was not able to calculate IC50 at 24h and 48h.

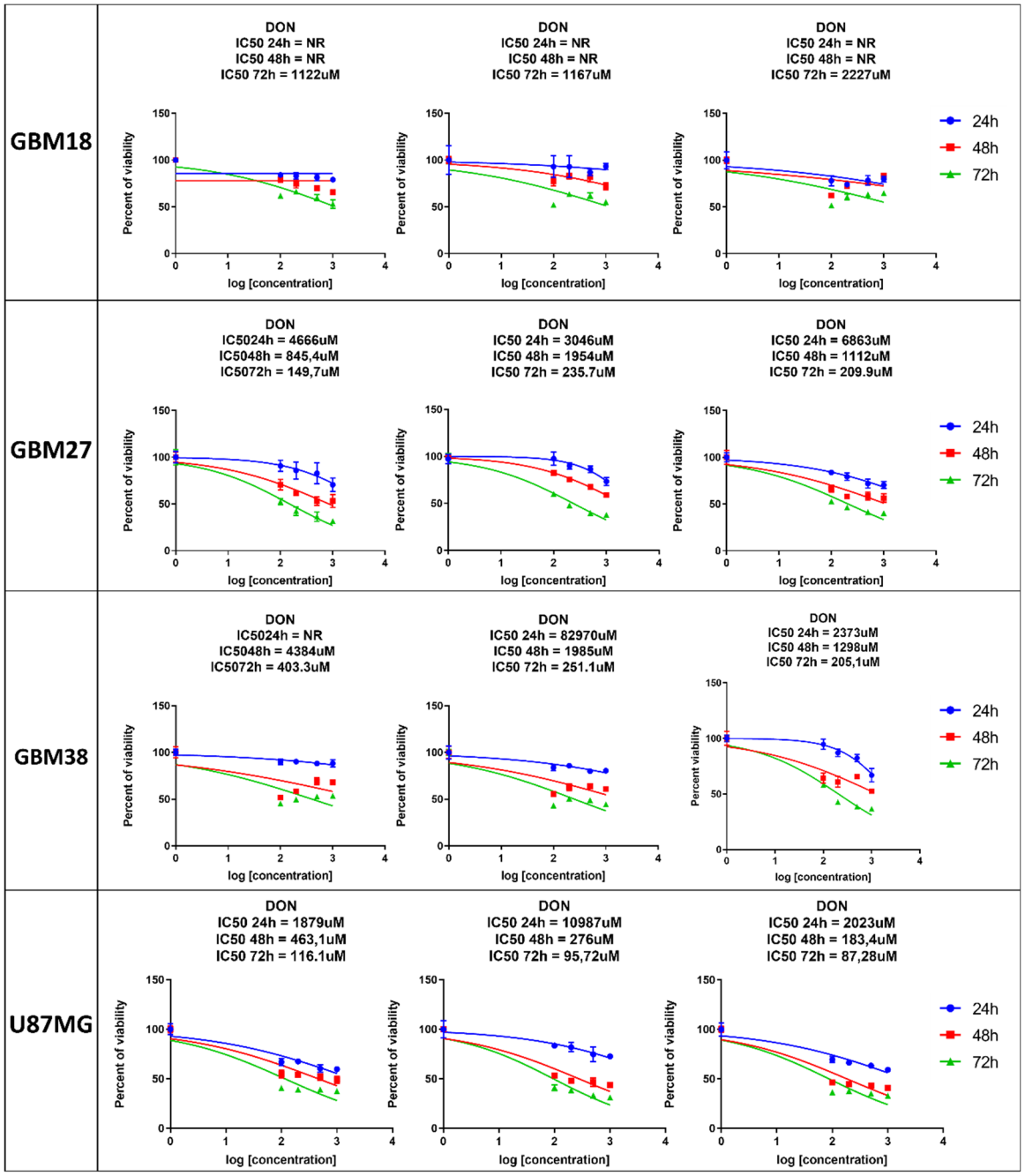

Figure S7: Inhibitory curves for metabolic inhibitor MF at 24h, 48h, 72h. Calculated IC50s for each cell line and time-point are included. In all cell lines, DON induces slow loss of viability at 24h, especially in GBM18 and GBM38. GBM27 and U87MG are more sensitive to the effects of DON. At 48h and 72h we can observe a clear dose-response in GBM27, but GBM18, GBM38 and U87MG do not show linear dose-response trends. This indicates a saturation point beyond which increasing DON doses further provides no additional benefit, with cytostatic, rather than cytotoxic effects. Abbreviations: NR (IC50 not reached).

8.3.5. Supplementary Figure S8. TMZ viability curves.

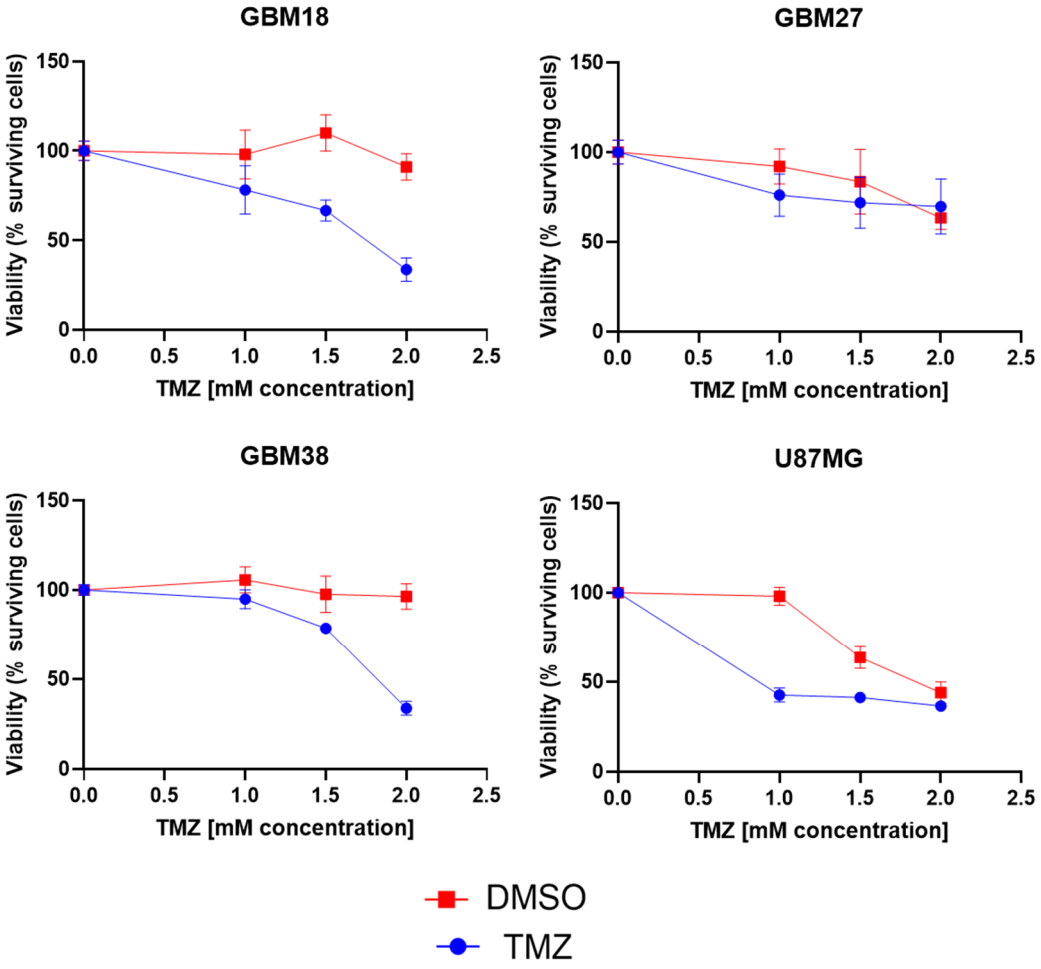

Figure S8. Viability profiles of cells treated with TMZ for 72 h relative to DMSO-controls. Maximal DMSO concentration was 2% *v*/*v* per experimental condition (corresponding to 2 mM of TMZ). High DMSO toxicity and interference should be noted in U87MG and GBM27. Groups were not compared due to ostensible reduction in viability in DMSO-treated controls. Any study of a drug dissolved in DMSO is, in essence, the analysis of two toxic substances, both of which could potentially reduce viability, and thus not suited for synergistic studies. Interference from DMSO has been reported at concentrations as low as 0.01% *v*/*v*, especially in stem-like GBM models [535]. Two biological replicates, each with n=4.

8.3.6. Supplementary Figure S9. Viability curves for radiomimetic bleomycin sulfate.

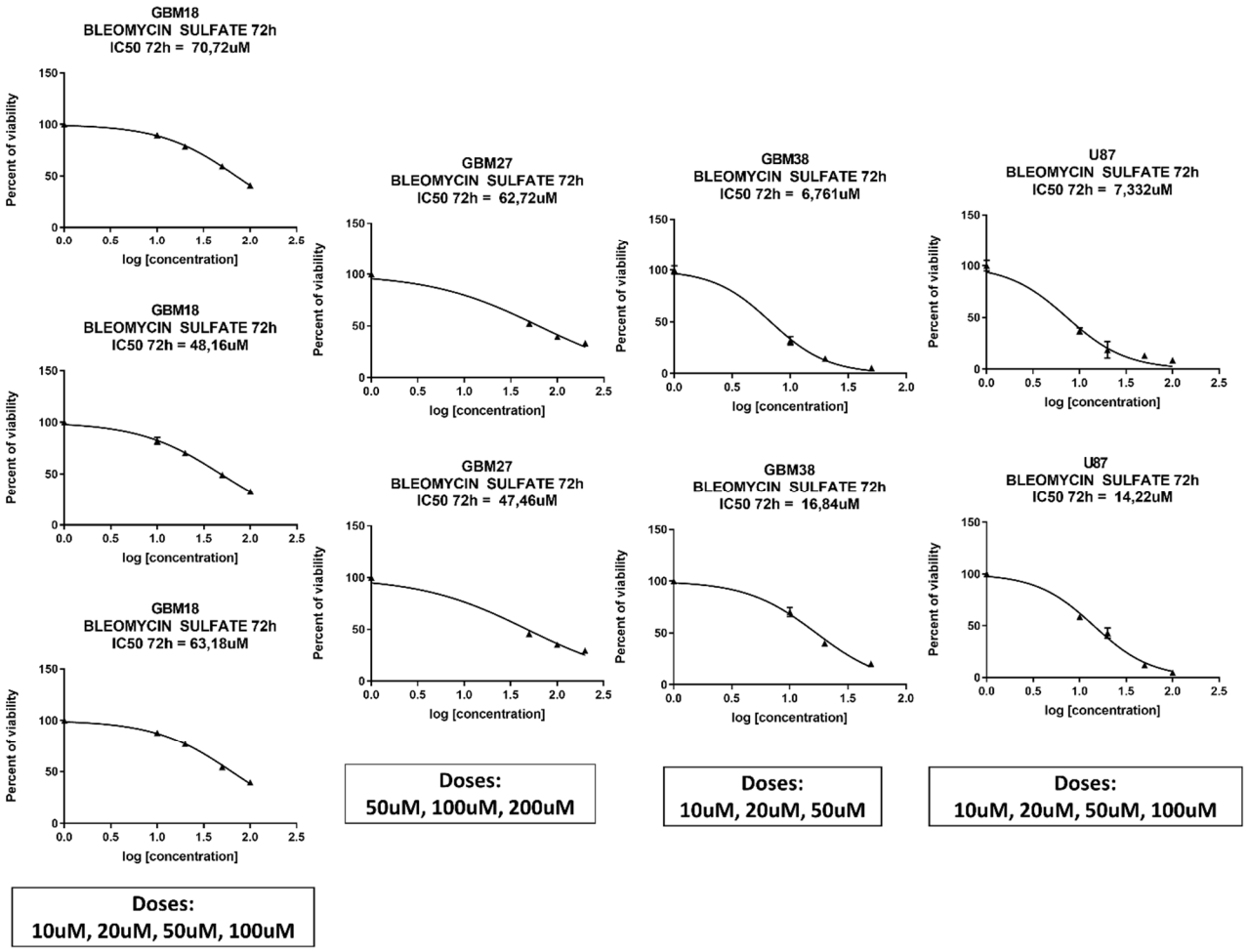

Figure S9: Inhibitory curves for bleomycin at 72h. Calculated IC50s for each cell line using the logarithmic variable slope equation are included. A minimum of 2 biological replicates were carried out for each cell line.

8.3.7. Supplementary Figure S10. MF dose-response curve with HBMEC.

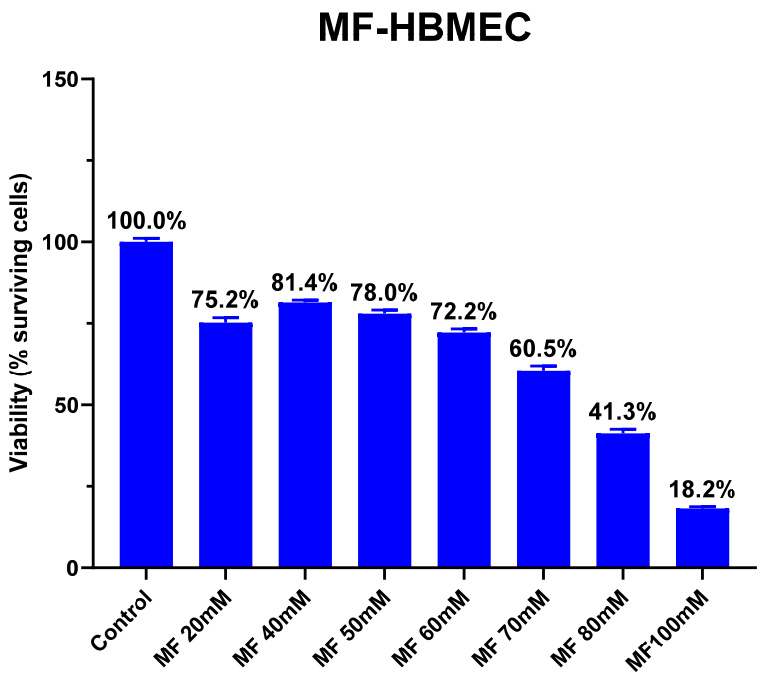

Figure S10: HBMEC inhibitory dose-response curve for MF at 72h. A sharp decrease in viability at concentrations > 60 mM can be observed in this cell line.

8.3.8. Supplementary Figure S11. Expression of OXCT1 in GSCs and U87MG.

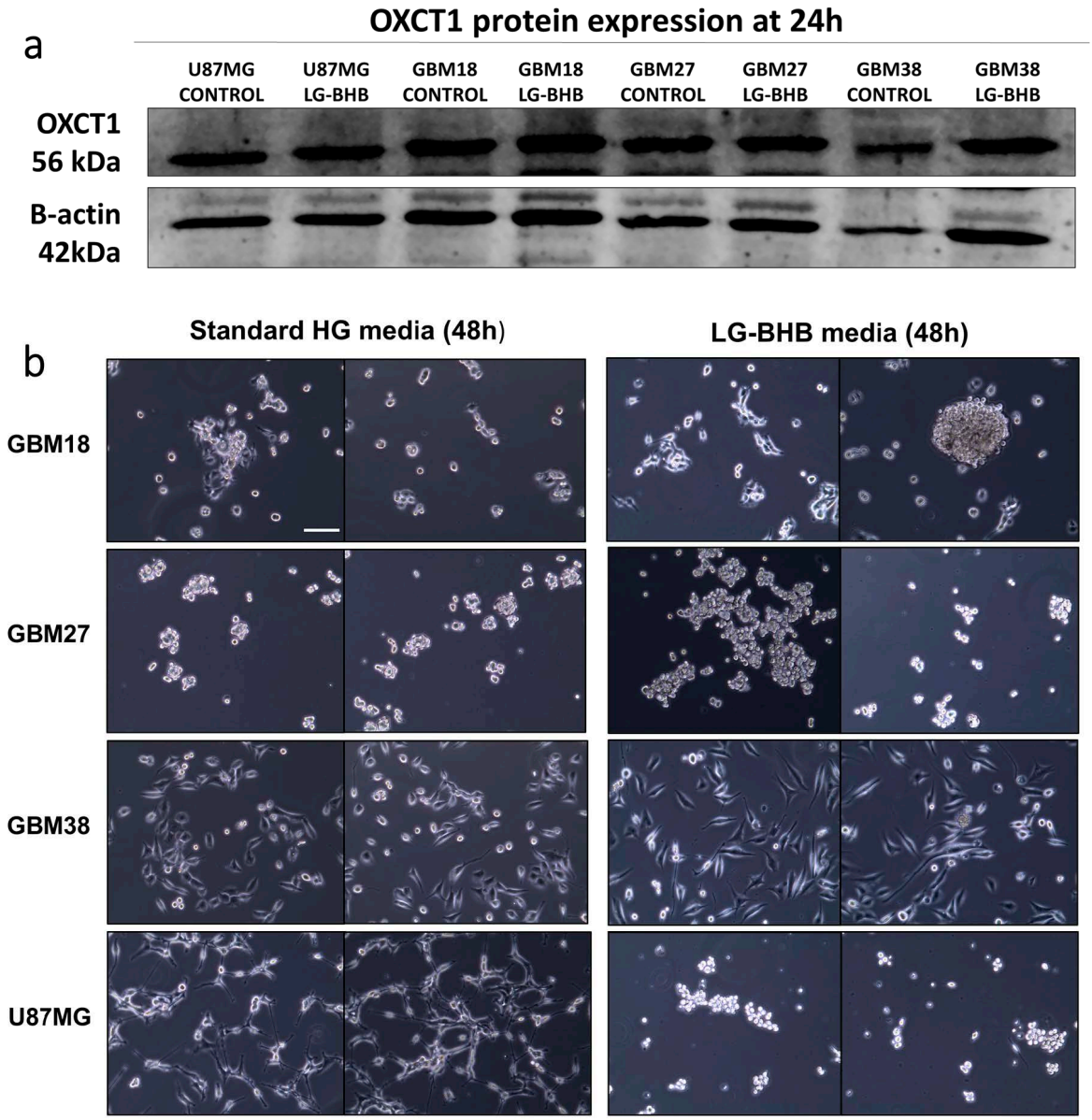

Figure S11. (a) Western Blot images of OXCT1 expression in GSCs and U87MG cell lines at 24 h. (b) Representative microscopy images of each cell line in normal media and LG-BHB media at 48h. Scale bar: 100um.

8.3.9. Supplementary Figure S12. Differences in ATP production of U87MG after normal subculturing and chronic exposure to BHB.

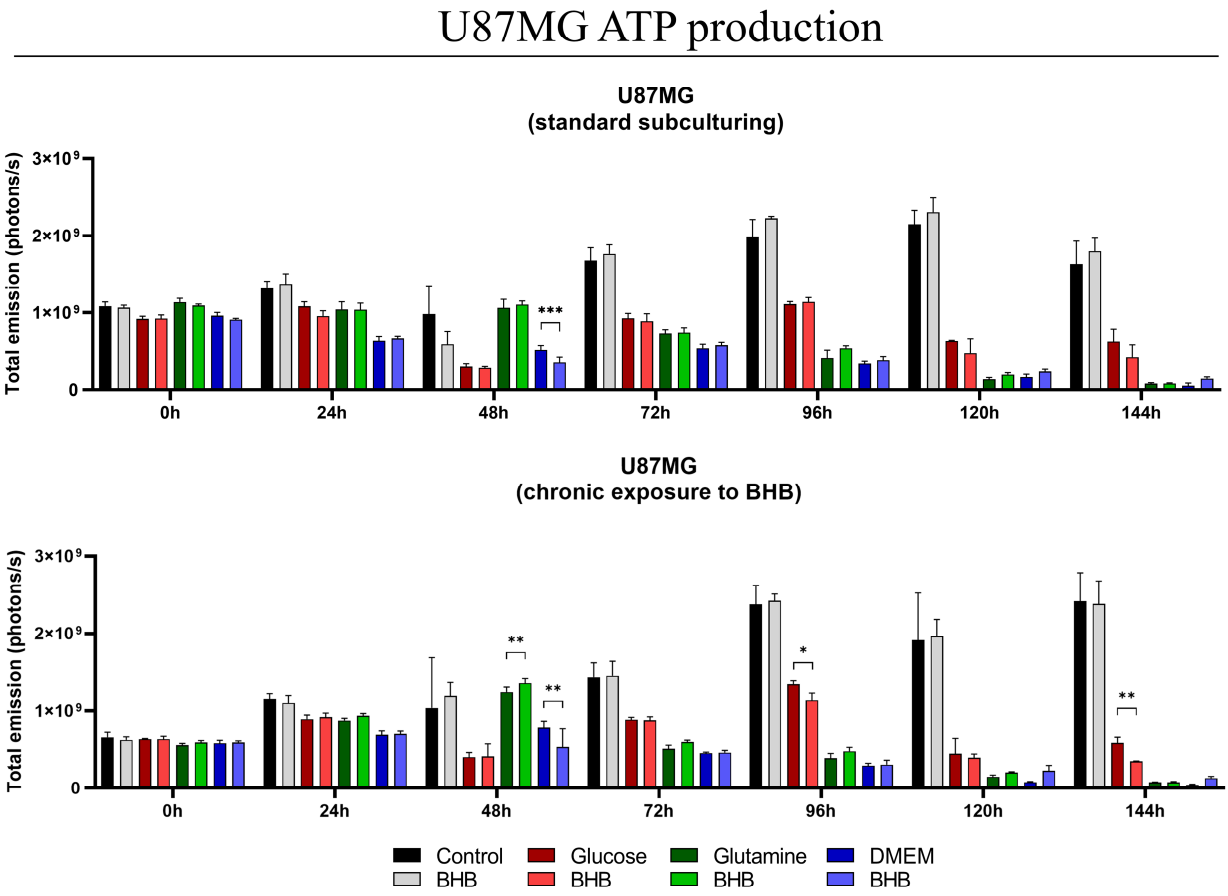

Figure S12. Comparison of ATP-linked bioluminescence of U87MG growing in standard subculturing conditions and 10 days of continuous exposure to intermediate concentrations of BHB. All experiments were performed in 2 biological replicates. Two-way ANOVA with Bonferroni correction. *** $p < 0.05$ *; $p < 0.01$ **; $p < 0.001$ ***.

8.3.10. Supplementary Figure S13. Changes of U87MG growing in intermediate glucose, BHB-compensated media.

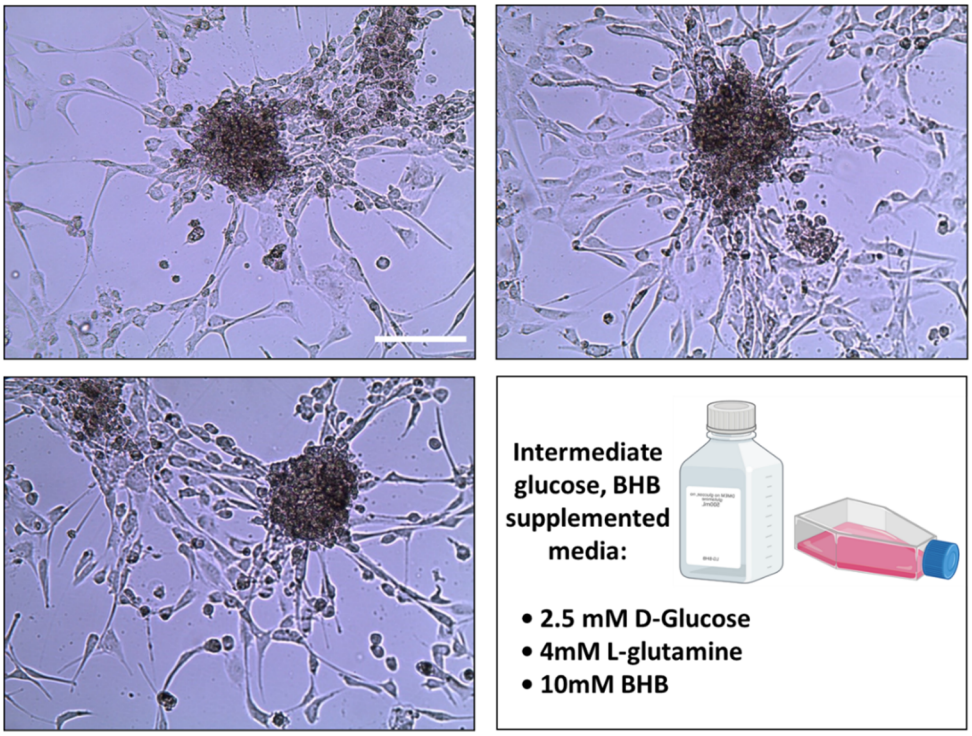

Figure S13. High magnification optical microscopy of U87MG growing in a medium equivalent to LG-BHB, but with a glucose concentration of 2.5 mM instead of 0.5 mM. Images taken at the end of the HG-FBS recovery period after 4 complete 7-day cycles of intermediate glucose adaptation. Scale bar: 100 μm.

8.3.11. Supplementary Figure S14. Cyclical LG-BHB exposure.

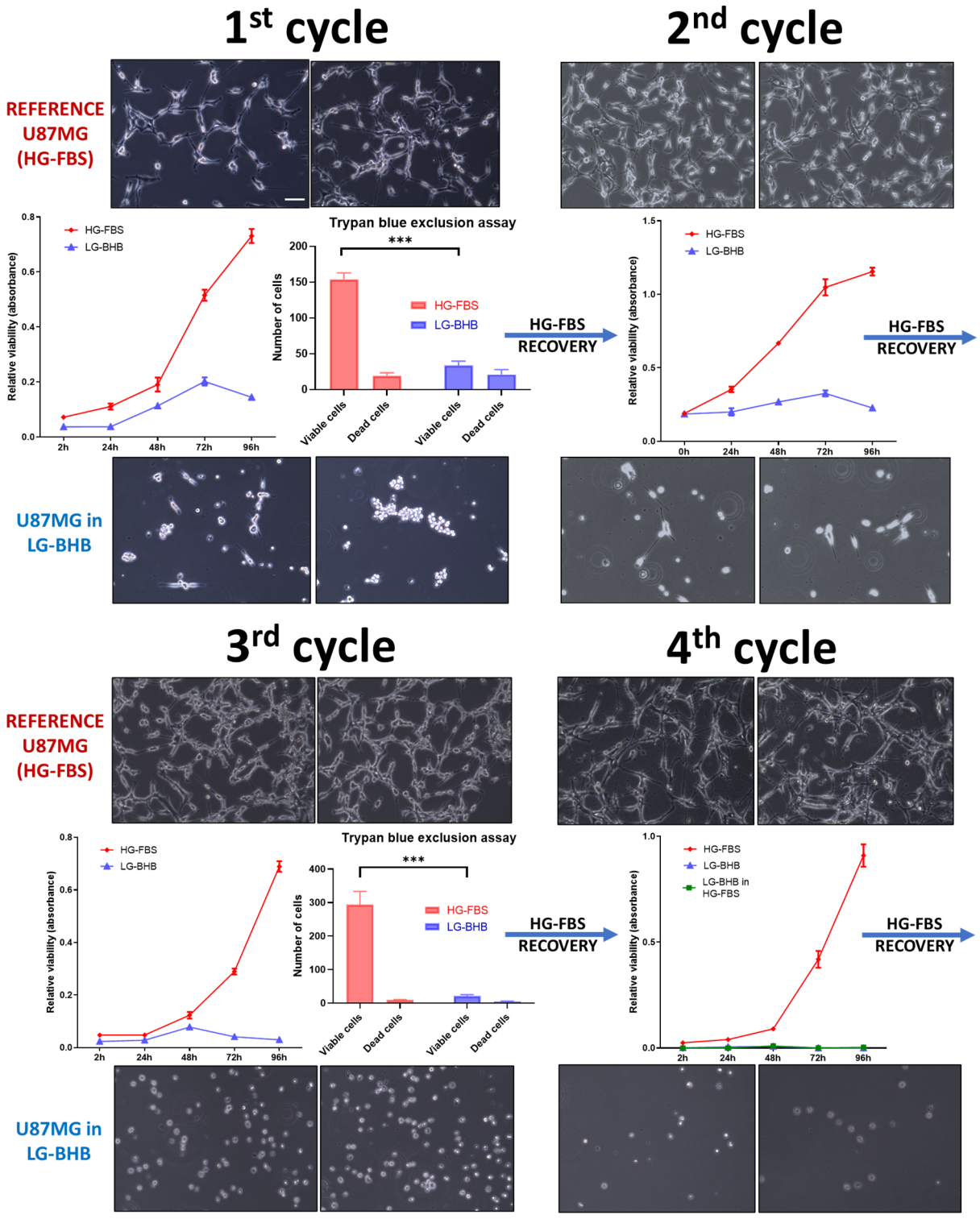

Figure S14. Summary of morphological changes during LG-BHB and HG-FBS cycles. Optical microscopy images were acquired at the end of each treatment cycle. MTS assays up to 96h were performed in each LG-BHB cycle, together with Trypan blue exclusion assays after cycle 1 and cycle 3. Comparisons between groups by unpaired t test with Welch's correction; *** $p < 0.05$ *; $p < 0.01$ **; $p < 0.001$ ***. Scale bar = 100 μm.

8.3.12. Supplementary Figure S15. Progression of LG-BHB cells after finalizing the cyclical glucose-deprivation, BHB-compensated metabolic treatment.

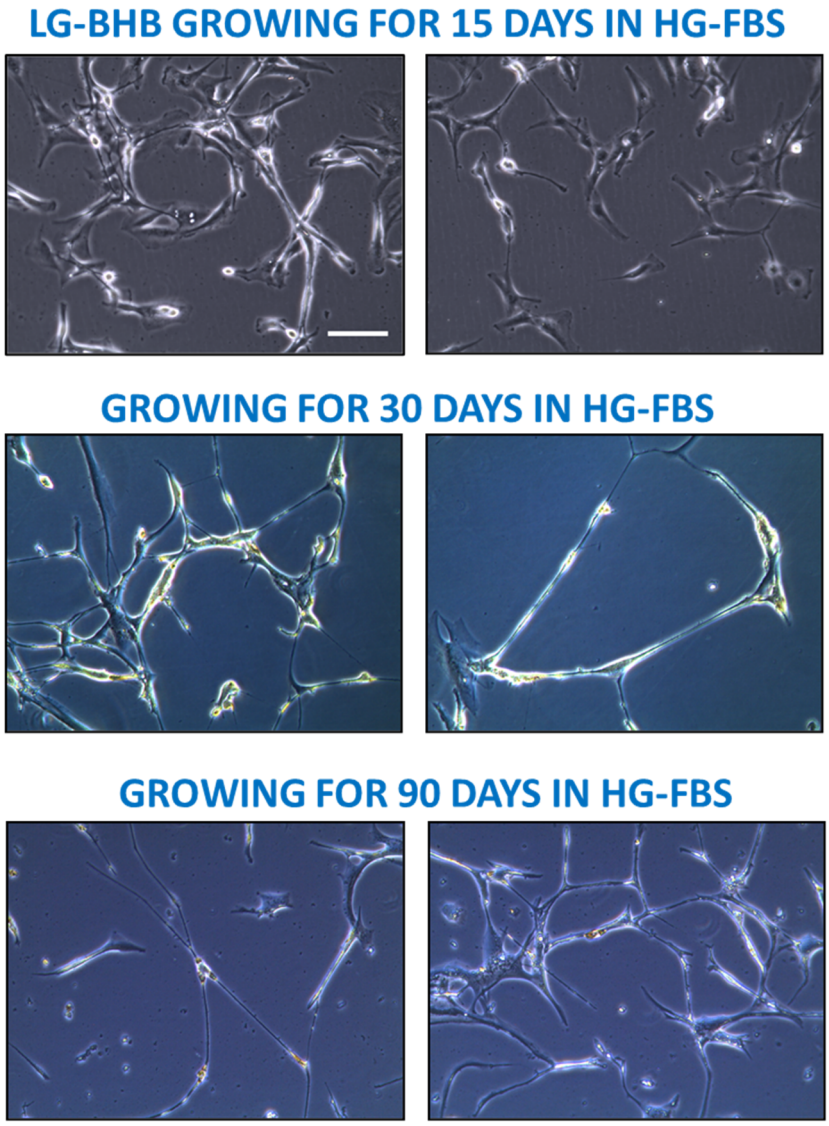

Figure S15. Representative morphological changes of U87MG after completing all LG-BHB cycles. Optical microscopy images with a scale bar = 100 μm.

8.3.13. Supplementary Figure S16. Representative images of LG-BHB adapted cells compared to controls.

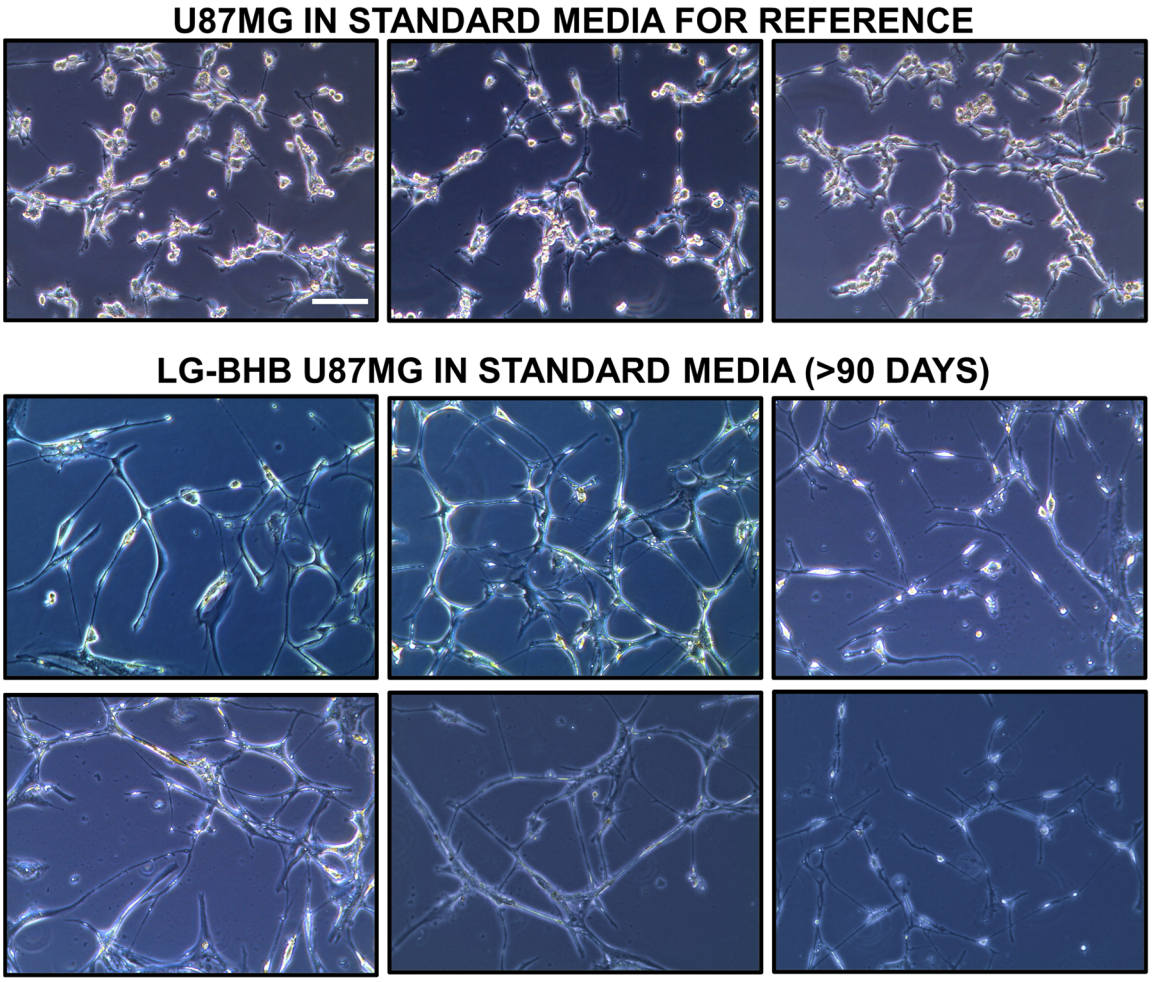

Figure S16. Representative morphological changes of U87MG after more than 90 days upon completion of LG-BHB cycles. Scale bar = 100 μm.

8.3.14. Supplementary Table S1. Manually curated list of metabolic target-genes.

Table S1. Genes involved in the targetable pathways of glycolysis, glutaminolysis and mitochondrial metabolism, based on KEGG pathways.

• **MF transport:**	*FOXO1*	*TSC1*	*NME6*
SLC29A4 (PMAT)	*GYS1*	*TSC2*	*NME7*
SLC47A1 (MATE1)	*LIPE*	*TBC1D7*	• **Monocarboxylate transporters:**
• **AMPK activation:**	*HMGCR 3*	*RHEB*	
STK11	*SREBF1*	• **Pyruvate junction:**	*SLC16A1*
CAB39	*FASN*	*LDHA*	*SLC16A2*
STRADA	*SCD*	*LDHB*	*SLC16A3*
STRADB	*SCD5*	*GOT1*	*SLC16A4*
PRKAA1	*ACACB*	*GOT2*	*SLC16A5*
PRKAA2	*CPT1A*	*PDHX*	*SLC16A7*
PRKAB1	*MLYCD*	*PDHB*	*SLC16A11*
PRKAB2	*MTOR*	*PDHA1*	*SLC16A13*
PRKAG2	*RPTOR*	*DLD*	*SLC16A14*
• **AMPK effectors:**	*AKT1S1*	*DLAT*	• **Metabolic regulators:**
PFKFB2	*RPS6KB1*	*PDK1*	*TP53*
PFKFB3	*RPS6KB2*	*PDK2*	*TP53BP1*
PFKFB4	*EIF4EBP1*	*PDK3*	*TP53BP2*
FBP1	*PPARG*	*PDK4*	*TIGAR*
G6PC3	*MLK1*	• **Glutaminolysis:**	*TP53RK*
PCK2	*BNIP3*	*GLS*	*MYC*
TBC1D1	*RRAGB*	*GLS2*	*MYCBP1*
RABL2A	*RRAGA*	*GLUD1*	*MYCBP2*
SLC2A4 (GLUT4)	• **Insulin regulators:**	*GLUD2*	*HIF1A*
MAP3K7	*IGF1R*	*OGDH*	*HIF1AN*
PPP2CA	*INSR*	• **TCA cycle:**	*DDIT4A (REDD1)*
CD36	*IRS1*	*SUCLG1*	*ARNT*
CRTC2	*PIK3CA*	*SUCLA2*	*EPAS1*
CREB1	*PIK3CB*	*SUCLG2*	*HK1*
PPARGC1A	*PIK3CD*	*SDHA*	*HK2*
ELAVL1	*PIK3R1*	*SDHB*	*GSK3A*
Cyclin D1	*PIK3R2*	*SDHC*	*GSK3B*
Cyclin A1	*PIK3R3*	*SDHD*	*CTNNB1*
Cyclin A2	*PDPK1*	*NME4*	*TCF4*
EEF2K	*AKT1*	*NME1*	*MDM2*
EEF2	*AKT2*	*NME2*	*MTBP*
SIRT1	*AKT3*	*NME3*	*EPAS1*

8.3.15. Supplementary Figure S17. RNA-Seq next-generation sequencing data of GSCs.

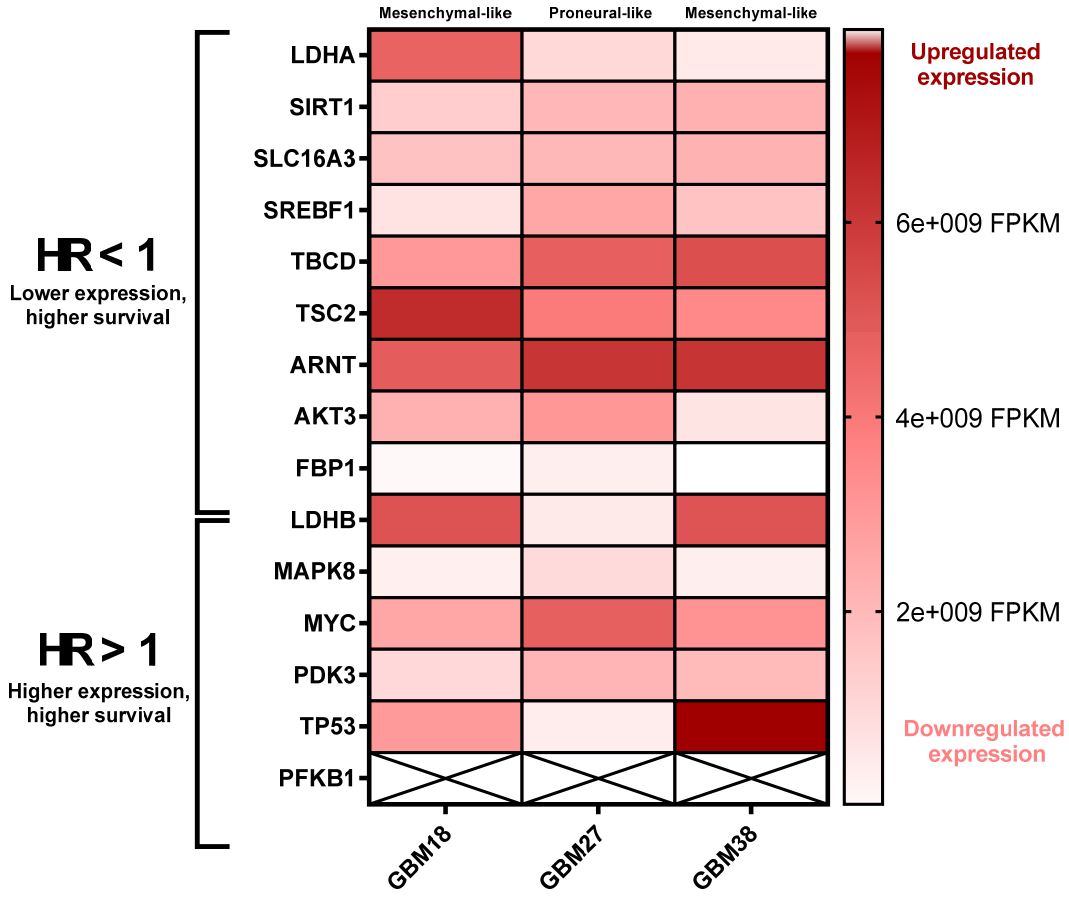

Figure S17. Correlations of RNA-Seq expression analysis in our GSCs to TCGA survival predictive genes. Our cells were previously classified by molecular and phenotypical characteristics as mesenchymal-like (GBM18 and GBM38) and proneural-like (GBM27) [158]. However, RNA-seq expression profiles cannot be compared to TCGA tissue samples, as cell line and bulk mRNA expression are not directly comparable. Tissue samples have a high contribution of diverse cancer and normal cells, whereas cell lines often isolate one specific hyper-proliferative subpopulation [536]. RNA-seq data expressed in relative normalized FPKM units (fragments per kilo base per million mapped reads).

8.3.16. Supplementary Figure S18. CGH analysis of selected genes.

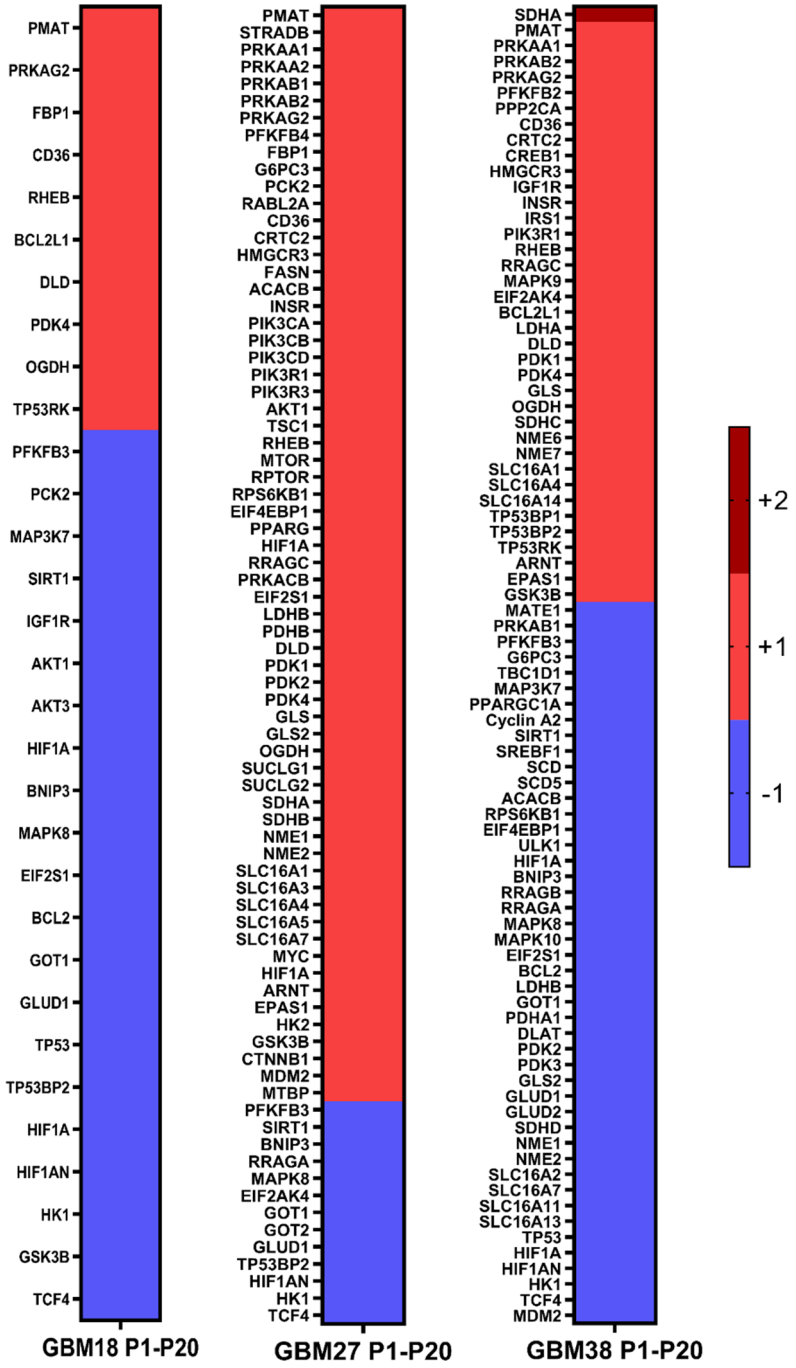

Figure S18. CGH analysis of the selected metabolic genes in GSCs (across cell culture passages 1, 5, 7, 10, 15, 20). Only stable and conserved amplifications and deletions across passages were analyzed. Dark red (+2) designates homozygous amplification, red (+1) heterozygous amplification and blue (-1) heterozygous deletion. No homozygous deletions (-2) were detected. Copy-number neutral regions as compared to reference genome were omitted for clarity. It can be observed that GBM18 has the most neutral copy-number variation profile.

8.3.17. Supplementary Figure S19. Oxygraphy and the OCR paradox.

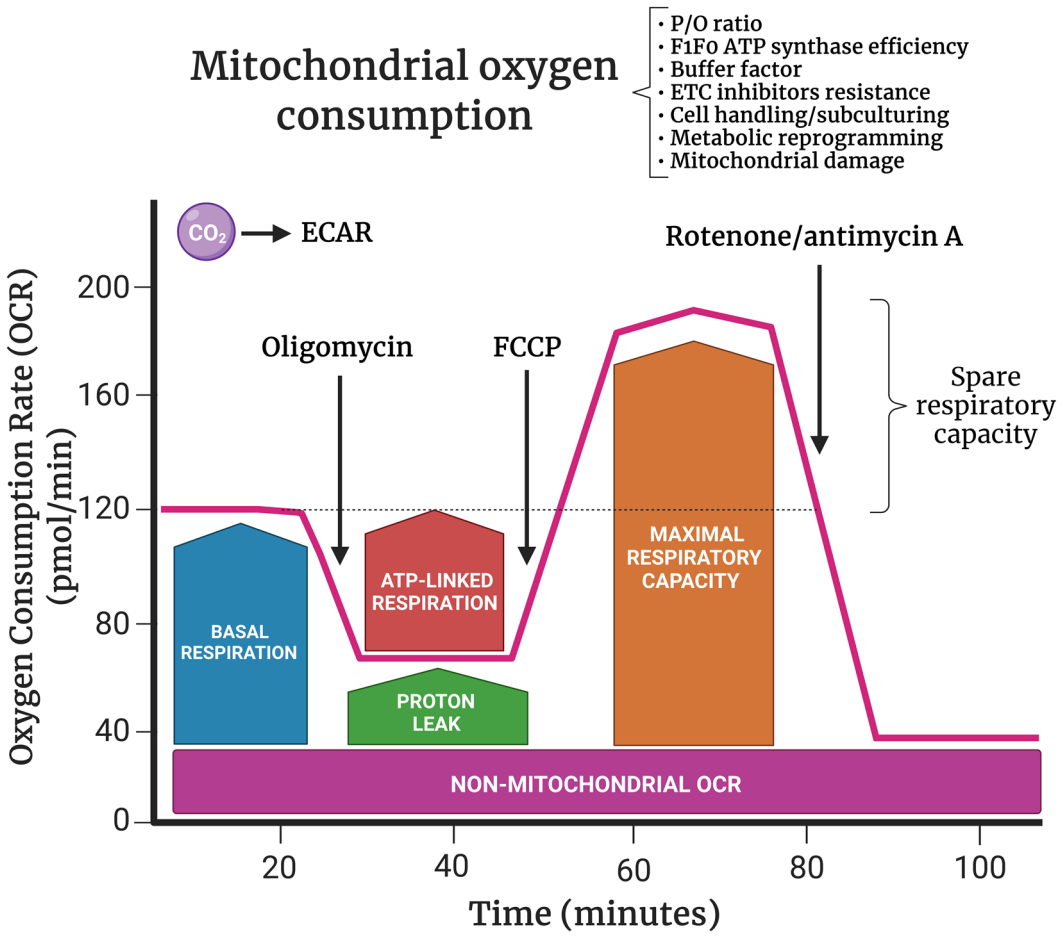

Figure S19. Interpretation of real-time oxygraphic measurements (Seahorse XF technology). ATP-linked respiration can be calculated after injection of oligomycin (complex V inhibitor). FCCP injection uncouples the proton gradient to estimate maximal respiratory capacity; this step is not present in the XF Real-Time ATP assay. After injection of rotenone/antimycin A (complex I and III inhibitors), the flow of electrons in the electron transport chain (ETC) is fully inhibited: differences between oligomycin and rotenone/AA indicate the "proton leak", i.e., the remaining basal respiration that is not coupled to ATP production. Proton leak can be a sign of mitochondrial damage or a regulator of ATP-synthesis. Non-mitochondrial respiration is defined as the OCR that persists despite maximal inhibition, due to a subset of cellular enzymes that still consume oxygen after rotenone/antimycin A injection. Mitochondrial OCR is modified by a number of external factors such as hypoxic metabolic reprograming, nutrient stress and cell culture conditions, as well as coupling efficiency and morphological cristae/lipid abnormalities. Mitochondrial-derived CO_2 also contributes to ECAR. Comparison of absolute values (raw OCR/ECAR) is limited by methodological standardization, which is not the norm across research groups. Own elaboration, adapted from [288; 537; 538].

Since the postulation of the Warburg hypothesis, researchers struggled with the fact that functional proteomics and oxygraphic measurements of tumor slices, whole cells and isolated mitochondria can detect residual activity of ETC components, membrane potential (ΔΨ), basal OCR, and, more importantly, meaningful shifts after specific inhibition of ETC complexes in highly buffered media (e.g., injection of oligomycin, FCCP, rotenone/antimycin A, as well as substrate inhibitors such as UK5099, BPTES and etomoxir) [84; 112; 539; 540]. Since the chemiosmotic theory gained traction in the mid-20th century, assaying mitochondrial function was based on the same set of principles; Warburg himself identified oxygen consumption in non-tumoral and cancer tissues using the Warburg apparatus, allowing calculation of respiratory ATP/O quotients [541]. Soon after, the group of Weinhouse argued that respiration was, in fact, normal in most cancer cells [542]. Wagner *et al.* reported a wide range of OCR in tumor cells, warning that "cell surface" (non-mitochondrial) oxygen consumption was an overlooked component and extrapolation from cell culture was problematic [543].

Judging from the accumulating oxygraphic evidence, it was concluded that OXPHOS must be functional in cancer cells, despite seemingly Warburgian behaviors under artefactual cell culture conditions [544; 545]. Despite technical limitations, there is a growing tendency to establish a direct link between relative changes in OCR and mitochondrial ATP [546-548]. Common estimations indicate that glycolysis contributes from 50 to 70% of total ATP production in cancer cells, while the rest comes from oxidation of pyruvate, glutamine and fatty acids [84; 112]. If mutations are the root cause of cancer, mitochondrial function can be completely normal, upregulated or downregulated depending on metabolic reprogramming [292]. If mitochondrial damage is the root cause of cancer, the chondriome must be, at minimum, partially dysfunctional [69].

In the same way the somatic mutation theory must explain the oncogenic paradox, the mitochondrial theory must account for highly variable OCRs in cell culture and dynamic changes upon inhibition of ETC complexes [64; 549]. This is not merely a theoretical exercise: if OCR translates into OXPHOS, metabolic therapy needs to bring attention to mitochondrial inhibition and "reverse Warburg effect", which is problematic since normal cells also require undisrupted mitochondrial function to survive [441].

Solving the OCR paradox requires conceptualizing mitochondrial metabolism as part of a dynamic system [550; 551]. The chondriome is the sum of all mitochondria in any given cell. This number can vary widely by organism, tissue, and cell type: a negligible amount has been

detected in non-dividing terminally differentiated human erythrocytes, 100 to several 1000s in cells from mature tissues such as muscle and liver (making up to 1/5 of total cell volume), and up to 100,000 in oocytes [552-554]. The chondriome is not a static organelle network: it undergoes active remodeling via motility/transport, fusion/fission dynamics, reshaping, quality control and mitophagy [555].

In this view, the oncogenic threshold of mitochondrial dysfunction is defined as a "numbers game" (Supplementary Figure S3). Damage to the mitochondria is the initiating factor of tumorigenesis, solving the inconsistencies of the somatic theory, but keeping in mind that the chondriome is a living ensemble of independent organelles. As total bioenergetic capacity starts to dwindle upon mitochondrial injury, surpassing a cell-specific threshold that depends on origin/genotype leads to irreversible reprogramming towards SLP. Consequently, cancer cells start to behave like a prokaryotic organism in hypoxic conditions, with uncontrolled proliferation and free-living motility (metastatic potential) [72].

A large body of evidence shows that OCR is lower in cancer cells after normalizing for metabolic activity when compared to controls of the same origin and responds abnormally to mitochondrial inhibitors (especially in coupling efficiency and maximal respiration) [309; 556-558]. Mitochondrial dysfunction is linked to tumorigenesis, but admits variable OCRs, as cancer cells can upregulate the functional fraction of their chondriome to stabilize ΔG'ATP hydrolysis. The nebulous term "dysfunction" would be defined as undergoing a SLP shift, which involves both a relative failure in OXPHOS and retrograde mitochondria-nucleus signaling [58; 109].

It bears repeating that classical respirometry will detect changes in OCR after the injection of mitochondrial inhibitors, as cells have trespassed the SLP-threshold but still retain some OXPHOS function. This leads to numerous therapeutic approaches focused on restoring mitochondrial health, especially at early stages of cancer development. In this framework, the basis of therapy should be focused on SLP fuel depletion (glucose/glutamine), reversal of chondriome damage via microenvironment modification and mitochondrial transfer therapy [90; 559; 560]. Mitochondrial targeting is reserved for populations of cancer cells that are demonstrably dependent on OXPHOS [171], with careful and precise dosing due to off-target toxicity, as shown in GBM27 in our own data. Further research is needed to confirm whether injuring the chondriome beyond a specific threshold is universally oncogenic.

IX. REFERENCES

9. References

[1] Sung, H., Ferlay, J., Siegel, R.L., Laversanne, M., Soerjomataram, I., Jemal, A., et al., 2021. Global cancer statistics 2020: GLOBOCAN estimates of incidence and mortality worldwide for 36 cancers in 185 countries. 71(3):209-249.

[2] Senga, S.S., Grose, R.P.J.O.B., 2021. Hallmarks of cancer—the New Testament. 11(1):200358.

[3] Hanahan, D., Weinberg, R.A., 2011. Hallmarks of cancer: the next generation. Cell 144(5):646.

[4] Paul, D.J.P.i.B., Biology, M., 2021. Cancer as a form of life: Musings of the cancer and evolution symposium.

[5] Agnihotri, S., Burrell, K.E., Wolf, A., Jalali, S., Hawkins, C., Rutka, J.T., et al., 2013. Glioblastoma, a brief review of history, molecular genetics, animal models and novel therapeutic strategies. 61(1):25-41.

[6] Louis, D.N., Perry, A., Reifenberger, G., Von Deimling, A., Figarella-Branger, D., Cavenee, W.K., et al., 2016. The 2016 World Health Organization classification of tumors of the central nervous system: a summary. 131(6):803-820.

[7] Wen, P.Y., Packer, R.J., 2021. The 2021 WHO classification of tumors of the central nervous system: clinical implications. Oxford University Press US.

[8] Vigneswaran, K., Neill, S., Hadjipanayis, C.G.J.A.o.t.m., 2015. Beyond the World Health Organization grading of infiltrating gliomas: advances in the molecular genetics of glioma classification. 3(7).

[9] Medicine, C.G.A.R.N.J.N.E.J.o., 2015. Comprehensive, integrative genomic analysis of diffuse lower-grade gliomas. 372(26):2481-2498.

[10] Huang, L.E.J.C., 2019. Friend or foe—IDH1 mutations in glioma 10 years on. 40(11):1299-1307.

[11] Ostrom, Q.T., Gittleman, H., Farah, P., Ondracek, A., Chen, Y., Wolinsky, Y., et al., 2013. CBTRUS statistical report: Primary brain and central nervous system tumors diagnosed in the United States in 2006-2010. 15(suppl_2):ii1-ii56.

[12] Koshy, M., Villano, J.L., Dolecek, T.A., Howard, A., Mahmood, U., Chmura, S.J., et al., 2012. Improved survival time trends for glioblastoma using the SEER 17 population-based registries. 107(1):207-212.

[13] Tamimi, A.F., Juweid, M., 2017. Epidemiology and outcome of glioblastoma. Glioblastoma [Internet]. Codon Publications.

[14] Grech, N., Dalli, T., Mizzi, S., Meilak, L., Calleja, N., Zrinzo, A.J.C., 2020. Rising Incidence of Glioblastoma Multiforme in a Well-Defined Population. 12(5).

[15] Nelson, S.J., Cha, S.J.T.C.J., 2003. Imaging glioblastoma multiforme. 9(2):134-145.

[16] Houillier, C., Wang, X., Kaloshi, G., Mokhtari, K., Guillevin, R., Laffaire, J., et al., 2010. IDH1 or IDH2 mutations predict longer survival and response to temozolomide in low-grade gliomas. 75(17):1560-1566.

[17] Hegi, M.E., Diserens, A.-C., Gorlia, T., Hamou, M.-F., De Tribolet, N., Weller, M., et al., 2005. MGMT gene silencing and benefit from temozolomide in glioblastoma. 352(10):997-1003.

[18] Brat, D.J., Aldape, K., Colman, H., Holland, E.C., Louis, D.N., Jenkins, R.B., et al., 2018. cIMPACT-NOW update 3: recommended diagnostic criteria for "Diffuse astrocytic glioma, IDH-wildtype, with molecular features of glioblastoma, WHO grade IV". 136(5):805-810.

[19] Yao, M., Li, S., Wu, X., Diao, S., Zhang, G., He, H., et al., 2018. Cellular origin of glioblastoma and its implication in precision therapy. 15(8):737-739.

[20] Fan, X., Xiong, Y., Wang, Y.J.F.o.m., 2019. A reignited debate over the cell (s) of origin for glioblastoma and its clinical implications. 13(5):531-539.

[21] Verhaak, R.G., Hoadley, K.A., Purdom, E., Wang, V., Qi, Y., Wilkerson, M.D., et al., 2010. Integrated genomic analysis identifies clinically relevant subtypes of glioblastoma characterized by abnormalities in PDGFRA, IDH1, EGFR, and NF1. 17(1):98-110.

[22] Kim, Y., Varn, F.S., Park, S.-H., Yoon, B.W., Park, H.R., Lee, C., et al., 2021. Perspective of mesenchymal transformation in glioblastoma. 9(1):1-20.

[23] Van Meir, E.G., Hadjipanayis, C.G., Norden, A.D., Shu, H.K., Wen, P.Y., Olson, J.J.J.C.a.c.j.f.c., 2010. Exciting new advances in neuro-oncology: the avenue to a cure for malignant glioma. 60(3):166-193.

[24] Zhang, P., Xia, Q., Liu, L., Li, S., Dong, L.J.F.i.M.B., 2020. Current opinion on molecular characterization for GBM classification in guiding clinical diagnosis, prognosis, and therapy. 7:241.

[25] Colman, H., Zhang, L., Sulman, E.P., McDonald, J.M., Shooshtari, N.L., Rivera, A., et al., 2010. A multigene predictor of outcome in glioblastoma. 12(1):49-57.

[26] Madurga, R., García-Romero, N., Jiménez, B., Collazo, A., Pérez-Rodríguez, F., Hernández-Laín, A., et al., 2021. Normal tissue content impact on the GBM molecular classification. 22(3):bbaa129.

[27] Wang, Q., Hu, B., Hu, X., Kim, H., Squatrito, M., Scarpace, L., et al., 2017. Tumor evolution of glioma-intrinsic gene expression subtypes associates with immunological changes in the microenvironment. 32(1):42-56. e46.

[28] Molinaro, A.M., Taylor, J.W., Wiencke, J.K., Wrensch, M.R.J.N.R.N., 2019. Genetic and molecular epidemiology of adult diffuse glioma. 15(7):405-417.

[29] Zhang, L., Liu, Z., Li, J., Huang, T., Wang, Y., Chang, L., et al., 2019. Genomic analysis of primary and recurrent gliomas reveals clinical outcome related molecular features. 9(1):1-8.

[30] Mirchia, K., Richardson, T.E.J.C., 2020. Beyond IDH-Mutation: emerging molecular diagnostic and prognostic features in adult diffuse gliomas. 12(7):1817.

[31] Kanderi, T., Gupta, V.J.S., 2020. Glioblastoma Multiforme.

[32] Young, R.M., Jamshidi, A., Davis, G., Sherman, J.H.J.A.o.t.m., 2015. Current trends in the surgical management and treatment of adult glioblastoma. 3(9).

[33] Nakada, M., Kita, D., Watanabe, T., Hayashi, Y., Teng, L., Pyko, I.V., et al., 2011. Aberrant signaling pathways in glioma. 3(3):3242-3278.

[34] Hanif, F., Muzaffar, K., Perveen, K., Malhi, S.M., Simjee, S.U.J.A.P.j.o.c.p.A., 2017. Glioblastoma multiforme: a review of its epidemiology and pathogenesis through clinical presentation and treatment. 18(1):3.

[35] Schiff, D., Lee, E.Q., Nayak, L., Norden, A.D., Reardon, D.A., Wen, P.Y.J.N.-o., 2015. Medical management of brain tumors and the sequelae of treatment. 17(4):488-504.

[36] Davis, M.E.J.C.j.o.o.n., 2016. Glioblastoma: overview of disease and treatment. 20(5):S2.

[37] Verger, A., Langen, K.-J.J.E.P., 2017. PET Imaging in glioblastoma: Use in clinical practice.155-174.

[38] Winnard, P.T., Pathak, A.P., Dhara, S., Cho, S.Y., Raman, V., Pomper, M.G.J.J.o.N.M., 2008. Molecular imaging of metastatic potential. 49(Suppl 2):96S-112S.

[39] Timm, K.N., Kennedy, B.W., Brindle, K.M.J.C.C.R., 2016. Imaging tumor metabolism to assess disease progression and treatment response. 22(21):5196-5203.

[40] Kim, M.M., Parolia, A., Dunphy, M.P., Venneti, S.J.N.R.C.O., 2016. Non-invasive metabolic imaging of brain tumours in the era of precision medicine. 13(12):725.

[41] Evans, S.M., Judy, K.D., Dunphy, I., Jenkins, W.T., Nelson, P.T., Collins, R., et al., 2004. Comparative measurements of hypoxia in human brain tumors using needle electrodes and EF5 binding. 64(5):1886-1892.

[42] Tabatabaei, P., Bergström, P., Henriksson, R., Bergenheim, A.T.J.J.o.n.-o., 2008. Glucose metabolites, glutamate and glycerol in malignant glioma tumours during radiotherapy. 90(1):35-39.

[43] Oudard, S., Arvelo, F., Miccoli, L., Apiou, F., Dutrillaux, A., Poisson, M., et al., 1996. High glycolysis in gliomas despite low hexokinase transcription and activity correlated to chromosome 10 loss. 74(6):839-845.

[44] Zhang, Y., Guillermier, C., De Raedt, T., Cox, A.G., Maertens, O., Yimlamai, D., et al., 2020. Imaging mass spectrometry reveals tumor metabolic heterogeneity. 23(8):101355.

[45] Nabors, L.B., Portnow, J., Ahluwalia, M., Baehring, J., Brem, H., Brem, S., et al., 2020. Central Nervous System Cancers, Version 3.2020, NCCN Clinical Practice Guidelines in Oncology. 18(11):1537-1570.

[46] McGirt, M.J., Chaichana, K.L., Gathinji, M., Attenello, F.J., Than, K., Olivi, A., et al., 2009. Independent association of extent of resection with survival in patients with malignant brain astrocytoma. 110(1):156-162.

[47] Lacroix, M., Abi-Said, D., Fourney, D.R., Gokaslan, Z.L., Shi, W., DeMonte, F., et al., 2001. A multivariate analysis of 416 patients with glioblastoma multiforme: prognosis, extent of resection, and survival. 95(2):190-198.

[48] Stummer, W., Pichlmeier, U., Meinel, T., Wiestler, O.D., Zanella, F., Reulen, H.-J., et al., 2006. Fluorescence-guided surgery with 5-aminolevulinic acid for resection of malignant glioma: a randomised controlled multicentre phase III trial. 7(5):392-401.

[49] Mukherjee, D., Quinones-Hinojosa, A., 2011. Impact of extent of resection on outcomes in patients with high-grade gliomas. Tumors of the Central Nervous System, Volume 2. Springer, p. 173-179.

[50] Walker, M.D., Strike, T.A., Sheline, G.E.J.I.J.o.R.O.B.P., 1979. An analysis of dose-effect relationship in the radiotherapy of malignant gliomas. 5(10):1725-1731.

[51] Kristiansen, K., Hagen, S., Kollevold, T., Torvik, A., Holme, I., Stat, M., et al., 1981. Combined modality therapy of operated astrocytomas grade III and IV. Confirmation of the value of postoperative

irradiation and lack of potentiation of bleomycin on survival time: a prospective multicenter trial of the Scandinavian Glioblastoma Study Group. 47(4):649-652.

[52] Stupp, R., Hegi, M.E., Mason, W.P., Van Den Bent, M.J., Taphoorn, M.J., Janzer, R.C., et al., 2009. Effects of radiotherapy with concomitant and adjuvant temozolomide versus radiotherapy alone on survival in glioblastoma in a randomised phase III study: 5-year analysis of the EORTC-NCIC trial. 10(5):459-466.

[53] Stupp, R., Taillibert, S., Kanner, A., Kesari, S., Toms, S.A., Barnett, G.H., et al., 2015. Tumor treating fields (TTFields): A novel treatment modality added to standard chemo-and radiotherapy in newly diagnosed glioblastoma—First report of the full dataset of the EF14 randomized phase III trial. American Society of Clinical Oncology.

[54] Guzauskas, G.F., Salzberg, M., Wang, B.C.J.C.o., 2018. Estimated lifetime survival benefit of tumor treating fields and temozolomide for newly diagnosed glioblastoma patients. 7(3):CNS23.

[55] Seyfried, T.N., Shelton, L., Arismendi-Morillo, G., Kalamian, M., Elsakka, A., Maroon, J., et al., 2019. Provocative question: should ketogenic metabolic therapy become the standard of care for glioblastoma? 44(10):2392-2404.

[56] Zielinski, D.C., Jamshidi, N., Corbett, A.J., Bordbar, A., Thomas, A., Palsson, B.O.J.S.r., 2017. Systems biology analysis of drivers underlying hallmarks of cancer cell metabolism. 7(1):1-14.

[57] Potter, M., Newport, E., Morten, K.J., 2016. The Warburg effect: 80 years on. Biochemical Society transactions 44(5):1499.

[58] Seyfried, T.N., Arismendi-Morillo, G., Mukherjee, P., Chinopoulos, C., 2020. On the Origin of ATP Synthesis in Cancer. iScience 23(11):101761.

[59] Pavlova, N.N., Thompson, C.B.J.C.m., 2016. The emerging hallmarks of cancer metabolism. 23(1):27-47.

[60] Cairns, R.A., Harris, I.S., Mak, T.W., 2011. Regulation of cancer cell metabolism. Nature Reviews Cancer 11(2):85.

[61] Weinberg, R.A., 2014. Coming full circle—from endless complexity to simplicity and back again. Cell 157(1):267.

[62] Wishart, D.S., 2015. Is cancer a genetic disease or a metabolic disease? EBioMedicine 2(6):478.

[63] Ladanie, A., Schmitt, A.M., Speich, B., Naudet, F., Agarwal, A., Pereira, T.V., et al., 2020. Clinical Trial Evidence Supporting US Food and Drug Administration Approval of Novel Cancer Therapies Between 2000 and 2016. 3(11):e2024406-e2024406.

[64] Soto, A.M., Sonnenschein, C., 2004. The somatic mutation theory of cancer: growing problems with the paradigm? Bioessays 26(10):1097.

[65] Brücher, B.L., Jamall, I.S.J.C.P., Biochemistry, 2016. Somatic mutation theory-why it's wrong for most cancers. 38(5):1663-1680.

[66] Adashek, J.J., Kato, S., Lippman, S.M., Kurzrock, R.J.G.m., 2020. The paradox of cancer genes in non-malignant conditions: implications for precision medicine. 12(1):1-19.

[67] Sonnenschein, C., Soto, A.M.J.P.b., 2020. Over a century of cancer research: Inconvenient truths and promising leads. 18(4):e3000670.

[68] Schwartz, L., T Supuran, C., O Alfarouk, K., 2017. The Warburg effect and the Hallmarks of Cancer. Anti-Cancer Agents in Medicinal Chemistry (Formerly Current Medicinal Chemistry-Anti-Cancer Agents) 17(2):164.

[69] Seyfried, T.N., Chinopoulos, C.J.M., 2021. Can the Mitochondrial Metabolic Theory Explain Better the Origin and Management of Cancer than Can the Somatic Mutation Theory? 11(9):572.

[70] Vyas, S., Zaganjor, E., Haigis, M.C., 2016. Mitochondria and cancer. Cell 166(3):555.

[71] Kulish, O., Wright, A., Terentjev, E.J.S.r., 2016. F 1 rotary motor of ATP synthase is driven by the torsionally-asymmetric drive shaft. 6(1):1-14.

[72] Davila, A.F., Zamorano, P.J.P.b., 2013. Mitochondria and the evolutionary roots of cancer. 10(2):026008.

[73] Saxton, R.A., Sabatini, D.M., 2017. mTOR signaling in growth, metabolism, and disease. Cell 168(6):960.

[74] Clark, J., Rager, J.E.J.E.E.i.T., Health, P., 2020. Epigenetics: An overview of CpG methylation, chromatin remodeling, and regulatory/noncoding RNAs.3-32.

[75] Fu, Y., Tigano, M., Sfeir, A.J.N.S., Biology, M., 2020. Safeguarding mitochondrial genomes in higher eukaryotes. 27(8):687-695.

[76] Stuart, J.A., Brown, M.F.J.B.e.B.A.-B., 2006. Mitochondrial DNA maintenance and bioenergetics. 1757(2):79-89.

[77] Sonugür, F.G., Akbulut, H.J.F.i.g., 2019. The role of tumor microenvironment in genomic instability of malignant tumors. 10:1063.

[78] Ibrahim-Hashim, A., Estrella, V.J.C., Reviews, M., 2019. Acidosis and cancer: from mechanism to neutralization. 38(1):149-155.

[79] Butow, R.A., Avadhani, N.G.J.M.c., 2004. Mitochondrial signaling: the retrograde response. 14(1):1-15.

[80] Jose, C., Bellance, N., Rossignol, R.J.B.e.B.A.-B., 2011. Choosing between glycolysis and oxidative phosphorylation: a tumor's dilemma? 1807(6):552-561.

[81] Seyfried, T.N., Shelton, L.M., 2010. Cancer as a metabolic disease. Nutrition & Metabolism 7(1):7.

[82] Baker, S.G.J.C., 2021. The case for a cancer paradox initiative.

[83] Bonuccelli, G., Tsirigos, A., Whitaker-Menezes, D., Pavlides, S., Pestell, R.G., Chiavarina, B., et al., 2010. Ketones and lactate "fuel" tumor growth and metastasis: Evidence that epithelial cancer cells use oxidative mitochondrial metabolism. Cell Cycle 9(17):3506.

[84] DeBerardinis, R.J., Sayed, N., Ditsworth, D., Thompson, C.B.J.C.o.i.g., development, 2008. Brick by brick: metabolism and tumor cell growth. 18(1):54-61.

[85] Li, R., Wang, W., Yang, Y., Gu, C.J.O.R., 2020. Exploring the role of glucose-6-phosphate dehydrogenase in cancer.

[86] Johannsen, D.L., Ravussin, E.J.C.o.i.p., 2009. The role of mitochondria in health and disease. 9(6):780-786.

[87] Nicholls, D.G., Budd, S.L.J.P.r., 2000. Mitochondria and neuronal survival. 80(1):315-360.

[88] Benard, G., Rossignol, R.J.A., signaling, r., 2008. Ultrastructure of the mitochondrion and its bearing on function and bioenergetics. 10(8):1313-1342.

[89] Pfeiffer, T., Schuster, S., Bonhoeffer, S.J.S., 2001. Cooperation and competition in the evolution of ATP-producing pathways. 292(5516):504-507.

[90] Seyfried, T.N., Yu, G., Maroon, J.C., D'Agostino, D.P., 2017. Press-pulse: a novel therapeutic strategy for the metabolic management of cancer. Nutrition & Metabolism 14(1):19.

[91] Porporato, P.E., Filigheddu, N., Bravo-San Pedro, J.M., Kroemer, G., Galluzzi, L.J.C.r., 2018. Mitochondrial metabolism and cancer. 28(3):265-280.

[92] Grasso, D., Zampieri, L.X., Capelôa, T., Van de Velde, J.A., Sonveaux, P.J.C.s., 2020. Mitochondria in cancer. 4(6):114.

[93] Elliott, R., Barnett, B.J.M., Microanalysis, 2011. Ultrastructural observation of mitochondria in human breast carcinoma cells. 17(S2):194-195.

[94] Arismendi-Morillo, G.J., Castellano-Ramirez, A.V.J.J.o.e.m., 2008. Ultrastructural mitochondrial pathology in human astrocytic tumors: potentials implications pro-therapeutics strategies. 57(1):33-39.

[95] Brand, M.D., Nicholls, D.G.J.B.J., 2011. Assessing mitochondrial dysfunction in cells. 435(2):297-312.

[96] Alberts, B., Johnson, A., Lewis, J., Raff, M., Roberts, K., Walter, P., 2002. The evolution of electron-transport chains. Molecular Biology of the Cell. 4th edition. Garland Science.

[97] Seyfried, T., 2012. Cancer as a metabolic disease: on the origin, management, and prevention of cancer. John Wiley & Sons.

[98] Chen, J.-Q., Russo, J.J.B.e.B.A.-R.o.C., 2012. Dysregulation of glucose transport, glycolysis, TCA cycle and glutaminolysis by oncogenes and tumor suppressors in cancer cells. 1826(2):370-384.

[99] Parsons, D.W., Jones, S., Zhang, X., Lin, J.C.-H., Leary, R.J., Angenendt, P., et al., 2008. An integrated genomic analysis of human glioblastoma multiforme. 321(5897):1807-1812.

[100] Yang, M., Soga, T., Pollard, P.J.J.T.J.o.c.i., 2013. Oncometabolites: linking altered metabolism with cancer. 123(9):3652-3658.

[101] Seyfried, T.N., Shivane, A.G., Kalamian, M., Maroon, J.C., Mukherjee, P., Zuccoli, G.J.F.i.N., 2021. Ketogenic Metabolic Therapy, Without Chemo or Radiation, for the Long-Term Management of IDH1-Mutant Glioblastoma: An 80-Month Follow-Up Case Report. 8:281.

[102] Platten, M., Bunse, L., Wick, A., Bunse, T., Le Cornet, L., Harting, I., et al., 2021. A vaccine targeting mutant IDH1 in newly diagnosed glioma. 592(7854):463-468.

[103] Elliott, R., Jiang, X., Head, J.J.B.c.r., treatment, 2012. Mitochondria organelle transplantation: introduction of normal epithelial mitochondria into human cancer cells inhibits proliferation and increases drug sensitivity. 136(2):347-354.

[104] Seyfried, T.N.J.F.i.c., biology, d., 2015. Cancer as a mitochondrial metabolic disease. 3:43.

[105] Singh, K.K., Kulawiec, M., Still, I., Desouki, M.M., Geradts, J., Matsui, S.-I.J.G., 2005. Inter-genomic cross talk between mitochondria and the nucleus plays an important role in tumorigenesis. 354:140-146.

[106] Mintz, B., Illmensee, K.J.P.o.t.N.A.o.S., 1975. Normal genetically mosaic mice produced from malignant teratocarcinoma cells. 72(9):3585-3589.

[107] Kaipparettu, B.A., Ma, Y., Park, J.H., Lee, T.-L., Zhang, Y., Yotnda, P., et al., 2013. Crosstalk from non-cancerous mitochondria can inhibit tumor properties of metastatic cells by suppressing oncogenic pathways. PLoS One 8(5):e61747.

[108] Israel, B.A., Schaeffer, W.I.J.I.v.c., biology, d., 1988. Cytoplasmic mediation of malignancy. 24(5):487-490.

[109] Schmidt, C.A., Fisher-Wellman, K.H., Neufer, P.D.J.J.o.B.C., 2021. From OCR and ECAR to energy: perspectives on the design and interpretation of bioenergetics studies.101140.

[110] Ramanathan, A., Wang, C., Schreiber, S.L.J.P.o.t.N.A.o.S., 2005. Perturbational profiling of a cell-line model of tumorigenesis by using metabolic measurements. 102(17):5992-5997.

[111] Tan, A.S., Baty, J.W., Dong, L.-F., Bezawork-Geleta, A., Endaya, B., Goodwin, J., et al., 2015. Mitochondrial genome acquisition restores respiratory function and tumorigenic potential of cancer cells without mitochondrial DNA. 21(1):81-94.

[112] Vander Heiden, M.G., Cantley, L.C., Thompson, C.B., 2009. Understanding the Warburg effect: the metabolic requirements of cell proliferation. Science (New York, N.Y.) 324(5930):1029.

[113] Kapelner, A., Vorsanger, M., 2015. Starvation of cancer via induced ketogenesis and severe hypoglycemia. Medical hypotheses 84(3):162.

[114] Tran, Q., Lee, H., Park, J., Kim, S.-H., Park, J.J.T.r., 2016. Targeting cancer metabolism-revisiting the Warburg effects. 32(3):177-193.

[115] Acker, M.G., Auld, D.S.J.P.i.S., 2014. Considerations for the design and reporting of enzyme assays in high-throughput screening applications. 1(1-6):56-73.

[116] Gu, X., Ma, Y., Liu, Y., Wan, Q.J.S.p., 2021. Measurement of mitochondrial respiration in adherent cells by Seahorse XF96 Cell Mito Stress Test. 2(1):100245.

[117] Zielonka, J., Kalyanaraman, B.J.F.R.B., Medicine, 2010. Hydroethidine-and MitoSOX-derived red fluorescence is not a reliable indicator of intracellular superoxide formation: another inconvenient truth. 48(8):983-1001.

[118] Chen, X., Zhong, Z., Xu, Z., Chen, L., Wang, Y.J.F.r.r., 2010. 2′, 7′-Dichlorodihydrofluorescein as a fluorescent probe for reactive oxygen species measurement: forty years of application and controversy. 44(6):587-604.

[119] Strickland, M., Stoll, E.A.J.F.i.c., biology, d., 2017. Metabolic reprogramming in glioma. 5:43.

[120] Koppenol, W.H., Bounds, P.L., Dang, C.V.J.N.R.C., 2011. Otto Warburg's contributions to current concepts of cancer metabolism. 11(5):325-337.

[121] Torresano, L., Nuevo-Tapioles, C., Santacatterina, F., Cuezva, J.M.J.B.e.B.A.-M.B.o.D., 2020. Metabolic reprogramming and disease progression in cancer patients. 1866(5):165721.

[122] Vidali, S., Aminzadeh, S., Lambert, B., Rutherford, T., Sperl, W., Kofler, B., et al., 2015. Mitochondria: The ketogenic diet—A metabolism-based therapy. 63:55-59.

[123] Lin, H., Patel, S., Affleck, V.S., Wilson, I., Turnbull, D.M., Joshi, A.R., et al., 2017. Fatty acid oxidation is required for the respiration and proliferation of malignant glioma cells. 19(1):43-54.

[124] Chinopoulos, C., Seyfried, T.N.J.A.n., 2018. Mitochondrial substrate-level phosphorylation as energy source for glioblastoma: review and hypothesis. 10:1759091418818261.

[125] Xu, X.D., Shao, S.X., Jiang, H.P., Cao, Y.W., Wang, Y.H., Yang, X.C., et al., 2015. Warburg effect or reverse Warburg effect? A review of cancer metabolism. 38(3):117-122.

[126] Sengupta, D., Pratx, G.J.M.c., 2016. Imaging metabolic heterogeneity in cancer. 15(1):4.

[127] Di Gialleonardo, V., Wilson, D.M., Keshari, K.R., 2016. The potential of metabolic imaging, Seminars in nuclear medicine. Elsevier, pp. 28-39.

[128] Clarke, M.F.J.B.o.B., Transplantation, M., 2005. Self-renewal and solid-tumor stem cells. 11(2):14-16.

[129] Reya, T., Morrison, S.J., Clarke, M.F., Weissman, I.L.J.n., 2001. Stem cells, cancer, and cancer stem cells. 414(6859):105-111.

[130] Pattabiraman, D.R., Weinberg, R.A.J.N.r.D.d., 2014. Tackling the cancer stem cells—what challenges do they pose? 13(7):497-512.

[131] Singh, S.K., Hawkins, C., Clarke, I.D., Squire, J.A., Bayani, J., Hide, T., et al., 2004. Identification of human brain tumour initiating cells. 432(7015):396-401.

[132] Gerdes, M.J., Sood, A., Sevinsky, C., Pris, A.D., Zavodszky, M.I., Ginty, F.J.F.i.o., 2014. Emerging understanding of multiscale tumor heterogeneity. 4:366.

[133] Michor, F., Polyak, K.J.C.p.r., 2010. The origins and implications of intratumor heterogeneity. 3(11):1361-1364.

[134] Medema, J.P.J.N.c.b., 2013. Cancer stem cells: the challenges ahead. 15(4):338-344.

[135] Orsi, W.D., Schink, B., Buckel, W., Martin, W.F.J.F.m.r., 2020. Physiological limits to life in anoxic subseafloor sediment. 44(2):219-231.

[136] Sonnenschein, C., Soto, A.M.J.O.J.o.B.S., 2021. Control of Cell Proliferation: Is the Default State of Cells Quiescence or Proliferation? :33-42.

[137] Pacini, N., Borziani, F.J.I.j.o.m.s., 2014. Cancer stem cell theory and the warburg effect, two sides of the same coin? 15(5):8893-8930.

[138] MENENDEZ, J., Joven, J., Cufí, S., Corominas-Faja, B., Oliveras-Ferraros, C., Cuyàs, E., et al., 2013. The Warburg effect version 2.0: metabolic reprogramming of cancer stem cells. 12(8):1166-1179.

[139] Shi, Y., Inoue, H., Wu, J.C., Yamanaka, S.J.N.r.D.d., 2017. Induced pluripotent stem cell technology: a decade of progress. 16(2):115-130.

[140] Warburg, O., 1956. On respiratory impairment in cancer cells. Science (New York, N.Y.) 124(3215):269.

[141] Warburg, O., 1956. On the origin of cancer cells. Science (New York, N.Y.) 123(3191):309.

[142] Beck, B., Blanpain, C.J.N.R.C., 2013. Unravelling cancer stem cell potential. 13(10):727-738.

[143] Huysentruyt, L.C., Seyfried, T.N.J.C., Reviews, M., 2010. Perspectives on the mesenchymal origin of metastatic cancer. 29(4):695-707.

[144] Munzarová, M., Kovarík, J.J.T.L., 1987. Is cancer a macrophage-mediated autoaggressive disease? 329(8539):952-954.

[145] Taha, M., Ahmad, A., Wharton, S., Jellinek, D.J.B.j.o.n., 2005. Extra-cranial metastasis of glioblastoma multiforme presenting as acute parotitis. 19(4):348-351.

[146] Hoffman, H.J., Duffner, P.K.J.C., 1985. Extraneural metastases of central nervous system tumors. 56(S7):1778-1782.

[147] Rubinstein, L.J., 1972. Tumors of the central nervous system. Armed Forces Institute of Pathology; sold by American Registry of Pathology.

[148] Wang, X., Zhu, Y., Ma, Y., Wang, J., Zhang, F., Xia, Q., et al., 2013. The role of cancer stem cells in cancer metastasis: new perspective and progress. 37(1):60-63.

[149] Vaupel, P., Multhoff, G.J.T.J.o.P., 2020. Revisiting the warburg effect: historical dogma versus current understanding.

[150] Lathia, J.D., Mack, S.C., Mulkearns-Hubert, E.E., Valentim, C.L., Rich, J.N.J.G., development, 2015. Cancer stem cells in glioblastoma. 29(12):1203-1217.

[151] Vlashi, E., Lagadec, C., Vergnes, L., Matsutani, T., Masui, K., Poulou, M., et al., 2011. Metabolic state of glioma stem cells and nontumorigenic cells. 108(38):16062-16067.

[152] Mao, P., Joshi, K., Li, J., Kim, S.-H., Li, P., Santana-Santos, L., et al., 2013. Mesenchymal glioma stem cells are maintained by activated glycolytic metabolism involving aldehyde dehydrogenase 1A3. 110(21):8644-8649.

[153] Marin-Valencia, I., Yang, C., Mashimo, T., Cho, S., Baek, H., Yang, X.-L., et al., 2012. Analysis of tumor metabolism reveals mitochondrial glucose oxidation in genetically diverse human glioblastomas in the mouse brain in vivo. Cell metabolism 15(6):827.

[154] Li, Z., Bao, S., Wu, Q., Wang, H., Eyler, C., Sathornsumetee, S., et al., 2009. Hypoxia-inducible factors regulate tumorigenic capacity of glioma stem cells. 15(6):501-513.

[155] Calabrese, C., Poppleton, H., Kocak, M., Hogg, T.L., Fuller, C., Hamner, B., et al., 2007. A perivascular niche for brain tumor stem cells. 11(1):69-82.

[156] Saga, I., Shibao, S., Okubo, J., Osuka, S., Kobayashi, Y., Yamada, S., et al., 2014. Integrated analysis identifies different metabolic signatures for tumor-initiating cells in a murine glioblastoma model. 16(8):1048-1056.

[157] Shibao, S., Minami, N., Koike, N., Fukui, N., Yoshida, K., Saya, H., et al., 2018. Metabolic heterogeneity and plasticity of glioma stem cells in a mouse glioblastoma model. 20(3):343-354.

[158] Garcia-Romero, N., Gonzalez-Tejedo, C., Carrion-Navarro, J., Esteban-Rubio, S., Rackov, G., Rodriguez-Fanjul, V., et al., 2016. Cancer stem cells from human glioblastoma resemble but do not mimic original tumors after in vitro passaging in serum-free media. Oncotarget 7(40):65888.

[159] Arismendi-Morillo, G.J.T.i.j.o.b., biology, c., 2009. Electron microscopy morphology of the mitochondrial network in human cancer. 41(10):2062-2068.

[160] Peiris-Pagès, M., Martinez-Outschoorn, U.E., Pestell, R.G., Sotgia, F., Lisanti, M.P.J.B.C.R., 2016. Cancer stem cell metabolism. 18(1):1-10.

[161] Chiu, M., Ottaviani, L., Bianchi, M.G., Franchi-Gazzola, R., Bussolati, O.J.A.B., 2012. Towards a metabolic therapy of cancer. 83(3):168-176.

[162] Martinez-Outschoorn, U.E., Peiris-Pagès, M., Pestell, R.G., Sotgia, F., Lisanti, M.P., 2017. Cancer metabolism: a therapeutic perspective. Nature Reviews Clinical Oncology 14(1):11.

[163] Seyfried, T.N., Shelton, L.M.J.N., metabolism, 2010. Cancer as a metabolic disease. 7(1):1-22.

[164] Roy, S., Kumaravel, S., Sharma, A., Duran, C.L., Bayless, K.J., Chakraborty, S.J.E.B., et al., 2020. Hypoxic tumor microenvironment: Implications for cancer therapy. 245(13):1073-1086.

[165] Wei, Q., Qian, Y., Yu, J., Wong, C.C.J.O., 2020. Metabolic rewiring in the promotion of cancer metastasis: mechanisms and therapeutic implications. 39(39):6139-6156.

[166] Abdel-Wahab, A.F., Mahmoud, W., Al-Harizy, R.M.J.P.r., 2019. Targeting glucose metabolism to suppress cancer progression: prospective of anti-glycolytic cancer therapy. 150:104511.

[167] Yu, T., Dong, T., Eyvani, H., Fang, Y., Wang, X., Zhang, X., et al., 2020. Metabolic interventions: A new insight into the cancer immunotherapy.108659.

[168] Allen, B.G., Bhatia, S.K., Anderson, C.M., Eichenberger-Gilmore, J.M., Sibenaller, Z.A., Mapuskar, K.A., et al., 2014. Ketogenic diets as an adjuvant cancer therapy: History and potential mechanism. Redox biology 2:963.

[169] Agnihotri, S., Zadeh, G.J.N.-o., 2015. Metabolic reprogramming in glioblastoma: the influence of cancer metabolism on epigenetics and unanswered questions. 18(2):160-172.

[170] Katsetos, C.D., Anni, H., Dráber, P., 2013. Mitochondrial dysfunction in gliomas, Seminars in pediatric neurology. Elsevier, pp. 216-227.

[171] Sica, V., Bravo-San Pedro, J.M., Stoll, G., Kroemer, G.J.I.j.o.c., 2020. Oxidative phosphorylation as a potential therapeutic target for cancer therapy. 146(1):10-17.

[172] Poteet, E., Choudhury, G.R., Winters, A., Li, W., Ryou, M.-G., Liu, R., et al., 2013. Reversing the Warburg effect as a treatment for glioblastoma. 288(13):9153-9164.

[173] Edmond, J., Robbins, R.A., Bergstrom, J.D., Cole, R.A., De Vellis, J., 1987. Capacity for substrate utilization in oxidative metabolism by neurons, astrocytes, and oligodendrocytes from developing brain in primary culture. Journal of neuroscience research 18(4):551.

[174] Chechik, T., Roeder, L.M., Tildon, J.T., Poduslo, S.E., 1987. Ketone body enzyme activities in purified neurons, astrocytes and oligodendroglia. Neurochemistry international 10(1):95.

[175] Duraj, T., Carrión-Navarro, J., Seyfried, T.N., García-Romero, N., Ayuso-Sacido, A.J.M.M., 2021. Metabolic therapy and bioenergetic analysis: the missing piece of the puzzle.101389.

[176] Harris, A.L., 2020. Development of cancer metabolism as a therapeutic target: New pathways, patient studies, stratification and combination therapy. Nature Publishing Group.

[177] Anderson, N.M., Mucka, P., Kern, J.G., Feng, H.J.P., cell, 2018. The emerging role and targetability of the TCA cycle in cancer metabolism. 9(2):216-237.

[178] Mallick, S., Benson, R., Hakim, A., Rath, G.K.J.J.o.t.E.N.C.I., 2016. Management of glioblastoma after recurrence: A changing paradigm. 28(4):199-210.

[179] Cervantes-Madrid, D., Dominguez-Gomez, G., Gonzalez-Fierro, A., Perez-Cardenas, E., Taja-Chayeb, L., Trejo-Becerril, C., et al., 2017. Feasibility and antitumor efficacy in vivo, of simultaneously targeting glycolysis, glutaminolysis and fatty acid synthesis using lonidamine, 6-diazo-5-oxo-L-norleucine and orlistat in colon cancer. Oncology letters 13(3):1905.

[180] Khodabakhshi, A., Akbari, M.E., Mirzaei, H.R., Seyfried, T.N., Kalamian, M., Davoodi, S.H.J.C.N., 2021. Effects of Ketogenic metabolic therapy on patients with breast Cancer: a randomized controlled clinical trial. 40(3):751-758.

[181] İyikesici, M.S., Slocum, A.K., Winters, N., Kalamian, M., Seyfried, T.N.J.C., 2021. Metabolically Supported Chemotherapy for Managing End-Stage Breast Cancer: A Complete and Durable Response. 13(4).

[182] Amoedo, N.D., Obre, E., Rossignol, R., 2017. Drug discovery strategies in the field of tumor energy metabolism: limitations by metabolic flexibility and metabolic resistance to chemotherapy. Biochimica et Biophysica Acta (BBA)-Bioenergetics 1858(8):674.

[183] Fan, T.W.-M., Higashi, R.M., Chernayavskaya, Y., Lane, A.N.J.M., 2020. Resolving metabolic heterogeneity in experimental models of the tumor microenvironment from a stable isotope resolved metabolomics perspective. 10(6):249.

[184] Heaster, T.M., Landman, B.A., Skala, M.C.J.F.i.o., 2019. Quantitative spatial analysis of metabolic heterogeneity across in vivo and in vitro tumor models. 9:1144.

[185] Sharick, J.T., Walsh, C.M., Sprackling, C.M., Pasch, C.A., Pham, D.L., Esbona, K., et al., 2020. Metabolic heterogeneity in patient tumor-derived organoids by primary site and drug treatment. 10:553.

[186] Connealy, L.E., Diagnostic Tests for Early Detection of Cancer: An Integrative Approach.

[187] Lee, J., Campbell, D., Singh, A., Phelps, M., Satyamurthy, N., Czernin, J., et al., 2011. Tumor metabolic phenotyping and treatment stratification by positron emission tomography. 52(supplement 1):23-23.

[188] Goveia, J., Pircher, A., Conradi, L.C., Kalucka, J., Lagani, V., Dewerchin, M., et al., 2016. Meta-analysis of clinical metabolic profiling studies in cancer: challenges and opportunities. 8(10):1134-1142.

[189] Lemberg, K.M., Vornov, J.J., Rais, R., Slusher, B.S.J.M.c.t., 2018. We're not "DON" yet: optimal dosing and prodrug delivery of 6-Diazo-5-oxo-L-norleucine. 17(9):1824-1832.

[190] Tataranni, T., Piccoli, C.J.O.M., Longevity, C., 2019. Dichloroacetate (DCA) and Cancer: An Overview towards Clinical Applications. 2019.

[191] Kasznicki, J., Sliwinska, A., Drzewoski, J.J.A.o.t.m., 2014. Metformin in cancer prevention and therapy. 2(6).

[192] Granchi, C., Paterni, I., Rani, R., Minutolo, F.J.F.m.c., 2013. Small-molecule inhibitors of human LDH5. 5(16):1967-1991.

[193] Pedersen, P.L.J.M.a.o.t.c., 1978. Tumor mitochondria and the bioenergetics of cancer cells. 22:190-274.

[194] Modica-Napolitano, J.S., Singh, K.K.J.M., 2004. Mitochondrial dysfunction in cancer. 4(5-6):755-762.

[195] Schumacker, P.T.J.C.c., 2006. Reactive oxygen species in cancer cells: live by the sword, die by the sword. 10(3):175-176.

[196] Sullivan, L.B., Chandel, N.S.J.C., metabolism, 2014. Mitochondrial reactive oxygen species and cancer. 2(1):1-12.

[197] Liou, G.-Y., Storz, P.J.F.r.r., 2010. Reactive oxygen species in cancer. 44(5):479-496.

[198] Nadege, B., Patrick, L., Rodrigue, R.J.F.i.b., 2009. Mitochondria: from bioenergetics to the metabolic regulation of carcinogenesis. 14(11):4015-4034.

[199] Raj, L., Ide, T., Gurkar, A.U., Foley, M., Schenone, M., Li, X., et al., 2011. Selective killing of cancer cells by a small molecule targeting the stress response to ROS. 475(7355):231-234.

[200] Singh, A., Faccenda, D., Campanella, M.J.E., 2021. Pharmacological advances in mitochondrial therapy. 65:103244.

[201] Vasan, K., Werner, M., Chandel, N.S.J.C.m., 2020. Mitochondrial Metabolism as a Target for Cancer Therapy.

[202] Iliopoulos, D., Hirsch, H.A., Struhl, K.J.C.r., 2011. Metformin decreases the dose of chemotherapy for prolonging tumor remission in mouse xenografts involving multiple cancer cell types. 71(9):3196-3201.

[203] Gritti, M., Würth, R., Angelini, M., Barbieri, F., Peretti, M., Pizzi, E., et al., 2014. Metformin repositioning as antitumoral agent: selective antiproliferative effects in human glioblastoma stem cells, via inhibition of CLIC1-mediated ion current. 5(22):11252.

[204] Chevalier, B., Pasquier, D., Lartigau, E.F., Chargari, C., Schernberg, A., Jannin, A., et al., 2020. Metformin:(future) best friend of the radiation oncologist? 151:95-105.

[205] Bowker, S., Yasui, Y., Veugelers, P., Johnson, J.J.D., 2010. Glucose-lowering agents and cancer mortality rates in type 2 diabetes: assessing effects of time-varying exposure. 53(8):1631-1637.

[206] Libby, G., Donnelly, L.A., Donnan, P.T., Alessi, D.R., Morris, A.D., Evans, J.M.J.D.c., 2009. New users of metformin are at low risk of incident cancer: a cohort study among people with type 2 diabetes. 32(9):1620-1625.

[207] Erices, R., Bravo, M.L., Gonzalez, P., Oliva, B., Racordon, D., Garrido, M., et al., 2013. Metformin, at concentrations corresponding to the treatment of diabetes, potentiates the cytotoxic effects of carboplatin in cultures of ovarian cancer cells. 20(12):1433-1446.

[208] Wen, K.-C., Sung, P.-L., Wu, A.T., Chou, P.-C., Lin, J.-H., Huang, C.-Y.F., et al., 2020. Neoadjuvant metformin added to conventional chemotherapy synergizes anti-proliferative effects in ovarian cancer. 13(1):1-13.

[209] Ugwueze, C.V., Ogamba, O.J., Young, E.E., Onyenekwe, B.M., Ezeokpo, B.C.J.A.C.P., 2020. Metformin: a possible option in cancer chemotherapy. 2020.

[210] Ward, N.P., Poff, A.M., Koutnik, A.P., D'Agostino, D.P., 2017. Complex I inhibition augments dichloroacetate cytotoxicity through enhancing oxidative stress in VM-M3 glioblastoma cells. PLoS One 12(6):e0180061.

[211] Ben Sahra, I., Laurent, K., Giuliano, S., Larbret, F., Ponzio, G., Gounon, P., et al., 2010. Targeting cancer cell metabolism: the combination of metformin and 2-deoxyglucose induces p53-dependent apoptosis in prostate cancer cells. Cancer research 70(6):2465.

[212] Lea, M.A., Chacko, J., Bolikal, S., Hong, J.Y., Chung, R., Ortega, A., et al., 2011. Addition of 2-deoxyglucose enhances growth inhibition but reverses acidification in colon cancer cells treated with phenformin. Anticancer Research 31(2):421.

[213] Singh, D., Banerji, A.K., Dwarakanath, B.S., Tripathi, R.P., Gupta, J.P., Mathew, T.L., et al., 2005. Optimizing cancer radiotherapy with 2-deoxy-D-glucose. Strahlentherapie und Onkologie 181(8):507.

[214] Cheong, J.H., Park, E.S., Liang, J., Dennison, J.B., Tsavachidou, D., Nguyen-Charles, C., et al., 2011. Dual inhibition of tumor energy pathway by 2-deoxyglucose and metformin is effective against a broad spectrum of preclinical cancer models. Molecular cancer therapeutics 10(12):2350.

[215] Zhuang, Y., Chan, D.K., Haugrud, A.B., Miskimins, W.K., 2014. Mechanisms by which low glucose enhances the cytotoxicity of metformin to cancer cells both in vitro and in vivo. PLoS One 9(9):e108444.

[216] Bittar, P.G., Charnay, Y., Pellerin, L., Bouras, C., Magistretti, P.J.J.J.o.C.B.F., Metabolism, 1996. Selective distribution of lactate dehydrogenase isoenzymes in neurons and astrocytes of human brain. 16(6):1079-1089.

[217] Brooks, G.A.J.C.m., 2018. The science and translation of lactate shuttle theory. 27(4):757-785.

[218] Bonuccelli, G., Whitaker-Menezes, D., Castello-Cros, R., Pavlides, S., Pestell, R.G., Fatatis, A., et al., 2010. The reverse Warburg effect: glycolysis inhibitors prevent the tumor promoting effects of caveolin-1 deficient cancer associated fibroblasts. 9(10):1960-1971.

[219] Chiche, J., Fur, Y.L., Vilmen, C., Frassineti, F., Daniel, L., Halestrap, A.P., et al., 2012. In vivo pH in metabolic-defective Ras-transformed fibroblast tumors: Key role of the monocarboxylate transporter, MCT4, for inducing an alkaline intracellular pH. 130(7):1511-1520.

[220] Pietras, K., Östman, A.J.E.c.r., 2010. Hallmarks of cancer: interactions with the tumor stroma. 316(8):1324-1331.

[221] Dienel, G.A.J.J.o.C.B.F., Metabolism, 2012. Brain lactate metabolism: the discoveries and the controversies. 32(7):1107-1138.

[222] Virtuoso, A., Giovannoni, R., De Luca, C., Gargano, F., Cerasuolo, M., Maggio, N., et al., 2021. The Glioblastoma Microenvironment: Morphology, Metabolism, and Molecular Signature of Glial Dynamics to Discover Metabolic Rewiring Sequence. 22(7):3301.

[223] Turner, D.A., Adamson, D.C.J.J.o.N., Neurology, E., 2011. Neuronal-astrocyte metabolic interactions: understanding the transition into abnormal astrocytoma metabolism. 70(3):167-176.

[224] Lutterbach, J., Sauerbrei, W., Guttenberger, R.J.S.u.O., 2003. Multivariate analysis of prognostic factors in patients with glioblastoma. 179(1):8-15.

[225] Koukourakis, M.I., Giatromanolaki, A.J.I.j.o.r.b., 2019. Warburg effect, lactate dehydrogenase, and radio/chemo-therapy efficacy. 95(4):408-426.

[226] Boudreau, A., Purkey, H.E., Hitz, A., Robarge, K., Peterson, D., Labadie, S., et al., 2016. Metabolic plasticity underpins innate and acquired resistance to LDHA inhibition. 12(10):779-786.

[227] Kim, E.-Y., Chung, T.-W., Han, C.W., Park, S.Y., Park, K.H., Jang, S.B., et al., 2019. A novel lactate dehydrogenase inhibitor, 1-(phenylseleno)-4-(trifluoromethyl) benzene, suppresses tumor growth through apoptotic cell death. 9(1):1-12.

[228] Jafary, F., Ganjalikhany, M.R., Moradi, A., Hemati, M., Jafari, S.J.S.r., 2019. Novel peptide Inhibitors for Lactate Dehydrogenase A (LDHA): A survey to Inhibit LDHA Activity via Disruption of protein-protein Interaction. 9(1):1-13.

[229] Ward, R.A., Brassington, C., Breeze, A.L., Caputo, A., Critchlow, S., Davies, G., et al., 2012. Design and synthesis of novel lactate dehydrogenase A inhibitors by fragment-based lead generation. 55(7):3285-3306.

[230] Payen, V.L., Mina, E., Van Hée, V.F., Porporato, P.E., Sonveaux, P.J.M.m., 2020. Monocarboxylate transporters in cancer. 33:48-66.

[231] Oshima, N., Ishida, R., Kishimoto, S., Beebe, K., Brender, J.R., Yamamoto, K., et al., 2020. Dynamic imaging of LDH inhibition in tumors reveals rapid in vivo metabolic rewiring and vulnerability to combination therapy. 30(6):1798-1810. e1794.

[232] Saunier, E., Benelli, C., Bortoli, S.J.I.j.o.c., 2016. The pyruvate dehydrogenase complex in cancer: An old metabolic gatekeeper regulated by new pathways and pharmacological agents. 138(4):809-817.

[233] McFate, T., Mohyeldin, A., Lu, H., Thakar, J., Henriques, J., Halim, N.D., et al., 2008. Pyruvate dehydrogenase complex activity controls metabolic and malignant phenotype in cancer cells. 283(33):22700-22708.

[234] Stacpoole, P.W.J.J.J.o.t.N.C.I., 2017. Therapeutic targeting of the pyruvate dehydrogenase complex/pyruvate dehydrogenase kinase (PDC/PDK) axis in cancer. 109(11).

[235] STACPOOLE, P.W.J.T.J.o.c.p., drugs, t.j.o.n., 1969. Review of the pharmacologic and therapeutic effects of diisopropylammonium dichloroacetate (DIPA). 9(5):282-291.

[236] Evans, O.B., Stacpoole, P.W.J.B.p., 1982. Prolonged hypolactatemia and increased total pyruvate dehydrogenase activity by dichloroacetate. 31(7):1295-1300.

[237] Bonnet, S., Archer, S.L., Allalunis-Turner, J., Haromy, A., Beaulieu, C., Thompson, R., et al., 2007. A mitochondria-K+ channel axis is suppressed in cancer and its normalization promotes apoptosis and inhibits cancer growth. 11(1):37-51.

[238] Garon, E.B., Christofk, H.R., Hosmer, W., Britten, C.D., Bahng, A., Crabtree, M.J., et al., 2014. Dichloroacetate should be considered with platinum-based chemotherapy in hypoxic tumors rather than as a single agent in advanced non-small cell lung cancer. 140(3):443-452.

[239] Michelakis, E., Sutendra, G., Dromparis, P., Webster, L., Haromy, A., Niven, E., et al., 2010. Metabolic modulation of glioblastoma with dichloroacetate. 2(31):31ra34-31ra34.

[240] Sutendra, G., Dromparis, P., Kinnaird, A., Stenson, T., Haromy, A., Parker, J., et al., 2013. Mitochondrial activation by inhibition of PDKII suppresses HIF1a signaling and angiogenesis in cancer. 32(13):1638-1650.

[241] Dunbar, E., Coats, B., Shroads, A., Langaee, T., Lew, A., Forder, J., et al., 2014. Phase 1 trial of dichloroacetate (DCA) in adults with recurrent malignant brain tumors. 32(3):452-464.

[242] Pathak, R.K., Marrache, S., Harn, D.A., Dhar, S.J.A.c.b., 2014. Mito-DCA: a mitochondria targeted molecular scaffold for efficacious delivery of metabolic modulator dichloroacetate. 9(5):1178-1187.

[243] DeBerardinis, R.J., Cheng, T., 2010. Q's next: the diverse functions of glutamine in metabolism, cell biology and cancer. Oncogene 29(3):313.

[244] Yuneva, M., 2008. Finding an “Achilles’ heel” of cancer: the role of glucose and glutamine metabolism in the survival of transformed cells. Cell Cycle 7(14):2083.

[245] Daykin, C.A., Bro, R., Wulfert, F.J.M., 2012. Data handling for interactive metabolomics: tools for studying the dynamics of metabolome-macromolecule interactions. 8(1):52-63.

[246] Cluntun, A.A., Lukey, M.J., Cerione, R.A., Locasale, J.W.J.T.i.c., 2017. Glutamine metabolism in cancer: understanding the heterogeneity. 3(3):169-180.

[247] Bhutia, Y.D., Ganapathy, V.J.B.e.B.A.-M.C.R., 2016. Glutamine transporters in mammalian cells and their functions in physiology and cancer. 1863(10):2531-2539.

[248] Thangavelu, K., Chong, Q.Y., Low, B.C., Sivaraman, J.J.S.r., 2014. Structural basis for the active site inhibition mechanism of human kidney-type glutaminase (KGA). 4(1):1-7.

[249] Saha, S.K., Islam, S., Abdullah-Al-Wadud, M., Islam, S., Ali, F., Park, K.S.J.J.o.c.m., 2019. Multiomics analysis reveals that GLS and GLS2 differentially modulate the clinical outcomes of cancer. 8(3):355.

[250] Zielke, H.R., Zielke, C.L., Ozand, P.T., 1984. Glutamine: a major energy source for cultured mammalian cells. Federation proceedings 43(1):121.

[251] Yoo, H.C., Yu, Y.C., Sung, Y., Han, J.M.J.E., Medicine, M., 2020. Glutamine reliance in cell metabolism. 52(9):1496-1516.

[252] Metallo, C.M., Gameiro, P.A., Bell, E.L., Mattaini, K.R., Yang, J., Hiller, K., et al., 2012. Reductive glutamine metabolism by IDH1 mediates lipogenesis under hypoxia. 481(7381):380-384.

[253] Huang, W., Choi, W., Chen, Y., Zhang, Q., Deng, H., He, W., et al., 2013. A proposed role for glutamine in cancer cell growth through acid resistance. 23(5):724-727.

[254] Wise, D.R., DeBerardinis, R.J., Mancuso, A., Sayed, N., Zhang, X.Y., Pfeiffer, H.K., et al., 2008. Myc regulates a transcriptional program that stimulates mitochondrial glutaminolysis and leads to glutamine addiction. Proceedings of the National Academy of Sciences of the United States of America 105(48):18782.

[255] Kim, S.-Y.J.B., Therapeutics, 2018. Cancer energy metabolism: shutting power off cancer factory. 26(1):39.

[256] Wang, J.-B., Erickson, J.W., Fuji, R., Ramachandran, S., Gao, P., Dinavahi, R., et al., 2010. Targeting mitochondrial glutaminase activity inhibits oncogenic transformation. 18(3):207-219.

[257] Cruzat, V., Macedo Rogero, M., Noel Keane, K., Curi, R., Newsholme, P.J.N., 2018. Glutamine: metabolism and immune function, supplementation and clinical translation. 10(11):1564.

[258] Mueller, C., Al-Batran, S., Jaeger, E., Schmidt, B., Bausch, M., Unger, C., et al., 2008. A phase IIa study of PEGylated glutaminase (PEG-PGA) plus 6-diazo-5-oxo-L-norleucine (DON) in patients with advanced refractory solid tumors. 26(15_suppl):2533-2533.

[259] Mukherjee, P., Augur, Z.M., Li, M., Hill, C., Greenwood, B., Domin, M.A., et al., 2019. Therapeutic benefit of combining calorie-restricted ketogenic diet and glutamine targeting in late-stage experimental glioblastoma. 2(1):1-14.

[260] Durán, R.V., Oppliger, W., Robitaille, A.M., Heiserich, L., Skendaj, R., Gottlieb, E., et al., 2012. Glutaminolysis activates Rag-mTORC1 signaling. 47(3):349-358.

[261] Dhillon, K.K., Gupta, S.J.S., 2020. Biochemistry, ketogenesis.

[262] Allen, B.G., Bhatia, S.K., Buatti, J.M., Brandt, K.E., Lindholm, K.E., Button, A.M., et al., 2013. Ketogenic diets enhance oxidative stress and radio-chemo-therapy responses in lung cancer xenografts. Clinical cancer research : an official journal of the American Association for Cancer Research 19(14):3905.

[263] Poff, A.M., Ari, C., Seyfried, T.N., D'Agostino, D.P., 2013. The ketogenic diet and hyperbaric oxygen therapy prolong survival in mice with systemic metastatic cancer. PLoS One 8(6):e65522.

[264] Kim, H.S., Masko, E.M., Poulton, S.L., Kennedy, K.M., Pizzo, S.V., Dewhirst, M.W., et al., 2012. Carbohydrate restriction and lactate transporter inhibition in a mouse xenograft model of human prostate cancer. BJU international 110(7):1062.

[265] Masko, E.M., Thomas, J.A., 2nd, Antonelli, J.A., Lloyd, J.C., Phillips, T.E., Poulton, S.H., et al., 2010. Low-carbohydrate diets and prostate cancer: how low is "low enough"? Cancer prevention research (Philadelphia, Pa.) 3(9):1124.

[266] Klement, R.J.J.C.O.i.C.N., Care, M., 2019. The emerging role of ketogenic diets in cancer treatment. 22(2):129-134.

[267] Winter, S.F., Loebel, F., Dietrich, J., 2017. Role of ketogenic metabolic therapy in malignant glioma: A systematic review. Critical reviews in oncology/hematology 112:41.

[268] Schroeder, U., Himpe, B., Pries, R., Vonthein, R., Nitsch, S., Wollenberg, B., 2013. Decline of lactate in tumor tissue after ketogenic diet: in vivo microdialysis study in patients with head and neck cancer. Nutrition and cancer 65(6):843.

[269] Ji, C.C., Hu, Y.Y., Cheng, G., Liang, L., Gao, B., Ren, Y.P., et al., 2020. A ketogenic diet attenuates proliferation and stemness of glioma stem-like cells by altering metabolism resulting in increased ROS production. 56(2):606-617.

[270] Leszczyniecka, M., Roberts, T., Dent, P., Grant, S., Fisher, P.B.J.P., therapeutics, 2001. Differentiation therapy of human cancer: basic science and clinical applications. 90(2-3):105-156.

[271] Silber, J., Lim, D.A., Petritsch, C., Persson, A.I., Maunakea, A.K., Yu, M., et al., 2008. miR-124 and miR-137 inhibit proliferation of glioblastoma multiforme cells and induce differentiation of brain tumor stem cells. 6(1):1-17.

[272] Campos, B., Wan, F., Farhadi, M., Ernst, A., Zeppernick, F., Tagscherer, K.E., et al., 2010. Differentiation therapy exerts antitumor effects on stem-like glioma cells. 16(10):2715-2728.

[273] Piccirillo, S., Reynolds, B.A., Zanetti, N., Lamorte, G., Binda, E., Broggi, G., et al., 2006. Bone morphogenetic proteins inhibit the tumorigenic potential of human brain tumour-initiating cells. 444(7120):761-765.

[274] Meidenbauer, J.J., Mukherjee, P., Seyfried, T.N., 2015. The glucose ketone index calculator: a simple tool to monitor therapeutic efficacy for metabolic management of brain cancer. Nutrition & Metabolism 12(1):12.

[275] Jensen, N.J., Wodschow, H.Z., Nilsson, M., Rungby, J.J.I.J.o.M.S., 2020. Effects of Ketone Bodies on Brain Metabolism and Function in Neurodegenerative Diseases. 21(22):8767.

[276] Puchalska, P., Crawford, P.A.J.C.m., 2017. Multi-dimensional roles of ketone bodies in fuel metabolism, signaling, and therapeutics. 25(2):262-284.

[277] Maalouf, M., Sullivan, P.G., Davis, L., Kim, D.Y., Rho, J.M.J.N., 2007. Ketones inhibit mitochondrial production of reactive oxygen species production following glutamate excitotoxicity by increasing NADH oxidation. 145(1):256-264.

[278] Srivastava, S., Kashiwaya, Y., King, M.T., Baxa, U., Tam, J., Niu, G., et al., 2012. Mitochondrial biogenesis and increased uncoupling protein 1 in brown adipose tissue of mice fed a ketone ester diet. 26(6):2351-2362.

[279] Shimazu, T., Hirschey, M.D., Newman, J., He, W., Shirakawa, K., Le Moan, N., et al., 2013. Suppression of oxidative stress by β-hydroxybutyrate, an endogenous histone deacetylase inhibitor. 339(6116):211-214.

[280] Hartman, A.L., Rho, J.M.J.E.c., 2014. The New Ketone Alphabet Soup: BHB, HCA, and HDAC: The New Ketone Alphabet Soup: BHB, HCA, and HDAC. 14(6):355-357.

[281] Shelton, L.M., Huysentruyt, L.C., Mukherjee, P., Seyfried, T.N.J.A.n., 2010. Calorie restriction as an anti-invasive therapy for malignant brain cancer in the VM mouse. 2(3):AN20100002.

[282] Artzi, M., Liberman, G., Vaisman, N., Bokstein, F., Vitinshtein, F., Aizenstein, O., et al., 2017. Changes in cerebral metabolism during ketogenic diet in patients with primary brain tumors: 1 H-MRS study. Journal of neuro-oncology 132(2):267.

[283] Maurer, G.D., Brucker, D.P., Bahr, O., Harter, P.N., Hattingen, E., Walenta, S., et al., 2011. Differential utilization of ketone bodies by neurons and glioma cell lines: a rationale for ketogenic diet as experimental glioma therapy. BMC cancer 11:315.

[284] Weber, D.D., Aminzadeh-Gohari, S., Tulipan, J., Catalano, L., Feichtinger, R.G., Kofler, B.J.M.m., 2020. Ketogenic diet in the treatment of cancer–where do we stand? 33:102-121.

[285] Obara-Michlewska, M., Szeliga, M.J.C., 2020. Targeting Glutamine Addiction in Gliomas. 12(2):310.

[286] Sperry, J., Condro, M.C., Guo, L., Braas, D., Vanderveer-Harris, N., Kim, K.K., et al., 2020. Glioblastoma utilizes fatty acids and ketone bodies for growth allowing progression during ketogenic diet therapy. 23(9):101453.

[287] Tildon, J.T., McKenna, M.C., Stevenson, J.H., 1994. Transport of 3-hydroxybutyrate by cultured rat brain astrocytes. Neurochemical research 19(10):1237.

[288] Romero, N., Swain, P.M., Kam, Y., Rogers, G., Dranka, B.P., 2018. Bioenergetic profiling of cancer cell lines: quantifying the impact of glycolysis on cell proliferation, Cancer research. AMER ASSOC CANCER RESEARCH 615 CHESTNUT ST, 17TH FLOOR, PHILADELPHIA, PA ….

[289] Arismendi-Morillo, G., Castellano-Ramírez, A., Seyfried, T.N., 2017. Ultrastructural characterization of the Mitochondria-associated membranes abnormalities in human astrocytomas: Functional and therapeutics implications. Ultrastructural pathology 41(3):234.

[290] Martinez-Outschoorn, U.E., Lin, Z., Whitaker-Menezes, D., Howell, A., Lisanti, M.P., Sotgia, F.J.C.c., 2012. Ketone bodies and two-compartment tumor metabolism: stromal ketone production fuels mitochondrial biogenesis in epithelial cancer cells. 11(21):3956-3963.

[291] Grabacka, M., Pierzchalska, M., Dean, M., Reiss, K.J.I.j.o.m.s., 2016. Regulation of ketone body metabolism and the role of PPARα. 17(12):2093.

[292] DeBerardinis, R.J., Chandel, N.S.J.N.m., 2020. We need to talk about the Warburg effect. 2(2):127-129.

[293] Vidali, S., Aminzadeh-Gohari, S., Vatrinet, R., Iommarini, L., Porcelli, A.M., Kofler, B., et al., 2019. Lithium and not acetoacetate influences the growth of cells treated with lithium acetoacetate. 20(12):3104.

[294] Held, P.J.B.A.N., 2018. Using phenol red to assess pH in tissue culture media.1-7.

[295] Dulbecco, R.J.V., 1969. Plaque production by polyoma virus. 8:396-397.

[296] Chou, T.-C.J.C.r., 2010. Drug combination studies and their synergy quantification using the Chou-Talalay method. 70(2):440-446.

[297] Chou, T.J.P.R., 2007. Theoretical basis, experimental design, and computerized simulation of synergism and antagonism in drug-combination studies (vol 58, pg 621, 2006). 59(1):124-124.

[298] Strober, W.J.C.P.I., 2001. Trypan blue test of cell viability. 21.

[299] Huysentruyt, L.C., Mukherjee, P., Banerjee, D., Shelton, L.M., Seyfried, T.N.J.I.j.o.c., 2008. Metastatic cancer cells with macrophage properties: evidence from a new murine tumor model. 123(1):73-84.

[300] Sena-Esteves, M., Tebbets, J.C., Steffens, S., Crombleholme, T., Flake, A.W.J.J.o.v.m., 2004. Optimized large-scale production of high titer lentivirus vector pseudotypes. 122(2):131-139.

[301] Oraiopoulou, M.-E., Tzamali, E., Tzedakis, G., Vakis, A., Papamatheakis, J., Sakkalis, V.J.B.r.i., 2017. In vitro/in silico study on the role of doubling time heterogeneity among primary glioblastoma cell lines. 2017.

[302] Rueden, C.T., Schindelin, J., Hiner, M.C., DeZonia, B.E., Walter, A.E., Arena, E.T., et al., 2017. ImageJ2: ImageJ for the next generation of scientific image data. 18(1):1-26.

[303] Ferrucci, M., Biagioni, F., Lenzi, P., Gambardella, S., Ferese, R., Calierno, M.T., et al., 2017. Rapamycin promotes differentiation increasing βIII-tubulin, NeuN, and NeuroD while suppressing nestin expression in glioblastoma cells. 8(18):29574.

[304] Kumar, A., Chordia, N., 2015. In silico PCR primer designing and validation. PCR Primer Design. Springer, p. 143-151.

[305] Mahmood, T., Yang, P.-C.J.N.A.j.o.m.s., 2012. Western blot: technique, theory, and trouble shooting. 4(9):429.

[306] Divakaruni, A.S., Paradyse, A., Ferrick, D.A., Murphy, A.N., Jastroch, M., 2014. Analysis and interpretation of microplate-based oxygen consumption and pH data. Methods in enzymology. Elsevier, p. 309-354.

[307] Yépez, V.A., Kremer, L.S., Iuso, A., Gusic, M., Kopajtich, R., Koňaříková, E., et al., 2018. OCR-Stats: Robust estimation and statistical testing of mitochondrial respiration activities using Seahorse XF Analyzer. 13(7):e0199938.

[308] Zhang, J., Zhang, Q., 2019. Using seahorse machine to measure OCR and ECAR in cancer cells. Cancer Metabolism. Springer, p. 353-363.

[309] Romero, N., Rogers, G., Neilson, A., Dranka, B.P.J.A.T., Inc, 2018. Quantifying cellular ATP production rate using Agilent Seahorse XF Technology.

[310] Bowman, R.L., Wang, Q., Carro, A., Verhaak, R.G., Squatrito, M.J.N.-o., 2017. GlioVis data portal for visualization and analysis of brain tumor expression datasets. 19(1):139-141.

[311] Zhou, W., Wahl, D.R.J.C., 2019. Metabolic abnormalities in glioblastoma and metabolic strategies to overcome treatment resistance. 11(9):1231.

[312] Madurga, R., García-Romero, N., Jiménez, B., Collazo, A., Pérez-Rodríguez, F., Hernández-Laín, A., et al., 2020. Normal tissue content impact on the GBM molecular classification.

[313] Subramanian, A., Tamayo, P., Mootha, V.K., Mukherjee, S., Ebert, B.L., Gillette, M.A., et al., 2005. Gene set enrichment analysis: a knowledge-based approach for interpreting genome-wide expression profiles. 102(43):15545-15550.

[314] Hänzelmann, S., Castelo, R., Guinney, J.J.B.b., 2013. GSVA: gene set variation analysis for microarray and RNA-seq data. 14(1):7.

[315] Kanehisa, M., Sato, Y., Kawashima, M., Furumichi, M., Tanabe, M.J.N.a.r., 2016. KEGG as a reference resource for gene and protein annotation. 44(D1):D457-D462.

[316] Gonzalez Tejedo, C., 2016. Integración de aproximaciones proteómicas y transcriptómicas para el estudio de células madre de glioblastoma humano.

[317] Teo, W.-Y., Sekar, K., Seshachalam, P., Shen, J., Chow, W.-Y., Lau, C.C., et al., 2019. Relevance of a tCGA-derived Glioblastoma subtype Gene-Classifier among Patient populations. 9(1):1-10.

[318] Behnan, J., Finocchiaro, G., Hanna, G.J.B., 2019. The landscape of the mesenchymal signature in brain tumours. 142(4):847-866.

[319] Levenson, C.W., Morgan, T.J., Twigg, P.D., Logan, T.M., Schepkin, V.D.J.C.D.R., 2019. Use of MRI, metabolomic, and genomic biomarkers to identify mechanisms of chemoresistance in glioma. 2(3):862-876.

[320] Chopra, S., Foltz, W.D., Milosevic, M.F., Toi, A., Bristow, R.G., Ménard, C., et al., 2009. Comparing oxygen-sensitive MRI (BOLD R2*) with oxygen electrode measurements: a pilot study in men with prostate cancer. 85(9):805-813.

[321] Zhu, L., Ploessl, K., Zhou, R., Mankoff, D., Kung, H.F., 2017. Metabolic Imaging of Glutamine in Cancer. Journal of nuclear medicine : official publication, Society of Nuclear Medicine 58(4):533.

[322] Spehalski, E.I., Lee, J.A., Peters, C., Tofilon, P., Camphausen, K.J.J.o.p., bioinformatics, 2019. The quiescent metabolic phenotype of glioma stem cells. 12(6):96.

[323] Allen, M., Bjerke, M., Edlund, H., Nelander, S., Westermark, B.J.S.t.m., 2016. Origin of the U87MG glioma cell line: Good news and bad news. 8(354):354re353-354re353.

[324] Zhang, W., Zhang, S.-L., Hu, X., Tam, K.Y.J.I.j.o.b.s., 2015. Targeting tumor metabolism for cancer treatment: is pyruvate dehydrogenase kinases (PDKs) a viable anticancer target? 11(12):1390.

[325] Fan, T., Sun, G., Sun, X., Zhao, L., Zhong, R., Peng, Y.J.C., 2019. Tumor energy metabolism and potential of 3-bromopyruvate as an inhibitor of aerobic glycolysis: Implications in tumor treatment. 11(3):317.

[326] Wise, D.R., Thompson, C.B.J.T.i.b.s., 2010. Glutamine addiction: a new therapeutic target in cancer. 35(8):427-433.

[327] Aljofan, M., Riethmacher, D.J.F.s.O., 2019. Anticancer activity of metformin: a systematic review of the literature. 5(8):FSO410.

[328] Michelakis, E., Webster, L., Mackey, J.J.B.j.o.c., 2008. Dichloroacetate (DCA) as a potential metabolic-targeting therapy for cancer. 99(7):989-994.

[329] Zhang, S., Hulver, M.W., McMillan, R.P., Cline, M.A., Gilbert, E.R.J.N., metabolism, 2014. The pivotal role of pyruvate dehydrogenase kinases in metabolic flexibility. 11(1):10.

[330] Jha, M.K., Suk, K.J.B.t.r., treatment, 2013. Pyruvate dehydrogenase kinase as a potential therapeutic target for malignant gliomas. 1(2):57-63.

[331] Baker, J.C., Yan, X., Peng, T., Kasten, S., Roche, T.E.J.J.o.B.C., 2000. Marked differences between two isoforms of human pyruvate dehydrogenase kinase. 275(21):15773-15781.

[332] Bowker-Kinley, M.M., DAVIS, I.W., Wu, P., HARRIS, A.R., POPOV, M.K.J.B.J., 1998. Evidence for existence of tissue-specific regulation of the mammalian pyruvate dehydrogenase complex. 329(1):191-196.

[333] Yeaman, S.J., Hutcheson, E.T., Roche, T.E., Pettit, F.H., Brown, J.R., Reed, L.J., et al., 1978. Sites of phosphorylation on pyruvate dehydrogenase from bovine kidney and heart. 17(12):2364-2370.

[334] Korotchkina, L.G., Patel, M.S.J.J.o.B.C., 2001. Site specificity of four pyruvate dehydrogenase kinase isoenzymes toward the three phosphorylation sites of human pyruvate dehydrogenase. 276(40):37223-37229.

[335] Thul, P.J., Åkesson, L., Wiking, M., Mahdessian, D., Geladaki, A., Blal, H.A., et al., 2017. A subcellular map of the human proteome. 356(6340).

[336] Amjad, M.T., Kasi, A.J.S., 2020. Cancer Chemotherapy.

[337] Hendry, J.H., Cai, W., Roberts, S.A., Potten, C.S.J.R.r., 1997. p53 deficiency sensitizes clonogenic cells to irradiation in the large but not the small intestine. 148(3):254-259.

[338] Eigenmann, D.E., Xue, G., Kim, K.S., Moses, A.V., Hamburger, M., Oufir, M.J.F., et al., 2013. Comparative study of four immortalized human brain capillary endothelial cell lines, hCMEC/D3,

hBMEC, TY10, and BB19, and optimization of culture conditions, for an in vitro blood–brain barrier model for drug permeability studies. 10(1):1-17.

[339] Turner, T.H., Alzubi, M.A., Harrell, J.C.J.S.r., 2020. Identification of synergistic drug combinations using breast cancer patient-derived xenografts. 10(1):1-20.

[340] Duraj, T., García-Romero, N., Carrión-Navarro, J., Madurga, R., Mendivil, A.O.d., Prat-Acin, R., et al., 2021. Beyond the Warburg Effect: Oxidative and Glycolytic Phenotypes Coexist within the Metabolic Heterogeneity of Glioblastoma. 10(2):202.

[341] Sesen, J., Dahan, P., Scotland, S.J., Saland, E., Dang, V.-T., Lemarié, A., et al., 2015. Metformin inhibits growth of human glioblastoma cells and enhances therapeutic response. 10(4):e0123721.

[342] Velpula, K.K., Guda, M.R., Sahu, K., Tuszynski, J., Asuthkar, S., Bach, S.E., et al., 2017. Metabolic targeting of EGFRvIII/PDK1 axis in temozolomide resistant glioblastoma. 8(22):35639.

[343] Prabhu, A., Sarcar, B., Miller, C.R., Kim, S.-H., Nakano, I., Forsyth, P., et al., 2015. Ras-mediated modulation of pyruvate dehydrogenase activity regulates mitochondrial reserve capacity and contributes to glioblastoma tumorigenesis. 17(9):1220-1230.

[344] Kroemer, G., Pouyssegur, J.J.C.c., 2008. Tumor cell metabolism: cancer's Achilles' heel. 13(6):472-482.

[345] Mazurek, M., Litak, J., Kamieniak, P., Kulesza, B., Jonak, K., Baj, J., et al., 2020. Metformin as Potential Therapy for High-Grade Glioma. 12(1):210.

[346] Seyfried, T., Sanderson, T., El-Abbadi, M., McGowan, R., Mukherjee, P.J.B.j.o.c., 2003. Role of glucose and ketone bodies in the metabolic control of experimental brain cancer. 89(7):1375-1382.

[347] Zuccoli, G., Marcello, N., Pisanello, A., Servadei, F., Vaccaro, S., Mukherjee, P., et al., 2010. Metabolic management of glioblastoma multiforme using standard therapy together with a restricted ketogenic diet: Case Report. 7(1):33.

[348] Fine, E.J., Segal-Isaacson, C.J., Feinman, R.D., Herszkopf, S., Romano, M.C., Tomuta, N., et al., 2012. Targeting insulin inhibition as a metabolic therapy in advanced cancer: a pilot safety and feasibility dietary trial in 10 patients. Nutrition 28(10):1028.

[349] Duraj, T., 2016. Tratamiento metabólico del cáncer, Registro de Propiedad Intelectual.

[350] Stewart, W., Fleming, L.W.J.P.m.j., 1973. Features of a successful therapeutic fast of 382 days' duration. 49(569):203-209.

[351] Owen, O.E., Felig, P., Morgan, A.P., Wahren, J., Cahill, G.F.J.T.J.o.c.i., 1969. Liver and kidney metabolism during prolonged starvation. 48(3):574-583.

[352] Schwartz, K., Chang, H.T., Nikolai, M., Pernicone, J., Rhee, S., Olson, K., et al., 2015. Treatment of glioma patients with ketogenic diets: report of two cases treated with an IRB-approved energy-restricted ketogenic diet protocol and review of the literature. Cancer & metabolism 3(1):1.

[353] Chang, H.T., Olson, L.K., Schwartz, K.A., 2013. Ketolytic and glycolytic enzymatic expression profiles in malignant gliomas: implication for ketogenic diet therapy. Nutrition & Metabolism 10(1):1.

[354] Veech, R.L.J.J.o.L.R., 2014. Ketone ester effects on metabolism and transcription. 55(10):2004-2006.

[355] Cotter, D.G., Schugar, R.C., Wentz, A.E., André d'Avignon, D., Crawford, P.A.J.A.J.o.P.-E., Metabolism, 2013. Successful adaptation to ketosis by mice with tissue-specific deficiency of ketone body oxidation. 304(4):E363-E374.

[356] Gameiro, P.A., Struhl, K.J.C.r., 2018. Nutrient deprivation elicits a transcriptional and translational inflammatory response coupled to decreased protein synthesis. 24(6):1415-1424.

[357] Andreev, D.E., O'Connor, P.B., Zhdanov, A.V., Dmitriev, R.I., Shatsky, I.N., Papkovsky, D.B., et al., 2015. Oxygen and glucose deprivation induces widespread alterations in mRNA translation within 20 minutes. 16(1):1-14.

[358] Zhou, W., Mukherjee, P., Kiebish, M.A., Markis, W.T., Mantis, J.G., Seyfried, T.N., 2007. The calorically restricted ketogenic diet, an effective alternative therapy for malignant brain cancer. Nutrition & Metabolism 4(1):5.

[359] D'Agostino, D., Kesl, S., Bennett, A., Dean, J.B., 2011. Beta-hydroxybutyrate reduces superoxide production in cultured U87 cells and hippocampal neurons: implications for metabolic therapy in cancer and CNS oxygen toxicity. Wiley Online Library.

[360] Law, M.E., Templeton, K.L., Kitange, G., Smith, J., Misra, A., Feuerstein, B.G., et al., 2005. Molecular cytogenetic analysis of chromosomes 1 and 19 in glioma cell lines. 160(1):1-14.

[361] Squire, J.A., Arab, S., Marrano, P., Bayani, J., Karaskova, J., Taylor, M., et al., 2001. Molecular cytogenetic analysis of glial tumors using spectral karyotyping and comparative genomic hybridization. 6(2):93-108.

[362] PontÉN, J., MACINTYRE, E.H.J.A.P.M.S., 1968. Long term culture of normal and neoplastic human glia. 74(4):465-486.

[363] Esteller, M.J.N.E.J.o.M., 2008. Epigenetics in cancer. 358(11):1148-1159.

[364] Cahill, G.F., Jr., 2006. Fuel metabolism in starvation. Annual Review of Nutrition 26:1.

[365] Drenick, E.J., Alvarez, L.C., Tamasi, G.C., Brickman, A.S.J.T.J.o.c.i., 1972. Resistance to symptomatic insulin reactions after fasting. 51(10):2757-2762.

[366] Ceccarelli, M., Barthel, F.P., Malta, T.M., Sabedot, T.S., Salama, S.R., Murray, B.A., et al., 2016. Molecular profiling reveals biologically discrete subsets and pathways of progression in diffuse glioma. 164(3):550-563.

[367] Hermsen, M.A., Meijer, G.A., Baak, J.P., Joenje, H., Walboomers, J.J.J.H.p., 1996. Comparative genomic hybridization: a new tool in cancer pathology. 27(4):342-349.

[368] Zhang, C., Wang, M., Ji, F., Peng, Y., Wang, B., Zhao, J., et al., 2021. A Novel Glucose Metabolism-Related Gene Signature for Overall Survival Prediction in Patients with Glioblastoma. 2021.

[369] Lei, C., Chen, W., Wang, Y., Zhao, B., Liu, P., Kong, Z., et al., 2020. Prognostic prediction model for glioblastoma: a metabolic gene signature and independent external validation.

[370] Zhang, W., Wan, Y.-w., Allen, G.I., Pang, K., Anderson, M.L., Liu, Z.J.B.g., 2013. Molecular pathway identification using biological network-regularized logistic models. 14(S8):S7.

[371] Celiku, O., Johnson, S., Zhao, S., Camphausen, K., Shankavaram, U.J.P.o., 2014. Visualizing molecular profiles of glioblastoma with GBM-BioDP. 9(7).

[372] Liu, Y., Beyer, A., Aebersold, R.J.C., 2016. On the dependency of cellular protein levels on mRNA abundance. 165(3):535-550.

[373] Garnier, D., Renoult, O., Alves-Guerra, M.-C., Paris, F., Pecqueur, C.J.F.i.o., 2019. Glioblastoma stem-like cells, metabolic strategy to kill a challenging target. 9:118.

[374] Schroeder, A.B., Pointer, K.B., Clark, P.A., Datta, R., Kuo, J.S., Eliceiri, K.W.J.J.o.b.o., 2020. Metabolic mapping of glioblastoma stem cells reveals NADH fluxes associated with glioblastoma phenotype and survival. 25(3):036502.

[375] Stupp, R., Mason, W.P., Van Den Bent, M.J., Weller, M., Fisher, B., Taphoorn, M.J., et al., 2005. Radiotherapy plus concomitant and adjuvant temozolomide for glioblastoma. 352(10):987-996.

[376] Brown, D.V., Stylli, S.S., Kaye, A.H., Mantamadiotis, T., 2019. Multilayered Heterogeneity of Glioblastoma Stem Cells: Biological and Clinical Significance. Stem Cells Heterogeneity in Cancer. Springer, p. 1-21.

[377] Eidelman, E., Tripathi, H., Fu, D.-X., Siddiqui, M.M.J.T.a., urology, 2018. Linking cellular metabolism and metabolomics to risk-stratification of prostate cancer clinical aggressiveness and potential therapeutic pathways. 7(Suppl 4):S490.

[378] Avril, N., Sassen, S., Roylance, R.J.J.o.N.M., 2009. Response to therapy in breast cancer. 50(Suppl 1):55S-63S.

[379] Farwell, M.D., Pryma, D.A., Mankoff, D.A.J.C., 2014. PET/CT imaging in cancer: current applications and future directions. 120(22):3433-3445.

[380] Julià-Sapé, M., Candiota, A.P., Arús, C.J.N.i.B., 2019. Cancer metabolism in a snapshot: MRS (I). 32(10):e4054.

[381] Marie, S.K.N., Shinjo, S.M.O.J.C., 2011. Metabolism and brain cancer. 66:33-43.

[382] Zhou, Y., Zhou, Y., Shingu, T., Feng, L., Chen, Z., Ogasawara, M., et al., 2011. Metabolic alterations in highly tumorigenic glioblastoma cells preference for hypoxia and high dependency on glycolysis. 286(37):32843-32853.

[383] Kiss, G., 2015. The role of matrix substrate-level phosphorylation during anoxia.

[384] Connolly, N.M., Theurey, P., Adam-Vizi, V., Bazan, N.G., Bernardi, P., Bolaños, J.P., et al., 2018. Guidelines on experimental methods to assess mitochondrial dysfunction in cellular models of neurodegenerative diseases. 25(3):542-572.

[385] Cvrljevic, A.N., Akhavan, D., Wu, M., Martinello, P., Furnari, F.B., Johnston, A.J., et al., 2011. Activation of Src induces mitochondrial localisation of de2-7EGFR (EGFRvIII) in glioma cells: implications for glucose metabolism. 124(17):2938-2950.

[386] Shen, H., Hau, E., Joshi, S., Dilda, P.J., McDonald, K.L.J.M.c.t., 2015. Sensitization of glioblastoma cells to irradiation by modulating the glucose metabolism. 14(8):1794-1804.

[387] Kim, J., Han, J., Jang, Y., Kim, S.J., Lee, M.J., Ryu, M.J., et al., 2015. High-capacity glycolytic and mitochondrial oxidative metabolisms mediate the growth ability of glioblastoma. 47(3):1009-1016.

[388] Luan, W., Wang, Y., Chen, X., Shi, Y., Wang, J., Zhang, J., et al., 2015. PKM2 promotes glucose metabolism and cell growth in gliomas through a mechanism involving a let-7a/c-Myc/hnRNPA1 feedback loop. 6(15):13006.

[389] Xing, F., Luan, Y., Cai, J., Wu, S., Mai, J., Gu, J., et al., 2017. The anti-warburg effect elicited by the camp-pgc1α pathway drives differentiation of glioblastoma cells into astrocytes. 18(2):468-481.

[390] Jones, J.E., Esler, W.P., Patel, R., Lanba, A., Vera, N.B., Pfefferkorn, J.A., et al., 2017. Inhibition of acetyl-CoA carboxylase 1 (ACC1) and 2 (ACC2) reduces proliferation and de novo lipogenesis of EGFRvIII human glioblastoma cells. 12(1).

[391] Staricha, K., Meyers, N., Garvin, J., Liu, Q., Rarick, K., Harder, D., et al., 2020. Effect of high glucose condition on glucose metabolism in primary astrocytes. 1732:146702.

[392] Li, W., Choudhury, G.R., Winters, A., Prah, J., Lin, W., Liu, R., et al., 2018. Hyperglycemia alters astrocyte metabolism and inhibits astrocyte proliferation. 9(4):674.

[393] Cordes, T., Lucas, A., Divakaruni, A.S., Murphy, A.N., Cabrales, P., Metallo, C.M.J.M.m., 2020. Itaconate modulates tricarboxylic acid and redox metabolism to mitigate reperfusion injury. 32:122-135.

[394] Thevenet, J., De Marchi, U., Domingo, J.S., Christinat, N., Bultot, L., Lefebvre, G., et al., 2016. Medium-chain fatty acids inhibit mitochondrial metabolism in astrocytes promoting astrocyte-neuron lactate and ketone body shuttle systems. 30(5):1913-1926.

[395] Potter, P.G.W., Walker, J.M.V., Robb, J.L., Chilton, J.K., Williamson, R., Randall, A., et al., 2018. Human primary astrocytes increase basal fatty acid oxidation following recurrent low glucose to maintain intracellular nucleotide levels.271981.

[396] Chumarina, M., Russ, K., Azevedo, C., Heuer, A., Pihl, M., Collin, A., et al., 2019. Cellular alterations identified in pluripotent stem cell-derived midbrain spheroids generated from a female patient with progressive external ophthalmoplegia and parkinsonism who carries a novel variation (p. Q811R) in the POLG1 gene. 7(1):1-19.

[397] Li, J., Liu, Q., Liu, Z., Xia, Q., Zhang, Z., Zhang, R., et al., 2018. KPNA2 promotes metabolic reprogramming in glioblastomas by regulation of c-myc. 37(1):1-15.

[398] Massalha, W., Markovits, M., Pichinuk, E., Feinstein-Rotkopf, Y., Tarshish, M., Mishra, K., et al., 2019. Minerval (2-hydroxyoleic acid) causes cancer cell selective toxicity by uncoupling oxidative phosphorylation and compromising bioenergetic compensation capacity. 39(1).

[399] Rinaldi, L., Sepe, M., Delle Donne, R., Conte, K., Arcella, A., Borzacchiello, D., et al., 2017. Mitochondrial AKAP1 supports mTOR pathway and tumor growth. 8(6):e2842-e2842.

[400] Chen, Z., Li, S., Shen, L., Wei, X., Zhu, H., Wang, X., et al., 2020. NF-kappa B interacting long noncoding RNA enhances the Warburg effect and angiogenesis and is associated with decreased survival of patients with gliomas. 11(5):1-18.

[401] Desai, V., Jain, A., Shaghaghi, H., Summer, R., Lai, J.C., Bhushan, A.J.A.r., 2019. Combination of biochanin A and temozolomide impairs tumor growth by modulating cell metabolism in glioblastoma multiforme. 39(1):57-66.

[402] Grigalavicius, M., Mastrangelopoulou, M., Arous, D., Juzeniene, A., Ménard, M., Skarpen, E., et al., 2020. Photodynamic efficacy of cercosporin in 3D tumor cell cultures. 96(3):699-707.

[403] Tomkova, S., Misuth, M., Lenkavska, L., Miskovsky, P., Huntosova, V.J.B.e.B.A.-M.C.R., 2018. In vitro identification of mitochondrial oxidative stress production by time-resolved fluorescence imaging of glioma cells. 1865(4):616-628.

[404] Cardoso, A.M., Sousa, M., Morais, C.M., Oancea-Castillo, L.R., Régnier-Vigouroux, A., Rebelo, O., et al., 2019. MiR-144 overexpression as a promising therapeutic strategy to overcome glioblastoma cell invasiveness and resistance to chemotherapy. 28(16):2738-2751.

[405] Woods, A., Vertommen, D., Neumann, D., Türk, R., Bayliss, J., Schlattner, U., et al., 2003. Identification of phosphorylation sites in AMP-activated protein kinase (AMPK) for upstream AMPK kinases and study of their roles by site-directed mutagenesis. 278(31):28434-28442.

[406] STEIN, S.C., WOODS, A., JONES, N.A., DAVISON, M.D., CARLING, D.J.B.J., 2000. The regulation of AMP-activated protein kinase by phosphorylation. 345(3):437-443.

[407] Liu, X., Chhipa, R.R., Pooya, S., Wortman, M., Yachyshin, S., Chow, L.M., et al., 2014. Discrete mechanisms of mTOR and cell cycle regulation by AMPK agonists independent of AMPK. 111(4):E435-E444.

[408] Rardin, M.J., Wiley, S.E., Naviaux, R.K., Murphy, A.N., Dixon, J.E.J.A.b., 2009. Monitoring phosphorylation of the pyruvate dehydrogenase complex. 389(2):157-164.

[409] Thornburg, J.M., Nelson, K.K., Clem, B.F., Lane, A.N., Arumugam, S., Simmons, A., et al., 2008. Targeting aspartate aminotransferase in breast cancer. 10(5):1-12.

[410] Valvona, C.J., Fillmore, H.L.J.B.s., 2018. Oxamate, but not selective targeting of LDH-A, inhibits medulloblastoma cell glycolysis, growth and motility. 8(4):56.

[411] Liu, X., Yang, Z., Chen, Z., Chen, R., Zhao, D., Zhou, Y., et al., 2015. Effects of the suppression of lactate dehydrogenase A on the growth and invasion of human gastric cancer cells. 33(1):157-162.

[412] Moreno-Sánchez, R., Marín-Hernández, Á., Del Mazo-Monsalvo, I., Saavedra, E., Rodríguez-Enríquez, S.J.B.e.B.A.-G.S., 2017. Assessment of the low inhibitory specificity of oxamate, aminooxyacetate and dichloroacetate on cancer energy metabolism. 1861(1):3221-3236.

[413] Zhai, X., Yang, Y., Wan, J., Zhu, R., Wu, Y.J.O.r., 2013. Inhibition of LDH-A by oxamate induces G2/M arrest, apoptosis and increases radiosensitivity in nasopharyngeal carcinoma cells. 30(6):2983-2991.

[414] Wu, M., Neilson, A., Swift, A.L., Moran, R., Tamagnine, J., Parslow, D., et al., 2007. Multiparameter metabolic analysis reveals a close link between attenuated mitochondrial bioenergetic function and enhanced glycolysis dependency in human tumor cells. 292(1):C125-C136.

[415] García-Castillo, V., López-Urrutia, E., Villanueva-Sánchez, O., Ávila-Rodríguez, M.Á., Zentella-Dehesa, A., Cortés-González, C., et al., 2017. Targeting metabolic remodeling in triple negative breast cancer in a murine model. 8(2):178.

[416] Hall, C.N., Klein-Flügge, M.C., Howarth, C., Attwell, D.J.J.o.N., 2012. Oxidative phosphorylation, not glycolysis, powers presynaptic and postsynaptic mechanisms underlying brain information processing. 32(26):8940-8951.

[417] Dienel, G.A.J.P.r., 2019. Brain glucose metabolism: integration of energetics with function. 99(1):949-1045.

[418] Miskimins, W.K., Ahn, H.J., Kim, J.Y., Ryu, S., Jung, Y.-S., Choi, J.Y.J.P.o., 2014. Synergistic anti-cancer effect of phenformin and oxamate. 9(1).

[419] An, J., Zhang, Y., He, J., Zang, Z., Zhou, Z., Pei, X., et al., 2017. Lactate dehydrogenase A promotes the invasion and proliferation of pituitary adenoma. 7(1):1-12.

[420] Ye, W., Zheng, Y., Zhang, S., Yan, L., Cheng, H., Wu, M.J.P.o., 2016. Oxamate improves glycemic control and insulin sensitivity via inhibition of tissue lactate production in db/db mice. 11(3):e0150303.

[421] Still, E.R., Yuneva, M.O.J.B.j.o.c., 2017. Hopefully devoted to Q: targeting glutamine addiction in cancer. 116(11):1375-1381.

[422] Ohba, S., Hirose, Y.J.J.o.N.-O., 2020. l-asparaginase and 6-diazo-5-oxo-l-norleucine synergistically inhibit the growth of glioblastoma cells. 146(3):469-475.

[423] Oizel, K., Chauvin, C., Oliver, L., Gratas, C., Geraldo, F., Jarry, U., et al., 2017. Efficient mitochondrial glutamine targeting prevails over glioblastoma metabolic plasticity. 23(20):6292-6304.

[424] Wang, G.S., Hoyte, C.J.J.o.i.c.m., 2019. Review of biguanide (metformin) toxicity. 34(11-12):863-876.

[425] Algharably, E.A.H., Kreutz, R., Gundert-Remy, U.J.A.o.t., 2019. Importance of in vitro conditions for modeling the in vivo dose in humans by in vitro–in vivo extrapolation (IVIVE). 93(3):615-621.

[426] Aharon, L.J.A., 2020. Correlation between In-vitro and In-vivo Studies based on Pharmacokinetic Considerations. 8:48-50.

[427] Brandsma, D., Dorlo, T.P., Haanen, J.H., Beijnen, J.H., Boogerd, W.J.J.o.n., 2010. Severe encephalopathy and polyneuropathy induced by dichloroacetate. 257(12):2099-2100.

[428] Stacpoole, P.W., Kurtz, T.L., Han, Z., Langaee, T.J.A.d.d.r., 2008. Role of dichloroacetate in the treatment of genetic mitochondrial diseases. 60(13-14):1478-1487.

[429] Sun, R.C., Fadia, M., Dahlstrom, J.E., Parish, C.R., Board, P.G., Blackburn, A.C.J.B.c.r., et al., 2010. Reversal of the glycolytic phenotype by dichloroacetate inhibits metastatic breast cancer cell growth in vitro and in vivo. 120(1):253-260.

[430] Heshe, D., Hoogestraat, S., Brauckmann, C., Karst, U., Boos, J., Lanvers-Kaminsky, C.J.C.c., et al., 2011. Dichloroacetate metabolically targeted therapy defeats cytotoxicity of standard anticancer drugs. 67(3):647-655.

[431] Madhok, B., Yeluri, S., Perry, S., Hughes, T., Jayne, D.J.B.j.o.c., 2010. Dichloroacetate induces apoptosis and cell-cycle arrest in colorectal cancer cells. 102(12):1746-1752.

[432] Stockwin, L.H., Yu, S.X., Borgel, S., Hancock, C., Wolfe, T.L., Phillips, L.R., et al., 2010. Sodium dichloroacetate selectively targets cells with defects in the mitochondrial ETC. 127(11):2510-2519.

[433] Shen, H., Decollogne, S., Dilda, P.J., Hau, E., Chung, S.A., Luk, P.P., et al., 2015. Dual-targeting of aberrant glucose metabolism in glioblastoma. 34(1):14.

[434] Pinkus, L.M., 1977. [45] Glutamine binding sites. Methods in enzymology. Elsevier, p. 414-427.

[435] Alt, J., Potter, M.C., Rojas, C., Slusher, B.S.J.A.b., 2015. Bioanalysis of 6-diazo-5-oxo-l-norleucine in plasma and brain by ultra-performance liquid chromatography mass spectrometry. 474:28-34.

[436] Rais, R., Jancarik, A., Tenora, L.s., Nedelcovych, M., Alt, J., Englert, J., et al., 2016. Discovery of 6-diazo-5-oxo-l-norleucine (DON) prodrugs with enhanced CSF delivery in monkeys: a potential treatment for glioblastoma. 59(18):8621-8633.

[437] Song, M., Kim, S.-H., Im, C.Y., Hwang, H.-J.J.C.t.i.m.c., 2018. Recent development of small molecule glutaminase inhibitors. 18(6):432-443.

[438] Wang, Z., Liu, F., Fan, N., Zhou, C., Li, D., Macvicar, T., et al., 2020. Targeting Glutaminolysis: New Perspectives to Understand Cancer Development and Novel Strategies for Potential Target Therapies. 10:2321.

[439] Kankotia, S., Stacpoole, P.W.J.B.e.B.A.-R.o.C., 2014. Dichloroacetate and cancer: new home for an orphan drug? 1846(2):617-629.

[440] Cuyàs, E., Fernández-Arroyo, S., Corominas-Faja, B., Rodríguez-Gallego, E., Bosch-Barrera, J., Martin-Castillo, B., et al., 2015. Oncometabolic mutation IDH1 R132H confers a metformin-hypersensitive phenotype. 6(14):12279.

[441] Ashton, T.M., McKenna, W.G., Kunz-Schughart, L.A., Higgins, G.S.J.C.C.R., 2018. Oxidative phosphorylation as an emerging target in cancer therapy. 24(11):2482-2490.

[442] Yu, Z., Zhao, G., Xie, G., Zhao, L., Chen, Y., Yu, H., et al., 2015. Metformin and temozolomide act synergistically to inhibit growth of glioma cells and glioma stem cells in vitro and in vivo. 6(32):32930.

[443] Jiang, W., Finniss, S., Cazacu, S., Xiang, C., Brodie, Z., Mikkelsen, T., et al., 2016. Repurposing phenformin for the targeting of glioma stem cells and the treatment of glioblastoma. 7(35):56456.

[444] Yang, S.H., Li, S., Lu, G., Xue, H., Kim, D.H., Zhu, J.-J., et al., 2016. Metformin treatment reduces temozolomide resistance of glioblastoma cells. 7(48):78787.

[445] Kast, R., Karpel-Massler, G., Halatsch, M.E.J.B.j.o.p., 2011. Can the therapeutic effects of temozolomide be potentiated by stimulating AMP-activated protein kinase with olanzepine and metformin? 164(5):1393-1396.

[446] Agrawal, S., Vamadevan, P., Mazibuko, N., Bannister, R., Swery, R., Wilson, S., et al., 2019. A new method for ethical and efficient evidence generation for off-label medication use in oncology (A case study in Glioblastoma). 10:681.

[447] Yu, Z., Zhao, G., Li, P., Li, Y., Zhou, G., Chen, Y., et al., 2016. Temozolomide in combination with metformin act synergistically to inhibit proliferation and expansion of glioma stem-like cells. 11(4):2792-2800.

[448] Gao-feng, X., Mao-de, W., Xiao-bin, B., Wan-fu, X., Rui-chun, L., Chuan-kun, L.J.J.o.X.a.J.U., 2014. Combining dichloroacetate with temozolomide increases the antitumor efficacy of temozolomide by inhibiting HIF-1α and promoting p53 signaling pathway. 35(1).

[449] Wicks, R.T., Azadi, J., Mangraviti, A., Zhang, I., Hwang, L., Joshi, A., et al., 2015. Local delivery of cancer-cell glycolytic inhibitors in high-grade glioma. 17(1):70-80.

[450] Valtorta, S., Dico, A.L., Raccagni, I., Gaglio, D., Belloli, S., Politi, L.S., et al., 2017. Metformin and temozolomide, a synergic option to overcome resistance in glioblastoma multiforme models. 8(68):113090.

[451] Chou, T.-C., Talalay, P.J.A.i.e.r., 1984. Quantitative analysis of dose-effect relationships: the combined effects of multiple drugs or enzyme inhibitors. 22:27-55.

[452] Gayvert, K.M., Aly, O., Platt, J., Bosenberg, M.W., Stern, D.F., Elemento, O.J.P.c.b., 2017. A computational approach for identifying synergistic drug combinations. 13(1):e1005308.

[453] Boik, J.C., Newman, R.A., Boik, R.J.J.S.i.m., 2008. Quantifying synergism/antagonism using nonlinear mixed-effects modeling: A simulation study. 27(7):1040-1061.

[454] García-Fuente, A., Vázquez, F., Viéitez, J.M., Alonso, F.J.G., Martín, J.I., Ferrer, J.J.S.r., 2018. CISNE: An accurate description of dose-effect and synergism in combination therapies. 8(1):1-9.

[455] İyikesici, M.S.J.N.j.o.c.p., 2020. Survival outcomes of metabolically supported chemotherapy combined with ketogenic diet, hyperthermia, and hyperbaric oxygen therapy in advanced gastric cancer. 23(5):734-740.

[456] Iyikesici, M.S., Slocum, A.K., Slocum, A., Berkarda, F.B., Kalamian, M., Seyfried, T.N., 2017. Efficacy of Metabolically Supported Chemotherapy Combined with Ketogenic Diet, Hyperthermia, and Hyperbaric Oxygen Therapy for Stage IV Triple-Negative Breast Cancer. Cureus 9(7):e1445.

[457] Kim, J.H., Lee, K.J., Seo, Y., Kwon, J.-H., Yoon, J.P., Kang, J.Y., et al., 2018. Effects of metformin on colorectal cancer stem cells depend on alterations in glutamine metabolism. 8(1):1-13.

[458] Sancho, P., Burgos-Ramos, E., Tavera, A., Kheir, T.B., Jagust, P., Schoenhals, M., et al., 2015. MYC/PGC-1α balance determines the metabolic phenotype and plasticity of pancreatic cancer stem cells. 22(4):590-605.

[459] Shen, H., Yu, M., Tsoli, M., Chang, C., Joshi, S., Liu, J., et al., 2020. Targeting reduced mitochondrial DNA quantity as a therapeutic approach in pediatric high-grade gliomas. 22(1):139-151.

[460] Abildgaard, C., Dahl, C., Basse, A.L., Ma, T., Guldberg, P.J.J.o.t.m., 2014. Bioenergetic modulation with dichloroacetate reduces the growth of melanoma cells and potentiates their response to BRAF V600E inhibition. 12(1):247.

[461] Tataranni, T., Agriesti, F., Pacelli, C., Ruggieri, V., Laurenzana, I., Mazzoccoli, C., et al., 2019. Dichloroacetate affects mitochondrial function and stemness-associated properties in pancreatic cancer cell lines. 8(5):478.

[462] Park, S., Jeon, J.-H., Min, B.-K., Ha, C.-M., Thoudam, T., Park, B.-Y., et al., 2018. Role of the pyruvate dehydrogenase complex in metabolic remodeling: differential pyruvate dehydrogenase complex functions in metabolism. 42(4):270-281.

[463] Shelton, L.M., Huysentruyt, L.C., Seyfried, T.N.J.I.j.o.c., 2010. Glutamine targeting inhibits systemic metastasis in the VM-M3 murine tumor model. 127(10):2478-2485.

[464] Cervantes-Madrid, D., Romero, Y., Dueñas-González, A.J.B.r.i., 2015. Reviving lonidamine and 6-diazo-5-oxo-L-norleucine to be used in combination for metabolic cancer therapy. 2015.

[465] Olsen, R.R., Mary-Sinclair, M.N., Yin, Z., Freeman, K.W.J.P.o., 2015. Antagonizing Bcl-2 family members sensitizes neuroblastoma and Ewing's sarcoma to an inhibitor of glutamine metabolism. 10(1).

[466] Wu, F., Lukinius, A., Bergström, M., Eriksson, B., Watanabe, Y., Långström, B.J.E.J.o.C., 1999. A mechanism behind the antitumour effect of 6-diazo-5-oxo-L-norleucine (DON): disruption of mitochondria. 35(7):1155-1161.

[467] Huber, K., Mayer, E., Mitchell, D., Roberts, J.J.B.j.o.c., 1987. Cell cycle phase perturbations by 6-diazo-5-oxo-L-norleucine and acivicin in normal and neoplastic human cell lines. 55(6):653.

[468] Dranoff, G., Elion, G.B., Friedman, H.S., Bigner, D.D.J.C.r., 1985. Combination chemotherapy in vitro exploiting glutamine metabolism of human glioma and medulloblastoma. 45(9):4082-4086.

[469] Kam, Y., Romero, N., Swain, P., Dranka, B.P., 2017. Characterization of fuel dependencies in multidrug resistant breast cancer cells, Presented at the American Association of Cancer Researchers Annual Meeting.

[470] Klement, R.J.J.J.o.t., medicine, c., 2019. Wilhelm Brünings' forgotten contribution to the metabolic treatment of cancer utilizing hypoglycemia and a very low carbohydrate (ketogenic) diet. 9(3):192-200.

[471] Oleksyszyn, J., 2011. The complete control of glucose level utilizing the composition of ketogenic diet with the gluconeogenesis inhibitor, the anti-diabetic drug metformin, as a potential anti-cancer therapy. Medical hypotheses 77(2):171.

[472] Thomson, T.J., Runcie, J., Miller, V., 1966. Treatment of obesity by total fasting for up to 249 days. The Lancet 288(7471):992.

[473] Stewart, W.K., Fleming, L.W., 1973. Features of a successful therapeutic fast of 382 days' duration. Postgraduate medical journal 49(569):203.

[474] Longo, R., Peri, C., Cricrì, D., Coppi, L., Caruso, D., Mitro, N., et al., 2019. Ketogenic Diet: A New Light Shining on Old but Gold Biochemistry. 11(10):2497.

[475] Sperry, J., Le Belle, J.E., Condro, M.C., Guo, L., Kim, K.K., Vanderveer-Harris, N., et al., 2019. Metabolism of fatty acids and ketone bodies for glioblastoma growth: Implications for Ketogenic Diet Therapy.659474.

[476] Kalra, S.J.D.T., 2014. Sodium glucose co-transporter-2 (SGLT2) inhibitors: a review of their basic and clinical pharmacology. 5(2):355-366.

[477] van Poelje, P.D., Potter, S.C., Erion, M.D.J.D.-P.i.D.T., 2011. Fructose-1, 6-bisphosphatase inhibitors for reducing excessive endogenous glucose production in type 2 diabetes.279-301.

[478] Oleksyszyn, J., Wietrzyk, J., Psurski, M.J.A.S.R.o.C., Cancer Energy Metabolism, Hyperglycemia-Hypoglycemia, Metformin, Warburg, Effects, C., Ther, a.N.P.i.C.T.J.C.S., 2014. Cancer–Could it be Cured. 6:056-061.

[479] McCall, A.L., Fixman, L.B., Fleming, N., Tornheim, K., Chick, W., Ruderman, N.B.J.A.J.o.P.-E., et al., 1986. Chronic hypoglycemia increases brain glucose transport. 251(4):E442-E447.

[480] Maldonado, R., Talana, C.A., Song, C., Dixon, A., Uehara, K., Weichhaus, M.J.O.L., 2021. β-hydroxybutyrate does not alter the effects of glucose deprivation on breast cancer cells. 21(1):1-1.

[481] Pastò, A., Pagotto, A., Pilotto, G., De Paoli, A., De Salvo, G.L., Baldoni, A., et al., 2017. Resistance to glucose starvation as metabolic trait of platinum-resistant human epithelial ovarian cancer cells. 8(4):6433.

[482] Mathews, E.H., Visagie, M.H., Meyer, A.A., Joubert, A.M., Mathews, G.E.J.N., 2020. In vitro quantification: long-term effect of glucose deprivation on various cancer cell lines. 74:110748.

[483] Menendez, J.A., Oliveras-Ferraros, C., Cufí, S., Corominas-Faja, B., Joven, J., Martin-Castillo, B., et al., 2012. Metformin is synthetically lethal with glucose withdrawal in cancer cells. 11(15):2782-2792.

[484] Bardaweel, S.K., Alsalamat, H.A., Aleidi, S.M., Bashatwah, R.M.J.A.P., 2018. Glucose deprivation enhances the antiproliferative effects of oral hypoglycemic biguanides in different molecular subtypes of breast cancer: An in vitro study. 68(4):517-524.

[485] Chiodi, I., Picco, G., Martino, C., Mondello, C.J.O.r., 2019. Cellular response to glutamine and/or glucose deprivation in in vitro transformed human fibroblasts. 41(6):3555-3564.

[486] Javier, R., Horbinski, C.J.b., 2020. The ketogenic diet is not effective in preclinical models of IDH1 wild-type and IDH1 mutant glioma.

[487] Jiang, J., Srivastava, S., Zhang, J.J.C., 2019. Starve cancer cells of glutamine: break the spell or make a hungry monster? 11(6):804.

[488] Iyikesici, M.S.J.I.J.o.H., 2019. Feasibility study of metabolically supported chemotherapy with weekly carboplatin/paclitaxel combined with ketogenic diet, hyperthermia and hyperbaric oxygen therapy in metastatic non-small cell lung cancer. 36(1):445-454.

[489] Iyikesici, M.S.J.C.m.r., 2020. Long-term survival outcomes of metabolically supported chemotherapy with gemcitabine-based or FOLFIRINOX regimen combined with ketogenic diet, hyperthermia, and hyperbaric oxygen therapy in metastatic pancreatic cancer. 27(1):31-39.

[490] Zhang, S., Xie, C.J.L.s., 2017. The role of OXCT1 in the pathogenesis of cancer as a rate-limiting enzyme of ketone body metabolism. 183:110-115.

[491] Skinner, R., Trujillo, A., Ma, X., Beierle, E.A.J.J.o.p.s., 2009. Ketone bodies inhibit the viability of human neuroblastoma cells. 44(1):212-216.

[492] Magee, B.A., Potezny, N., Rofe, A.M., Conyers, R.A.J.A.J.o.E.B., Science, M., 1979. The inhibition of malignant cell growth by ketone bodies. 57(5):529-539.

[493] Tisdale, M., Brennan, R.J.B.j.o.c., 1983. Loss of acetoacetate coenzyme A transferase activity in tumours of peripheral tissues. 47(2):293-297.

[494] SAWAI, M., YASHIRO, M., NISHIGUCHI, Y., OHIRA, M., HIRAKAWA, K.J.A.r., 2004. Growth-inhibitory effects of the ketone body, monoacetoacetin, on human gastric cancer cells with succinyl-CoA: 3-oxoacid CoA-transferase (SCOT) deficiency. 24(4):2213-2218.

[495] Martuscello, R.T., Vedam-Mai, V., McCarthy, D.J., Schmoll, M.E., Jundi, M.A., Louviere, C.D., et al., 2016. A supplemented high-fat low-carbohydrate diet for the treatment of glioblastoma. 22(10):2482-2495.

[496] Klepin, H.D., Neuendorff, N.R., Larson, R.A., Hamaker, M.E., Breccia, M., Montesinos, P., et al., 2020. Treatment of acute promyelocytic leukemia in older patients: recommendations of an International Society of Geriatric Oncology (SIOG) task force.

[497] Seyfried, T.N., Mukherjee, P., Adams, E., Mulrooney, T., Abate, L.E., 2014. Metabolic control of brain cancer: role of glucose and ketone bodies. Cancer research 65(9 Supplement):267.

[498] Hong, X., Chedid, K., Kalkanis, S.N.J.I.j.o.o., 2012. Glioblastoma cell line-derived spheres in serum-containing medium versus serum-free medium: A comparison of cancer stem cell properties. 41(5):1693-1700.

[499] Lorenz, C., Lesimple, P., Bukowiecki, R., Zink, A., Inak, G., Mlody, B., et al., 2017. Human iPSC-derived neural progenitors are an effective drug discovery model for neurological mtDNA disorders. 20(5):659-674. e659.

[500] Delp, J., Gutbier, S., Cerff, M., Zasada, C., Niedenführ, S., Zhao, L., et al., 2018. Stage-specific metabolic features of differentiating neurons: implications for toxicant sensitivity. 354:64-80.

[501] Han, J., Nichols, J.H., Rice, M., Klonoff, D.C.J.J.o.d.s., technology, 2020. The End of the Road for the YSI 2300 Analyzer: Where Do We Go Now? 14(3):595-600.

[502] Lee, M.-J., Fried, S.K.J.M.i.e., 2014. Optimal protocol for the differentiation and metabolic analysis of human adipose stromal cells. 538:49-65.

[503] Agostini, M., Romeo, F., Inoue, S., Niklison-Chirou, M.V., Elia, A.J., Dinsdale, D., et al., 2016. Metabolic reprogramming during neuronal differentiation. 23(9):1502-1514.

[504] Iacopino, F., Angelucci, C., Piacentini, R., Biamonte, F., Mangiola, A., Maira, G., et al., 2014. Isolation of cancer stem cells from three human glioblastoma cell lines: characterization of two selected clones. 9(8):e105166.

[505] Giraud, S., Bessette, B., Boda, C., Lalloué, F., Petit, D., Mathonnet, M., et al., 2007. In vitro apoptotic induction of human glioblastoma cells by Fas ligand plus etoposide and in vivo antitumour activity of combined drugs in xenografted nude rats. 30(1):273-281.

[506] Wappler, J., Arts, M., Röth, A., Heeren, R.M., Neumann, U.P., Damink, S.W.O., et al., 2020. Glutamine deprivation counteracts hypoxia-induced chemoresistance. 22(1):22-32.

[507] Flavahan, W.A., Wu, Q., Hitomi, M., Rahim, N., Kim, Y., Sloan, A.E., et al., 2013. Brain tumor initiating cells adapt to restricted nutrition through preferential glucose uptake. 16(10):1373.

[508] Joly, J.H., Chew, B.T., Graham, N.A.J.P.C.B., 2021. The landscape of metabolic pathway dependencies in cancer cell lines. 17(4):e1008942.

[509] Willems, S.M., Abeln, S., Feenstra, K.A., de Bree, R., van der Poel, E.F., de Jong, R.J.B., et al., 2019. The potential use of big data in oncology. 98:8-12.

[510] Niu, N., Liu, T., Cairns, J., Ly, R.C., Tan, X., Deng, M., et al., 2016. Metformin pharmacogenomics: a genome-wide association study to identify genetic and epigenetic biomarkers involved in metformin anticancer response using human lymphoblastoid cell lines. 25(21):4819-4834.

[511] Dunwoodie, L.J., Poehlman, W.L., Ficklin, S.P., Feltus, F.A.J.O., 2018. Discovery and validation of a glioblastoma co-expressed gene module. 9(13):10995.

[512] Forman, A., Sotelo, J.J.C.S.H.p.i.m., 2020. Tumor-based genetic testing and familial cancer risk. 10(8):a036590.

[513] Dermani, F.K., Samadi, P., Rahmani, G., Kohlan, A.K., Najafi, R.J.J.o.c.p., 2019. PD-1/PD-L1 immune checkpoint: Potential target for cancer therapy. 234(2):1313-1325.

[514] Azuaje, F.J.N.p.o., 2019. Artificial intelligence for precision oncology: beyond patient stratification. 3(1):1-5.

[515] Andersen, F., Anjum, R.L., Rocca, E.J.E., 2019. Philosophy of Biology: Philosophical bias is the one bias that science cannot avoid. 8:e44929.

[516] Kwasniewski, W., Stupak, A., Kotarski, J., Gozdzicak-Jozefiak, A.J.G.P., 2021. Chaos and cancers. Theories concerning carcinogenesis. 92(4):318-321.

[517] Ravetz, J.J.N., 1961. Origins of the Copernican Revolution. 189(4767):859-860.

[518] Aleksandr Nikoláyevich Bálmont, On the neurobiology of human nature. Lomonósov Institute, Essay Series (Limitibus naturae humanae):786.

[519] Lander, E.S., Linton, L.M., Birren, B., Nusbaum, C., Zody, M.C., Baldwin, J., et al., 2001. Initial sequencing and analysis of the human genome.

[520] Garber, K.J.J.o.t.N.C.I., 2005. Human Cancer Genome Project moving forward despite some doubts in community. 97(18):1322-1324.

[521] Gyamfi, J., Kim, J., Choi, J.J.I.J.o.M.S., 2022. Cancer as a Metabolic Disorder. 23(3):1155.

[522] Larivière, V., Gingras, Y., Archambault, É.J.J.o.t.A.S.f.I.S., Technology, 2009. The decline in the concentration of citations, 1900–2007. 60(4):858-862.

[523] Woolf, E.C., Syed, N., Scheck, A.C.J.F.i.m.n., 2016. Tumor metabolism, the ketogenic diet and β-hydroxybutyrate: novel approaches to adjuvant brain tumor therapy. 9:122.

[524] Akins, N.S., Nielson, T.C., Le, H.V.J.C.t.i.m.c., 2018. Inhibition of glycolysis and glutaminolysis: an emerging drug discovery approach to combat cancer. 18(6):494-504.

[525] Jin, L., Alesi, G., Kang, S.J.O., 2016. Glutaminolysis as a target for cancer therapy. 35(28):3619-3625.

[526] Liu, Y.e., Shi, Y.J.M., 2020. Mitochondria as a target in cancer treatment. 1(2):129-139.

[527] Ma, Y., Temkin, S.M., Hawkridge, A.M., Guo, C., Wang, W., Wang, X.-Y., et al., 2018. Fatty acid oxidation: an emerging facet of metabolic transformation in cancer. 435:92-100.

[528] Brennan, C.W., Verhaak, R.G., McKenna, A., Campos, B., Noushmehr, H., Salama, S.R., et al., 2013. The somatic genomic landscape of glioblastoma. 155(2):462-477.

[529] Deighton, R.F., Le Bihan, T., Martin, S.F., Gerth, A.M., McCulloch, M., Edgar, J.M., et al., 2014. Interactions among mitochondrial proteins altered in glioblastoma. 118(2):247-256.

[530] Arismendi-Morillo, G.J., Castellano-Ramirez, A.V., 2008. Ultrastructural mitochondrial pathology in human astrocytic tumors: potentials implications pro-therapeutics strategies. Journal of electron microscopy 57(1):33.

[531] Hassan, A., Mosley, J., Singh, S., Zinn, P.O.J.T.i.M.R.I., 2017. A comprehensive review of genomics and noncoding RNA in gliomas. 26(1):3-14.

[532] Munzarova, M., Lauerova, L., Kovarik, J., Rejthar, A., Brezina, V., Kellnerova, R., et al., 1992. Fusion-induced malignancy? A preliminary study.(a challenge to today's common wisdom). 39(2):79-86.

[533] Baker, S.G.J.O.J.o.B.S., 2018. The detached pericyte hypothesis: A novel explanation for many puzzling aspects of tumorigenesis. 2(1):25-42.

[534] Seliger, C., Leukel, P., Moeckel, S., Jachnik, B., Lottaz, C., Kreutz, M., et al., 2013. Lactate-modulated induction of THBS-1 activates transforming growth factor (TGF)-beta2 and migration of glioma cells in vitro. 8(11):e78935.

[535] Herbener, V.J., Burster, T., Goreth, A., Pruss, M., von Bandemer, H., Baisch, T., et al., 2020. Considering the Experimental Use of Temozolomide in Glioblastoma Research. 8(6):151.

[536] Uhlen, M., Zhang, C., Lee, S., Sjöstedt, E., Fagerberg, L., Bidkhori, G., et al., 2017. A pathology atlas of the human cancer transcriptome. 357(6352).

[537] Bioscience, S., 2010. XF Cell Mito Stress Test Kit User Manual XF24 Instructions.

[538] Glancy, B., Kim, Y., Katti, P., Willingham, T.B.J.F.i.p., 2020. The functional impact of mitochondrial structure across subcellular scales. 11.

[539] Singleterry, J., Sreedhar, A., Zhao, Y.J.M., 2014. Components of cancer metabolism and therapeutic interventions. 17:50-55.

[540] Nakashima, R.A., Paggi, M.G., Pedersen, P.L.J.C.r., 1984. Contributions of glycolysis and oxidative phosphorylation to adenosine 5′-triphosphate production in AS-30D hepatoma cells. 44(12 Part 1):5702-5706.

[541] Oesper, P., 1964. The history of the Warburg apparatus: Some reminiscences on its use. ACS Publications.

[542] House, S.W., Warburg, O., Burk, D., Schade, A.L.J.S., 1956. On respiratory impairment in cancer cells. 124(3215):267-272.

[543] Wagner, B.A., Venkataraman, S., Buettner, G.R.J.F.R.B., Medicine, 2011. The rate of oxygen utilization by cells. 51(3):700-712.

[544] Childers, G., Harry, G.J., 2021. Mitochondrial Stress Assay and Glycolytic Rate Assay in Microglia Using Agilent Seahorse Extracellular Flux Analyzers. Experimental Neurotoxicology Methods. Springer, p. 305-324.

[545] Diaz-Ruiz, R., Rigoulet, M., Devin, A., 2011. The Warburg and Crabtree effects: On the origin of cancer cell energy metabolism and of yeast glucose repression. Biochimica et Biophysica Acta (BBA)-Bioenergetics 1807(6):568.

[546] Koppenol, W.H., Bounds, P.L., Dang, C.V., 2011. Otto Warburg's contributions to current concepts of cancer metabolism. Nature Reviews Cancer 11(5):325.

[547] Pascale, R.M., Calvisi, D.F., Simile, M.M., Feo, C.F., Feo, F.J.C., 2020. The Warburg effect 97 years after its discovery. 12(10):2819.

[548] Potter, M., Badder, L., Hoade, Y., Johnston, I.G., Morten, K.J., 2016. Monitoring intracellular oxygen concentration: Implications for hypoxia studies and real-time oxygen monitoring. Oxygen Transport to Tissue XXXVII. Springer, p. 257-263.

[549] Kaambre, T., Chekulayev, V., Shevchuk, I., Tepp, K., Timohhina, N., Varikmaa, M., et al., 2013. Metabolic control analysis of respiration in human cancer tissue. 4:151.

[550] Majerus, M.J.M.h., 2002. The relationship between the cancer cell and the oocyte. 58(6):544-551.

[551] Gonzalez, M.J., Massari, J.R.M., Duconge, J., Riordan, N.H., Ichim, T., Quintero-Del-Rio, A.I., et al., 2012. The bio-energetic theory of carcinogenesis. 79(4):433-439.

[552] Voet, D., Voet, J.G., Pratt, C.W., 2016. Fundamentals of biochemistry: life at the molecular level. John Wiley & Sons.

[553] Monnot, S., Samuels, D.C., Hesters, L., Frydman, N., Gigarel, N., Burlet, P., et al., 2013. Mutation dependance of the mitochondrial DNA copy number in the first stages of human embryogenesis. 22(9):1867-1872.

[554] Moras, M., Lefevre, S.D., Ostuni, M.A.J.F.i.p., 2017. From erythroblasts to mature red blood cells: organelle clearance in mammals. 8:1076.

[555] Logan, D.C., Paszkiewicz, G.J.A.P.R.o., 2018. The dynamic chondriome: control of number, shape, size and motility of mitochondria.67-110.

[556] Yang, L., Moss, T., Mangala, L.S., Marini, J., Zhao, H., Wahlig, S., et al., 2014. Metabolic shifts toward glutamine regulate tumor growth, invasion and bioenergetics in ovarian cancer. 10(5):728.

[557] Dier, U., Shin, D.-H., Hemachandra, L.M.P., Uusitalo, L.M., Hempel, N.J.P.o., 2014. Bioenergetic analysis of ovarian cancer cell lines: profiling of histological subtypes and identification of a mitochondria-defective cell line. 9(5):e98479.

[558] Russell, S., Wojtkowiak, J., Neilson, A., Gillies, R.J.J.S.r., 2017. Metabolic Profiling of healthy and cancerous tissues in 2D and 3D. 7(1):1-11.

[559] Patananan, A.N., Sercel, A.J., Wu, T.-H., Ahsan, F.M., Torres Jr, A., Kennedy, S.A., et al., 2020. Pressure-Driven mitochondrial transfer pipeline generates mammalian cells of desired genetic combinations and fates. 33(13):108562.

[560] Zampieri, L.X., Silva-Almeida, C., Rondeau, J.D., Sonveaux, P.J.I.J.o.M.S., 2021. Mitochondrial Transfer in Cancer: A Comprehensive Review. 22(6):3245.

cells

MDPI

Article

Beyond the Warburg Effect: Oxidative and Glycolytic Phenotypes Coexist within the Metabolic Heterogeneity of Glioblastoma

Tomás Duraj [1], Noemí García-Romero [2,3], Josefa Carrión-Navarro [2,3], Rodrigo Madurga [2,3], Ana Ortiz de Mendivil [4], Ricardo Prat-Acin [5], Lina Garcia-Cañamaque [6] and Angel Ayuso-Sacido [2,3,*]

1 Faculty of Medicine, Institute for Applied Molecular Medicine (IMMA), CEU San Pablo University, 28668 Madrid, Spain; tom.duraj.ce@ceindo.ceu.es
2 Faculty of Experimental Sciences, Universidad Francisco de Vitoria, 28223 Madrid, Spain; noemi.garcia@ufv.es (N.G.-R.); pepa.carrion@ufv.es (J.C.-N.); rodrigo.madurga@ufv.es (R.M.)
3 Brain Tumor Laboratory, Fundación Vithas, Grupo Hospitales Vithas, 28043 Madrid, Spain
4 Fundación de Investigación HM Hospitales, HM Hospitales, 28015 Madrid, Spain; aomendivil@yahoo.es
5 Neurosurgery Department, Hospital Universitario La Fe, 46026 Valencia, Spain; ricprat@hotmail.com
6 Departamento de Medicina Nuclear, HM Hospitales, 28015 Madrid, Spain; lgarciacanamaque@hmhospitales.com
* Correspondence: ayusosa@vithas.es; Tel.: +34-686-966-904

Abstract: Glioblastoma (GBM) is the most aggressive primary brain tumor, with a median survival at diagnosis of 16–20 months. Metabolism represents a new attractive therapeutic target; however, due to high intratumoral heterogeneity, the application of metabolic drugs in GBM is challenging. We characterized the basal bioenergetic metabolism and antiproliferative potential of metformin (MF), dichloroacetate (DCA), sodium oxamate (SOD) and diazo-5-oxo-L-norleucine (DON) in three distinct glioma stem cells (GSCs) (GBM18, GBM27, GBM38), as well as U87MG. GBM27, a highly oxidative cell line, was the most resistant to all treatments, except DON. GBM18 and GBM38, Warburg-like GSCs, were sensitive to MF and DCA, respectively. Resistance to DON was not correlated with basal metabolic phenotypes. In combinatory experiments, radiomimetic bleomycin exhibited therapeutically relevant synergistic effects with MF, DCA and DON in GBM27 and DON in all other cell lines. MF and DCA shifted the metabolism of treated cells towards glycolysis or oxidation, respectively. DON consistently decreased total ATP production. Our study highlights the need for a better characterization of GBM from a metabolic perspective. Metabolic therapy should focus on both glycolytic and oxidative subpopulations of GSCs.

Keywords: glioblastoma; energy metabolism; glycolysis; oxidative phosphorylation; therapeutics; gene expression profiling

Citation: Duraj, T.; García-Romero, N.; Carrión-Navarro, J.; Madurga, R.; Ortiz de Mendivil, A.; Prat-Acin, R.; Garcia-Cañamaque, L.; Ayuso-Sacido, A. Beyond the Warburg Effect: Oxidative and Glycolytic Phenotypes Coexist within the Metabolic Heterogeneity of Glioblastoma. *Cells* **2021**, *10*, 202. https://doi.org/10.3390/cells10020202

Academic Editor: Javier S. Castresana
Received: 31 December 2020
Accepted: 18 January 2021
Published: 20 January 2021

1. Introduction

Glioblastoma (GBM) is the most common, heterogeneous and aggressive primary brain tumor in adults (54% of all gliomas) [1–3]. The World Health Organization (WHO, Geneva, Switzerland) classifies GBM based on histopathological findings and molecular features (especially IDH mutation status) [4]. At a gene-expression level, GBM can be classified into four subtypes: mesenchymal, classical, proneural and neural [5,6].

Standard treatment of GBM consists of maximally safe surgical resection, followed by radiotherapy and chemotherapy, usually in the form of temozolomide (TMZ). Despite decades of extensive research and advancements in therapeutics, such as tumor treating fields (TTF), prognosis remains extremely poor, with a median overall survival of 20.9 months [7]. GBM has a low global incidence (less than 10 per 100,000 persons/year), but cumulative survival after five years from diagnosis is less than 10%, making it a critical public health issue [8,9]. Dismal survival is partly owed to GBM's highly invasive,

chemo-resistant and recurrent nature [10]. As standard of care is not a curative option, new therapies are sorely needed, with efforts to characterize GBM from multiple viewpoints, predominantly the omics sciences.

Setting aside the uncertainty behind the origin of cancer [11,12], one of its defining characteristics, at a functional, bioenergetic level, is its ability to exploit glycolytic metabolism even in the presence of oxygen, a phenomenon known as the "Warburg effect" [13]. Among many other solid tumors, this metabolic shift has been extensively documented in gliomas [14,15]. In the mitochondrial theory of cancer, aerobic glycolysis represents a universal feature of transformed cells, allowing the reduction of vast molecular heterogeneity into a smaller number of metabolic categories [16]. Metabolic reprogramming is not merely an in vitro artifact, but has wide-ranging clinical applications [11,17,18]. Nowadays, 18F-fluorodeoxyglucose PET (18F-FDG PET) is a common technique for cancer diagnosis and staging, with novel metabolic markers, such as lactate, glutamine, oxygen and even ketone bodies under clinical evaluation [19–21]. Within ample cell diversity, however, the predominance of aerobic glycolysis does not necessarily abrogate ancillary energetic sources: functional oxidative metabolism (glucose, fatty acids, glutamine) and the "reverse Warburg" effect [22,23]. Characteristically, in vitro, GBM has shown high variability in mitochondrial respiration, while tissue-derived cell lines revealed glucose dependency and fatty acid oxidation (FAO) [23–26]. Intratumoral heterogeneity makes development of targeted strategies against specific mutations very challenging [27]; therefore, patient stratification based on metabolic pathways should be a key component of improved therapeutic strategies.

The main challenge facing GBM management is the eradication of all malignant cells, including those able to survive drastic changes in the tumor microenvironment and toxic interventions. For this reason, GBM presents as a unique model to study bioenergetic alterations, as both aerobic glycolysis and oxidative phosphorylation (OXPHOS) have been described in high grade gliomas [28–30]. Furthermore, discouraging survival rates are a compelling reason to explore new therapeutic opportunities, either stand-alone or, more likely, in combination with standard of care. To this effect, metabolic inhibitors such as metformin hydrochloride (MF), dichloroacetate (DCA), sodium oxamate (SOD) and 6-diazo-5-oxo-L-norleucine (DON) have a longstanding history in this field, undergoing extensive evaluation in animal models and clinical trials with a variable rate of success [31–34].

To accurately model this disease in vitro, it has been proposed that GBM stem cells (GSCs) have a remarkable proliferative ability, sufficient to drive tumor maintenance, recurrence and therapeutic resistance [35–38]. GSCs are a highly heterogeneous and metabolically adaptive cell population: surviving in both perivascular aerobic and hypoxic regions [39,40], seemingly able to shift between glycolytic and oxidative phenotypes [28,29]. Whether these parameters are permanent, stable, independent or complementary, operating on a spectrum, remains to be elucidated [41].

To help us illuminate this question, we performed a Gene Set Variation Analysis (GSVA) [42] for canonical glycolytic/oxidative pathways in The Cancer Genome Atlas (TCGA) GBM datasets. A clustering of highly oxidative signatures was observed in normal tissues, whereas highly glycolytic tumors matched with the mesenchymal subtype; interestingly, mesenchymal signatures are associated with increased inflammation and wound healing pathways, a higher degree of necrosis and the worst survival when restricting for samples with low transcriptional heterogeneity [5,43]. Between these two categories, a high degree of heterogeneity was recognized. Clinically, 18F-FDG PET imaging of GBM can exhibit high or low glucose uptake, but allocation of metabolic substrates is not routine practice.

To verify these observations in vitro, we analyzed the basal metabolic phenotype of three tissue-derived and molecularly distinct GSCs (GBM18, GBM27, GBM38), in addition to traditional established cell line U87MG. As metabolic plasticity is being touted as a distinctive feature of GSCs, we wanted to explore antiproliferative responses to metabolic inhibitors and their correlation with basal bioenergetics. High resistance to MF (a mild

mitochondrial inhibitor) and DCA (glycolytic modulator) was detected in GBM27, a distinctively oxidative cell line. GBM38 displayed Warburg-like properties, with higher sensitivity to DCA. Responses to DON (glutaminase inhibitor) varied between cell lines, without a clear correlation with basal metabolic phenotypes. Subsequently, we combined promising drug candidates with bleomycin, a radiomimetic drug that causes single-strand and double-strand DNA breaks [44,45]. Synergism at therapeutically relevant outcomes was detected with all drugs in GBM27, and all cell lines with DON. Lastly, Seahorse XF analysis was performed in surviving, metabolically treated cells to determine vulnerabilities in bioenergetic phenotypes ("metabolic priming").

Here, we propose that strategic targeting of dysregulated bioenergetic pathways, after an initial assessment of the metabolic phenotypes coexisting within a tumor, could become a valuable stratification and therapeutic tool, improving the efficacy of adjuvant metabolic therapy.

2. Materials and Methods

2.1. Culture of GSCs from Human GBM Samples, U87MG and Mesenchymal Stem Cells

GSCs were originally isolated from surgical human GBM specimens, as described by our group in [46]. The GSCs used in this study are characterized by distinct molecular and morphological features, differential drug sensitivity profiles and in vivo dissemination patterns that reflect the original tumors. GSCs were cultured under a humidified atmosphere of 5% CO_2 at 37 °C, in a media containing, as a base, DMEM/F-12 (catalog number 11039, Gibco, Grand Island, NY, USA), supplemented with: Non Essential Amino Acids (1% *v/v*; 11140, Gibco), HEPES (38 mM; 15630, Gibco), D-Glucose (0,54% *v/v* or 30 mM; G8769, Sigma-Aldrich, St. Louis, MI, USA), BSA-FV (0,01% *v/v*; 15260037, Invitrogen, Carlsbad, CA, USA), Sodium Pyruvate (1 mM; Invitrogen), L-Glutamine (4 mM; 25030, Gibco), Antibiotic-Antimycotic (0.4% *v/v*; Invitrogen), N1 Supplement (1% *v/v*; Invitrogen), Hydrocortisone (0.3 µg/mL; H0135, Sigma-Aldrich), Tri-iodothyronine (0.03 µg/mL; T5516, Sigma-Aldrich), EGF (10 ng/µL; E9644, Sigma-Aldrich), bFGF (20 ng/mL; F0291, Sigma-Aldrich) and Heparin (2 µg/mL; H3393, Sigma-Aldrich).

U87MG was purchased from ATCC, Rockville, MD, USA and cultured in DMEM/F-12 (11039, Gibco) supplemented with 10% fetal bovine serum (FBS) and 2% penicillin-streptomycin (PS). Cells were maintained at 37 °C in humidified atmosphere air, CO_2 5%.

Human mesenchymal stem cells (hMSCs) (a gift from Dr. Carmen Escobedo Lucea) were cultured in DMEM, high glucose, GlutaMAX (10566016, Gibco), supplemented with a final concentration of 20% FBS and 1% P/S. All hMSCs experiments were performed in the first five passages from isolation.

2.2. Reagents and Metabolic Inhibitors

1,1-Dimethylbiguanide hydrochloride (D150959), sodium oxamate (O2751), sodium dichloroacetate (347795) and 6-Diazo-5-oxo-L-norleucine (D2141) were purchased from Sigma-Aldrich. Bleomycin sulfate (HY-17565) was acquired from MedChemExpress, Monmouth Junction, NJ, USA.

2.3. MTS Assays and Drug Combination Studies using the Chou-Talalay Method

The sensitivity to different metabolic drugs was assessed using [3-(4,5-dimethylthiazol-2-yl)-5-(3-carboxymethoxyphenyl)-2-(4-sulfophenyl)-2H-tetrazolium, inner salt (MTS) containing solution from Promega, Madison, WI, USA (CellTiter 96 AQueous One Solution, G3582). Briefly, single-cell suspensions of GSCs were plated in a 96-well plate, 3000 cells/well, and allowed to grow and form spheres for 72 h. U87MG were seeded at 3000 cells/well and allowed to grow for 24 h. Cultures were then treated with their respective culture media (control cells) or increasing concentrations of each drug for 0 h, 24 h, 48 h or 72 h. At each timepoint, MTS reactant was added, incubated at 37 °C for 2 to 4 h and absorbance was measured at 490 nm/630 nm, using a Varioskan Flash (5250030, Thermo Scientific, Waltham, MA, USA) or a Sunrise Absorbance Reader (Tecan

Trading AG, Männedorf, Switzerland). For IC50 calculations, corrected absorbance was transformed, normalized and extrapolated in GraphPad Prism version 8.0.1, using the logarithmic variable slope equation:

$$Y = 100/(1 + 10\hat{}((LogIC50 - X) \times HillSlope)).$$

In specific dose experiments, hMSCs were seeded at 6000 cells/well and allowed to grow for 72 h. Fresh cell culture media was then added to control wells and dissolved treatments to experimental wells. Cells were treated for 72 h before MTS read-out.

Combinatory studies were performed in the same manner as single-drug assays. After seeding and cell-specific recovery/attachment intervals, combined treatments were added in the following final concentrations: IC50 for drug A alone; IC50 for drug B alone; full dose IC50 for drug A + drug B; IC50(A + B)/2; IC50(A + B)/8. Experimentally, drug "A" was one of the metabolic inhibitors (MF, DCA or DON), whereas drug "B" was the radiomimetic bleomycin. CompuSyn software (version 1.0), based on the Chou-Talalay method, was employed to determine the interaction between the drugs [47,48]. This method utilizes a multiple drug-effect equation derived from enzyme kinetics, generating a "combination index" (CI) for each drug combination, at each fraction of affected cells (Fa) level. CompuSyn software defines synergy as a CI value lower than 1, CI = 1 equals to additive effects and CI values > 1 indicate antagonistic effects. We have determined CI values for each metabolic inhibitor and bleomycin across all tested cell lines using a constant ratio experimental design, as well as other valuable parameters such as the Dose-Reduction Index (DRI), which indicates how many folds of dose-reduction for each drug, at any given effect, would be allowed in synergistic combination.

2.4. Real-Time Quantitative Reverse Transcription PCR (RT-qRT-PCR) Analysis

For RT-qRT-PCR, total RNA was isolated from cell pellets using NZYol (MB18501, NZYTech, Lda.), following the manufacturer's recommendations. For chronological parity with other experiments, GSCs were seeded in 6-well plates at a density of 90000 cells/well, allowed to grow for 72 h, fresh cell culture media was added (1:1) and pellets were collected after 72 h; the same protocol was applicable to U87MG, but fresh cell culture media was added after 24 h from seeding. Purity of RNA was assessed based on 260/280 and 260/230 ratios using a Thermo Scientific NanoDrop 2000/2000c. RNA was retrotranscribed to cDNA (High-Capacity cDNA Reverse Transcription Kit; Applied BioSystems). Resulting samples were amplified with specific primers (Table 1) in a CFX Connect Real-Time PCR Detection System (Bio-Rad). *β-actin* and *GAPDH* were used as housekeeping genes. For relativization and comparison with a non-tumoral control, we compared our samples with a pool of retrotranscribed RNA from brain tissue obtained from epileptic patients, provided courtesy of Hospital Universitario y Politécnico La Fe (Valencia).

Table 1. Forward (FW) and reverse (RV) primers for real-time quantitative reverse transcription PCR (RT-qRT-PCR).

Name	5′-Sequence-3′
β-actin FW	TTCTACAATGAGCTGCGTGTG
β-actin RV	GGGGTGTTGAAGGTCTCAAA
GAPDH FW	TCCTCCACCTTTGACGCTG
GAPDH RV	ACCACCCTGTTGCTGTAGCC
GLS1 FW	GCCCGCTTTGTGTGACTAAA
GLS1 RV	CAGGGGTAAATAACGGCACA
GLS2 FW	GCACTAAAGGCCACTGGAC
GLS2 RV	CCAAGAGGCCACCACTACTG
MTOR FW	CTGACCGCTAGTAGGGAGGT
MTOR RV	AACATCCCAGAACCCTGCTG
PDK1 FW	ATCCTCCTGCCTGAGTCTCT
PDK1 RV	CAAATGCCAAGGACTGCTGT
PDK2 FW	TGCCTACGACATGGCTAAGCTC
PDK2 RV	GACGTAGACCATGTGAATCGGC
PDK3 FW	TGGAAGGAGTGGGTACTGATGC
PDK3 RV	GGATTGCTCCAATCATCGGCTTC
PDK4 FW	AACTCGGGATGTTGGGGATT
PDK4 RV	AGAGAAAAGCCCTTCCTACTGA
PRKAA1 FW	GTCCAGGGCTTGTTCTATTCA
PRKAA1 RV	ATGCTGCACTTAGAGACCCT
PRKAA2 FW	TGGAACATTGTTACAGCAGGC
PRKAA2 RV	AGCTCTTCTCCCGTGTCTTC

2.5. Antibodies

All primary and secondary antibodies were purchased from commercial sources, listed as follows: AMPKα Antibody (2532, Cell Signaling, Danvers, MA, USA), phospho-AMPKα (Thr172) (2535, Cell Signaling), Anti-Pyruvate Dehydrogenase E1-alpha subunit antibody (ab110334, Abcam, Cambridge, UK), Anti-PDHA1 (phospho S293) antibody (ab177461, Abcam), β-Actin (A5441, Sigma-Aldrich), α-Tubulin (sc-8035, Santa Cruz Biotechnology, Santa Cruz, CA, USA). The secondary antibodies for horseradish peroxidase (HRP) detection were anti-rabbit IgG (sc-2004, Santa Cruz Biotechnology) and anti-mouse IgG (PI-2000, Vector Laboratories, Burlingame, CA, USA).

2.6. Protein Isolation/Quantification and Western Blotting

Centrifuged and pelleted U87MG and GSCs were resuspended in 100 µL of radioimmunoprecipitation buffer [RIPA; 100 mM Tris-HCl (pH 8.5), 200 mM NaCl, 5 mM EDTA and 0.2% SDS, with phosphatase and a protease inhibitor cocktail and stored at −80 °C for a minimum of 24 h. Samples were then centrifuged at 13,200 RPM for 20 min at 4 °C; protein-containing supernatant was conserved.

Total protein concentration was determined using Bio-Rad Protein Assay according to the manufacturer instructions; after corresponding incubation, absorbance was read at 595 nm.

In phosphorylation experiments, treatments dissolved at 1:1 concentration in serum-free medium were added 3–4 days after seeding GSCs, and 24 h in the case of U87MG. U87MG cells were washed twice with PBS and serum-deprived for 1 h prior to sample

collection. Protein was subsequently recovered at the indicated timepoints (30 min, 60 min, 2 h, 6 h).

Western blotting experiments were performed adapting the protocol from Mahmood et al. [49]. Briefly, protein extracts were separated by 8%–12% SDS-PAGE and transferred to nitrocellulose membranes. After blocking for 1 h with 5% Bovine Serum Albumin (BSA) in Tween-Tris Buffered Saline 1× [T-TBS; 10 mM Tris-HCl (pH 7.6), 150 mM NaCl and 0.1% Tween-20], membranes were incubated with the corresponding primary antibody O/N at 4 °C. After washing three times for 10 min with T-TBS, membranes were incubated with HRP-linked secondary antibody for 1 h at room temperature (RT). Detection was performed using ECL reagents (GE Healthcare) according to the manufacturer's guidelines and revealed in a BioRad ChemiDoc chemiluminescence system. The same membranes were then incubated with a housekeeping primary antibody O/N at 4 °C, washed the next day and incubated with an HRP-linked secondary antibody for 1 h RT before ECL detection.

2.7. Seahorse XFp Protocol for Real-Time Metabolic Evaluation of U87MG Adherent Cells and GSCs Neurospheres

Experiments were performed in an XFp 8-well microplate using the Seahorse XFp Analyzer (Agilent, Santa Clara, CA, USA). Briefly, GSCs were seeded at a density of 10,000 cells/well and allowed to grow for 72 h, in wells previously coated with 20 µL of Collagen Type IV at 20 µg/mL (C6745-1ML, Sigma Aldrich). U87MG cells were seeded at 6000 cells/well and allowed to grow for 24 h. Metabolic drugs were added to the treatment wells and fresh media was added to the control wells. After 72 h, the original media was carefully pipetted out of each well into a centrifuge tube without disturbing the attached cells; then, Seahorse XF DMEM medium, pH 7.4 (103575-100, Agilent) was used to wash, pipetted out and centrifuged with the original media at 1000 rpm for 5 min at 25 °C. After centrifugation, supernatant was aspirated from each tube, conserving only the cell pellet, resuspended in Seahorse medium and added back to respective wells.

We then followed the standard protocol for Standard XF Real-Time ATP Rate Assay, as described in the Seahorse XF Real-Time ATP Rate Assay User Guide (Kit 103592-100, Agilent). Seahorse XF technology measures two key parameters of cellular bioenergetics: oxygen consumption rate (OCR; an estimation of mitochondrial ATP) and extracellular acidification rate (ECAR; quantification of glycolytic activity through changes in pH by lactate production) [50,51]. Results were analyzed in Seahorse Wave software (version 2.6.1), with analysis of OCR and ECAR carried out using the Seahorse XF Real-Time ATP Rate Assay Report Generator (version 4.0.17). For normalization, total protein was quantified using an Invitrogen Qubit 3 Fluorometer (Q33216, Invitrogen).

2.8. TCGA Gene-Set Variation Analysis

Affymetrix (HG-U133A) normalized gene expression datasets of GBM and non-tumor tissue samples from TCGA were downloaded from GlioVis repository (gliovis.bioinfo.cnio.es) [52]. As IDH mutation status confers characteristic metabolic rewiring of the TCA cycle, IDH mutant and IDH unknown samples were removed from the analysis [53]. The remaining 498 GBM IDH-wt and 10 non-tumor samples were classified in proneural, classical, mesenchymal and those with a high content in non-tumoral tissue (low cellularity), as proposed elsewhere [54]. Four different canonical gene sets (two oxidative and two glycolytic) were obtained from the Molecular Signatures Database (MSigDB) [55]: KEGG (oxidative phosphorylation and TCA cycle), Hallmark (glycolysis, mTORC1 signaling). Gene set variation analysis (GSVA) was performed on each sample to obtain an enrichment score (ES) using the GSVA R package [42].

2.9. Statistical Analysis

Statistical analysis was performed using a 2-tailed Student t test (when comparing two groups) and One-Way ANOVA (three or more groups). Data are presented as means ± standard deviation and calculated using the software package GraphPad Prism version 8.0.1 for Windows, GraphPad Software, San Diego, California USA. RT-qRT-PCR expression data was graphed and analyzed directly in CFX Maestro 1.1 software, version

4.1.2433.1219 (Bio-Rad Laboratories). p values < 0.05 were considered as statistically significant. For all figures, p values were expressed according to GraphPad 8 NEJM p-value style.: $p > 0.05$ (ns); $p < 0.05$ (*); $p < 0.01$ (**); $p < 0.001$ (***).

3. Results

3.1. GBM can be Stratified into Glycolytic and Oxidative Phenotypes

Molecular heterogeneity is a key feature of GBM, with clinical and therapeutic repercussions. To better understand if the vast molecular landscape of GBM could be reduced into a manageable number of metabolic categories, we explored the TCGA expression databases using a GSVA approach. Filtering for canonical gene sets of glycolytic and oxidative pathways, Warburg-like phenotypes were enriched in the mesenchymal subgroup, whereas functional mitochondrial metabolism predominated in healthy tissues (Figure 1a). Between these two extremes, however, we still encountered ample metabolic heterogeneity. Clinically, 18F-FDG PET is valuable for staging and detection of recurrence, but not necessarily to guide treatments. Without further stratification, GBM can be identified as a malignancy with high glucose uptake or low glucose uptake (Figure 1b). Nevertheless, common standardized procedures such as 18F-FDG PET do not allow for differentiation between high glucose uptake due to increased aerobic glycolysis or OXPHOS, or low glucose uptake due to compensatory glutaminolysis, necrosis or quiescent metabolic phenotypes.

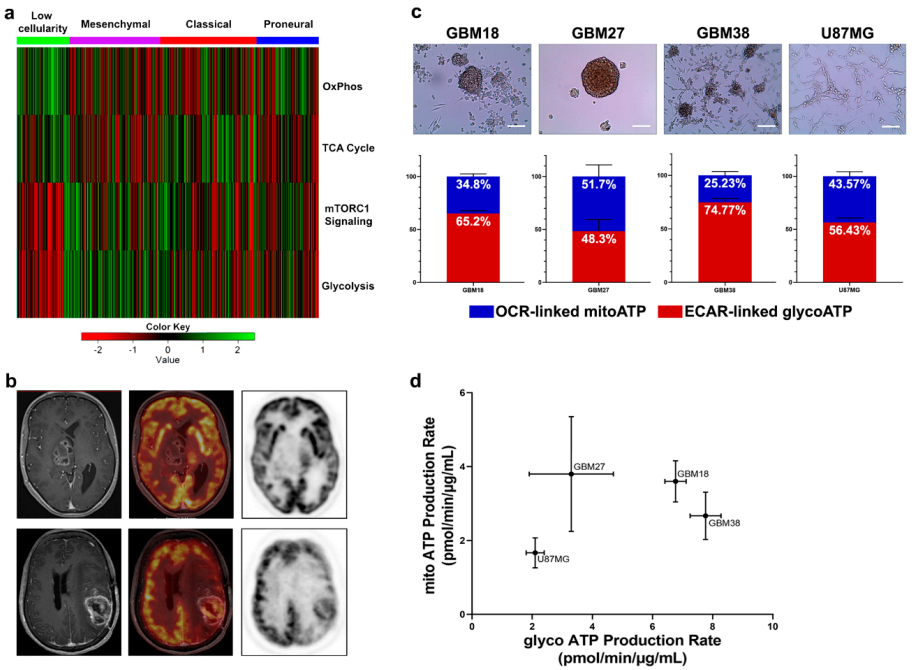

Figure 1. (**a**) Heatmap of the scaled enrichment score (ES) obtained by Gene Set Variation Analysis (GSVA) with the samples grouped by their gene expression subtype (proneural, classical or mesenchymal) including those with high content of non-tumor tissue (low cellularity). (**b**) Clinically, standard imaging techniques such as 18F-FDG PET-MRI can classify tumors into low glucose uptake (upper) and high glucose uptake (lower). Upper images: Right thalamic glioblastoma shows patchy contrast enhanced areas on 3DT1 (right side) and no uptake of 18F-FDG PET (medium and left side). Lower images: Parietal recurrent glioblastoma in the left hemisphere shows heterogeneous enhancement on axial three-dimensional T1-weighted imaging (3DT1) and extensive uptake of 18F-FDG PET (right and medium side), despite high uptake in surrounding normal brain tissue. (**c**) Representative optical microscopy images of cellular morphology. Scale bar = 100 µm. Under each cell line, average distribution of total ATP production from extracellular acidification rate (ECAR)-linked ATP production and oxygen consumption rate (OCR)-linked ATP production in basal (non-treated) conditions. (**d**) Seahorse XF Energetic Map. GBM18 and GBM38 clustered together as highly glycolytic-like cells. GBM27 displayed the highest variation in the metabolic profiles, with increased mitochondrial respiration, at a similar level to GBM18, but, in comparison, lower glycolysis. U87MG were not as metabolically active as glioma stem cells (GSCs). Data from three independent experiments, each with $n = 3$, normalized to total protein concentration (µg/mL).

Subsequently, to examine the differences in bioenergetic metabolism in phenotypically and molecularly distinct gliomas in vitro, we determined OCR and ECAR of our set of GSCs and U87MG (Figure 1c). We can observe that, in basal conditions, GBM27 and U87MG are close to a 1:1 ratio of glycolytic/oxidative metabolism, whereas GBM18 and GBM38 have a strong preference towards a glycolytic phenotype. Furthermore, U87MG, a typically Warburg-like cell line [30], also exhibited a relative elevation in OCR-linked ATP production rate (up to 43.57% of total ATP). As shown in Figure 1d, GBM27 demonstrated high mitochondrial ATP production as well as lower glycolytic ATP production when compared to GSCs GBM18 and GBM38; as much as 50% of its bioenergetic needs were met by OCR-linked ATP production. GBM18 and, especially, GBM38, relied predominantly on glycolytic metabolism (Warburg effect). In GBM27, OCR and ECAR fluctuated slightly between sets of biological experiments, indicating a range of metabolic flexibility: further investigation into metabolite allocation for energy production would be necessary to fully characterize this adaptive capacity. Our data indicate that even under the same cell culture conditions, distinct molecular characteristics of GSCs can in fact produce unique metabolic phenotypes. Interestingly, the global metabolic activity of U87MG is actually lower than GSCs.

Taken together, our data suggest that a high degree of metabolic variability is present between our GSCs, and their ATP production rates are faster than those of U87MG. GSCs and U87MG maintain a stable, basal, metabolic profile, and seem to be able to shift, to some extent, between aerobic glycolysis and OXPHOS to meet their bioenergetic needs.

3.2. GSCs Display a Heterogeneous Pattern of Resistance to Metabolic Inhibitors

At the outset, in order to determine the optimal doses to be used in future experiments, we exposed our GSCs (GBM18, GBM27, GBM38) and the U87MG cell line to escalating concentrations of selected metabolic drugs. Inhibitory curves for all time points are presented in Supplementary Figure S1.

After conducting these experiments, we ascertained maximum inhibitory effects and reliable trends in the viability data at 72 h; therefore, for every cell line, IC50 at 72 h was considered as the optimal inhibitory concentration.

As we can appreciate in Figure 2, GBM27 had the highest resistance to all metabolic treatments except for DON, where, in turn, GBM18 required the highest concentrations to achieve IC50. For MF, GBM18 and GBM38 were the most sensitive cell lines (10.66 $\pm$ 3.162 mM and 21.33 $\pm$ 7.08 mM, respectively) and GBM27 the most resistant (77.41 $\pm$ 34.02 mM). U87MG revealed an intermediate resistance (42.51 $\pm$ 2.742 mM). For DCA, GBM38 required the lowest concentrations (13.52 $\pm$ 5.235 mM) and GBM27 the highest (40.61 $\pm$ 7.400 mM). In this case, GBM18 (29.20 $\pm$ 5.627 mM) and U87MG (27.10 $\pm$ 0.955 mM) showed no statistically significant differences in IC50 concentrations. For SOD, all cell lines required relatively high in vitro concentrations to reach 50% growth inhibition; no statistical significance was reached between groups. Lastly, regarding glutaminolysis inhibition by DON, U87MG required the lowest IC50 DON dose (99.70 $\pm$ 14.82 μM), followed by GBM27 (198.4 $\pm$ 44.13 μM) and GBM38 (286.9 $\pm$ 103.2 μM), whereas GBM18 was the most resistant (1505 $\pm$ 625.4 μM). It should be noted, however, that a closer look at the growth inhibition curves for DON in GBM18 reveals a cytostatic "threshold" around the IC50 value regardless of the dose, suggesting a non-linear inhibitory slope (Figure S1). Therefore, the IC50 provided is a statistical approximation owed to the resistance against the drug, but we should not always assume a linear correlation between dose and effect; this will become especially relevant in subsequent combinatory studies.

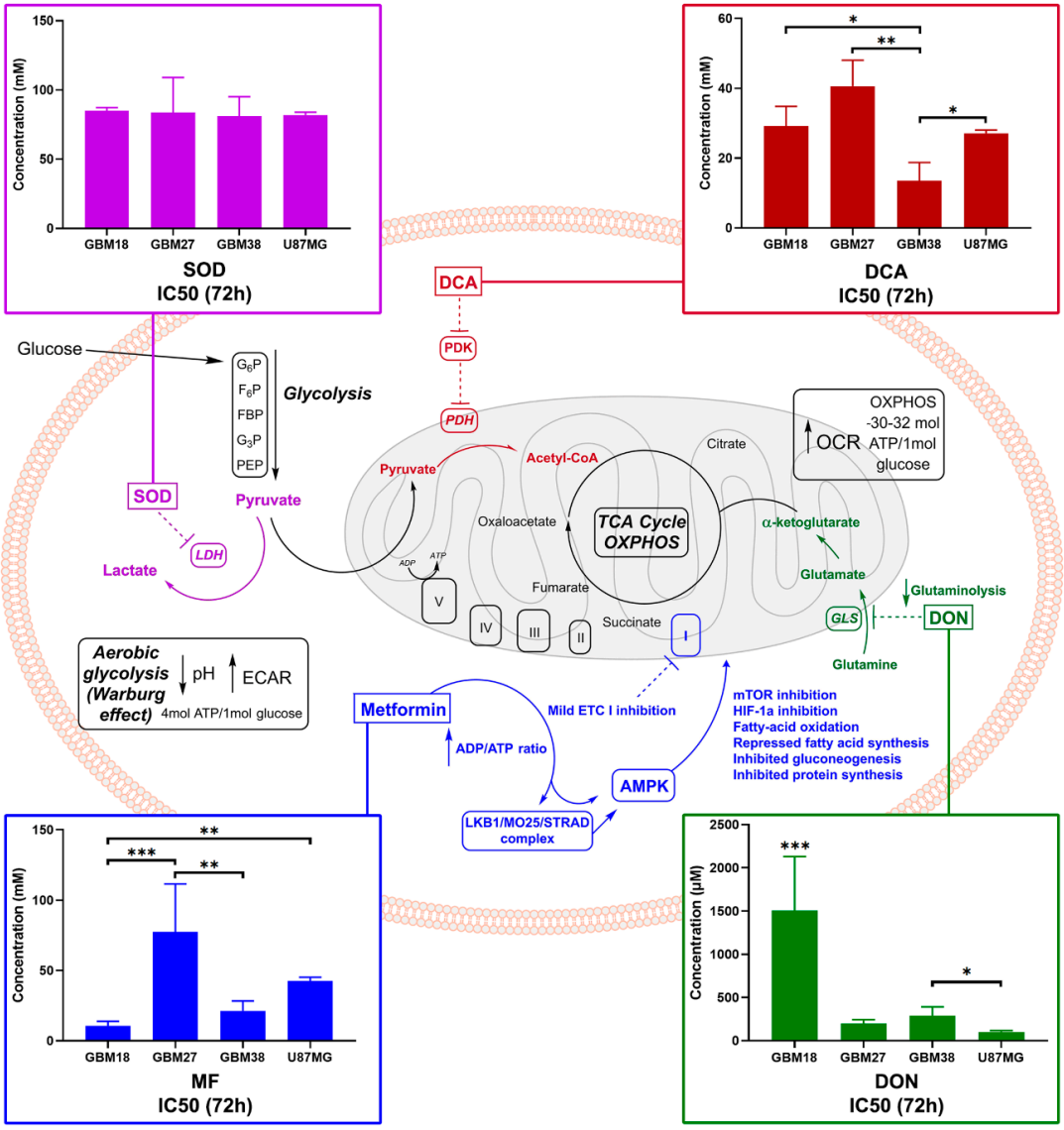

Figure 2. Cancer metabolism at a glance, with experimental in vitro IC50 values for selected metabolic inhibitors. Glucose enters cells and undergoes glycolysis, converted into pyruvate. Cancer cells can divert up to 85% of pyruvate to lactate, regardless of the presence of oxygen (Warburg effect, yielding two net ATP); an estimated 10% of pyruvate goes towards biosynthesis and 5% to OXPHOS [56]. In normal, non-tumoral cells, the majority of pyruvate undergoes OXPHOS (30–32 ATP molecules). To decrease the Warburg effect and facilitate oxidative metabolic reprogramming, PDKs can be inhibited by dichloroacetate (DCA), supporting the entry of pyruvate in the mitochondria, and LDH can be targeted via sodium oxamate (SOD). "Glutamine addiction" can be regulated by glutaminase inhibitors such as 6-diazo-5-oxo-L-norleucine (DON) [57]. Lastly, metformin hydrochloride (MF) has pleiotropic effects: ETC complex I inhibition leads to downstream signaling via AMPK and mTOR [58]. In color-matching boxes, we display concentrations required for 50% viability inhibition (IC50) after 72 h of treatment. One-way ANOVA statistical significance of three biological experiments was calculated with normalized raw fluorometric data; $p < 0.05$ *; $p < 0.01$ **; $p < 0.001$ ***. Abbreviations: ETC (electron transport chain), mTOR (mammalian target of rapamycin), PDK (pyruvate dehydrogenase kinase), PDH (pyruvate dehydrogenase), GLS (glutaminase), LDH (lactate dehydrogenase), GLS (glutaminase), ECAR (extracellular acidification rate), OCR (oxygen consumption rate).

In summary, GBM18 was the most sensitive to MF, GBM38 to DCA and U87MG to DON; on the other hand, GBM27 was the most resistant to MF and DCA, while GBM18 required the highest doses of DON. A very high resistance towards SOD, as well as low

variability in responses, was observed across all cell lines, so this drug was discarded from further assays.

3.3. Differences of Target Enzymes across Cell Lines Predicts Responses to Metabolic Inhibitors

To further investigate the relative sensitivity/resistance profiles of each cell line to our selection of metabolic drugs, we aimed to evaluate their basal genetic expression profiles (Figure 3a).

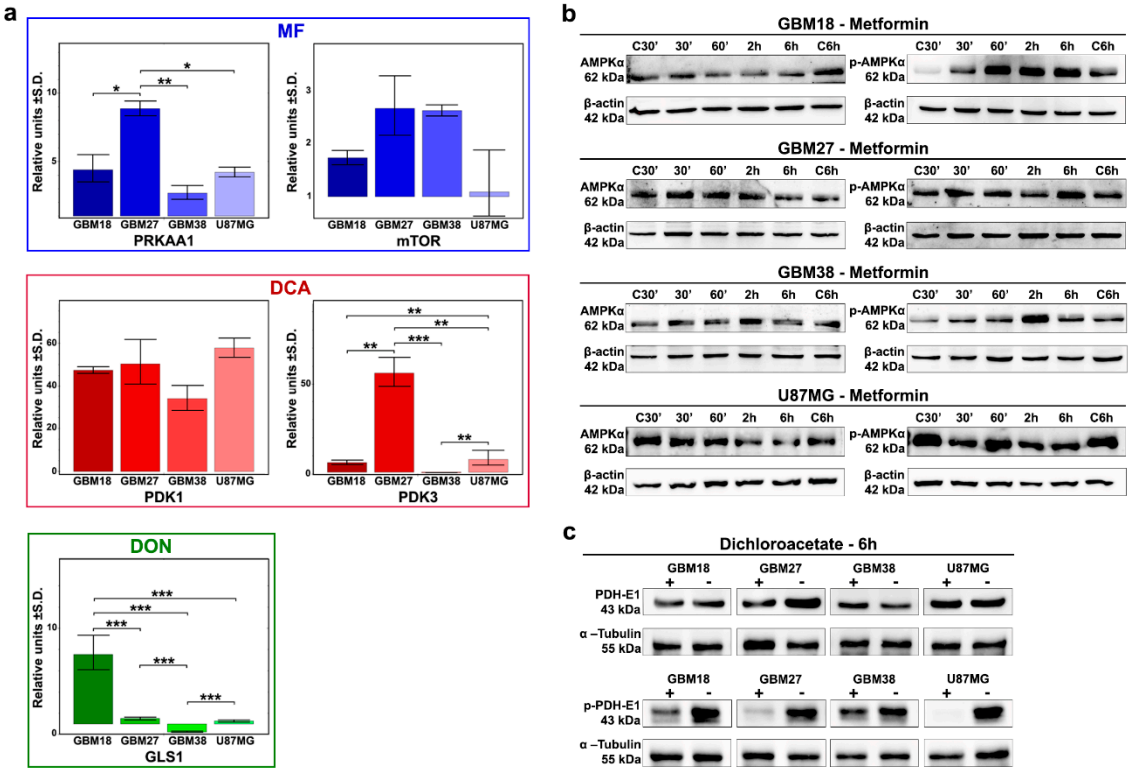

Figure 3. (**a**) Expression profiles of target enzymes for our selection of metabolic drugs under basal conditions determined by RT-qRT-PCR. Representative results from a minimum of two replicates ($n = 2$). One-way ANOVA with Tukey correction. $p < 0.05$ *; $p < 0.01$ **; $p < 0.001$ ***. (**b**) Western Blot analysis at 30 min, 60 min, 2 h, 6 h after MF 72h-IC50 treatment for AMPKα and phospho-Thr172 AMPKα. (**c**) Western Blot analysis after 6 h of treatment with respective DCA 72h-IC50 doses for phospho-Ser293 PDH-E1 and total PDH-E1.

MF acts through inhibition of the electron transport chain (ETC) complex I, increasing the ADP/ATP ratio, but its primary downstream target is the activation of AMPK (phosphorylation of Thr172 of AMPKα1), which ultimately leads to mammalian target of rapamycin (mTOR) inhibition. We therefore evaluated expression of PRKAA1 and PRKAA2 (together, catalytic subunits of AMPK) and the mTOR gene. Although PRKAA2 was not expressed in our samples, PRKAA1 was significantly upregulated in GBM27 (9-fold relative to control) and, at similar levels (approximately 3 to 4-fold), in GBM18, GBM38 and U87MG. We also found the highest relative expression levels of mTOR in GBM27 and GBM38, but differences did not reach statistical significance. Additionally, we analyzed the phosphorylation of AMPKα to investigate the biological effects of MF (Figure 3b). We observed strong phosphorylation of Thr172 AMPKα relative to control in GBM18 (60 min, 2 h, 6 h) and GBM38 (2 h). Cell lines GBM27 and U87MG did not phosphorylate AMPKα in the first 6 h, consistent with their need for higher concentrations of MF and slower responses against the drug.

Next, we studied DCA activity in our GBM cell lines. Altough we analyzed all PDK subunits, PDK2 and PDK4 were not expressed, with major differences detected primarily

in PDK3 expression, exceptionally upregulated in GBM27, consistent with sensitivity profiles to DCA. At the protein level, the catalytic subunit PDH-E1α has three major phosphorylation sites, with site 1 (Ser-293) being the most frequent and efficient target, sufficient to fully inhibit PDH activity [59,60]. With inhibition of PDKs by DCA treatment, we detected rapid, visually discernable, de-phosphorylation of Ser-293 in all cell lines after 6 h of treatment with 72h-IC50 concentrations (Figure 3c and Supplementary Figure S2). The expression of PDKs in our dataset could provide a predictive biomarker to explain differential responses to DCA.

When we evaluated GLS genes, our analysis revealed no detectable amplification of GLS2; therefore, we focused on GLS1 as a potential predictor for DON's antiproliferative effects. Relativized to epilepsy control, GLS1 was significantly upregulated in GBM18, neutral in GBM27/U87MG and downregulated in GBM38. Higher GLS1 expression correlated with the relative resistance against DON in GBM18, but comparatively lower expression in GBM38 was not associated with lower doses.

3.4. Doses of Metabolic Inhibitors and Radiomimetic Bleomycin Corresponding to Warburg-Like Phenotypes Spare Viability of Non-Tumoral hMSCs

After completing this set of experiments, we questioned whether our cell lines would respond favorably to bleomycin, a radiomimetic/DNA-targeting drug.

The mechanism of action and IC50-72h concentrations for bleomycin are presented in Figure 4a. To substantiate our following combinatory studies, we first performed exploratory MTS assays to determine optimal concentrations of bleomycin for each cell line: we observed relative resistance in GBM18 and GBM27, whereas GBM38 and U87MG were equally sensitive to the drug (Supplementary Figure S3).

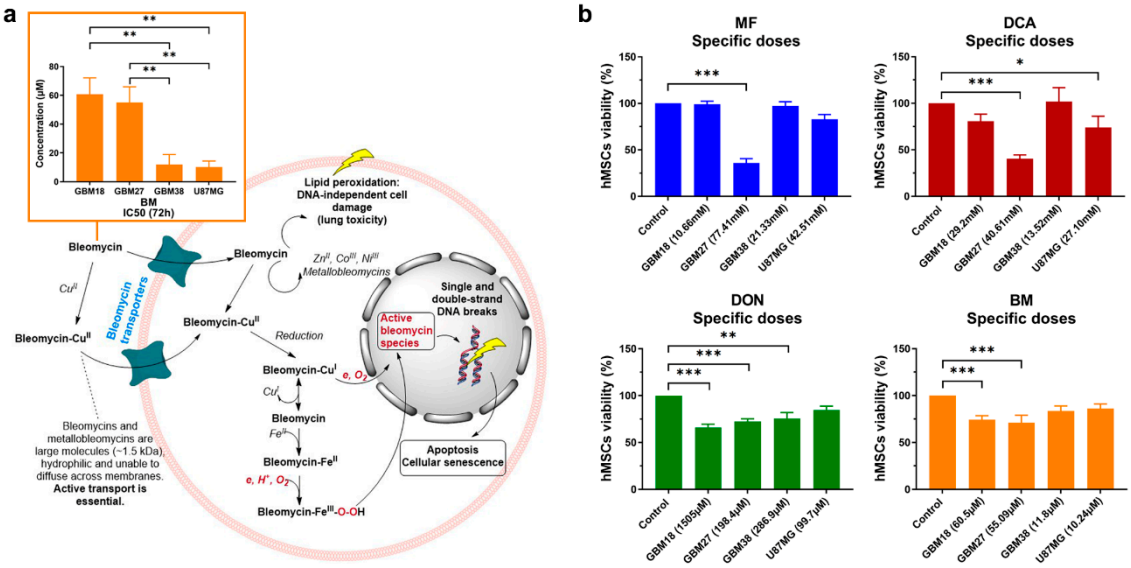

Figure 4. (**a**) IC50 values at 72 h and mechanism of action of radiomimetic drug bleomycin (BM). Bleomycin is a large molecule (~1.5 kDa) and cannot freely diffuse cell membranes; it is transported into cells either alone or as a bleomycin-Cu(II) complex, then reduced to bleomycin-Cu(I), which reacts with oxygen leading to DNA strand breaks. Successful chemotherapy with bleomycin is dependent on active transport; however, there is currently no consensus about the uptake mechanism or the transporters involved. Bleomycin-Cu(I) can also dissociate inside the cell to form bleomycin-Fe(II) complexes, transforming into «activated bleomycin species» resulting in DNA fragmentation and chromosomal aberrations. Complexes with zinc (II), iron (II) and cobalt (III) have also been characterized. Calculated IC50, as per inner salt (MTS) assay, with a minimum of two biological replicates. One-way ANOVA with Tukey correction, $p < 0.05$ *; $p < 0.01$ **; $p < 0.001$ ***. (**b**) Viability profiles relative to control mesenchymal stem cells (hMSCs) treated with all calculated 72h-IC50 doses ($n = 2$). One-way ANOVA with Dunn's correction, $p < 0.05$ *; $p < 0.01$ **; $p < 0.001$ ***.

As with any other form of treatment, the success of metabolic therapies could be limited by toxicity to healthy cells. Therefore, we investigated whether all IC50 concentrations determined thus far could be a realistic goal in vitro, exploring their effects on non-tumoral hMSCs (Figure 4b). MF/DCA affected more than 60% of cells when using GBM27 IC50s (oxidative-like metabolic phenotype), but all other doses were very well tolerated (toxicity less than 20%). DCA 72h-IC50 from GBM38 actually slightly increased "cell viability" relative to control (as per metabolic activity measured by MTS assay). DON inhibited cell growth up to 35% at the highest dose (1505 µM), suggesting a saturation point after which increased dosages do not linearly correlate with antiproliferative effects. Bleomycin, in contrast, only affects up to 30% of hMSCs at the highest IC50, correlating well with slower proliferation rates. In summary, cell lines with predominantly Warburg-like phenotypes could be targeted with metabolic inhibitors without affecting normal stem cells, but oxidative-like phenotypes, such as GBM27, will require individualized, unique approaches.

3.5. Synergy between Bleomycin and Metabolic Inhibitors Helps to Overcome Dose-Limitng Toxicity in Predominantly Oxidative Metabolic Phenotypes

One way to solve the challenge of non-specific damage to healthy cells is to exploit coexisting weaknesses of tumoral cells in combinatory strategies. Since GBM27 doses of MF/DCA were also affecting the viability of normal cells, we explored the possibility of dose-reduction attributable to synergistic effects with radiomimetic bleomycin. After individually confirming the validity of each calculated 72h-IC50, we performed combinatory studies to determine the existence of synergy, additive or antagonistic effects. Using the Chou-Talalay theorem, the Combination Index (CI) and the Dose Reduction Index (DRI) were calculated for each drug combination.

As shown in Table 2, drug mixtures with CI < 1 and DRI > 1 at a fraction of affected cells (Fa) = 0.6 were considered as the optimal cutoff to identify promising therapeutic combinations. Nevertheless, in constant ratio combinatory experiments, close attention needs to be paid to the full range of Fa and CI/DRI to evaluate synergy for any given combination/antiproliferative effect.

Table 2. Summary of synergy/antagonism at an optimal Fa cutoff of = 0.6. All combinatory experiments were performed in two biological replicates (n = 2).

	MF + Bleomycin		DCA + Bleomycin		DON + Bleomycin	
Cell Line	**Effect at Fa = 0.6**	**DRI at Fa = 0.6**	**Effect at Fa = 0.6**	**DRI at Fa = 0.6**	**Effect at Fa = 0.6**	**DRI at Fa = 0.6**
GBM18	Additive	DRI > 1 for both	Antagonism	DRI > 1 for both	Synergism	DRI > 1 for both
GBM27	Synergism	DRI > 1 for both	Synergism	DRI > 1 for both	Synergism	DRI > 1 for both
GBM38	Synergism	DRI > 1 for both	Antagonism	DRI > 1 for bleomycin	Synergism	DRI > 1 for both
U87MG	Synergism	DRI > 1 for both	Antagonism	DRI > 1 for both	Synergism	DRI > 1 for both

All final reports with complete datasets, including Median-Effect Plot, CI Plot, Logarithmic CI Plot, DRI, Isobologram and Sequential Deletion Analysis (SDA; confidence intervals for CI values), are included in Supplementary Material File S1.

Our results describe a wide variety of combinatory effects depending on the cell subtype and Fa level. Figure 5a describes the combined effects of MF and bleomycin. GBM18 exhibits mostly additive effects (no synergy). GBM27, on the other hand, is a prototypical example of synergistic effects when affecting most tumoral cells (at high Fa values): in the CI index, Fa $\geq$ 0.75 has a CI < 0.4, indicative of strong synergism. Consequently, DRI is > 1 for both MF and bleomycin, with significant dose reductions at Fa $\geq$ 0.6, potentially reducing the toxicity of both agents. GBM38 is synergistic at Fa $\approx$ 0.5 but has a tendency towards antagonism at Fa > 0.75. GBM38 appears to have a threshold for both MF and bleomycin, where even small doses produce significant anti-proliferative

effects, but further increases provide no additional benefit. Finally, the CI in U87MG is close to synergistic/additive up to Fa = 0.75, then turning antagonistic.

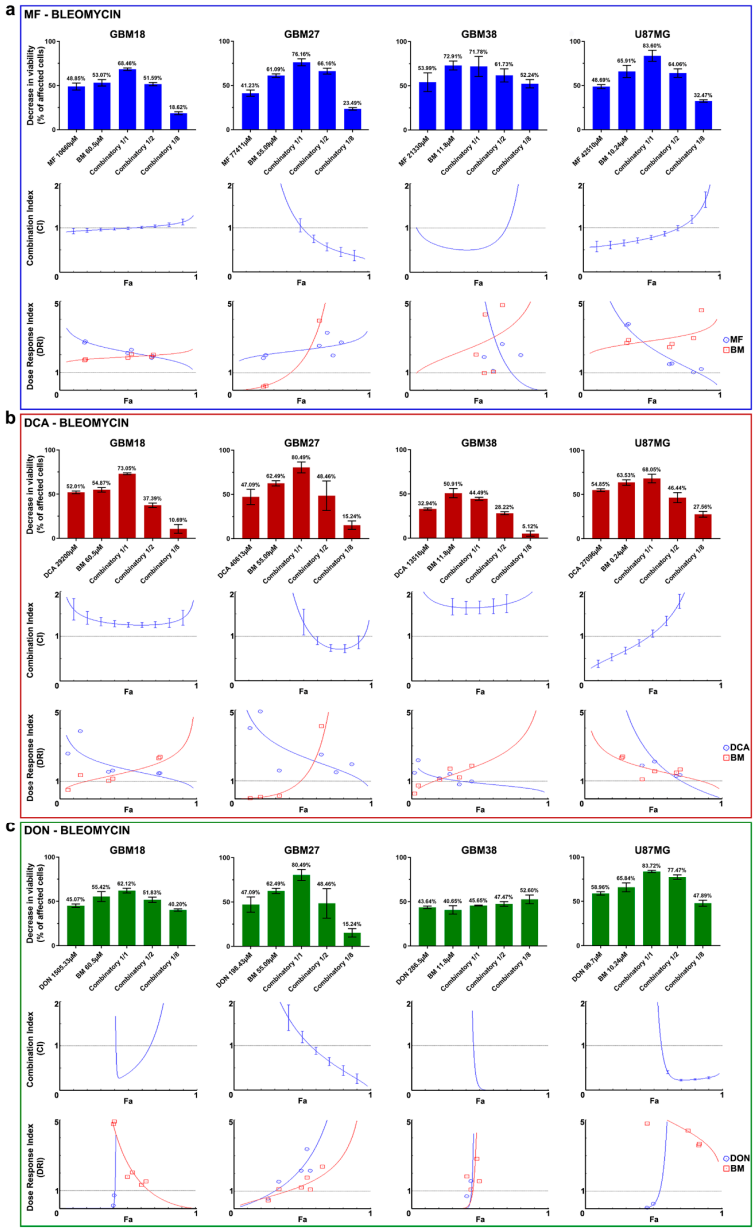

Figure 5. (**a**–**c**) Combinatory drug studies between metabolic drugs (MF, DCA, DON) and bleomycin (BM). From top to bottom, three graphs for each cell line comprehensively describe synergy/antagonism. First graph: Bar charts of decrease in viability (% of affected cells) relative to control. Second graph: Combination index (CI) is given as a function of the fraction of affected cells (Fa) by the drug combination with a continuous line. The central dashed line indicates a CI = 1. According to the Chou-Talalay's Combination Index Theorem, CI = 0.9 to 1.1 indicates an additive effect. CI < 1 is indicative of synergism, whereas CI > 1 indicates antagonism. The vertical bars indicate 95% confidence intervals for CI values based on Sequential Deletion Analysis (SDA); in some cases, SDA values cannot be graphed in CompuSyn software, but they were always calculated and are available in Supplementary File S1. Third graph: The Dose-Reduction Index (DRI) (also known as the Chou-Martin plot) signifies how many folds of dose-reduction for each drug at any given effect (Fa) are allowed in synergistic combination. In blue, metabolic drug DRI index; in red, bleomycin DRI index. DRI = 1 indicates no dose-reduction, DRI > 1 favorable dose-reduction and DRI < 1 no favorable dose-reduction. All experiments were performed in two biological replicates (n = 2).

Next, Figure 5b describes the combinatory effects of DCA and bleomycin. For GBM18, the CI is > 1 (antagonistic) at any given Fa; despite this, DRI > 1 for bleomycin at high Fa levels indicates the possibility of dose-reduction. In GBM27, therapeutic effects are determined by Fa cutoff: close to Fa ≈ 0.75, CI is <1 (synergistic), with dose reduction predicted at this value. GBM38, on the other hand, represents a clear example of strong antagonism (CI values > 1.5 at any Fa level); consequently, the combination of drugs does not surpass the effects of bleomycin by itself. Even still, DRI suggests that bleomycin concentrations could be decreased at the expense of DCA. Lastly, up to Fa = 0.5, U87MG displays synergistic/additive effects, with antagonism prevailing thereafter; this translates to unfavorable dosing at Fa > 0.8 (DRI < 1 for both drugs).

To conclude, Figure 5c details the interaction between DON and bleomycin. For GBM18, combining the compounds presents a strong synergistic relationship at Fa close to 0.5; however, at higher Fa, this synergy is lost. Ascending DRI for DON indicates the potential of important dose-reduction. GBM27 benefits from additive effects close to Fa ≈ 0.5, and, as we move closer to Fa = 1, the combination becomes strongly synergistic; this too would allow for dose reduction. In GBM38, the combined treatment has a similar threshold as in U87MG, as even one eighth of the concentrations significantly decreases proliferation: in these two cell lines, CI is <1 and DRI > 1 at Fa levels > 0.5, making DON and bleomycin a very promising therapeutic combination.

In summary, for GBM27, synergism with radiomimetic bleomycin was observed for all metabolic inhibitors at therapeutically relevant Fa = 0.9. Combining metabolic inhibitors and bleomycin could be leveraged to reduce dosing requirements of oxidative-like GSC subtypes.

3.6. Bioenergetic Profiling after Metabolic Treatment Reveals Opportunities for Metabolic Priming in Surviving Cell Populations

Using Seahorse XF technology, we determined total ATP production and ratios of mitoATP/glycoATP production under metabolically treated conditions.

As shown in Figure 6a,b, normalized total ATP production was decreased in all treated cells, with the exception of DCA-treated GBM27; in this case, rather than a significant drop in total ATP, production shifted from glycolytic to oxidative metabolism, with total ATP rates remaining unaltered. Furthermore, consistent with the proposed biological function for each drug, we observed a reduction in mitoATP production and a shift toward glycolysis using MF. Even though IC50 values should affect all cell lines proportionately, we noticed that the reduction in total ATP production was less pronounced with lower doses; e.g., in GBM18 (lowest MF IC50 of 10.66 mM), mitochondrial ATP was almost completely abolished, but total glycolytic ATP dropped only marginally, indicating a surviving population of almost exclusively glycolytic cells. Mitochondrial ATP production was increased after treatment with DCA, especially in GBM27, a GSC with a clear preference towards oxidative metabolism under both basal and treated conditions. The XF Rate Index for DCA can provide an idea of the oxidative potential of each cell line: highest in GBM27, followed by GBM18 and lowest in GBM38/U87MG. In the case of DON, we can appreciate a notable reduction of total ATP for each calculated IC50 value. As previously stated, DON is a glutamine analog predominantly targeting GLS (inhibition of TCA cycle intermediaries from glutamine would be expected to reduce mitoATP, unless glutamine derived α-ketoglutarate was diverted towards biosynthesis or mitochondrial substrate-level phosphorylation rather than oxidized). Examining the XF ATP Rate Index, GBM18 and especially GBM27 shifted towards oxidative metabolism, whereas GBM38 and U87MG remained unaltered. In conclusion, DON did not consistently change the metabolic phenotype of surviving cells; interestingly, however, in U87MG, a characteristically glutaminolytic cell line, even small concentrations of DON (99.7 μM) were enough to drastically reduce total ATP production.

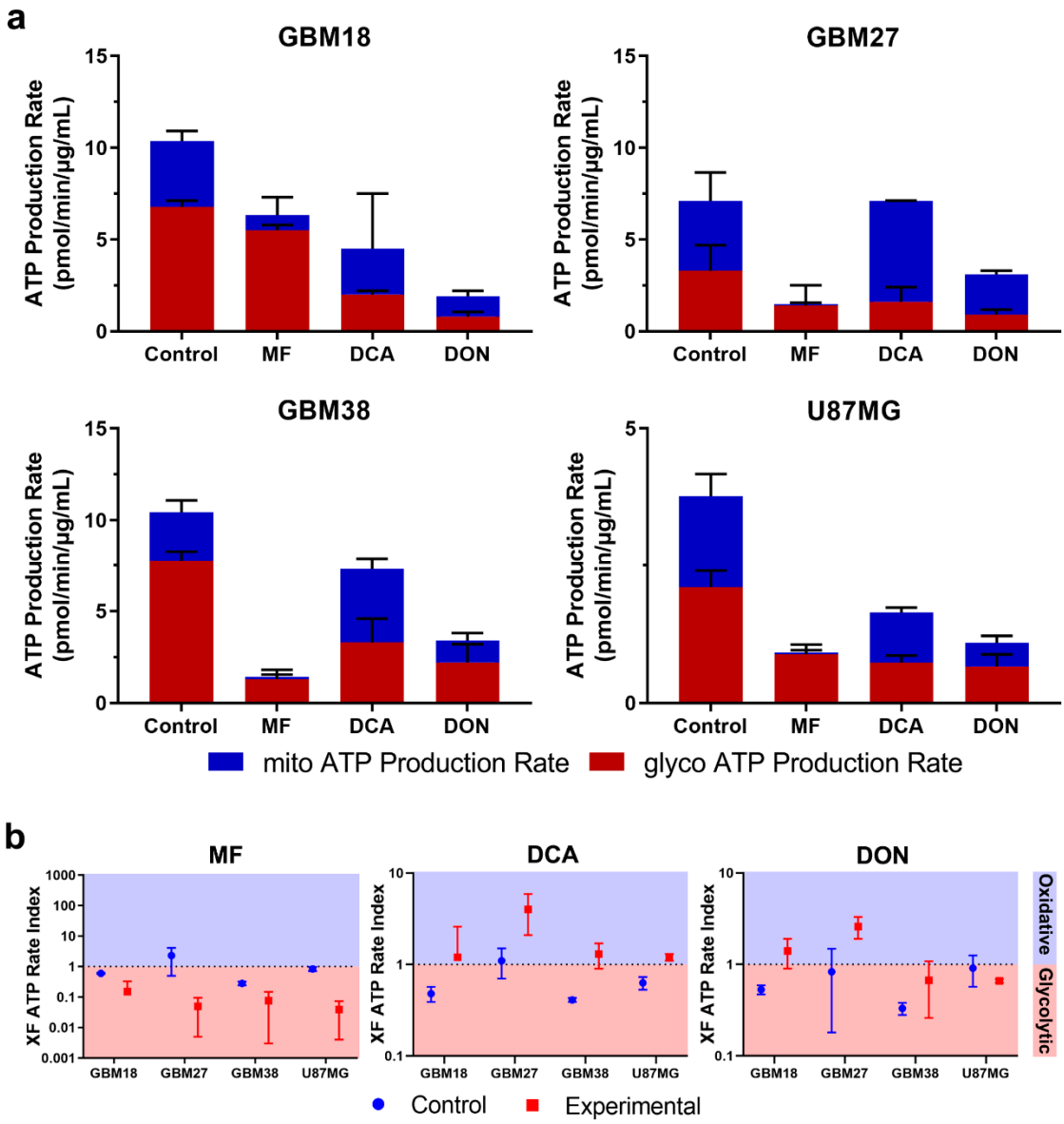

Figure 6. (**a**) Changes in metabolic phenotypes after IC50 treatment for 72 h with metformin (MF), dichloroacetate (DCA) and 6-Diazo-5-oxo-L-norleucine (DON). (**b**) XF ATP Rate Index for GSCs and U87MG. The ATP Rate Index is the ratio of the mitoATP Production Rate divided by glycoATP Production Rate, indicating higher oxidative or glycolytic bioenergetic profile.

Normalized values of OCR/Proton Efflux Rate (PER) in real-time after each drug injection of the Seahorse XF protocol are provided in Supplementary Figure S4. These kinetic graphs allow us to examine how previous metabolic treatments changed the basal metabolic state and acute responses to mitochondrial inhibitors included in the assay: oligomycin (complex V inhibitor, i.e., mitochondrial ATP synthesis) and rotenone/antimycin A (total inhibition of mitochondrial respiration, complex I and complex III, respectively). Glycolytic upregulation in response to partial and complete mitochondrial inhibition (Warburg phenotype) and residual non-mitochondrial OCR should be highlighted in GBM18 and GBM38.

In conclusion, pre-treatment with metabolic drugs could become a valuable tool to characterize the bioenergetic phenotypes of surviving, resistant fraction of cells, priming them for further treatments. To our knowledge, this is the first time chronic metabolic treatments (>72 h) with DCA and DON have been characterized in GSCs. Despite methodological differences, our results also confirm the bioenergetic changes after low-dose MF in

GSCs [61] and DCA in established glioma cell lines [62,63]. Finally, oxidative GSCs such as GBM27, an abnormality in the predominantly glycolytic phenotypes of solid tumors, need to be fully recognized in order to improve metabolic therapies. Based on our results, sequential drug strategies targeting previously weakened ATP-generating pathways warrant further exploration.

4. Discussion

Cancer metabolism has recently regained interest as a promising therapeutic target, coinciding with the development of standardized techniques for real-time assessment of bioenergetics. Given high intratumoral molecular and metabolic heterogeneity, it is necessary to target glycolytic, glutaminolytic and oxidative phenotypes; for this purpose, primary GSCs cultured from human surgical samples are an excellent model [64].

In this paper, we describe how metabolic modulators (MF, DCA, DON) could be leveraged to inhibit GSCs proliferation, demonstrating that distinct, stable, metabolic phenotypes contrast in their response to these treatments. A comparison between untreated and metabolically treated GSCs populations is presented here for the first time, leading us to hypothesize that inhibiting metabolic pathways might not only kill malignant cells, but also turn them vulnerable to successive targeted treatments ("metabolic priming").

Consistent with our results, GSCs have been characterized by ample metabolic heterogeneity, exhibiting both glycolytic/oxidative characteristics [29,65,66]. Surprisingly, GBM27 exhibited a highly oxidative phenotype, at odds with Warburg's central hypothesis of dysfunctional mitochondria; the presence of such metabolic subpopulations will need to be addressed to prevent tumor recurrence after antiglycolytic therapy. Similarly, U87MG had been described numerous times as highly glycolytic (high basal ECAR); however, we and others also described simultaneous elevations in OCR [30,67–70].

Regarding our selection of metabolic inhibitors, GBM27 was the most resistant to all drugs, with the exception of DON. One of the reasons for this might be owed to GBM27's characteristically oxidative metabolism (up to 50% oxidative) and slower proliferation rates. Metabolic flexibility may grant a survival advantage even if mitochondrial energy production is targeted via MF or glycolysis via DCA. GBM18 and GBM38, on the other hand, were significantly more sensitive to MF; this would be consistent with their Warburg-like metabolic phenotypes. At the protein level, our results are consistent with previous research, where 10 mM MF did not significantly increase phospho-Thr172 at 6 h in U87MG [71]. Next, we hypothesized whether upregulated or downregulated PDK expression could be useful in predicting responses to DCA. While PDK1 was upregulated with respect to non-tumoral controls, expression was similar across all cell lines. PDK3 expression was relatively downregulated in GBM38 and exceptionally upregulated in GBM27. This would be consistent with previous reports where the PDK3 subunit was the most resistant to inhibition by DCA (higher expression of PDK3 would therefore translate into higher doses of DCA) [72,73]. In contrast, PDK2 subunits are the most sensitive to DCA treatment, while PDK1 and PDK4 display intermediate sensitivity (*Ki* PDK2 < PDK1 $\simeq$ PDK4 < PDK3). As PDK1 was equally distributed, and PDK2/PDK4 were undetectable in our samples, variances in dose-response profiles were likely related to differences in PDK3. SOD treatment was equally inefficacious in all tested cell lines, but we suspect this was partly related to poor cell membrane permeability of this compound [74–76]. Despite issues with potency, our GSCs appear as highly resistant to SOD, as evidenced by much lower reported IC50s in nasopharyngeal carcinoma and gastric cell lines [77,78]. Concerning DON, glutamine addiction is thought to play an important role in supporting cancer proliferation [79,80]. In our case, GBM18 was the most resistant to DON, while other GSCs and U87MG turned more vulnerable to glutaminase inhibition. Our results confirm the inhibition profile for U87MG/DON at 72 h recounted by Ohba et al., with a similarly flattened inhibitory curve but higher "theoretical" IC50 [81]. With DON, rather than linear, dose-dependent cytotoxicity, we noted a more cytostatic-like effect in GBM18, GBM38 and, to a lesser extent, GBM27. Higher relative mRNA expression of GLS1 was evidenced in

GBM18, accompanied with, indeed, higher doses of DON for the same inhibitory effect; correlations between doses and GLS1 expression was not as clear in other cell lines.

The heterogeneity of cancer could also be managed by combinatorial strategies, focusing on multiple molecular pathways to achieve compounded effects. Even though stand-alone metabolic modulation could become a possibility in the future, a more realistic and approachable goal is to design safe and effective combinations together with well-established chemotherapeutics and radiotherapy. Here, we show that non-tumoral hMSCs are not affected by low/intermediate doses of MF, DCA, DON or bleomycin. Concentrations of MF and DCA corresponding to GBM27, however, decreased viability by more than half in hMSCs, revealing that oxidative cancer cells would require a different management strategy: combinatory therapies could be such an option.

To the extent of our knowledge, ours is the first report of the combinatorial effects in GSCs of the radiomimetic drug bleomycin together with MF, DCA and DON. Bleomycin acts by inducing single and double strand DNA breaks, causing apoptosis and cell cycle arrest in early G2 phase [44]; it is FDA-approved as a clinical prescription against lymphomas, squamous-cell carcinomas and germ-cell tumours, as well as brain cancer [45,82]. IC50 profiles for bleomycin revealed significant disparities among cell lines, with GBM38 and U87MG being more sensitive than GBM18 and GBM27. Direct comparisons with radiotherapy are scarce, however, as we only encounter combined evaluation in traditional glioblastoma cell lines (not GSCs) for MF [61] and DCA [69]. Discussing our results, we want to bring attention to the fact that GBM27, identified as distinctly "oxidative", was potentially the most benefited by pairing bleomycin and metabolic modulators. Synergistic opportunities in GBM27 would allow for significant dose reduction, as individual IC50 concentrations for MF and DCA are higher than in all other cell lines, thus reducing toxicity in normal cells. One of the strengths of our combinatory approach is the experimental design in a constant drug ratio: this allows for a data-driven, more accurate and comprehensive description of synergy/antagonism using the Chou-Talalay method [83], without relying solely on computer simulations.

As far as we know, sustained metabolic changes in GSCs after extended treatment with DCA and DON had not been properly illustrated until now. In terms of OCR/ECAR, all metabolic modulators exerted biologically coherent responses, especially well-defined for MF and DCA. In the case of MF, as would be expected, surviving cells shifted to a primarily glycolytic behavior, with a very low percentage of mitoATP generation; these results are consistent with Seahorse XF assays in established glioma cell lines and colon cancer CSCs [61]. The metabolic effects of MF were mainly determined by dose-response profiles. Similarly, DCA induced bioenergetic changes consistent with the forced activation of the PDH complex, in congruence with previous reports [69,84]. Interestingly, when comparing total ATP production rates, DCA only reached a maximal attenuation of approximately 50% relative to control. Indeed, DCA is believed to act more as a "metabolic modulator", not simply reducing cell proliferation, but also "shifting" the glycolytic/OXPHOS ratio via increased mitochondrial uptake of pyruvate [85,86]. Lastly, evaluating the effects of DON, we detected consistent ATP inhibition but heterogeneous metabolic adaptations. In previous reports, no response was observed to low concentrations of DON in U87MG [87]. Preclinical data shows that relatively high in vitro doses of DON are required in some cell lines, which might explain the high variability in antiproliferative effects [88–91]. After chronic treatment with DON, we observed either an unchanged (GBM38, U87MG) or increased (GBM18, GBM27) ATP Rate Index. The third alternative, a decrease in ATP Rate Index (enhanced Warburg effect), was not detected; in contrast, this shift was noted with MF in all cell lines. Therefore, after GLS inhibition, we can hypothesize that increased mitoATP cannot be originated from glutamine oxidation: this was apparent in GBM27, where inhibition of glutaminolysis led to preferential oxidation of glucose (indicative of metabolic flexibility). GBM18 displayed a similar trend, albeit less pronounced, whereas GBM38 and U87MG saw their total ATP production diminished without compensatory shifts in mito/glycoATP.

From a translational medicine perspective, avoiding the risk of toxicity associated with high concentrations of MF might be feasible, as even very low doses of this drug revealed antiproliferative effects and radiotherapy enhancement [92,93]. Furthermore, combinatory strategies would allow for meaningful dose reductions, as shown with improved efficacy in radioresistant stem cells [94]. Moreover, DCA could be applied synergistically to prevent MF-induced lactic acidosis [95–97]. Our results agree with previously published data, showing that concentrations of DCA in the range of $\geq$ 10 mM are required for consistent anti-proliferative responses [98–101]. Finally, the prospective of DON for GBM therapy is hindered by a polar structure and reactive moiety that significantly reduces its ability to cross the blood-brain barrier (BBB) [102,103]. Nevertheless, most GBM patients present with a disrupted BBB [104], and, where this might not be applicable, prodrugs and novel glutaminase inhibitors are in active development [31,105].

We believe the origin of cancer is complex, with involvement of both oncogenic signaling and metabolic reprogramming [106,107]. Future directions in this field might entail a more precise molecular classification of tumor biopsies, expanding the comparison between gene expression subtypes and their metabolic milieu, and imaging of patients for improved, tailor-made therapeutics. Stratification and metabolic analysis will be crucial to discover malignancies that could benefit from adjuvant anti-glycolytic therapy [108,109], specific pathway inhibition (e.g., mitochondrial, glutamine and FAO inhibitors [110–112]) and tumors where, due to molecular rewiring, glycolysis inhibition with compensatory fuels might even be contraindicated [25,113,114].

5. Conclusions

In summary, we show that molecularly distinct GSCs show a high degree of heterogeneity, both in basal metabolic phenotypes and in response to metabolic inhibitors. Subpopulations of GSCs presented both highly glycolytic and highly oxidative characteristics. Stratification of patients according to coexisting metabolic phenotypes could be advanced into clinical tools for improved metabolic therapies. In highly oxidative GSCs (e.g., GBM27), there is potential for synergistic effects with radiomimetic bleomycin. Inhibition of glutaminolysis (via DON) is also an attractive therapeutic target, as synergy was described regardless of basal metabolism. Application of metabolic drugs produces stable changes in the bioenergetic states of GSCs, which could be leveraged as a form of metabolic priming.

Supplementary Materials: The following are available online at https://www.mdpi.com/2073-4409/10/2/202/s1. Figure S1: Inhibitory curves for MF, DCA, SOD and DON at 24 h, 48 h, 72 h. Figure S2: Western Blot time-course analysis of phospho-Ser293 PDH-E1 in GBM38. Figure S3: Inhibitory curves for bleomycin at 72 h. Figure S4: Seahorse XF real-time kinetic graphs. File S1: Comprehensive analysis of Chou–Talalay combinatory experiments, as exported from CompuSyn software.

Author Contributions: Conceptualization, T.D., N.G.-R. and A.A-S.; methodology, T.D., J.C.-N., N.G.-R. and A.A.-S.; investigation, T.D. and N.G.-R.; formal analysis, R.M.; resources, A.O.d.M. and L.G.-C. (MRI imaging assistance); data curation, T.D.; writing—original draft preparation, T.D.; writing—review and editing, T.D., J.C.-N., R.P.-A., N.G.-R. and A.A.-S.; project administration, N.G.-R. and A.A.-S.; funding acquisition, A.A.-S. All authors have read and agreed to the published version of the manuscript.

Funding: This research was funded by grants from the "Fondo de Investigaciones Sanitarias" (FIS) (PI17-01489), the Miguel Servet Program (CP11/00147) del Instituto de Salud Carlos III (AAS), the Ministerio de Economía y Competitividad-FEDERER (RTC-2016-4990-1). Research funded by Ministerio de Educación, Cultura y Deporte (FPU16/03198).

Institutional Review Board Statement: The study was conducted according to the guidelines of the Declaration of Helsinki, and approved by the Ethics Committee 14.06.632-GHM.

Informed Consent Statement: Informed consent was obtained from all subjects involved in the study.

Data Availability Statement: The data presented in this study is available in the Supplementary Materials of this article. The results shown in the GSVA analysis are in part based upon data generated by the TCGA Research Network: https://www.cancer.gov/tcga.

Acknowledgments: We thank Irina Palacín-Aliana, Gorjana Rackov and Susana Esteban-Rubio for methodological support and technical help.

Conflicts of Interest: The authors declare no conflict of interest.

References

1. Ostrom, Q.T.; Gittleman, H.; Farah, P.; Ondracek, A.; Chen, Y.; Wolinsky, Y.; Stroup, N.E.; Kruchko, C.; Barnholtz-Sloan, J.S. CBTRUS Statistical Report: Primary Brain and Central Nervous System Tumors Diagnosed in the United States in 2006–2010. *Neuro-Oncology* **2013**, *15*, ii1–ii56. [CrossRef] [PubMed]
2. Koshy, M.; Villano, J.L.; Dolecek, T.A.; Howard, A.; Mahmood, U.; Chmura, S.J.; Weichselbaum, R.R.; McCarthy, B.J. Improved survival time trends for glioblastoma using the SEER 17 population-based registries. *J. Neuro-Oncol.* **2012**, *107*, 207–212. [CrossRef] [PubMed]
3. Tamimi, A.F.; Juweid, M. Epidemiology and Outcome of Glioblastoma. In *Glioblastoma [Internet]*; 201921345W; Codon Publications: Singapore, 2017.
4. Louis, D.N.; Perry, A.; Reifenberger, G.; Von Deimling, A.; Figarella-Branger, D.; Cavenee, W.K.; Ohgaki, H.; Wiestler, O.D.; Kleihues, P.; Ellison, D.W. The 2016 World Health Organization Classification of Tumors of the Central Nervous System: A summary. *Acta Neuropathol.* **2016**, *131*, 803–820. [CrossRef] [PubMed]
5. Verhaak, R.G.; Hoadley, K.A.; Purdom, E.; Wang, V.; Qi, Y.; Wilkerson, M.D.; Miller, C.R.; Ding, L.; Golub, T.; Mesirov, J.P.; et al. Integrated Genomic Analysis Identifies Clinically Relevant Subtypes of Glioblastoma Characterized by Abnormalities in PDGFRA, IDH1, EGFR, and NF1. *Cancer Cell* **2010**, *17*, 98–110. [CrossRef] [PubMed]
6. Teo, W.-Y.; Sekar, K.; Seshachalam, P.; Shen, J.; Chow, W.-Y.; Lau, C.C.; Yang, H.; Park, J.; Kang, S.-G.; Li, X.; et al. Relevance of a TCGA-derived Glioblastoma Subtype Gene-Classifier among Patient Populations. *Sci. Rep.* **2019**, *9*, 7442. [CrossRef] [PubMed]
7. Stupp, R.; Taillibert, S.; Kanner, A.; Read, W.; Steinberg, D.M.; Lhermitte, B.; Toms, S.; Idbaih, A.; Ahluwalia, M.S.; Fink, K.J.J. Effect of tumor-treating fields plus maintenance temozolomide vs maintenance temozolomide alone on survival in patients with glioblastoma: A randomized clinical trial. *JAMA* **2017**, *318*, 2306–2316. [CrossRef]
8. Ostrom, Q.T.; Bauchet, L.; Davis, F.G.; Deltour, I.; Fisher, J.L.; Langer, C.E.; Pekmezci, M.; Schwartzbaum, J.A.; Turner, M.C.; Walsh, K.M.; et al. The epidemiology of glioma in adults: A "state of the science" review. *Neuro-Oncology* **2014**, *16*, 896–913. [CrossRef]
9. Johnson, D.R.; O'Neill, B.P. Glioblastoma survival in the United States before and during the temozolomide era. *J. Neuro-Oncol.* **2012**, *107*, 359–364. [CrossRef]
10. Han, X.; Xue, X.; Zhou, H.; Zhang, G. A molecular view of the radioresistance of gliomas. *Oncotarget* **2017**, *8*, 100931–100941. [CrossRef]
11. Seyfried, T.N.; Shelton, L.M. Cancer as a metabolic disease. *Nutr. Metab.* **2010**, *7*, 7. [CrossRef]
12. Jose, C.; Bellance, N.; Rossignol, R. Choosing between glycolysis and oxidative phosphorylation: A tumor's dilemma? *Biochim. Biophys. Acta* **2011**, *1807*, 552–561. [CrossRef] [PubMed]
13. Hanahan, D.; Weinberg, R.A. Hallmarks of cancer: The next generation. *Cell* **2011**, *144*, 646–674. [CrossRef] [PubMed]
14. Potter, M.; Newport, E.; Morten, K.J. The Warburg effect: 80 years on. *Biochem. Soc. Trans.* **2016**, *44*, 1499–1505. [CrossRef] [PubMed]
15. Hsu, P.P.; Sabatini, D.M. Cancer Cell Metabolism: Warburg and Beyond. *Cell* **2008**, *134*, 703–707. [CrossRef] [PubMed]
16. Seyfried, T.N.; Flores, R.E.; Poff, A.M.; D'Agostino, D.P. Cancer as a metabolic disease: Implications for novel therapeutics. *Carcinogenesis* **2014**, *35*, 515–527. [CrossRef]
17. Ristow, M. Oxidative metabolism in cancer growth. *Curr. Opin. Clin. Nutr. Metab. Care* **2006**, *9*, 339–345. [CrossRef]
18. Semenza, G.L.; Artemov, D.; Bedi, A.; Bhujwalla, Z.; Chiles, K.; Feldser, D.; Laughner, E.; Ravi, R.; Simons, J.; Taghavi, P.; et al. 'The Metabolism of Tumours': 70 Years Later. In Proceedings of the Novartis Foundation Symposium, Singapore, 30 August–1 September 2004; pp. 251–259.
19. Timm, K.N.; Kennedy, B.W.; Brindle, K.M. Imaging Tumor Metabolism to Assess Disease Progression and Treatment Response. *Clin. Cancer Res.* **2016**, *22*, 5196–5203. [CrossRef]
20. Kim, M.M.; Parolia, A.; Dunphy, M.P.; Venneti, S. Non-invasive metabolic imaging of brain tumours in the era of precision medicine. *Nat. Rev. Clin. Oncol.* **2016**, *13*, 725–739. [CrossRef]
21. Paech, D.; Nagel, A.M.; Schultheiss, M.N.; Umathum, R.; Regnery, S.; Scherer, M.; Wick, A.; Platt, T.; Wick, W.; Bendszus, M.; et al. Quantitative Dynamic Oxygen 17 MRI at 7.0 T for the Cerebral Oxygen Metabolism in Glioma. *Radiology* **2020**, *295*, 181–189. [CrossRef]
22. Grasso, D.; Zampieri, L.X.; Capelôa, T.; van de Velde, J.A.; Sonveaux, P. Mitochondria in Cancer. *Cell Stress* **2020**, *4*, 114–146. [CrossRef]
23. Xu, X.D.; Shao, S.X.; Jiang, H.P.; Cao, Y.W.; Wang, Y.H.; Yang, X.C.; Wang, Y.L.; Wang, X.S.; Niu, H.T. Warburg Effect or Reverse Warburg Effect? A Review of Cancer Metabolism. *Oncol. Res. Treat.* **2015**, *38*, 117–122. [CrossRef]

24. Vidali, S.; Aminzadeh, S.; Lambert, B.; Rutherford, T.; Sperl, W.; Kofler, B.; Feichtinger, R.G. Mitochondria: The ketogenic diet—A metabolism-based therapy. *Int. J. Biochem. Cell Biol.* **2015**, *63*, 55–59. [CrossRef] [PubMed]
25. Lin, H.; Patel, S.; Affleck, V.S.; Wilson, I.; Turnbull, D.M.; Joshi, A.R.; Maxwell, R.; Stoll, E.A. Fatty acid oxidation is required for the respiration and proliferation of malignant glioma cells. *Neuro-Oncology* **2017**, *19*, 43–54. [CrossRef] [PubMed]
26. Chinopoulos, C.; Seyfried, T.N. Mitochondrial substrate-level phosphorylation as energy source for glioblastoma: Review and hypothesis. *ASN Neuro* **2018**, *10*, 1759091418818261. [CrossRef]
27. Hinohara, K.; Polyak, K. Intratumoral heterogeneity: More than just mutations. *Trends Cell Biol.* **2019**, *29*, 569–579. [CrossRef]
28. Saga, I.; Shibao, S.; Okubo, J.; Osuka, S.; Kobayashi, Y.; Yamada, S.; Fujita, S.; Urakami, K.; Kusuhara, M.; Yoshida, K.; et al. Integrated analysis identifies different metabolic signatures for tumor-initiating cells in a murine glioblastoma model. *Neuro-Oncology* **2014**, *16*, 1048–1056. [CrossRef]
29. Shibao, S.; Minami, N.; Koike, N.; Fukui, N.; Yoshida, K.; Saya, H.; Sampetrean, O. Metabolic heterogeneity and plasticity of glioma stem cells in a mouse glioblastoma model. *Neuro-Oncology* **2018**, *20*, 343–354. [CrossRef]
30. Vlashi, E.; Lagadec, C.; Vergnes, L.; Matsutani, T.; Masui, K.; Poulou, M.; Popescu, R.; Della Donna, L.; Evers, P.; Dekmezian, C.; et al. Metabolic state of glioma stem cells and nontumorigenic cells. *Proc. Natl. Acad. Sci. USA* **2011**, *108*, 16062–16067. [CrossRef]
31. Lemberg, K.M.; Vornov, J.J.; Rais, R.; Slusher, B.S. We're not "DON" yet: Optimal dosing and prodrug delivery of 6-Diazo-5-oxo-L-norleucine. *Mol. Cancer Ther.* **2018**, *17*, 1824–1832. [CrossRef]
32. Tataranni, T.; Piccoli, C. Dichloroacetate (DCA) and Cancer: An Overview towards Clinical Applications. *Oxidative Med. Cell. Longev.* **2019**, *2019*, 8201079. [CrossRef]
33. Kasznicki, J.; Sliwinska, A.; Drzewoski, J. Metformin in cancer prevention and therapy. *Ann. Transl. Med.* **2014**, *2*, 57.
34. Granchi, C.; Paterni, I.; Rani, R.; Minutolo, F. Small-molecule inhibitors of human LDH5. *Future Med. Chem.* **2013**, *5*, 1967–1991. [CrossRef] [PubMed]
35. Al-Hajj, M.; Clarke, M.F. Self-renewal and solid-tumor stem cells. *Oncogene* **2005**, *11*, 14–16. [CrossRef] [PubMed]
36. Pattabiraman, D.R.; Weinberg, R.A. Tackling the cancer stem cells—What challenges do they pose? *Nat. Rev. Drug Discov.* **2014**, *13*, 497–512. [CrossRef] [PubMed]
37. Singh, S.K.; Hawkins, C.; Clarke, I.D.; Squire, J.A.; Bayani, J.; Hide, T.; Henkelman, R.M.; Cusimano, M.D.; Dirks, P.B. Identification of human brain tumour initiating cells. *Nature* **2004**, *432*, 396–401. [CrossRef]
38. Reya, T.; Morrison, S.J.; Clarke, M.F.; Weissman, I.L. Stem cells, cancer, and cancer stem cells. *Nature* **2001**, *414*, 105–111. [CrossRef]
39. Li, Z.; Bao, S.; Wu, Q.; Wang, H.; Eyler, C.; Sathornsumetee, S.; Shi, Q.; Cao, Y.; Lathia, J.; McLendon, R.E.; et al. Hypoxia-Inducible Factors Regulate Tumorigenic Capacity of Glioma Stem Cells. *Cancer Cell* **2009**, *15*, 501–513. [CrossRef]
40. Calabrese, C.; Poppleton, H.; Kocak, M.; Hogg, T.L.; Fuller, C.; Hamner, B.; Oh, E.Y.; Gaber, M.W.; Finklestein, D.; Allen, M.; et al. A Perivascular Niche for Brain Tumor Stem Cells. *Cancer Cell* **2007**, *11*, 69–82. [CrossRef]
41. Peiris-Pagès, M.; Martinez-Outschoorn, U.E.; Pestell, R.G.; Sotgia, F.; Lisanti, M.P. Cancer stem cell metabolism. *Breast Cancer Res.* **2016**, *18*, 1–10. [CrossRef]
42. Hänzelmann, S.; Castelo, R.; Guinney, J. GSVA: Gene set variation analysis for microarray and RNA-Seq data. *BMC Bioinform.* **2013**, *14*, 7. [CrossRef]
43. Behnan, J.; Finocchiaro, G.; Hanna, G. The landscape of the mesenchymal signature in brain tumours. *Brain* **2019**, *142*, 847–866. [CrossRef] [PubMed]
44. Povirk, L.F.; Mutagenesis, M. DNA damage and mutagenesis by radiomimetic DNA-cleaving agents: Bleomycin, neocarzinostatin and other enediynes. *Mutat. Res.* **1996**, *355*, 71–89. [CrossRef]
45. Chen, J.; Stubbe, J. Bleomycins: Towards better therapeutics. *Nat. Rev. Cancer* **2005**, *5*, 102–112. [CrossRef] [PubMed]
46. García-Romero, N.; González-Tejedo, C.; Carrión-Navarro, J.; Esteban-Rubio, S.; Rackov, G.; Rodríguez-Fanjul, V.; Oliver-De La Cruz, J.; Prat-Acín, R.; Peris-Celda, M.; Blesa, D.; et al. Cancer stem cells from human glioblastoma resemble but do not mimic original tumors after in vitro passaging in serum-free media. *Oncotarget* **2016**, *7*, 65888–65901. [CrossRef]
47. Chou, T.-C. Drug Combination Studies and Their Synergy Quantification Using the Chou-Talalay Method. *Cancer Res.* **2010**, *70*, 440–446. [CrossRef]
48. Chou, T.-C. Theoretical Basis, Experimental Design, and Computerized Simulation of Synergism and Antagonism in Drug Combination Studies. *Pharmacol. Rev.* **2006**, *58*, 621–681. [CrossRef]
49. Mahmood, T.; Yang, P.-C. Western blot: Technique, theory, and trouble shooting. *N. Am. J. Med. Sci.* **2012**, *4*, 429–434. [CrossRef]
50. Divakaruni, A.S.; Paradyse, A.; Ferrick, D.A.; Murphy, A.N.; Jastroch, M. Analysis and Interpretation of Microplate-Based Oxygen Consumption and pH Data. In *Methods in Enzymology*; Elsevier: Amsterdam, The Netherlands, 2014; Volume 547, pp. 309–354.
51. Yépez, V.A.; Kremer, L.S.; Iuso, A.; Gusic, M.; Kopajtich, R.; Koňaříková, E.; Nadel, A.; Wachutka, L.; Prokisch, H.; Gagneur, J. OCR-Stats: Robust estimation and statistical testing of mitochondrial respiration activities using Seahorse XF Analyzer. *PLoS ONE* **2018**, *13*, e0199938. [CrossRef]
52. Bowman, R.L.; Wang, Q.; Carro, A.; Verhaak, R.G.; Squatrito, M. GlioVis data portal for visualization and analysis of brain tumor expression datasets. *Neuro-Oncology* **2017**, *19*, 139–141. [CrossRef]
53. Zhou, W.; Wahl, D.R. Metabolic Abnormalities in Glioblastoma and Metabolic Strategies to Overcome Treatment Resistance. *Cancers* **2019**, *11*, 1231. [CrossRef]

54. Madurga, R.; García-Romero, N.; Jiménez, B.; Collazo, A.; Pérez-Rodríguez, F.; Hernández-Laín, A.; Fernández-Carballal, C.; Prat-Acín, R.; Zanin, M.; Menasalvas, E.; et al. Normal tissue content impact on the GBM molecular classification. *Brief. Bioinform.* **2020**, bbaa129. [CrossRef] [PubMed]
55. Subramanian, A.; Tamayo, P.; Mootha, V.K.; Mukherjee, S.; Ebert, B.L.; Gillette, M.A.; Paulovich, A.; Pomeroy, S.L.; Golub, T.R.; Lander, E.S.; et al. Gene set enrichment analysis: A knowledge-based approach for interpreting genome-wide expression profiles. *Proc. Natl. Acad. Sci. USA* **2005**, *102*, 15545–15550. [CrossRef] [PubMed]
56. Fan, T.; Sun, G.; Sun, X.; Zhao, L.; Zhong, R.; Peng, Y. Tumor Energy Metabolism and Potential of 3-Bromopyruvate as an Inhibitor of Aerobic Glycolysis: Implications in Tumor Treatment. *Cancers* **2019**, *11*, 317. [CrossRef] [PubMed]
57. Wise, D.R.; Thompson, C.B. Glutamine addiction: A new therapeutic target in cancer. *Trends Biochem. Sci.* **2010**, *35*, 427–433. [CrossRef] [PubMed]
58. Aljofan, M.; Riethmacher, D. Anticancer activity of metformin: A systematic review of the literature. *Future Sci. OA* **2019**, *5*, FSO410. [CrossRef] [PubMed]
59. Yeaman, S.J.; Hutcheson, E.T.; Roche, T.E.; Pettit, F.H.; Brown, J.R.; Reed, L.J.; Watson, D.C.; Dixon, G.H. Sites of phosphorylation on pyruvate dehydrogenase from bovine kidney and heart. *Biochemistry* **1978**, *17*, 2364–2370. [CrossRef]
60. Korotchkina, L.G.; Patel, M.S. Site specificity of four pyruvate dehydrogenase kinase isoenzymes toward the three phosphorylation sites of human pyruvate dehydrogenase. *J. Biol. Chem.* **2001**, *276*, 37223–37229. [CrossRef]
61. Sesen, J.; Dahan, P.; Scotland, S.J.; Saland, E.; Dang, V.-T.; Lemarié, A.; Tyler, B.M.; Brem, H.; Toulas, C.; Moyal, E.C.-J.; et al. Metformin Inhibits Growth of Human Glioblastoma Cells and Enhances Therapeutic Response. *PLoS ONE* **2015**, *10*, e0123721. [CrossRef] [PubMed]
62. Velpula, K.K.; Guda, M.R.; Sahu, K.; Tuszynski, J.; Asuthkar, S.; Bach, S.E.; Lathia, J.D.; Tsung, A.J. Metabolic targeting of EGFRvIII/PDK1 axis in temozolomide resistant glioblastoma. *Oncotarget* **2017**, *8*, 35639–35655. [CrossRef]
63. Prabhu, A.; Sarcar, B.; Miller, C.R.; Kim, S.-H.; Nakano, I.; Forsyth, P.; Chinnaiyan, P. Ras-mediated modulation of pyruvate dehydrogenase activity regulates mitochondrial reserve capacity and contributes to glioblastoma tumorigenesis. *Neuro-Oncology* **2015**, *17*, 1220–1230. [CrossRef]
64. Brown, D.V.; Stylli, S.S.; Kaye, A.H.; Mantamadiotis, T. Multilayered Heterogeneity of Glioblastoma Stem Cells: Biological and Clinical Significance. In *Cannabinoids and Neuropsychiatric Disorders*; Springer: Berlin/Heidelberg, Germany, 2019; pp. 1–21.
65. Spehalski, E.I.; Lee, J.A.; Peters, C.; Tofilon, P.; Camphausen, K. The Quiescent Metabolic Phenotype of Glioma Stem Cells. *J. Proteom. Bioinform.* **2019**, *12*, 1–8. [CrossRef] [PubMed]
66. Zhou, Y.; Zhou, Y.; Shingu, T.; Feng, L.; Chen, Z.; Ogasawara, M.; Keating, M.J.; Kondo, S.; Huang, P. Metabolic alterations in highly tumorigenic glioblastoma cells preference for hypoxia and high dependency on glycolysis. *J. Biol. Chem.* **2011**, *286*, 32843–32853. [CrossRef]
67. Massalha, W.; Markovits, M.; Pichinuk, E.; Feinstein-Rotkopf, Y.; Tarshish, M.; Mishra, K.; Llado, V.; Weil, M.; Escriba, P.V.; Kakhlon, O. Minerval (2-hydroxyoleic acid) causes cancer cell selective toxicity by uncoupling oxidative phosphorylation and compromising bioenergetic compensation capacity. *Biosci. Rep.* **2019**, *39*, 39. [CrossRef] [PubMed]
68. Cvrljevic, A.; Akhavan, D.; Wu, M.; Martinello, P.; Furnari, F.B.; Johnston, A.J.; Guo, D.; Pike, L.; Cavenee, W.K.; Scott, A.M.; et al. Activation of Src induces mitochondrial localisation of de2-7EGFR (EGFRvIII) in glioma cells: Implications for glucose metabolism. *J. Cell Sci.* **2011**, *124*, 2938–2950. [CrossRef] [PubMed]
69. Shen, H.; Hau, E.; Joshi, S.; Dilda, P.J.; McDonald, K.L. Sensitization of Glioblastoma Cells to Irradiation by Modulating the Glucose Metabolism. *Mol. Cancer Ther.* **2015**, *14*, 1794–1804. [CrossRef]
70. Kim, J.; Han, J.; Jang, Y.; Kim, S.J.; Lee, M.J.; Ryu, M.J.; Kweon, G.R.; Heo, J.Y. High-capacity glycolytic and mitochondrial oxidative metabolisms mediate the growth ability of glioblastoma. *Int. J. Oncol.* **2015**, *47*, 1009–1016. [CrossRef]
71. Liu, X.; Chhipa, R.R.; Pooya, S.; Wortman, M.; Yachyshin, S.; Chow, L.M.L.; Kumar, A.; Zhou, X.; Sun, Y.; Quinn, B.; et al. Discrete mechanisms of mTOR and cell cycle regulation by AMPK agonists independent of AMPK. *Proc. Natl. Acad. Sci. USA* **2014**, *111*, E435–E444. [CrossRef]
72. Baker, J.C.; Yan, X.; Peng, T.; Kasten, S.; Roche, T.E. Marked Differences between Two Isoforms of Human Pyruvate Dehydrogenase Kinase. *J. Biol. Chem.* **2000**, *275*, 15773–15781. [CrossRef]
73. Bowker-Kinley, M.M.; Davis, I.W.; Wu, P.; Harris, A.R.; Popov, M.K. Evidence for existence of tissue-specific regulation of the mammalian pyruvate dehydrogenase complex. *Biochem. J.* **1998**, *329*, 191–196. [CrossRef]
74. Goldberg, E.B.; Colowick, S.P. The role of glycolysis in the growth of tumor cells. 3. Lactic dehydrogenase as the site of action of oxamate on the growth of cultured cells. *J. Biol. Chem.* **1965**, *240*, 2786–2790. [CrossRef]
75. Elwood, J.C. Effect of oxamate on glycolysis and respiration in sarcoma 37 ascites cells. *Cancer Res.* **1968**, *28*, 2056–2060. [PubMed]
76. Fiume, L.; Manerba, M.; Vettraino, M.; Di Stefano, G. Impairment of Aerobic Glycolysis by Inhibitors of Lactic Dehydrogenase Hinders the Growth of Human Hepatocellular Carcinoma Cell Lines. *Pharmacology* **2010**, *86*, 157–162. [CrossRef] [PubMed]
77. Zhai, X.; Yang, Y.; Wan, J.; Zhu, R.; Wu, Y. Inhibition of LDH-A by oxamate induces G2/M arrest, apoptosis and increases radiosensitivity in nasopharyngeal carcinoma cells. *Oncol. Rep.* **2013**, *30*, 2983–2991. [CrossRef] [PubMed]
78. Liu, X.; Yang, Z.; Chen, Z.; Chen, R.; Zhaofeng, C.; Zhou, Y.; Qiao, L. Effects of the suppression of lactate dehydrogenase A on the growth and invasion of human gastric cancer cells. *Oncol. Rep.* **2014**, *33*, 157–162. [CrossRef] [PubMed]
79. Still, E.R.; Yuneva, M.O. Hopefully devoted to Q: Targeting glutamine addiction in cancer. *Br. J. Cancer* **2017**, *116*, 1375–1381. [CrossRef]

80. DeBerardinis, R.J.; Cheng, T. Q's next: The diverse functions of glutamine in metabolism, cell biology and cancer. *Oncogene* **2010**, *29*, 313–324. [CrossRef] [PubMed]
81. Ohba, S.; Hirose, Y. L-asparaginase and 6-diazo-5-oxo-L-norleucine synergistically inhibit the growth of glioblastoma cells. *J. Neuro-Oncol.* **2020**, *146*, 469–475. [CrossRef]
82. Linnert, M.; Gehl, J. Bleomycin treatment of brain tumors: An evaluation. *Anti-Cancer Drugs* **2009**, *20*, 157–164. [CrossRef]
83. Chou, T.-C.; Talalay, P. Quantitative analysis of dose-effect relationships: The combined effects of multiple drugs or enzyme inhibitors. *Adv. Enzym. Regul.* **1984**, *22*, 27–55. [CrossRef]
84. Shen, H.; Decollogne, S.; Dilda, P.J.; Hau, E.; Chung, S.A.; Luk, P.P.; Hogg, P.J.; McDonald, K.L. Dual-targeting of aberrant glucose metabolism in glioblastoma. *J. Exp. Clin. Cancer Res.* **2015**, *34*, 14. [CrossRef]
85. Park, S.; Jeon, J.-H.; Min, B.-K.; Ha, C.-M.; Thoudam, T.; Park, B.-Y.; Lee, I. Role of the Pyruvate Dehydrogenase Complex in Metabolic Remodeling: Differential Pyruvate Dehydrogenase Complex Functions in Metabolism. *Diabetes Metab. J.* **2018**, *42*, 270–281. [CrossRef] [PubMed]
86. Zhang, W.; Zhang, S.-L.; Hu, X.; Tam, K.Y. Targeting Tumor Metabolism for Cancer Treatment: Is Pyruvate Dehydrogenase Kinases (PDKs) a Viable Anticancer Target? *Int. J. Biol. Sci.* **2015**, *11*, 1390–1400. [CrossRef] [PubMed]
87. Oizel, K.; Chauvin, C.; Oliver, L.; Gratas, C.; Geraldo, F.; Jarry, U.; Scotet, E.; Rabe, M.; Alves-Guerra, M.-C.; Teusan, R.; et al. Efficient Mitochondrial Glutamine Targeting Prevails Over Glioblastoma Metabolic Plasticity. *Clin. Cancer Res.* **2017**, *23*, 6292–6304. [CrossRef] [PubMed]
88. Shelton, L.M.; Huysentruyt, L.C.; Seyfried, T.N. Glutamine targeting inhibits systemic metastasis in the VM-M3 murine tumor model. *Int. J. Cancer* **2010**, *127*, 2478–2485. [CrossRef] [PubMed]
89. Cervantes-Madrid, D.; Romero, Y.; Dueñas-González, A. Reviving Lonidamine and 6-Diazo-5-oxo-L-norleucine to Be Used in Combination for Metabolic Cancer Therapy. *BioMed Res. Int.* **2015**, *2015*, 690492. [CrossRef]
90. Wu, F.; Lukinius, A.; Bergström, M.; Eriksson, B.; Watanabe, Y.; Långström, B. A mechanism behind the antitumour effect of 6-diazo-5-oxo-L-norleucine (DON): Disruption of mitochondria. *Eur. J. Cancer* **1999**, *35*, 1155–1161. [CrossRef]
91. Huber, K.R.; Mayer, E.P.; Mitchell, D.; Roberts, J.W. Cell cycle phase perturbations by 6-diazo-5-oxo-L-norleucine and acivicin in normal and neoplastic human cell lines. *Br. J. Cancer* **1987**, *55*, 653–656. [CrossRef]
92. Wang, G.S.; Hoyte, C. Review of biguanide (metformin) toxicity. *J. Intensive Care Med.* **2019**, *34*, 863–876. [CrossRef]
93. Erices, R.; Bravo, M.L.; Gonzalez, P.; Oliva, B.; Racordon, D.; Garrido, M.; Ibañez, C.; Kato, S.; Brañes, J.; Pizarro, J.; et al. Metformin, at Concentrations Corresponding to the Treatment of Diabetes, Potentiates the Cytotoxic Effects of Carboplatin in Cultures of Ovarian Cancer Cells. *Reprod. Sci.* **2013**, *20*, 1433–1446. [CrossRef]
94. Song, C.W.; Lee, H.; Dings, R.P.M.; Williams, B.; Powers, J.; Dos Santos, T.; Choi, B.-H.; Park, H.J. Metformin kills and radiosensitizes cancer cells and preferentially kills cancer stem cells. *Sci. Rep.* **2012**, *2*, 362. [CrossRef]
95. Stacpoole, P.W.; Kurtz, T.L.; Han, Z.; Langaee, T.Y. Role of dichloroacetate in the treatment of genetic mitochondrial diseases. *Adv. Drug Deliv. Rev.* **2008**, *60*, 1478–1487. [CrossRef] [PubMed]
96. Brandsma, D.; Dorlo, T.P.; Haanen, J.H.; Beijnen, J.H.; Boogerd, W. Severe encephalopathy and polyneuropathy induced by dichloroacetate. *J. Neurol.* **2010**, *257*, 2099–2100. [CrossRef] [PubMed]
97. Bonnet, S.; Archer, S.L.; Allalunis-Turner, J.; Haromy, A.; Beaulieu, C.; Thompson, R.B.; Lee, C.T.; Lopaschuk, G.D.; Puttagunta, L.; Bonnet, S.; et al. A Mitochondria-K+ Channel Axis Is Suppressed in Cancer and Its Normalization Promotes Apoptosis and Inhibits Cancer Growth. *Cancer Cell* **2007**, *11*, 37–51. [CrossRef]
98. Sun, R.C.; Fadia, M.; Dahlstrom, J.E.; Parish, C.R.; Board, P.G.; Blackburn, A.C. Reversal of the glycolytic phenotype by dichloroacetate inhibits metastatic breast cancer cell growth in vitro and in vivo. *Breast Cancer Res. Treat.* **2009**, *120*, 253–260. [CrossRef] [PubMed]
99. Heshe, D.; Hoogestraat, S.; Brauckmann, C.; Karst, U.; Boos, J.; Lanvers-Kaminsky, C. Dichloroacetate metabolically targeted therapy defeats cytotoxicity of standard anticancer drugs. *Cancer Chemother. Pharmacol.* **2010**, *67*, 647–655. [CrossRef] [PubMed]
100. Madhok, B.M.; Yeluri, S.; Perry, S.L.; Hughes, T.A.; Jayne, D.G. Dichloroacetate induces apoptosis and cell-cycle arrest in colorectal cancer cells. *Br. J. Cancer* **2010**, *102*, 1746–1752. [CrossRef] [PubMed]
101. Stockwin, L.H.; Yu, S.X.; Borgel, S.; Hancock, C.; Wolfe, T.L.; Phillips, L.R.; Hollingshead, M.G.; Newton, D.L. Sodium dichloroacetate selectively targets cells with defects in the mitochondrial ETC. *Int. J. Cancer* **2010**, *127*, 2510–2519. [CrossRef]
102. Pinkus, L.M. [45] Glutamine binding sites. In *Methods in Enzymology*; Elsevier: Amsterdam, The Netherlands, 1977; Volume 46, pp. 414–427.
103. Alt, J.; Potter, M.C.; Rojas, C.; Slusher, B.S. Bioanalysis of 6-diazo-5-oxo-l-norleucine in plasma and brain by ultra-performance liquid chromatography mass spectrometry. *Anal. Biochem.* **2015**, *474*, 28–34. [CrossRef]
104. Sarkaria, J.N.; Hu, L.S.; Parney, I.F.; Pafundi, D.H.; Brinkmann, D.H.; Laack, N.N.; Giannini, C.; Burns, T.C.; Kizilbash, S.H.; Laramy, J.K.; et al. Is the blood–brain barrier really disrupted in all glioblastomas? A critical assessment of existing clinical data. *Neuro-Oncology* **2018**, *20*, 184–191. [CrossRef]
105. Song, M.; Kim, S.-H.; Im, C.Y.; Hwang, H.-J. Recent development of small molecule glutaminase inhibitors. *Curr. Top. Med. Chem.* **2018**, *18*, 432–443. [CrossRef]
106. Strickland, M.; Stoll, E.A. Metabolic reprogramming in glioma. *Front. Cell Dev. Biol.* **2017**, *5*, 43. [CrossRef] [PubMed]
107. Woolf, E.C.; Syed, N.; Scheck, A.C. Tumor metabolism, the ketogenic diet and β-hydroxybutyrate: Novel approaches to adjuvant brain tumor therapy. *Front. Mol. Neurosci.* **2016**, *9*, 122. [CrossRef] [PubMed]

108. Akins, N.S.; Nielson, T.C.; Le, H.V. Inhibition of glycolysis and glutaminolysis: An emerging drug discovery approach to combat cancer. *Curr. Top. Med. Chem.* **2018**, *18*, 494–504. [CrossRef] [PubMed]
109. Abdel-Wahab, A.F.; Mahmoud, W.; Al-Harizy, R.M. Targeting glucose metabolism to suppress cancer progression: Prospective of anti-glycolytic cancer therapy. *Pharmacol. Res.* **2019**, *150*, 104511. [CrossRef] [PubMed]
110. Jin, L.; Alesi, G.; Kang, S. Glutaminolysis as a target for cancer therapy. *Oncogene* **2016**, *35*, 3619–3625. [CrossRef]
111. Liu, Y.; Shi, Y. Mitochondria as a target in cancer treatment. *MedComm* **2020**, *1*, 129–139. [CrossRef]
112. Ma, Y.; Temkin, S.M.; Hawkridge, A.M.; Guo, C.; Wang, W.; Wang, X.-Y.; Fang, X. Fatty acid oxidation: An emerging facet of metabolic transformation in cancer. *Cancer Lett.* **2018**, *435*, 92–100. [CrossRef]
113. Xia, S.; Lin, R.; Jin, L.; Zhao, L.; Kang, H.-B.; Pan, Y.; Liu, S.; Qian, G.; Qian, Z.; Konstantakou, E. Prevention of dietary-fat-fueled ketogenesis attenuates BRAF V600E tumor growth. *Cell Metab.* **2017**, *25*, 358–373. [CrossRef]
114. De Feyter, H.M.; Behar, K.L.; Rao, J.U.; Madden-Hennessey, K.; Ip, K.L.; Hyder, F.; Drewes, L.R.; Geschwind, J.-F.; De Graaf, R.A.; Rothman, D.L. A ketogenic diet increases transport and oxidation of ketone bodies in RG2 and 9L gliomas without affecting tumor growth. *Neuro-Oncology* **2016**, *18*, 1079–1087. [CrossRef]

Review

MOLECULAR METABOLISM

Metabolic therapy and bioenergetic analysis: The missing piece of the puzzle

Tomás Duraj [1], Josefa Carrión-Navarro [2,3], Thomas N. Seyfried [4], Noemí García-Romero [2,3,*], Angel Ayuso-Sacido [2,3,5,]**

ABSTRACT

Background: Aberrant metabolism is recognized as a hallmark of cancer, a pillar necessary for cellular proliferation. Regarding bioenergetics (ATP generation), most cancers display a preference not only toward aerobic glycolysis ("Warburg effect") and glutaminolysis (mitochondrial substrate level-phosphorylation) but also toward other metabolites such as lactate, pyruvate, and fat-derived sources. These secondary metabolites can assist in proliferation but cannot fully cover ATP demands.

Scope of review: The concept of a static metabolic profile is challenged by instances of heterogeneity and flexibility to meet fuel/anaplerotic demands. Although metabolic therapies are a promising tool to improve therapeutic outcomes, either via pharmacological targets or press-pulse interventions, metabolic plasticity is rarely considered. Lack of bioenergetic analysis *in vitro* and patient-derived models is hindering translational potential. Here, we review the bioenergetics of cancer and propose a simple analysis of major metabolic pathways, encompassing both affordable and advanced techniques. A comprehensive compendium of Seahorse XF bioenergetic measurements is presented for the first time.

Major conclusions: Standardization of principal readouts might help researchers to collect a complete metabolic picture of cancer using the most appropriate methods depending on the sample of interest.

Keywords Cancer; Energy metabolism; Glycolysis; Oxidative phosphorylation; Research design

1. INTRODUCTION

Study of cancer metabolism has seen a resurgence in recent years, with interest to guide therapies at the distinct metabolic characteristics of cancerous cells; this renewed focus is substantiated by the fact that altered metabolism has been integrated as one of the principal hallmarks of cancer [1].

Several theories about the metabolic origin of cancer have resulted in scientific debate due to their seeming confrontation with the somatic mutation theory [2]. Currently, research efforts are fundamentally directed at the study of genetic aberrations, with arguably limited cost-effectiveness and translational success [2–5]. This has led to a call for major revisions in the molecular paradigm of cancer [2,5,6].

Almost a century ago, Warburg postulated a theory where all cancer cells arise from mitochondrial defects in structure and function, making them avid consumers of glucose and other fermentable sources, even in the presence of oxygen [7]. This metabolic phenotype was termed "Warburg effect" or "aerobic glycolysis". Altered mitochondrial metabolism leads to variable dysfunction in oxidative phosphorylation (OXPHOS) [8,9]. In this model, genetic rewiring is a non-causal downstream epiphenomenon of mitochondrial failure, ROS-induced mutations and derailed inputs into primitive energy sensing pathways [10]. Instead of antagonizing genomic and mitochondrial contributions to tumorigenesis, metabolomics, proteomics, big data analysis, and mitochondrial respirometry can help us integrate conflicting results into a unified model. Notwithstanding the contentious origin problem, recent insights indicate a close connection between molecular and metabolic rewiring [11]. As a practical application, oncometabolic signatures from tumoral samples have been integrated into therapeutically relevant predictive models [12]. Unfortunately, the clarity of the accumulating evidence is obfuscated by a lack of systematic collection of relevant metabolic information.

In this review, we incorporated well-known and widely replicated experiments of bioenergetic metabolism as the backdrop to propel the need for standardized metabolic analysis. First, we describe all major metabolic pathways that lead to ATP production in normal and cancer cells. Second, we discuss the successes and pitfalls of metabolic

[1]Faculty of Medicine, Institute for Applied Molecular Medicine (IMMA), CEU San Pablo University, 28668, Madrid, Spain [2]Faculty of Experimental Sciences, Universidad Francisco de Vitoria, 28223, Madrid, Spain [3]Brain Tumor Laboratory, Fundación Vithas, Grupo Hospitales Vithas, 28043, Madrid, Spain [4]Biology Department, Boston College, 140 Commonwealth Ave, Chestnut Hill, MA, 02467, USA [5]Faculty of Medicine, Universidad Francisco de Vitoria, 28223, Madrid, Spain

*Corresponding author. Carretera Pozuelo-Majadahonda (M-515) Km. 1.800, Facultad de Ciencias Experimentales, Edificio E, planta 0, Universidad Francisco de Vitoria, Pozuelo de Alarcón, 28223, Madrid, Spain.

**Corresponding author. Carretera Pozuelo-Majadahonda (M-515) Km. 1.800, Facultad de Ciencias Experimentales, Edificio E, planta 0, Universidad Francisco de Vitoria, Pozuelo de Alarcón, 28223, Madrid, Spain.

E-mails: tom.duraj.ce@ceindo.ceu.es (T. Duraj), pepa.carrion@ufv.es (J. Carrión-Navarro), thomas.seyfried@bc.edu (T.N. Seyfried), noemi.garcia@ufv.es (N. García-Romero), ayusosacido@gmail.com (A. Ayuso-Sacido).

Received September 23, 2021 • Revision received October 29, 2021 • Accepted November 1, 2021 • Available online 5 November 2021

https://doi.org/10.1016/j.molmet.2021.101389

Abbreviations

OXPHOS	oxidative phosphorylation
SLP	substrate-level phosphorylation
ETC	electron transport chain
FAO	fatty acid oxidation
mtDNA	mitochondrial DNA
OCR	oxygen consumption rate
KBs	ketone bodies
BHB	β-hydroxybutyrate
AcAc	acetoacetate
LDH	lactate dehydrogenase
BCAAs	branched-chain amino acids
ORR	optical redox ratio
TPEF	two-photon excited fluorescence
ECAR	extracellular acidification rates
MMP	mitochondrial membrane potential
CEB	Cell Energy Budget Platform
SCM-PAM	single-cell metabolic photoacoustic microscopy
PET	positron emission tomography
MRS	magnetic resonance spectroscopy
CT	computed tomography
MRI	magnetic resonance imaging
CEST	chemical exchange saturation transfer
BIRDS	biosensor imaging of redundant deviation in shifts
LC/GC—MS	liquid and gas chromatography-mass spectrometry
SIRM	stable isotope-resolved metabolomics
DGE	dynamic glucose-enhanced
DNP	dynamic nuclear polarization

therapies, emphasizing the lack of appropriate patient stratification as a key unresolved challenge. Third, we offer a summary of tools and techniques to obtain *in vitro* and *in vivo* measurements of bioenergetic metabolism. Seahorse XF technology is spotlighted as a widespread method for metabolic analysis that requires careful interpretation and experimental design.

We conclude that guiding research endeavors towards evolutionarily conserved bioenergetic or biosynthetic pathways could be a way of reducing molecular complexity and increasing the effectiveness of cancer therapies. A better characterization of tumoral and healthy samples could cast new light about cancer growth, designing comprehensive studies which include altered metabolism as a prominent driver of proliferation.

2. MASTER METABOLIC REGULATORS

Despite the ample genetic and histological heterogeneity of cancer, a relatively small number of metabolic processes is responsible for maintaining ATP generation and redox balance [13]. ATP can only be physically generated in two distinct processes: substrate-level phosphorylation (SLP) or fueling the proton gradient of the mitochondrial electron transport chain (ETC). Their adequate functioning is essential for the maintenance of a proliferative status, redox balance and cell viability [14].

As shown in Figure 1, healthy cells exhibit efficient, fine-tuned bioenergetic metabolism. Under physiological conditions, glycolysis is the cytosolic conversion of glucose into two molecules of pyruvate, which are then oxidized in the mitochondria, yielding ≈30 ATP, CO_2 and H_2O per glucose molecule [15]. In most normal cells, glucose-driven OXPHOS entails the primary mechanism for energy production [16]. However, in the absence of oxygen (anaerobic glycolysis), pyruvate can be enzymatically reduced to lactic acid, generating a net total of 2 ATP. In cancer cells, the persistent production of lactate from pyruvate, regardless of the presence of oxygen and forgoing mitochondrial oxidation, is known as "aerobic fermentation," "aerobic glycolysis," or "Warburg effect." Catabolic fuels (glucose, glutamine, pyruvate, lactate, free fatty acids, ketone bodies, cysteine, serine, and other amino acids) can be obtained from circulation, stroma, *de novo*

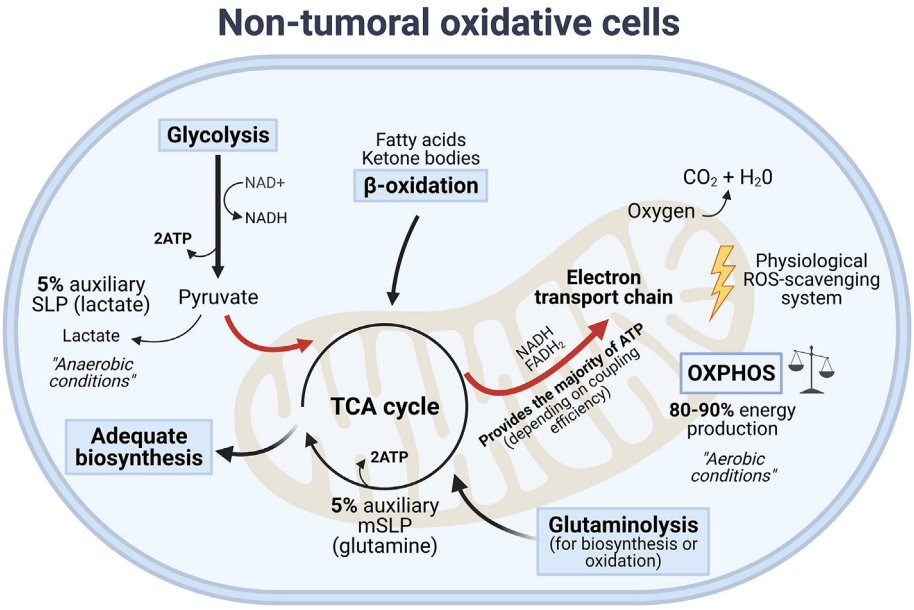

Figure 1: Simplified diagram of the distribution of fuels in non-tumoral, oxidative cells. OXPHOS is estimated to provide at least 80% of ATP under conditions of oxygen abundance, generating a manageable amount of ROS. SLP-ATP generation is upregulated in anaerobic conditions. This diagram is intended to serve as a point of comparison between nontumoral and transformed cells, but it does not encompass all the dynamic properties of metabolic regulation in physiological conditions.

synthesis, and/or autophagy within the cell itself [17,18]. Tumors are metabolically heterogeneous and different cell populations can express preferences toward specific microenvironmental metabolites [19].

Warburg-like and oxygen consuming phenotypes have been extensively described in cancer as both discreet and plastic categories, as summarized in Figure 2. Oxygen consumption, however, cannot be interpreted as functioning ATP generation at the mitochondrial level due to ample evidence of mitochondrial defects in almost all subtypes of cancer [9]. Despite the supporting role of other metabolites, cancer cells are largely dependent on glucose and glutamine as either fermentable or oxidative fuels. The reach and scope of metabolic flexibility, that is, the ability of any given cancer cell to shift between metabolic states, remains unclear.

3. CATABOLIC PATHWAYS CONTRIBUTING TO ATP SYNTHESIS

3.1. Warburg effect: selfish, rapid, and oxygen-independent ATP production to fuel proliferation over bioenergetic efficiency

The Warburg effect embodies perhaps the single most studied and misunderstood metabolic alteration of cancer [20]. An unresolved debate stands about its independence from the microenvironment, mitochondrial fitness, and sufficiency/necessity for malignant transformation [21]. It was hypothesized that this metabolic switch might be a preemptive adaptation to variations in intratumoral blood flow by improper angiogenesis [22]. In the endosymbiotic mitochondrial model, the Warburg effect signifies a regression to an evolutionary conserved glycolytic, proliferative phenotype, triggered by compromised mitochondrial integrity/function [23]. Speed of energy production is another reason to consider SLP an advantageous, rapidly adjustable metabolic state: although the amount of ATP per mole of substrate produced by OXPHOS is higher, aerobic glycolysis is almost 100 times faster [24]. Awareness about the predominance of the Warburg phenotype in most cultured cells should not be an excuse to underestimate its relevance, especially when outlining cancer as unchecked proliferation with a primary metabolic component.

Glucose is avidly consumed by most cancer cells through metabolic rewiring to compensate for the low ATP generation yields due to mitochondrial defects as well as the predominance of the glycolytic PKM2 isoform, which produces intermediary metabolites rather than ATP [25,26]. Glucose is destined mainly for fermentation and biosynthetic processes, not OXPHOS. To date, Warburgian phenotypes had been observed in almost all solid tumors [16,27]. Counterpoint evidence for a more nuanced metabolic heterogeneity was suggested in oxygen-consuming phenotypes [28], but it is important to emphasize that extracellular measurements of oxygen do not translate to ATP synthesis by the ETC. As ATP levels in cancer cells are still maintained under irreversible mitochondrial inhibition, normal OXPHOS cannot occur in the majority of cancer cells [29,30]. As a juxtaposition, a hybrid model of metabolic clustering termed the “reverse Warburg effect” or “Autophagic Tumor Stroma Model” has been put forward to describe the interactions between cancer cells and tumoral stroma [31–35]. Lactate is an important source of TCA cycle intermediates in physiological conditions and should be recognized as a potential target in cancer, regardless of the discussion surrounding the oxidative fitness of cancer cells [36,37]. While ancillary metabolites could support tumor growth, especially for biosynthetic purposes, as discussed below, they cannot drive sufficient ATP synthesis in conditions of glucose and glutamine depletion [38,39]. Furthermore, glucose uptake is not necessarily destined for fermentation or oxidation, but can be diverted mostly to anabolic pathways [40].

Mitochondrial integrity and ATP-generating capacity could be understood as the underlaying factor that dictates the fate of glucose-derived pyruvate and metabolic heterogeneity. A more appropriate way to conceptualize the Warburg effect might be a spectrum, rather than a binary switch, with cancer cells displaying unique glucose and glutamine dependencies based on their degree of mitochondrial dysfunction, tissue of origin, and ROS-induced mutational landscapes [41]. While accurate measurement of mitochondrial function has not been accomplished in all models of cancer, it can elegantly explain apparent differences in metabolic phenotypes without the need to characterize each individual effector-gene, rewired in a non-causal manner. As a solution to this methodological issue, a wide variety of techniques to measure mitochondrial metabolism are highlighted in our review.

3.2. Oxidative phosphorylation: mitochondrial fitness as the arbitrator of respiration

OXPHOS produces energy through the transfer of electrons from high-energy electron carriers (NADH or FADH2) to a series of mitochondrial complexes located in the inner membrane and by the generation of a proton gradient. The resulting electromotive force converts ADP to ATP via ATP synthase. At the same time, redox carriers derive from cytoplasmatic glycolysis, tricarboxylic acid (TCA) cycle and fatty acid oxidation (FAO). The term OXPHOS itself is substrate-agnostic, although the majority of electron donors originate from glucose oxidation in normal cells [42], and between 25 and 60% in cancer cells, with a high degree of variability between subtypes [43].

Cancer cells have evidence of abnormalities in mitochondrial structure, biogenesis, and mitochondrial DNA (mtDNA), together with reduced activity of ETC complexes [29,44–48]. Normal cristae shape is essential to evaluate ATP synthesis, as structure and function cannot be separated [49,50]. Mitochondrial transfer studies corroborated that normal mitochondria can inhibit tumorigenesis and reverse the Warburg effect, even when coexisting with a tumorigenic genome [27,51,52]. Conversely, a compelling demonstration of the importance of mitochondrial regulation for neoplastic transformation comes from cancer cells lacking mtDNA, that required mitochondrial acquisition from neighboring cells to efficiently generate tumors *in vivo* [53]. In both healthy cells and cancer cells, mitochondria regulate cell proliferation, metabolic adaptation, and Ca_2^+ homeostasis [54]. Metabolic reprogramming enables proliferation despite varying degrees of mitochondrial dysfunction [55–57]. As a merely descriptive exercise, when OXPHOS decreases, SLP must increase to ensure constant ATP supply; this interplay has been replicated in direct measurement studies at the cellular level [58] and simulated in flow balance and mathematical models [59]. Nonetheless, the inhibition of glycolysis also increases other processes such as glutamine-dependent SLP/OXPHOS [60].

The relevance of mitochondrial alterations is still unclear, as definite determination of function without relying on indirect measurements, such as oxygen consumption rates (OCR), is a challenging endeavor [61].

Contemplating glycolytic capacity as a survival advantage and, at the same time, a vulnerably due to defective mitochondria are two opposing concepts [62]. Contrary to Warburg’s hypothesis, a relative dependence upon oxygen-consuming phenotypes has been described in specific cancer subtypes [63,64]. Even still, as indicated by metabolic profiling (described in subsection 5.1 and Table S2), cancer cells in which OCR is the predominant state are very rare, always coexisting with glycolytic compensation. Beyond ATP synthesis, identification of oxidative metabolism could be applied as a predictor of chemo-

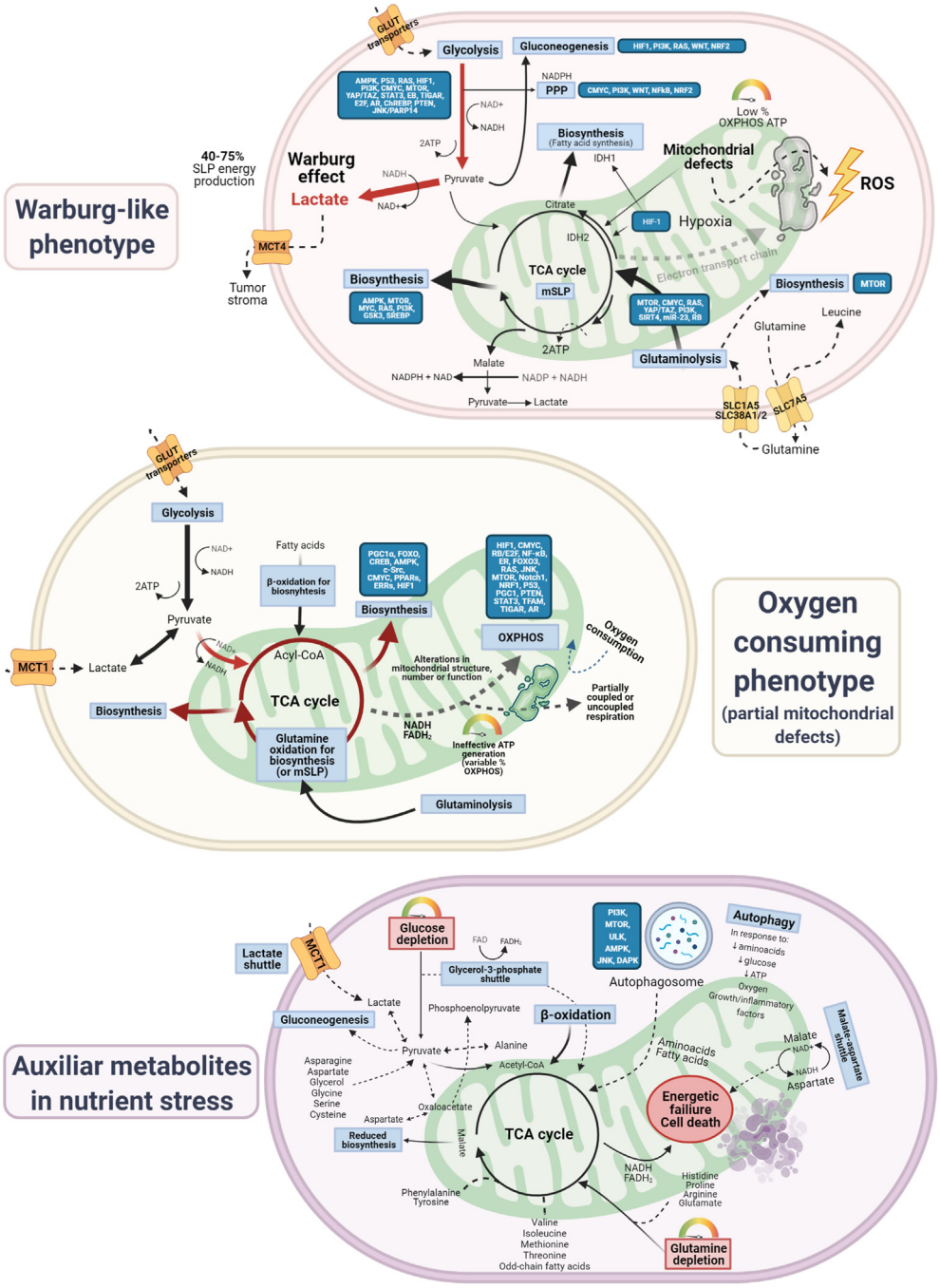

Figure 2: Tumoral bioenergetic metabolism at a glance. Glucose enters transformed cells via GLUT family transporters and undergoes glycolysis, converted into pyruvate (yielding 2 net ATP). Cancer cells preferentially divert pyruvate to lactate (SLP), regardless of the presence of oxygen (aerobic glycolysis or Warburg effect); an estimated 10% of pyruvate goes toward biosynthesis, and OXPHOS is variable, depending on mitochondrial dysfunction. Oxygen consuming, mitochondrially defective cancer cells can utilize glucose-derived pyruvate, glutamine, and fatty acids to drive TCA cycle intermediaries, but ATP-generation capacity through the ETC is impaired to a substantial degree. In conditions of glucose and glutamine deprivation, recycling of ancillary substrates could aid in ATP generation, including fatty acids/ketone bodies, lactate, amino acids and autophagic processes. Metabolic reprogramming involves the interconnected regulation of glycolysis, glutaminolysis and mitochondrial metabolism. Prominent regulators are *P53* (glycolysis/OXPHOS), *CMYC* (glycolysis, glutaminolysis and lipid synthesis), *KRAS* (glycolysis, glutaminolysis), *PI3K/AKT* (glycolysis), *AMPK* (nutrient stress), *HIF-1* (glycolysis, global metabolic rewiring), peroxisome proliferator-activated receptors (*PPARs*) and PPARγ coactivator-1α (*PGC-1α*) (FAO), forkead box O family (*FOXO*) (OXPHOS). The combination of preexisting oncogenic lesions and metabolic fluxes, along with tumoral milieu, is likely to govern metabolic flexibility of each individual cell. Abbreviations: PPP (Pentose phosphate pathway), SLP (substrate level phosphorylation), OXPHOS (oxidative phosphorylation), ROS (reactive oxygen species).

resistance [65]. OCR, measured by a variety of respirometry techniques, differed greatly between and within the same cell lines, further confused by cell handling and normalization issues [66]. To the extent of our knowledge, no experimental evidence of cancer cells sustained exclusively and self-sufficiently by oxidation of glucose, glutamine, or fatty acids has been described (Table S3). To which extent is OCR representative of healthy mitochondrial function is being questioned: it cannot detect glutamine-driven mitochondrial SLP (mSLP) or allocate any other metabolic fuels to their final destination; thus, measuring OCR alone should not be considered an unequivocal marker of functioning respiration [29,67].

3.3. Glutaminolysis: mitochondrial substrate-level phosphorylation and anaplerosis

Glutamine is a conditionally essential α-amino acid involved in cell proliferation, tumor growth, and nucleotide synthesis [68,69]. As an important anaplerotic source, it can be metabolized into glutamate and, subsequently, α-ketoglutarate, to enter the TCA cycle and drive biosynthesis and OXPHOS by generation of electron cofactors. Glutaminolysis can generate 2 ATP molecules through succinyl-CoA synthetase in a enzymatic reaction called mSLP [70], which is believed to generate substantial amounts of ATP in the absence of glucose, under hypoxic conditions, or when mitochondrial integrity is compromised [71–73].

Moreover, mSLP could be erroneously interpreted as a marker of mitochondrial fitness using flux analyzers, whereas stable isotope tracing studies demonstrated its role in response to moderate (catabolic) or severe (anabolic) OXPHOS dysfunction [74]. Under hypoxic conditions, glutaminolysis has been shown to produce most of the ATP and synergize with the Warburg effect to promote tumor growth [75]. Addiction to glutamine has now been documented in almost all subtypes of cancer, including lung, ovarian, pancreatic, colorectal, breast, and brain tumors, with metabolic reprogramming (principally by the *MYC* family of genes) for increased anaplerosis, regulation of nitrogen balance, redox homeostasis, and mSLP [76]. Because the contribution of glutamine is fluctuating and not fully characterized in all model systems, the absolute contribution of glucose and glutamine oxidation/SLP to ATP synthesis for any given cell line is largely unknown [59,77]. In cancer, glutamine-dependent reductive carboxylation becomes a major pathway of citrate formation for lipid synthesis, generation of TCA metabolites, and macromolecular precursors [56]. In addition to roles as a carbon/nitrogen biosynthetic source [78,79], glutamine has been implicated in enzymatic release of ammonia into the microenvironment [80]. Free ammonia can be recycled into central amino acid metabolism to maximize nitrogen utilization [81,82]. A participation in acidic protection was touted through enzymatic deamidation [83]. Cancer cells are likely able to acquire sufficient quantities of glutamine from circulation with increased blood levels reported in advanced stage cancers [84]. *De novo* synthesis of glutamine could be sufficient to compensate glutamine starvation via glutamine synthetase and rescued by other amino acids, particularly asparagine, aspartate, and arginine [85,86]. Although less understood from a cancer perspective, glutamine has been implicated in the regulation of autophagy [87,88]. Lastly, *in vitro* studies are generally performed under conditions of glutamine abundance to improve proliferation rates, thus reducing translational potential [89]. Likewise, levels of metabolites inside the tumor mass are variable: for example, colon, stomach, and oral cancers presented low glucose and glutamine levels with high lactate and glutathione, suggesting Warburg-like properties [90]. Synergistic inhibition of glycolysis and glutaminolysis is proposed as a promising therapeutic approach [91]. In clinical trials, metabolic flux analysis and stratification of patients according to glutaminolysis will be crucial to improve responses to both conventional therapy and metabolic drugs.

3.4. Fatty acid oxidation and ketone bodies

Saturated and unsaturated fatty acids can be oxidized for energy via medium and long-chain acyl-CoA dehydrogenases and β-oxidation input into the TCA cycle, generating acetyl-CoA and electron donors. FAO yields 2.5 times more ATP per mole of substrate than glucose (between 14 and 17 ATP every oxidation cycle) [92]. Elevated levels of FAO have been detected even in abundance of glucose and glutamine [93]. When the AMP/ATP ratio increases, AMPK activates fatty acid metabolism to provide catabolic substrates, maintain redox homeostasis, and biosynthesis. In hypoxia, FAO is suppressed by *HIF-1* [94,95]. Even though specific cell lines (e.g., ovarian, prostate, breast, brain, and colon) demonstrated relatively higher reliance upon FAO, complete ATP provision from this pathway without substantial contribution of glycolysis/glutaminolysis is uncommon [96]. Rather, lipid metabolism might contribute to redox balance and biosynthetic pathways, while also regulating glycolysis and glutaminolysis [97,98].

Ketone bodies (KBs), β-hydroxybutyrate (BHB) and acetoacetate (AcAc), and the short-chain fatty acid acetate, have been identified as non-fermentable substrates. KBs metabolism is especially relevant in metabolic therapies based on glucose/glutamine inhibition, where rescue of healthy cells via BHB has been proposed as an adjuvant therapeutic strategy [99,100]. In humans, acetate can be a secondary energy source, thought to play a very minor role in tumor growth, with very low *in vivo* levels [101]. Although tumor cells can express ketolytic enzymes, the argument has been made that most mitochondrially defective cells struggle to process fats and KBs for fuel, especially in conditions of low glucose [102,103]. It was also shown that hypoxia and nutrient stress can increase the dependence of some cancers upon FAO and KBs [104,105]. KBs generally possess antitumoral properties, but, under certain conditions, might promote cancer stemness [106,107]. Instead of relying on single pathway inhibition, combined press-pulse strategies might be the key to improve therapeutic responses [99].

In conclusion, KBs and fatty acids can be supplied either from circulation, autophagy, or adjacent stromal cells [108]. The importance of fat-derived sources to strictly bioenergetic production is heterogeneous and largely unspecified [59]. Identifying cancers with an abnormally high affinity for such obligate-OXPHOS catabolites is an appealing proposition for adequate patient stratification.

3.5. Ancillary metabolites and pathways: lactate and pyruvate in the reverse Warburg effect, anaplerotic amino acids and autophagy

Monocarboxylates have been examined extensively as central ATP-generating molecules [109,110].

Lactate, a downstream metabolite of pyruvate via lactate dehydrogenase (LDH), can itself act as a secondary energy source for tumor cells. Lactate can be synthetized independently of hypoxia and supplied by tumoral stroma [111,112]. Lactate can be derived to both alanine and glutamate synthesis [113,114]. In the two-compartment model of cancer metabolism, glucose fermentation leads to lactic acidosis, promoting a transition to oxidative metabolism in surrounding, well irrigated, oxygenated cells [115]. This assumes full metabolic flexibility of both cancer cells and associated fibroblasts, which might be limited to specific models and not representative of tumors with mitochondrial dysfunction [116,117]. High levels of lactate can partially rescue from nutrient depletion, but most cancer cells cannot proliferate with lactate alone [31,118]. Owing to the intrinsic regulation of glycolytic and mitochondrial metabolism, reversal of lactic acidosis showed

promising results in preclinical and pilot human studies [119,120]. Lactate acts as a pro-metastatic metabolite, with functions in extracellular matrix remodeling through hyaluronan synthesis, enhanced cell motility, upregulation of *VEFG* and *HIF1* signaling, and immunomodulatory effects [109,121].

The monocarboxylate pyruvate could be viewed independently, originating primarily from glycolysis but also TCA sources (malate), amino acids (serine, cysteine, threonine/glycine and alanine), as well as lactate itself by reversal of LDH [122,123]. Pyruvate constitutes a central metabolic junction that can lead to the production of lactate, alanine, oxaloacetate, or acetyl-CoA [38]. Acetyl-CoA can remain in the TCA cycle or be metabolized in the cytosol for *de novo* lipogenesis, protein acetylation, or KB production [124]. Exogenous pyruvate has been shown to enhance invasive phenotypes: pyruvate oxidation correlates with proliferation and malignancy in some cancer cells [125]. Consequently, targeting pyruvate upstream or downstream is essential for the design of metabolic therapies, as pyruvate stands as an arbitrator between glycolysis and OXPHOS [126].

Complementary amino acids (methionine, threonine, phenylalanine, tyrosine, asparagine/aspartate, histidine, proline, arginine, and glutamate), especially branched-chain amino acids (BCAAs) isoleucine and valine, can also enter the TCA cycle at different steps as anaplerotic sources [127,128]. BCAAs can be metabolized by transaminases in both the cytosol and mitochondria, but their contribution to cancer progression is unclear [129]. Anaplerotic intermediaries might exert a partial rescue effect on tumor proliferation [130]. In this process, cysteine plays a pivotal role, being incorporated into glutathione, serving as a carbon source for energy metabolism and biosynthesis (via folate and methionine cycles), and contributing to the ETC as an indirect electron donor via hydrogen sulfide [131]. Alternatively, serine, glycine, folate oxidation, alanine, succinate, and ammonia, as well as other minor metabolites (glycerol, propionate), could aid in the survival of cancer cells by strengthening their metabolic flexibility in response to glucose/glutamine depletion [132–135].

It should be noted that metabolic substrates are not imported exclusively from circulation or surrounding tissue, as autophagy, vesicular transport, and lysosomal digestion act as secondary sources [136,137]. Autophagy is a dynamic degradation process of cytoplasmic cellular self-constituents, allowing for macromolecule turnover even in a state of diminished nutrients (amino acids/glucose) and oxygen availability [138].

The question remains whether these supplementary metabolites, in quantities realistically achieved *in vivo*, be it from circulation, stroma, or autophagic processes, would be adequate to sustain tumor growth under synergistic targeting of glucose/glutamine. Thus far, it has been well established that glucose/glutamine are the two major bioenergetic and anaplerotic contributors, allowing adaptation to unfavorable microenvironment changes in oxygen and acidity by dynamic tuning of metabolic pathways [38,139,140].

4. METABOLIC FLEXIBILITY AND THERAPY IN THE ERA OF PRECISION MEDICINE

The incredible complexity of the genetic landscape and flow of information among genome, metabolome, and tumor microenvironment should be recognized as an important barrier for the translational success of molecular research [141]. One of the main limitations of applying metabolism-based strategies is the heterogeneity of cancer cells and their adaptive mechanisms against nutrient deprivation. In this paradigm, each individual cancer cell could have a unique metabolic profile [142]. Multiple inputs into the TCA cycle, in an everchanging microenvironment, compose a metabolic framework that is far more diverse than limiting our perspective to "glycolysis, glutaminolysis, and FAO". As with genetic heterogeneity, addressing these metabolic differences individually appears almost unmanageable.

In the reverse Warburg effect hypothesis, transformed cells (preserved OXPHOS, anabolic, stem-like) and adjacent fibroblasts (glycolytic, catabolic) coexist [143–145], whereas in the mitochondrial theory of cancer, this cooperative link is not relevant for mitochondrially impaired cancer cells [146]. Autophagy, mitochondrial dynamics, and metabolic coupling have been described as possible contributors to tumor growth, but they have never been shown to produce sufficient ATP to sustain proliferation on their own [63,111,147]. This dual metabolic model is only appliable to tumors with important stromal components [145,148]. Integrating new findings to determine whether glycolysis and OXPHOS can co-occur or are mutually exclusive is under active investigation [149–151].

In conclusion, a comprehensive metabolic analysis of neighboring tissues should be recommended [112]. Categorization of glycolysis/OXPHOS as "predominant" phenotypes would be a way to by-pass the heterogeneity of the molecular landscape, but additional studies to fully characterize metabolic flexibility are indispensable. Therapeutic targeting will require synergistic approaches to ensure single-pathway inhibition cannot be rescued.

4.1. The promises and limitations of metabolic therapy: reconsidering standardization and heterogeneity

Metabolic therapy has been proposed as a promising management strategy for cancers with very poor prognosis and ineffective standard of care. Glycolytic and glutaminolytic dependencies are a well-described and targetable feature of many tumors, such as brain, pancreatic, breast, lung, gastric, skin, and prostate, among others [152–154]. Multiple interventions were suggested under the metabolic therapy umbrella, e.g., calorically restricted ketogenic diets, fasting, tumor microenvironment and oxidative stress regulation, hyperbaric oxygen therapy, hyperthermia, controlled hypoglycemia, autophagy inhibition, metabolic reprogramming, and inhibitors [99,155–159]; however, standardization is needed.

As a good candidate for metabolic therapy, high-grade gliomas have glycolytic phenotypes [160,161] and partial mitochondrial defects [29,162]. Mitochondrial inhibitors (such as metformin or IACS-010759) epitomize an attractive opportunity to specifically increase mitochondrial stress in cancer cells, while concurrently targeting glycolysis by dietary or pharmacological interventions [163,164]. Inhibiting OXPHOS and mitochondrial dynamics requires careful dosing and tissue localization to avoid off-target toxicity, being only intended to manage tumoral subpopulations with a partially functioning chondriome [165]. Stratification of mitochondrial dependencies in different cancer models and individual patients would be essential prior to synergistic SLP-OXPHOS targeting. Ketogenic compensatory strategies could protect healthy neuronal tissues against glucose deprivation [166,167]. Despite identification of Warburg-like vulnerabilities in glioma, metabolic heterogeneity needs to be incorporated into therapeutic designs [168–170].

In the same way, pancreatic cancer is an appealing target for metabolic intervention due to specific metabolic subtypes, *KRAS* governance, mitochondrial defects, and generally poor prognosis [171,172]. Accordingly, tumors of this origin have been classified into metabolic categories, with significant differences in glucose, glutamine, and mitochondrial metabolism, as well as a stromal component (reverse Warburg effect), highlighting the need for improved stratification [173,174].

Other solid tumors with broader metabolic plasticity are breast and lung cancers, where anti-glycolytic targeting has been proposed as a first-line therapy, but additional tailor-made approaches might be necessary to target all possible metabolic phenotypes [175,176]. In breast cancers, Warburgian/OCR phenotypes have been shown to coexist, thus requiring synergistic approaches to manage glycolysis and reverse mitochondrial dysfunction [177,178]. Lung cancers integrate oncogenic lesions, stromal contributions, and basal metabolic states into Warburg-like, glutaminolytic, mitochondrial, and mixed dependencies (lactate, serine, fatty acids, autophagy) [175,179,180].
In summary, owing to the proposed universal nature of altered metabolism, metabolic therapy would encompass all tumors with obligate SLP-ATP generation and defects in mitochondrial metabolism [181,182]. However, the identification of tumors characterized by a higher reliance on oxidative metabolites (e.g., glutamine or fat-derived), not exclusively for ATP synthesis but also other proliferative requirements, could be useful for stratification [41,183].
Unfortunately, initial excitement in this field has been met with difficulties to translate preclinical research into advanced human trials. Metabolic interventions are being evaluated predominantly in phase I and II pilot studies (e.g., dichloroacetate, 2-deoxyglucose, metformin, ketogenic diets, fasting, hyperbaric oxygen), with mostly favorable and encouraging outcomes [100,184]. Case reports and pilot clinical trials are a promising first step to introduce metabolic therapy into clinical practice [182,184–186]. Phase III clinical trials focus almost exclusively on metabolic imaging, with only a handful of trials assessing concrete therapeutic interventions, such as metformin (NCT02201381, NCT03031821), sirolimus (NCT04775173), fasting-mimicking diets (NCT02126449), and dietary supplements/life-style interventions to improve quality of life. Only one phase IV metabolic study is underway with metformin (NCT04741204).
As discussed, metabolic flexibility should be assessed in a case-by-case basis, and easy-to-use tools for bioenergetic analysis are finally becoming accessible for researchers. In translational studies, however, metabolic profiling is still relatively unheard-of. Metabolic plasticity and heterogeneity are also key factors in treatment response and resistance to standard chemoradiotherapy, but even with this knowledge, such concepts are often overlooked in experimental designs unless specifically testing metabolic agents [187].

5. MEASUREMENT OF METABOLIC FUNCTION: A SUMMARY OF EQUIPMENT, TECHNIQUES AND THEIR ACCURACY

Routinely, all tumors are considered as metabolically equal regardless of their basal metabolism. In contrast, genetic aberrations are starting to be evaluated as a part of more personalized drug therapies, but their repercussions on metabolism are rarely assessed [188,189]. In our opinion, information about the ability of cancer cells to switch metabolic fuels is fundamental to improve therapeutic success and translational potential of basic research.
A summary of techniques to study metabolism is presented in Figure 3 and Table S1. Techniques were separated into *in vitro* and *in vivo* analysis of glycolysis, glutaminolysis, ATP production and mitochondrial function (including OCR, membrane potential, as well as structure and cristae shape). In addition, we propose a simple flow chart clinical model where results from metabolic analysis could guide subsequent treatments (Figure S1).

5.1. *In vitro* assessment of bioenergetic metabolism

As the bioenergetic profile of individual cells is under dynamic control of various microenvironmental stimuli, such as nutrient availability, oxygen, and acidity [190], numerous attempts have been made to increase the resolution of direct metabolic measurements. Historically, refinements to the Warburg apparatus [191] and Clark electrode chambers [192,193] allowed to measure oxygen consumption in increasingly reduced volumes, but required a high amount of purified mitochondria and removed cellular regulation of metabolism during isolation [194]. Now, these time-consuming techniques are being substituted by multiple-readout integrated solutions, such as oxygen-sensing fluorophores or oxygraphs [195,196]. Quantitative/functional proteomics can reveal the presence and activity of key metabolic enzymes and transporters in tumor tissues and cell cultures. Indirect estimations of metabolic phenotypes can be completed with bulk to single cell metabolic analysis, ranging in precision, price, and technical requirements.
In vitro, multiparameter metabolic analysis can be performed by individual assays or integrated solutions. Bench-top commercial solutions for metabolic assessment (nutrient uptake, enzymatic activity, ATP turnover, oxygen/pH/ROS probes, mitochondrial integrity) are available from most research suppliers.
Optical redox ratio (ORR) by two-photon excited fluorescence (TPEF) imaging of NAD(P)H and FAD co-enzymes designates relative changes in global metabolism and single-cell heterogeneity across cancer cells, organoids and animal models [197,198]. It is nondestructive, real-time and label-free, correlating well with both Seahorse flux and kit-based assays of glycolysis [199].
Glycolysis determination was previously reviewed by Tecla and Teitell, including useful tips and protocols [200]. Overall turnover of glucose, lactate, as well as glutamine and glutamate, can be measured using specialized biochemistry analyzers [201,202]. Bioluminescent assays can be adapted for high-throughput extracellular and intracellular detection of metabolites [203]. Focusing strictly on ATP production, the contribution of glycolysis and OXPHOS can be measured by conventional techniques, including enzymatic methods and targeted luciferase measurements [204]. It should be acknowledged that, even though many manufacturers are competing in this space, most commercial platforms are based on equivalent physicochemical principles (e.g., oxygen sensing probes for determination of OCR, redox-sensitive fluorophores, enzymatic assays). Common limitations include low throughput, single parameter readout, low specificity or signal, susceptibility to changes in pH, careful experimental design, and difficulty for normalization [205–208], Real-time respirometry using extracellular flux of live, adherent cells, is the most widespread technology to measure bioenergetics. In this set-up, mitochondrial respiration is extrapolated from oxygen-sensing electrodes or fluorescent/phosphorescent reporters to determine OCR over time, whereas the Warburg effect is calculated based on extracellular acidification rates (ECAR); specifically, extracellular pH changes due to proton extrusion coupled with lactate, imposing correction by the buffering power of the media and ignoring mitochondrial and pentose phosphate pathway (PPP) contributions to ECAR. OCR and ECAR are the two principal metabolic readouts in this field [209]. Intracellular O_2 can be compared to extracellular levels as an indicator of single-cell OXPHOS, using phosphorescent Pt-porphyrin-based probes [210,211]. To measure complementary parameters of intracellular metabolism, several exogenous and genetically-induced fluorescent reporters have been developed [61], as detailed in Table S1.
Even though polarography using high-resolution Clark electrodes (e.g., Oroboros oxygraphs) is considered the gold standard for assessing cellular oxygen dynamics, especially when multiplexed with mitochondrial membrane potential (MMP) or ADP–ATP exchange rates [212,213], higher-throughput and user-friendly devices such as Seahorse XF instruments (Agilent) are being validated by a higher number

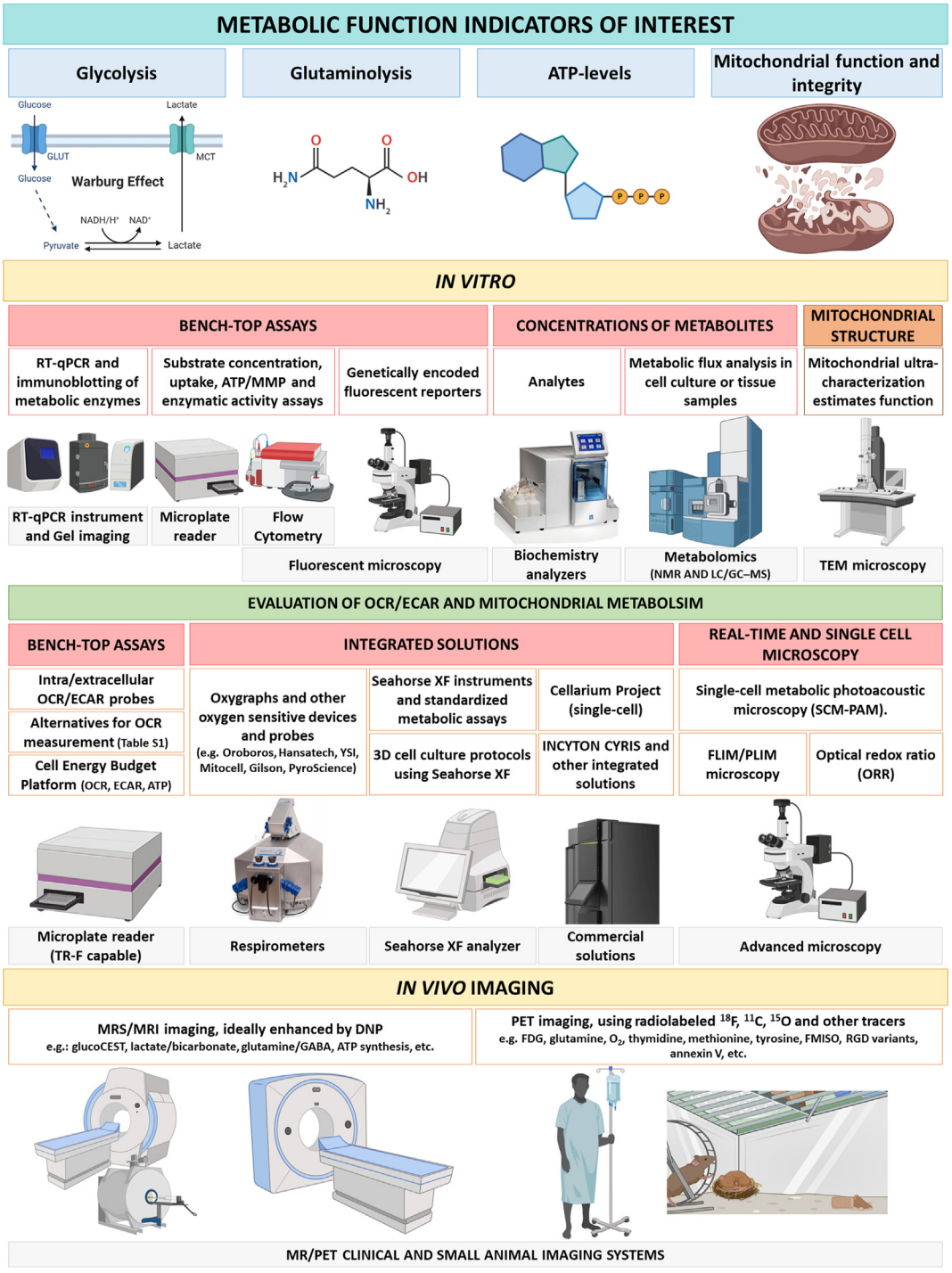

Figure 3: Methods to measure cancer metabolism *in vitro* and *in vivo*. Instruments and platforms required are indicated below each metabolic parameter. Detailed information about individual techniques, protocols and further reading is provided in Table S1.

of publications [214]. Oroboros and Seahorse XF are the leading platforms that are still continuously updated [215,216]. Rapid analysis of theoretical glycolytic and oxidative fluxes can be performed using the Seahorse XF and other microplate-based techniques, measuring relative changes in OCR/ECAR in response to different substrates (glucose, glutamine, fatty acids) and metabolic inhibitors [217]. For lower budgets, Takahashi et al. devised an inexpensive alternative for manually measuring OCR of adherent cells in a custom glassware sealed chamber, using an optical oxygen probe [218]. Basic overview of OCR measurements and guidelines have been extensively reviewed elsewhere [61,219,220]. If researchers opt to use extracellular flux analysis, raw OCR/ECAR data can be partitioned using special indexes [221]. Predictive models based on flux analysis have been postulated to quantify bioenergetic health, such as the "Bioenergetic Health Index" for peripheral blood cells [222] and "Mitochondrial Oncobioenergetic Index" for cultured tumoral cells [223].

Unfortunately, extracellular OCR has important caveats with regards to its interpretation as a marker of mitochondrial function. While extracellular flux analysis has become an accepted standard to measure metabolic parameters, without specific substrate inhibition it cannot granularly allocate their contribution to global OCR, be it destined for ATP generation, uncoupled respiration, and other pathways [220,224–226]. Careful attention needs to be devoted to "non-mitochondrial OCR", that is, cellular processes that consume oxygen outside the mitochondria, which has been shown to account for a large portion of OCR [194,227]. Contrary to what would be expected, data from numerous triple fuel inhibition Seahorse experiments (simultaneous targeting of pyruvate, glutamine, and FAO, detailed in Table S3) achieved only a small reduction in total OCR, suggestive of dysfunctional mitochondria or resistance to pathway inhibitors. Caution is advised when interpreting Seahorse results, as relative changes of basal OCR under mitochondrial inhibition are commonly presented as functional OXPHOS, but, OCR cannot fully evaluate mitochondrial function [29,228–230]. Schmidt et al. expertly reviewed the methodological concerns and limitations of extracellular flux analysis, recapitulating the high variability in coupling efficiency, need for normalization, avoidance of non-physiological and artefactual conditions, while also providing a workflow to reduce ambiguity when interrogating mitochondrial function [231]. OCR/ECAR readings should be complemented using additional techniques such as force flow analysis and single cell imaging to interrogate ATP synthesis, MMP, and confirm mitochondrial integrity.

For this purpose, Papkovsky et al. proposed a comprehensive protocol for bioenergetic assessment, the "Cell Energy Budget Platform" (CEB) [232]. Contrary to the Seahorse XF, CEB is designed to measure an extensive set of bioenergetic parameters without specialized equipment, except a time-resolved fluorescence reader. The CEB uses commercial fluorescent or luminescent probes and can be setup in a multi-well format to measure OCR, ECAR/pH (lactate and lactate/CO_2 extrusion), ATP production and total protein for normalization, as well as MMP, mitochondrial pH, redox state, NAD(P)H, and Ca2+.

An affordable and simple alternative for the measurement of oxygen uptake in biological samples has been developed using the Redflash technology from PyroScience [233]. This device can be adjusted to determine cell respiration, lactate excretion, and MMP where measuring actual lactate excretion is more specific of glycolysis than ECAR [234]. An added advantage is that oxygen-sensing optodes can be reutilized for years, circumventing repeated purchase of single-use cartridges [235].

The Cellarium platform was presented as an integrated solution with a significantly higher resolution, allowing for single cell analysis and confirming differences in the metabolic profiles of nearby cell populations [236]. Following these innovations, Hai et al. developed a high-throughput platform to assess OCR using single-cell metabolic photoacoustic microscopy (SCM-PAM), based on the hemoglobin exchange of oxygen in microwell arrays [237]. This method also avoids bulk-averaged measurements and further demonstrated metabolic heterogeneity at the cellular level. To match these technological advances, Agilent recently launched the Seahorse XF HS instrument with improved signal ratios and sensitivity [216].

Obtaining preclinical models to study tumor heterogeneity without the need of repeated, multi-site biopsies, is being facilitated by isolating circulating tumoral cells [238,239]. Still, the analysis of metabolism at the single-cell level is laborious and costly, not only by the intrinsic difficulty of isolating single cells, but also due to challenging computational workflows; therefore, streamlining these developments will be necessary to widen its adoption [240,241]

Single-cell analysis of intercellular heterogeneity should be examined in light of the tumoral microenvironment. Maintaining 3D cell-to-cell interactions and tissue structure could be crucial to truly recapitulate metabolic heterogeneity and avoid confounding factors of 2D cultures. Seahorse technology was adapted into a workflow to study 3D cultures and complex microtissues (organoids/organotypic models) [242]. Direct metabolic examination of tumor biopsies and healthy tissues is bridging the gap between *in vitro* and clinical studies [243,244]. Recently, a methodological summary for the characterization of organoids using the Seahorse technology was presented, circumventing common pitfalls by DNA-based normalization [245].

Statistical analysis of OCR/ECAR is especially problematic with a low number of samples, requiring careful design to avoid intra and inter-experimental background noise, invalid measurements, and outliers. Raw Seahorse XF measurements carry a complex data structure that requires advanced statistical modeling (e.g., OCR-Stats, OCRbayes) [219,246].

We consider the lack of absolute normalization as the main limiting factor to compare OCR/ECAR measurements between research groups. Currently, there is no standardized set of methods for normalization, leaving each researcher to normalize their experiments as they see fit. Data are regularly presented without advanced normalization, assuming it is comparable as long as an equal number of cells was seeded into each well, or normalized *ad-hoc* to protein/DNA content or cell number for each batch of experiments [247]. Therefore, inter-laboratory setups are personalized and virtually incomparable. As metabolism is highly dynamic due to cell handling and experimental conditions, as well as adjusted to specific normalization factors, the same cell lines measured in different circumstances can deliver vastly divergent results [248–251]. Flux rates, adjusted to cell number or DNA/protein, can be representative within the same experimental setup, but do not translate between research groups [247]. There have been strides towards a more universal normalization crystalized in Agilent's Seahorse XF Imaging and Normalization system, estimating cell number from brightfield and fluorescence images acquired by a compatible BioTek Cytation 1/5 Cytometer [252]. However, this upgrade is yet to see wide adoption and requires a separate instrument purchase. Complete platform integration would offer a standardized normalization factor across all applications.

A nondescriptive library of results acquired using Seahorse XF technology is assembled in the Cell Analysis Database from Agilent, but no attempts have been made to integrate this information. For the first time, we recapitulate metabolic heterogeneity *in vitro* determined by Seahorse XF technology in Figure 4. Seahorse Real-Time ATP assays (Figure 4 and Table S2) and Mito Fuel/Substrate Oxidation assays (Table S3) were selected for direct comparison between cell lines, irrespective of internal normalization factors. Raw OCR and ECAR rates cannot be accurately compared in different experimental setups unless following the same methodology for normalization. It is important to note that relative changes in OCR/ECAR-linked ATP ignore absolute ATP production rates, which can differ greatly depending on the basal metabolic activity of the cells.

In conclusion, mitochondrial dysfunction and the two-compartment model of cancer described earlier present numerous open questions that metabolic studies at the cellular and whole-tissue level could resolve. Primarily, characterize if oxidative and glycolytic phenotypes in cancers with proven mitochondrial defects are strict metabolic categories or various degrees of plasticity. Secondly, characterize if adaptive capacity evolves as a function of disease progression. Regarding metabolic therapy, glycolytic and oxidative compartments

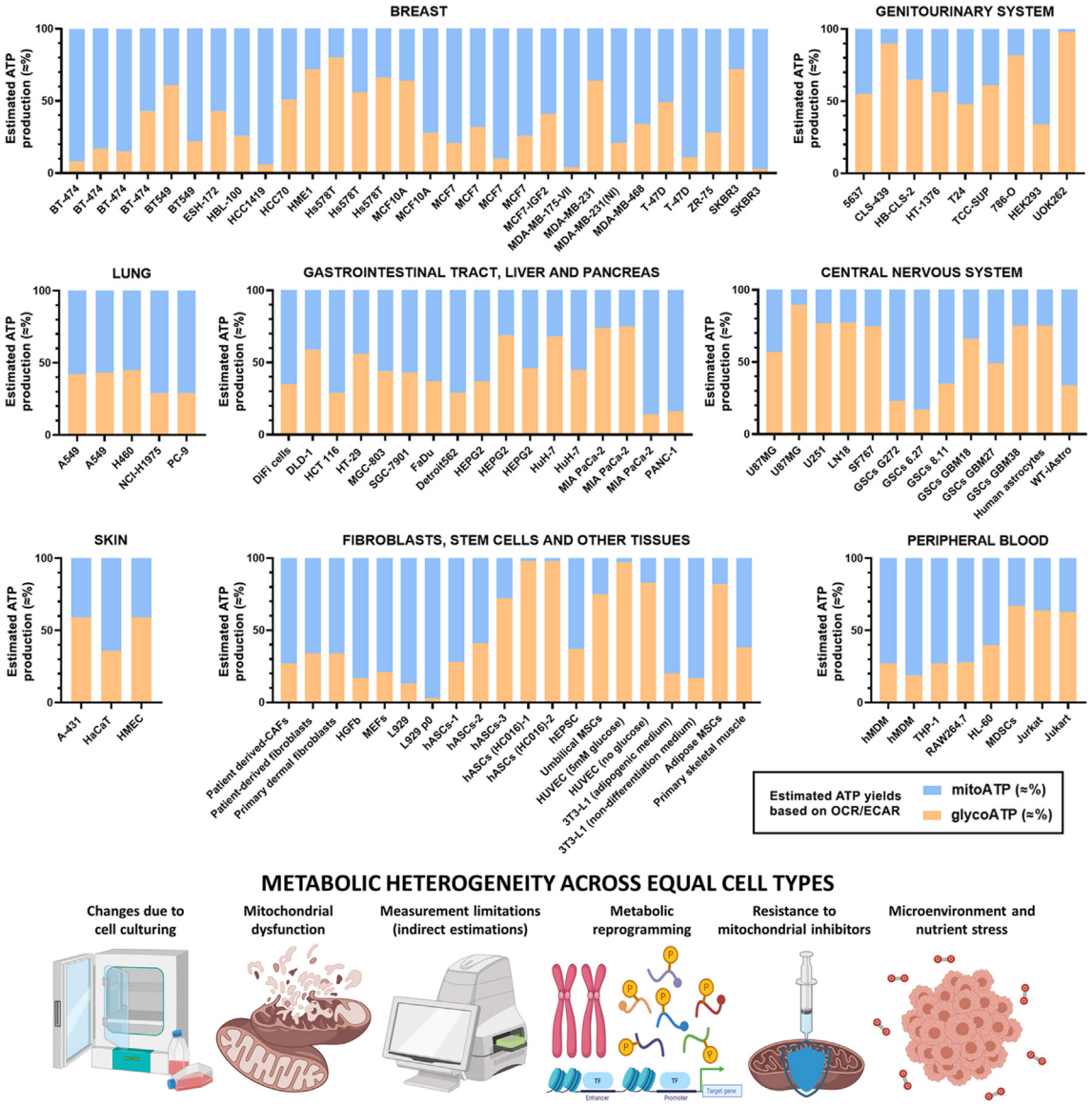

Figure 4: ECAR-linked (glycoATP) and OCR-linked (mitoATP) energy production, expressed as percentage of total ATP determined by Seahorse XF Real-Time ATP assays, in different cell lines and tissue origins. The ATP values are based on general stoichiometries, not cancer specific OXPHOS metabolic fluxes, and thus they represent only an assumed mathematical extrapolation. ATP is not being determined experimentally in this assay. High metabolic variability should be noted even in the same cell subtypes, especially when measured by independent authors (e.g., breast cancer cell lines SKBR3, BT549, Hs578T and T-47D; pancreatic cell line MIA PaCa-2; hepatic HEPG2 and others). Numerical values, methodology of analysis and references are provided in Tables S2 and S3.

should be determined and tackled simultaneously to improve therapeutic efficacy.

5.2. Additional considerations about *in vitro* experimental conditions and metabolic assays

Artificial environments need to be considered as powerful determinants of metabolic regulation. Metabolic changes can be partially owed to chemically treated, immortalized cell lines; arguably, such cells do not fully retain original metabolic phenotypes due to changes in nutrient concentrations, growth factors, lactate, oxygen/pH ranges, loss of complex 3D interactions, and other factors [253–255]. Cell culturing is directly responsible for several characteristics of altered metabolism, especially the interplay between the Warburg and Crabtree effect (an artifact of *in vitro* studies where fermentation represses respiration even under hyperoxia) [256]. Transformation is triggered by adherent cell growth and repeated cell detachment (metastatic phenotypes) [257–259], with cells having to transiently adapt to unfavorable medium compositions, as shown by glucose/glutamine deprivation experiments [260,261]. Mitochondrial defects can arise by subculturing, further obscuring oxidative ATP production [48]. Differences in cell handling and microenvironmental factors such as hypoxia can significantly alter readouts of direct measurements of metabolism in cell culture [66,262]. *In vivo*, nonlinear microenvironmental gradients regulate the metabolic state of tumoral cells [263,264]. Ideally, metabolic analysis would be performed on fresh tumor samples and organotypic/organoid models [265,266], or with the lowest passage number [267]. In recent years, significant strides have been made to design more physiological cell culture media and to characterize the

artifacts induced by an abnormal *in vitro* microenvironment [268–270]. Recognizing this issue and contrasting metabolic measurements performed in traditional cell culture with more representative and nuanced models could help to bridge the translational gap of metabolic therapy.

5.3. Metabolic imaging (PET/MRS)

Metabolic imaging is a noninvasive approach to measure bioenergetics *in vivo*. Positron emission tomography (PET) and proton magnetic resonance spectroscopy (^{1}H-MRS) are the two most widely adopted techniques. PET allows to visualize radioactive-labeled molecules as they travel across the body, with simultaneous anatomic localization by computed tomography (CT) or magnetic resonance imaging (MRI). Similarly, MRS is an MRI-based technique for the detection of spectral bands corresponding to several metabolites without the need for ionizing radiation. Acquisition can be performed in a relatively short time (10–15 min) but, without signal enhancements such as hyperpolarization, it is limited by low sensitivity.

To estimate glycolysis *in vivo*, PET-imaging with glucose analogues such as ^{18}F-fluorodeoxyglucose (^{18F}-FDG) is used to identify areas of high glucose uptake (GLUT1/3). ^{18}F-FDG has been standardized to image most anatomical enclaves. Despite poor sensitivity for tumors with low glycolysis and substantial cerebral/inflammatory background, FDG-PET has become an essential clinical tool for staging and response assessment [271,272]. To complete substrate allocation, alternative PET radiotracers are being investigated, as summarized in Table S1. One important limitation is that PET imaging can only evaluate uptake of tracers, which does not always correlate with real processing for fuel or biosynthesis.

MRS, in conjunction with metabolomic profiling, are a helpful combination to study intracellular flow of metabolites without radiolabeled tracers. ^{7}O-MRS and ^{31}P-MRS enable estimation of oxygen consumption and mitochondrial ATP synthesis, whereas ^{9}F-MRS has been proposed for measurement of glycolysis [273]. Metabolite concentrations correlated with survival [274,275], with quantification of metabolites such as glutamine, TCA cycle intermediaries, and lipids. Analysis of intratumoral/peritumoral pH and metabolites by enhanced ^{1}H-MRS methodologies such as the "chemical exchange saturation transfer" (CEST) and "biosensor imaging of redundant deviation in shifts" (BIRDS) allow for precise evaluation of glycolysis [276,277]. CEST can be used to detect the signal of glucose (glucoCEST) and lactate. T1ρ-weighted dynamic glucose-enhanced (DGE)-MRI has been used to reveal *in vivo* glucose metabolism [278]. D-glucose is also being evaluated as a biodegradable contrast, but its use to monitor metabolic responses remains unclear [279].

Under this section, we would like to highlight the promise of novel dynamic nuclear polarization (DNP)-enhanced ^{13}C tracers, which allow to study pyruvate to lactate/bicarbonate flux, KBs uptake, and other pathways such as the PPP or redox capacity, with improved signal ratios [280,281]. Integration into routine clinical practice could significantly improve pre/post-treatment metabolic evaluation [282].

Unfortunately, while conventional PET/MRS imaging can provide an overview of preferences towards specific metabolites, it does not inform about distribution inside cells. At this time, a wider array of methods should be employed to obtain a complete metabolic picture. There have been some successful pilot studies that included combined metabolic measurements; for example, Neveu et al. determined FDG uptake, lactate production, tumor oxygenation, and metabolic fluxes *in vivo*, using PET, microdialysis, electron paramagnetic resonance imaging, and [^{13}C]-hyperpolarized MRS, respectively [283,284]. CTs and case reports evaluating the safety and efficacy of metabolic therapies often include some form of basic metabolic imaging (mostly FDG-PET), but rarely direct tissue-level metabolic analysis, so patient stratification remains an unresolved problem [187,285]. In clinical contexts, reduced access to precise and easy-to-use tools to measure relevant metabolic information is likely responsible for this limitation.

5.4. Metabolomics and metabolic profiling

Metabolic profiling, using metabolomics, is the measurement of low-molecular-weight metabolites and intermediates from biological samples, and offers a panoramic view of the dynamic response to molecular and pathophysiological stimuli [286–289].

Flux of metabolites through metabolic pathways is key to understand how cancer cells meet their bioenergetic demands. A wide variety of metabolomic techniques can identify cancer related metabolites, such as liquid and gas chromatography-mass spectrometry (LC/GC–MS) and nuclear magnetic resonance spectroscopy (NMR). Dynamic characterization of metabolism is a daunting task due to cellular adjustments to everchanging concentrations and microenvironments [290,291]. Stable isotope-resolved metabolomics (SIRM) is a tool for such dynamic studies, illustrating the mechanism of action of pathway inhibitors and quantifying downstream metabolites [292,293].

Raw metabolomic data can be processed by "Pathway Activity Profiling (PAPi) to predict dysregulated metabolic pathways [294]. MS-based metabolomics are particularly relevant for direct evaluation of bioenergetic metabolism in bulk biological samples [295]. Clinical data from a broad range of cancers suggests that metabolomics can improve classification of biopsies [286]. In conclusion, when available, metabolomic approaches could be applied for patient stratification, especially as a first order overview of biopsies. Accurate tracing of metabolites uncovers a more detailed picture of their distribution than averaged OCR/ECAR measurements [296,297].

5.5. Mitochondrial structure and mtDNA mutations as indicators of mitochondrial function

Mitochondria are bioenergetic, biosynthetic and signaling organelles, playing a vital role in adaptation to changes in the microenvironment and tumorigenesis [298]. Ultrastructural characterization of mitochondrial membranes provides insights about the relative state of the mitochondria in a pool of cells, but it is not easy to perform and requires specialized equipment [299]. As previously discussed, the most widespread tool to assess mitochondrial function indirectly is to evaluate OCR fluctuations under sequential ETC inhibition. Nevertheless, mitochondrial health in cancer is a source of controversy. To examine function in light of structure, an argument has been made for the identification of structural defects, mitochondrial mass, and mtDNA mutations [29]. As cytotoxic drugs have been shown to inflict structural damage to the mitochondria, and resistance to chemotherapy is linked with their dysfunction, analyzing mitochondrial fitness may be warranted in chemoresistant tumors [300–302].

Moreover, mtDNA mutations have been proposed as biomarkers for early detection, acting as negative regulators of OXPHOS [303–305]. In certain cancers, such as bladder, lung, and head/neck tumors, mtDNA mutations were even more abundant than nuclear mutations [306]. Increased mitochondrial biogenesis is essential for tumorigenesis [307], and analysis of total mitochondrial mass reveals differences between tumoral and normal cells [308,309]. Although the functional effects of all mtDNA mutations have not been fully elucidated [310,311], mitochondrial intercellular transfer and transplantation experiments hold the promise of restoring oxidative function, reversing cancer proliferation and overcoming therapeutic resistance [312–315].

6. CONCLUDING REMARKS

For appropriate metabolic therapy, substrate flexibility needs to be studied in advance, as cancer subtypes will show distinct fuel preferences. To achieve this, we summarized techniques to measure key metabolic parameters *in vitro* and *in vivo*, accommodating different research needs and budgets. Our straightforward flow chart could be used to approach clinical metabolic analysis. Taking all these complexities into account will advance our understanding of the contribution of metabolism to cancer origin and progression. Where characterization drives subsequent treatment, the collection of metabolic data in different tumor specimens, interventions and microenvironments is essential. Our hope is that, as more researchers contemplate including metabolic measurements in their studies, bioenergetic classification will unlock fundamental insights for improved cancer treatments.

AUTHOR CONTRIBUTIONS

Writing - original draft, T.D.; Writing - review & editing, T.D., N.G.-R., T.N.S.; Visualization: P.C.N.; Supervision: A.A.-S. All authors have read and agreed to the published version of the manuscript.

FUNDING

This research was funded by grants from the "Fondo de Investigaciones Sanitarias" (FIS) (PI17-01489), the Ministerio de Economía y Competitividad (RTC2019-006918-1). Research funded by Ministerio de Educación, Cultura y Deporte (FPU16/03198).

DATA AVAILABILITY STATEMENT

The data presented in this review are available and individually cited in the Supplementary Materials.

ACKNOWLEDGMENTS

Original figures created with BioRender and GraphPad software.

CONFLICT OF INTEREST

None declared.

APPENDIX A. SUPPLEMENTARY DATA

Supplementary data to this article can be found online at https://doi.org/10.1016/j.molmet.2021.101389.

REFERENCES

[1] Hanahan, D., Weinberg, R.A.J., 2011. Hallmarks of cancer: the next generation. Cell 144(5):646—674.
[2] Soto, A.M., Sonnenschein, C., 2004. The somatic mutation theory of cancer: growing problems with the paradigm? BioEssays 26(10):1097.
[3] Vogelstein, B., Kinzler, K.W., 2015. The path to cancer -Three strikes and you're out. New England Journal of Medicine 373(20):1895.
[4] Ladanie, A., Schmitt, A.M., Speich, B., Naudet, F., Agarwal, A., Pereira, T.V., et al., 2020. Clinical trial evidence supporting US food and drug administration approval of novel cancer therapies between 2000 and 2016. JAMA Network Open 3(11) e2024406-e2024406.
[5] Burgio, E., Migliore, L.J., 2015. Towards a systemic paradigm in carcinogenesis: linking epigenetics and genetics. Molecular Biology Reports 42(4): 777—790.
[6] Sonnenschein, C., Soto, A.M., 2000. Somatic mutation theory of carcinogenesis: why it should be dropped and replaced. Molecular Carcinogenesis 29(4):205—211.
[7] Warburg, O., 1956. On the origin of cancer cells. Science (New York, N.Y.) 123(3191):309.
[8] Poljsak, B., Kovac, V., Dahmane, R., Levec, T., Starc, A.J.O.m., longevity, c., 2019. Cancer etiology: a metabolic disease originating from life's major evolutionary transition? 2019.
[9] Seyfried, T.N., Arismendi-Morillo, G., Mukherjee, P., Chinopoulos, C., 2020. On the origin of ATP synthesis in cancer. iScience 23(11):101761.
[10] Saxton, R.A., Sabatini, D.M., 2017. mTOR signaling in growth, metabolism, and disease. Cell 168(6):960.
[11] Cairns, R.A., Harris, I.S., Mak, T.W., 2011. Regulation of cancer cell metabolism. Nature Reviews Cancer 11(2):85.
[12] Yu, L., Lu, M., Jia, D., Ma, J., Ben-Jacob, E., Levine, H., et al., 2017. Modeling the genetic regulation of cancer metabolism: interplay between glycolysis and oxidative phosphorylation. Cancer Research 77(7):1564.
[13] Cantor, J.R., Sabatini, D.M., 2012. Cancer cell metabolism: one hallmark, many faces. Cancer Discovery 2(10):881.
[14] Kim, A., 2015. Mitochondria in cancer energy metabolism: culprits or bystanders? Toxicological Research 31(4):323.
[15] Berg, J.M., Tymoczko, J.L., Stryer, L., 2002. Biochemistry. New York: W. H. Freeman.
[16] Vander Heiden, M.G., Cantley, L.C., Thompson, C.B., 2009. Understanding the Warburg effect: the metabolic requirements of cell proliferation. Science (New York, N.Y.) 324(5930):1029.
[17] Vander Heiden, M.G., Cantley, L.C., Thompson, C.B., 2009. Understanding the Warburg effect: the metabolic requirements of cell proliferation. Science 324(5930):1029—1033.
[18] DeBerardinis, R.J., Mancuso, A., Daikhin, E., Nissim, I., Yudkoff, M., Wehrli, S., et al., 2007. Beyond aerobic glycolysis: transformed cells can engage in glutamine metabolism that exceeds the requirement for protein and nucleotide synthesis. Proceedings of the National Academy of Sciences 104(49):19345—19350.
[19] Pavlides, S., Whitaker-Menezes, D., Castello-Cros, R., Flomenberg, N., Witkiewicz, A.K., Frank, P.G., et al., 2009. The reverse Warburg effect: aerobic glycolysis in cancer associated fibroblasts and the tumor stroma. Cell Cycle 8(23):3984.
[20] Lin, X., Xiao, Z., Chen, T., Liang, S.H., Guo, H.J., 2020. Glucose metabolism on tumor plasticity, diagnosis, and treatment. Frontiers in Oncology 10:317.
[21] DeBerardinis, R.J., Chandel, N.S., 2020. We need to talk about the Warburg effect. Nature Metabolism 2(2):127—129.
[22] Gravenmier, C.A., Siddique, M., Gatenby, R.A., 2017. Adaptation to stochastic temporal variations in intratumoral blood flow: the Warburg effect as a bet hedging strategy. Bulletin of Mathematical Biology 1.
[23] Mazzocca, A.J., 2019. The systemic—evolutionary theory of the origin of cancer (SETOC): a new interpretative model of cancer as a complex biological system. International Journal of Molecular Sciences 20(19):4885.
[24] Epstein, T., Gatenby, R.A., Brown, J.S., 2017. The Warburg effect as an adaptation of cancer cells to rapid fluctuations in energy demand. PLoS One 12(9):e0185085.
[25] Zahra, K., Dey, T., Ashish, A., Pandey, U., Mishra, S.P., 2020. Pyruvate kinase M2 and cancer: the role of PKM2 in promoting tumorigenesis. Frontiers in Oncology 10:159.
[26] Vander Heiden, M.G., Locasale, J.W., Swanson, K.D., Sharfi, H., Heffron, G.J., Amador-Noguez, D., et al., 2010. Evidence for an alternative glycolytic pathway in rapidly proliferating cells. Science 329(5998):1492—1499.

[27] Seyfried, T.N., 2015. Cancer as a mitochondrial metabolic disease. Frontiers in Cell and Developmental 3:43.
[28] Koppenol, W.H., Bounds, P.L., Dang, C.V., 2011. Otto Warburg's contributions to current concepts of cancer metabolism. Nature Reviews Cancer 11(5): 325–337.
[29] Seyfried, T.N., Arismendi-Morillo, G., Mukherjee, P., Chinopoulos, C., 2020. On the origin of ATP synthesis in cancer. Iscience 23(11):101761.
[30] Kiebish, M.A., Han, X., Cheng, H., Chuang, J.H., Seyfried, T.N.J., 2008. Cardiolipin and electron transport chain abnormalities in mouse brain tumor mitochondria: lipidomic evidence supporting the Warburg theory of cancer. Journal of Lipid Research 49(12):2545–2556.
[31] Sonveaux, P., Vegran, F., Schroeder, T., Wergin, M.C., Verrax, J., Rabbani, Z.N., et al., 2008. Targeting lactate-fueled respiration selectively kills hypoxic tumor cells in mice. Journal of Clinical Investigation 118(12):3930.
[32] Payen, V.L., Mina, E., Van Hée, V.F., Porporato, P.E., Sonveaux, P., 2020. Monocarboxylate transporters in cancer. Molecular Metabolism 33:48–66.
[33] Witkiewicz, A.K., Whitaker-Menezes, D., Dasgupta, A., Philp, N.J., Lin, Z., Gandara, R., et al., 2012. Using the "reverse Warburg effect" to identify high-risk breast cancer patients: stromal MCT4 predicts poor clinical outcome in triple-negative breast cancers. Cell Cycle 11(6):1108.
[34] Whitaker-Menezes, D., Martinez-Outschoorn, U.E., Lin, Z., Ertel, A., Flomenberg, N., Witkiewicz, A.K., et al., 2011. Evidence for a stroma-epithelial "lactate shuttle" in human tumors: MCT4 is a marker of oxidative stress in cancer-associated fibroblasts. Cell Cycle 10(11):1772.
[35] Ko, Y.-H., Lin, Z., Flomenberg, N., Pestell, R.G., Howell, A., Sotgia, F., et al., 2011. Glutamine fuels a vicious cycle of autophagy in the tumor stroma and oxidative mitochondrial metabolism in epithelial cancer cells: implications for preventing chemotherapy resistance. Cancer Biology & Therapy 12(12):1085.
[36] TeSlaa, T., Bartman, C.R., Jankowski, C.S., Zhang, Z., Xu, X., Xing, X., et al., 2021. The source of glycolytic intermediates in mammalian tissues. Cell Metabolism 33(2):367–378 e365.
[37] Hui, S., Ghergurovich, J.M., Morscher, R.J., Jang, C., Teng, X., Lu, W., et al., 2017. Glucose feeds the TCA cycle via circulating lactate. Nature 551(7678): 115–118.
[38] Otto, A.M., 2020. Metabolic constants and plasticity of cancer cells in a limiting glucose and glutamine microenvironment—a pyruvate perspective. Frontiers in Oncology 10.
[39] Seyfried, T., 2012. Cancer as a metabolic disease: on the origin, management, and prevention of cancer. John Wiley & Sons.
[40] Pavlova, N.N., Thompson, C.B., 2016. The emerging hallmarks of cancer metabolism. Cell Metabolism 23(1):27.
[41] Kim, J., DeBerardinis, R.J., 2019. Mechanisms and implications of metabolic heterogeneity in cancer. Cell Metabolism 30(3):434–446.
[42] Fadaka, A., Ajiboye, B., Ojo, O., Adewale, O., Olayide, I., Emuowhochere, R.J., 2017. Biology of glucose metabolization in cancer cells. Journal of Oncological Sciences 3(2):45–51.
[43] Ashton, T.M., McKenna, W.G., Kunz-Schughart, L.A., Higgins, G.S., 2018. Oxidative phosphorylation as an emerging target in cancer therapy. Clinical Cancer Research 24(11):2482–2490.
[44] Sapandowski, A., Stope, M., Evert, K., Evert, M., Zimmermann, U., Peter, D., et al., 2015. Cardiolipin composition correlates with prostate cancer cell proliferation. Molecular and Cellular Biochemistry 410(1–2):175.
[45] Kiebish, M.A., Han, X., Cheng, H., Chuang, J.H., Seyfried, T.N., 2008. Cardiolipin and electron transport chain abnormalities in mouse brain tumor mitochondria: lipidomic evidence supporting the Warburg theory of cancer. Journal of Lipid Research 49(12):2545.
[46] Peyta, L., Jarnouen, K., Pinault, M., Guimaraes, C., de Barros, J.-P.P., Chevalier, S., et al., 2016. Reduced cardiolipin content decreases respiratory chain capacities and increases ATP synthesis yield in the human HepaRG cells. Biochimica et Biophysica Acta (BBA) - Bioenergetics 1857(4):443.
[47] Leznev, E.I., Popova Il, , Lavrovskaja, V.P., Evtodienko, Y.V., 2013. Comparison of oxygen consumption rates in minimally transformed BALB/3T3 and virus-transformed 3T3B-SV40 cells. Biochemistry (Moscow) 78(8):904.
[48] Kiebish, M.A., Han, X., Cheng, H., Seyfried, T.N., 2009. In vitro growth environment produces lipidomic and electron transport chain abnormalities in mitochondria from non-tumorigenic astrocytes and brain tumours. ASN Neuro 1(3):AN20090011.
[49] Quintana-Cabrera, R., Mehrotra, A., Rigoni, G., Soriano, M., 2018. Who and how in the regulation of mitochondrial cristae shape and function. Biochemical and Biophysical Research Communications 500(1):94–101.
[50] Zick, M., Rabl, R., Reichert, A.S., 2009. Cristae formation—linking ultrastructure and function of mitochondria. Biochimica et Biophysica Acta (BBA) - Molecular Cell Research 1793(1):5–19.
[51] Kaipparettu, B.A., Ma, Y., Park, J.H., Lee, T.-L., Zhang, Y., Yotnda, P., et al., 2013. Crosstalk from non-cancerous mitochondria can inhibit tumor properties of metastatic cells by suppressing oncogenic pathways. PLoS One 8(5): e61747.
[52] Sun, C., Liu, X., Wang, B., Wang, Z., Liu, Y., Di, C., et al., 2019. Endocytosis-mediated mitochondrial transplantation: transferring normal human astrocytic mitochondria into glioma cells rescues aerobic respiration and enhances radiosensitivity. Theranostics 9(12):3595.
[53] Tan, A.S., Baty, J.W., Dong, L.-F., Bezawork-Geleta, A., Endaya, B., Goodwin, J., et al., 2015. Mitochondrial genome acquisition restores respiratory function and tumorigenic potential of cancer cells without mitochondrial DNA. Cell Metabolism 21(1):81–94.
[54] Grasso, D., Zampieri, L.X., Capelôa, T., Van de Velde, J.A., Sonveaux, P., 2020. Mitochondria in cancer. Nature Reviews Cancer 4(6):114.
[55] Cardaci, S., Zheng, L., MacKay, G., Van Den Broek, N.J.F., MacKenzie, E.D., Nixon, C., et al., 2015. Pyruvate carboxylation enables growth of SDH-deficient cells by supporting aspartate biosynthesis. Nature Cell Biology 17(10):1317.
[56] Mullen, A.R., Wheaton, W.W., Jin, E.S., Chen, P.-H., Sullivan, L.B., Cheng, T., et al., 2012. Reductive carboxylation supports growth in tumour cells with defective mitochondria. Nature 481(7381):385.
[57] Guzy, R.D., Sharma, B., Bell, E., Chandel, N.S., Schumacker, P.T., 2008. Loss of the SdhB, but Not the SdhA, subunit of complex II triggers reactive oxygen species-dependent hypoxia-inducible factor activation and tumorigenesis. Molecular and Cellular Biology 28(2):718.
[58] Wu, M., Neilson, A., Swift, A.L., Moran, R., Tamagnine, J., Parslow, D., et al., 2007. Multiparameter metabolic analysis reveals a close link between attenuated mitochondrial bioenergetic function and enhanced glycolysis dependency in human tumor cells. American Journal of Physiology - Cell Physiology 292(1):C125–C136.
[59] Keibler, M.A., Wasylenko, T.M., Kelleher, J.K., Iliopoulos, O., Vander Heiden, M.G., Stephanopoulos, G., 2016. Metabolic requirements for cancer cell proliferation. Cancer & Metabolism 4(1):16.
[60] Shiratori, R., Furuichi, K., Yamaguchi, M., Miyazaki, N., Aoki, H., Chibana, H., et al., 2019. Glycolytic suppression dramatically changes the intracellular metabolic profile of multiple cancer cell lines in a mitochondrial metabolism-dependent manner. Scientific Reports 9(1):1–15.
[61] Connolly, N.M., Theurey, P., Adam-Vizi, V., Bazan, N.G., Bernardi, P., Bolaños, J.P., et al., 2018. Guidelines on experimental methods to assess mitochondrial dysfunction in cellular models of neurodegenerative diseases. Cell Death & Differentiation 25(3):542–572.
[62] Yuneva, M.O., Fan, T.W., Allen, T.D., Higashi, R.M., Ferraris, D.V., Tsukamoto, T., et al., 2012. The metabolic profile of tumors depends on both the responsible genetic lesion and tissue type. Cell Metabolism 15(2): 157–170.
[63] Vyas, S., Zaganjor, E., Haigis, M.C., 2016. Mitochondria and cancer. Nature Reviews Cancer 166(3):555–566.

[64] Viale, A., Corti, D., Draetta, G.F., 2015. Tumors and mitochondrial respiration: a neglected connection. Cancer Research 75(18):3687—3691.

[65] Ni Chonghaile, T., Sarosiek, K.A., Vo, T.T., Ryan, J.A., Tammareddi, A., Moore Vdel, G., et al., 2011. Pretreatment mitochondrial priming correlates with clinical response to cytotoxic chemotherapy. Science (New York, N.Y.) 334(6059):1129.

[66] Wagner, B.A., Venkataraman, S., Buettner, G.R., 2011. The rate of oxygen utilization by cells. Free Radical Biology and Medicine 51(3):700—712.

[67] Horan, M.P., Pichaud, N., Ballard, J.W.O.J., 2012. Quantifying mitochondrial dysfunction in complex diseases of aging. Journal of Gerontology 67(10): 1022—1035.

[68] DeBerardinis, R.J., Cheng, T., 2010. Q's next: the diverse functions of glutamine in metabolism, cell biology and cancer. Oncogene 29(3):313.

[69] Yuneva, M., 2008. Finding an "Achilles' heel" of cancer: the role of glucose and glutamine metabolism in the survival of transformed cells. Cell Cycle 7(14):2083.

[70] Zielke, H.R., Zielke, C.L., Ozand, P.T., 1984. Glutamine: a major energy source for cultured mammalian cells. Federation Proceedings 43(1):121.

[71] Chinopoulos, C., 2013. Which way does the citric acid cycle turn during hypoxia? The critical role of α-ketoglutarate dehydrogenase complex. Journal of Neuroscience Research 91(8):1030.

[72] Schwimmer, C., Lefebvre-Legendre, L., Rak, M., Devin, A., Slonimski, P.P., di Rago, J.P., et al., 2005. Increasing mitochondrial substrate-level phosphorylation can rescue respiratory growth of an ATP synthase-deficient yeast. Journal of Biological Chemistry 280(35):30751.

[73] Saragovi, A., Abramovich, I., Omar, I., Arbib, E., Toker, O., Gottlieb, E., et al., 2020. Systemic hypoxia inhibits T cell response by limiting mitobiogenesis via matrix substrate-level phosphorylation arrest. Elife 9:e56612.

[74] Chen, Q., Kirk, K., Shurubor, Y.I., Zhao, D., Arreguin, A.J., Shahi, I., et al., 2018. Rewiring of glutamine metabolism is a bioenergetic adaptation of human cells with mitochondrial DNA mutations. Cell Metabolism 27(5): 1007—1025 e1005.

[75] Fan, J., Kamphorst, J.J., Mathew, R., Chung, M.K., White, E., Shlomi, T., et al., 2013. Glutamine-driven oxidative phosphorylation is a major ATP source in transformed mammalian cells in both normoxia and hypoxia. Molecular Systems Biology 9:712.

[76] Wang, Z., Liu, F., Fan, N., Zhou, C., Li, D., Macvicar, T., et al., 2020. Targeting glutaminolysis: new perspectives to understand cancer development and novel strategies for potential target therapies. Frontiers in Oncology 10.

[77] Kiss, G., Konrad, C., Pour-Ghaz, I., Mansour, J.J., Nemeth, B., Starkov, A.A., et al., 2014. Mitochondrial diaphorases as NAD(+) donors to segments of the citric acid cycle that support substrate-level phosphorylation yielding ATP during respiratory inhibition. The FASEB Journal : Official Publication of the Federation of American Societies for Experimental Biology 28(4):1682.

[78] Hosios, A.M., Hecht, V.C., Danai, L.V., Johnson, M.O., Rathmell, J.C., Steinhauser, M.L., et al., 2016. Amino acids rather than glucose account for the majority of cell mass in proliferating mammalian cells. Developmental Cell 36(5):540.

[79] DeBerardinis, R.J., Mancuso, A., Daikhin, E., Nissim, I., Yudkoff, M., Wehrli, S., et al., 2007. Beyond aerobic glycolysis: transformed cells can engage in glutamine metabolism that exceeds the requirement for protein and nucleotide synthesis. Proceedings of the National Academy of Sciences of the United States of America 104(49):19345.

[80] Huang, W., Choi, W., Chen, Y., Zhang, Q., Deng, H., He, W., et al., 2013. A proposed role for glutamine in cancer cell growth through acid resistance. Cell Research 23(5):724.

[81] Spinelli, J.B., Yoon, H., Ringel, A.E., Jeanfavre, S., Clish, C.B., Haigis, M.C., 2017. Metabolic recycling of ammonia via glutamate dehydrogenase supports breast cancer biomass. Science 358(6365):941—946.

[82] Bott, A.J., Maimouni, S., Zong, W.-X., 2019. The pleiotropic effects of glutamine metabolism in cancer. Cancers 11(6):770.

[83] Huang, W., Choi, W., Chen, Y., Zhang, Q., Deng, H., He, W., et al., 2013. A proposed role for glutamine in cancer cell growth through acid resistance. Cell Research 23(5):724—727.

[84] Still, E.R., Yuneva, M.O.J., 2017. Hopefully devoted to Q: targeting glutamine addiction in cancer. British Journal of Cancer 116(11):1375—1381.

[85] Jiang, J., Srivastava, S., Zhang, J., 2019. Starve cancer cells of glutamine: break the spell or make a hungry monster? Cancers 11(6):804.

[86] Kim, G.W., Lee, D.H., Jeon, Y.H., Yoo, J., Kim, S.Y., Lee, S.W., et al., 2021. Glutamine synthetase as a therapeutic target for cancer treatment. International Journal of Molecular Sciences 22(4):1701.

[87] Nicklin, P., Bergman, P., Zhang, B., Triantafellow, E., Wang, H., Nyfeler, B., et al., 2009. Bidirectional transport of amino acids regulates mTOR and autophagy. Cell 136(3):521.

[88] Villar, V.H., Merhi, F., Djavaheri-Mergny, M., Durán, R.V., 2015. Glutaminolysis and autophagy in cancer. Autophagy 11(8):1198—1208.

[89] Hensley, C.T., Wasti, A.T., DeBerardinis, R.J., 2013. Glutamine and cancer: cell biology, physiology, and clinical opportunities. Journal of Clinical Investigation 123(9):3678.

[90] Hirayama, A., Kami, K., Sugimoto, M., Sugawara, M., Toki, N., Onozuka, H., et al., 2009. Quantitative metabolome profiling of colon and stomach cancer microenvironment by capillary electrophoresis time-of-flight mass spectrometry. Cancer Research 69(11):4918.

[91] Matés, J.M., Di Paola, F.J., Campos-Sandoval, J.A., Mazurek, S., Márquez, J., 2020. Therapeutic targeting of glutaminolysis as an essential strategy to combat cancer. In: Seminars in cell & developmental biology. Elsevier. p. 34—43.

[92] Rodwell, V.W., Bender, D.A., Botham, K.M., Kennelly, P.J., Weil, P.A., 2018. Harper's illustrated biochemistry. New York (NY): McGraw-Hill Education.

[93] Boroughs, L.K., DeBerardinis, R.J., 2015. Metabolic pathways promoting cancer cell survival and growth. Nature Cell Biology 17(4):351.

[94] Huang, D., Li, T., Li, X., Zhang, L., Sun, L., He, X., et al., 2014. HIF-1-mediated suppression of acyl-CoA dehydrogenases and fatty acid oxidation is critical for cancer progression. Cell Reports 8(6):1930—1942.

[95] Parks, S.K., Mazure, N.M., Counillon, L., Pouysségur, J., 2013. Hypoxia promotes tumor cell survival in acidic conditions by preserving ATP levels. Journal of Cellular Physiology 228(9):1854.

[96] Ma, Y., Temkin, S.M., Hawkridge, A.M., Guo, C., Wang, W., Wang, X.-Y., et al., 2018. Fatty acid oxidation: an emerging facet of metabolic transformation in cancer. Cancer Letters 435:92—100.

[97] Mikalayeva, V., Ceslevičienė, I., Sarapinienė, I., Žvikas, V., Skeberdis, V.A., Jakštas, V., et al., 2019. Fatty acid synthesis and degradation interplay to regulate the oxidative stress in cancer cells. International Journal of Molecular Sciences 20(6):1348.

[98] Koundouros, N., Poulogiannis, G.J.B., 2020. Reprogramming of fatty acid metabolism in cancer. Cancers 122(1):4—22.

[99] Seyfried, T.N., Yu, G., Maroon, J.C., D'Agostino, D.P., 2017. Press-pulse: a novel therapeutic strategy for the metabolic management of cancer. Nutrition & Metabolism 14(1):19.

[100] Weber, D.D., Aminzadeh-Gohari, S., Tulipan, J., Catalano, L., Feichtinger, R.G., Kofler, B.J., 2020. Ketogenic diet in the treatment of cancer—where do we stand? Molecular Metabolism 33:102—121.

[101] Jaworski, D.M., Namboodiri, A., Moffett, J.R., 2016. Acetate as a metabolic and epigenetic modifier of cancer therapy. Journal of Cellular Biochemistry 117(3):574.

[102] Poff, A.M., Ari, C., Arnold, P., Seyfried, T.N., D'Agostino, D.P., 2014. Ketone supplementation decreases tumor cell viability and prolongs survival of mice with metastatic cancer. International Journal of Cancer 135(7):1711.

[103] Maurer, G.D., Brucker, D.P., Bähr, O., Harter, P.N., Hattingen, E., Walenta, S., et al., 2011. Differential utilization of ketone bodies by neurons and glioma cell lines: a rationale for ketogenic diet as experimental glioma therapy. BMC Cancer 11(1):315.

[104] Schug, Z.T., Peck, B., Jones, D.T., Zhang, Q., Grosskurth, S., Alam, I.S., et al., 2015. Acetyl-CoA synthetase 2 promotes acetate utilization and maintains cancer cell growth under metabolic stress. Cancer Cell 27(1):57.
[105] De Oliveira, M.P., Liesa, M.J.C., 2020. The role of mitochondrial fat oxidation in. Cancer Cell Proliferation and Survival 9(12):2600.
[106] Magee, B.A., Potezny, N., Rofe, A.M., Conyers, R.A., 1979. The inhibition of malignant cell growth by ketone bodies. Australian Journal of Experimental Biology & Medical Science 57(5):529.
[107] Martinez-Outschoorn, U.E., Prisco, M., Ertel, A., Tsirigos, A., Lin, Z., Pavlides, S., et al., 2011. Ketones and lactate increase cancer cell "stemness," driving recurrence, metastasis and poor clinical outcome in breast cancer: achieving personalized medicine via Metabolo-Genomics. Cell Cycle 10(8):1271.
[108] Rabinowitz, J.D., White, E., 2010. Autophagy and metabolism. Science (New York, N.Y.) 330(6009):1344.
[109] Hirschhaeuser, F., Sattler, U.G., Mueller-Klieser, W., 2011. Lactate: a metabolic key player in cancer. Cancer Research 71(22):6921.
[110] Draoui, N., Feron, O., 2011. Lactate shuttles at a glance: from physiological paradigms to anti-cancer treatments. Disease Models & Mechanisms 4(6):727.
[111] Fu, Y., Liu, S., Yin, S., Niu, W., Xiong, W., Tan, M., et al., 2017. The reverse Warburg effect is likely to be an Achilles' heel of cancer that can be exploited for cancer therapy. Oncotarget 8(34):57813.
[112] Pavlides, S., Vera, I., Gandara, R., Sneddon, S., Pestell, R.G., Mercier, I., et al., 2012. Warburg meets autophagy: cancer-associated fibroblasts accelerate tumor growth and metastasis via oxidative stress, mitophagy, and aerobic glycolysis. Antioxidants and Redox Signaling 16(11):1264–1284.
[113] Martinez-Outschoorn, U.E., Sotgia, F., Lisanti, M.P., 2012. Power surge: supporting cells "fuel" cancer cell mitochondria. Cell Metabolism 15(1):4.
[114] Kennedy, K.M., Scarbrough, P.M., Ribeiro, A., Richardson, R., Yuan, H., Sonveaux, P., et al., 2013. Catabolism of exogenous lactate reveals it as a legitimate metabolic substrate in breast cancer. PLoS One 8(9):e75154.
[115] Fiaschi, T., Marini, A., Giannoni, E., Taddei, M.L., Gandellini, P., De Donatis, A., et al., 2012. Reciprocal metabolic reprogramming through lactate shuttle coordinately influences tumor-stroma interplay. Cancer Research 72(19):5130.
[116] Luo, Y., Ma, J., Lu, W.J.I., 2020. The significance of mitochondrial dysfunction in cancer. International Journal of Molecular Sciences 21(16):5598.
[117] Solaini, G., Sgarbi, G., Baracca, A., 2011. Oxidative phosphorylation in cancer cells. Biochimica et Biophysica Acta (BBA) - Bioenergetics 1807(6):534–542.
[118] Wu, H., Ding, Z., Hu, D., Sun, F., Dai, C., Xie, J., et al., 2012. Central role of lactic acidosis in cancer cell resistance to glucose deprivation-induced cell death. The Journal of Pathology 227(2):189.
[119] Chao, M., Wu, H., Jin, K., Li, B., Wu, J., Zhang, G., et al., 2016. A nonrandomized cohort and a randomized study of local control of large hepatocarcinoma by targeting intratumoral lactic acidosis. eLife 5. https://doi.org/10.7554/eLife.15691.
[120] Silva, A.S., Yunes, J.A., Gillies, R.J., Gatenby, R.A., 2009. The potential role of systemic buffers in reducing intratumoral extracellular pH and acid-mediated invasion. Cancer Research 69(6):2677.
[121] Walenta, S., Schroeder, T., Mueller-Klieser, W., 2004. Lactate in solid malignant tumors: potential basis of a metabolic classification in clinical oncology. Current Medicinal Chemistry 11(16):2195.
[122] Penkert, J., Ripperger, T., Schieck, M., Schlegelberger, B., Steinemann, D., Illig, T.J.O., 2016. On metabolic reprogramming and tumor biology: a comprehensive survey of metabolism in breast cancer. Oncotarget 7(41):67626.
[123] de la Cruz-López, K.G., Castro-Muñoz, L.J., Reyes-Hernández, D.O., García-Carrancá, A., Manzo-Merino, J., 2019. Lactate in the regulation of tumor microenvironment and therapeutic approaches. Frontiers in Oncology 9:1143.
[124] Martinez-Outschoorn, U.E., Peiris-Pagès, M., Pestell, R.G., Sotgia, F., Lisanti, M.P., 2017. Cancer metabolism: a therapeutic perspective. Nature Reviews Clinical Oncology 14(1):11.
[125] Diers, A.R., Broniowska, K.A., Chang, C.F., Hogg, N., 2012. Pyruvate fuels mitochondrial respiration and proliferation of breast cancer cells: effect of monocarboxylate transporter inhibition. Biochemical Journal 444(3):561.
[126] Olson, K.A., Schell, J.C., Rutter, J., 2016. Pyruvate and metabolic flexibility: illuminating a path toward selective cancer therapies. Trends in Biochemical Sciences 41(3):219–230.
[127] Mayers, J.R., Wu, C., Clish, C.B., Kraft, P., Torrence, M.E., Fiske, B.P., et al., 2014. Elevation of circulating branched-chain amino acids is an early event in human pancreatic adenocarcinoma development. Nature Medicine 20(10):1193.
[128] Owen, O.E., Kalhan, S.C., Hanson, R.W.J., 2002. The key role of anaplerosis and cataplerosis for citric acid cycle function. Journal of Biological Chemistry 277(34):30409–30412.
[129] Hiller, K., Metallo, C.M., Kelleher, J.K., Stephanopoulos, G., 2010. Non-targeted elucidation of metabolic pathways using stable-isotope tracers and mass spectrometry. Analytical Chemistry 82(15):6621.
[130] Carey, B.W., Finley, L.W.S., Cross, J.R., Allis, C.D., Thompson, C.B., 2015. Intracellular agr -ketoglutarate maintains the pluripotency of embryonic stem cells. Nature 518(7539):413.
[131] Serpa, J., 2020. Cysteine as a carbon source, a hot spot in cancer cells survival. Frontiers in Oncology 10.
[132] Possemato, R., Marks, K.M., Shaul, Y.D., Pacold, M.E., Kim, D., Birsoy, K., et al., 2011. Functional genomics reveal that the serine synthesis pathway is essential in breast cancer. Nature 476(7360):346–350.
[133] Locasale, J.W., Grassian, A.R., Melman, T., Lyssiotis, C.A., Mattaini, K.R., Bass, A.J., et al., 2011. Phosphoglycerate dehydrogenase diverts glycolytic flux and contributes to oncogenesis. Nature Genetics 43(9):869.
[134] Zhang, W.C., Shyh-Chang, N., Yang, H., Rai, A., Umashankar, S., Ma, S., et al., 2012. Glycine decarboxylase activity drives non-small cell lung cancer tumor-initiating cells and tumorigenesis. Cell 148(1):259.
[135] Fan, J., Ye, J., Kamphorst, J.J., Shlomi, T., Thompson, C.B., Rabinowitz, J.D., 2014. Quantitative flux analysis reveals folate-dependent NADPH production. Nature 510(7504):298.
[136] Fais, S., 2007. Cannibalism: a way to feed on metastatic tumors. Cancer Letters 258(2):155.
[137] Gonzalez, C.D., Alvarez, S., Ropolo, A., Rosenzvit, C., Gonzalez Bagnes, M.F., Vaccaro, M.I., 2014. Autophagy, Warburg, and Warburg reverse effects in human cancer. BioMed Research International 2014.
[138] Kuma, A., Mizushima, N., 2010. Physiological role of autophagy as an intracellular recycling system: with an emphasis on nutrient metabolism. In: Seminars in cell & developmental biology. Elsevier. p. 683–90.
[139] Mekuria, A., Abdi, A.J., 2018. Drivers of glucose and glutamine metabolism reprogramming in tumor cells and their potential as target for cancer. Journal of Tumor Research 4(139):2.
[140] Altman, B.J., Stine, Z.E., Dang, C.V., 2016. From Krebs to clinic: glutamine metabolism to cancer therapy. Nature Reviews Cancer 16(10):619.
[141] Gottesman, M.M., Lavi, O., Hall, M.D., Gillet, J.-P., 2016. Toward a better understanding of the complexity of cancer drug resistance. Annual Review of Pharmacology and Toxicology 56:85–102.
[142] Potter, M., Newport, E., Morten, K.J., 2016. The Warburg effect: 80 years on. Biochemical Society Transactions 44(5):1499.
[143] Benny, S., Mishra, R., Manojkumar, M.K., Aneesh, T., 2020. From Warburg effect to Reverse Warburg effect; the new horizons of anti-cancer therapy. Medical Hypotheses 144:110216.
[144] Aguilar, E., Marin de Mas, I., Zodda, E., Marin, S., Morrish, F., Selivanov, V., et al., 2016. Metabolic reprogramming and dependencies associated with epithelial cancer stem cells independent of the epithelial-mesenchymal transition program. Stem Cells 34(5):1163.

[145] Yoshida, G.J., 2015. Metabolic reprogramming: the emerging concept and associated therapeutic strategies. Journal of Experimental & Clinical Cancer Research 34(1):111.
[146] Seyfried, T.N., Flores, R.E., Poff, A.M., D'Agostino, D.P., 2013. Cancer as a metabolic disease: implications for novel therapeutics. Carcinogenesis 35(3):515.
[147] Zu, X.L., Guppy, M., 2004. Cancer metabolism: facts, fantasy, and fiction. Biochemical and Biophysical Research Communications 313(3):459–465.
[148] Fu, Y., Liu, S., Yin, S., Niu, W., Xiong, W., Tan, M., et al., 2017. The reverse Warburg effect is likely to be an Achilles' heel of cancer that can be exploited for cancer therapy. Oncotarget 8(34):57813.
[149] DeBerardinis, R.J., Chandel, N.S., 2016. Fundamentals of cancer metabolism. Science Advances 2(5):e1600200.
[150] Rohatgi, N., Ghoshdastider, U., Baruah, P., Skanderup, A.J., 2020. A pan-cancer metabolic atlas of the tumor microenvironment. bioRxiv.
[151] Porporato, P.E., Filigheddu, N., Bravo-San Pedro, J.M., Kroemer, G., Galluzzi, L., 2018. Mitochondrial metabolism and cancer. Cell Research 28(3):265–280.
[152] Chiu, M., Ottaviani, L., Bianchi, M.G., Franchi-Gazzola, R., Bussolati, O., 2012. Towards a metabolic therapy of cancer. Acta BioMedica 83(3): 168–176.
[153] Martinez-Outschoorn, U.E., Peiris-Pagés, M., Pestell, R.G., Sotgia, F., Lisanti, M.P., 2017. Cancer metabolism: a therapeutic perspective. Nature Reviews Clinical Oncology 14(1):11.
[154] Seyfried, T.N., Shelton, L.M., 2010. Cancer as a metabolic disease. Nutrition & Metabolism 7(1):1–22.
[155] Roy, S., Kumaravel, S., Sharma, A., Duran, C.L., Bayless, K.J., Chakraborty, S., et al., 2020. Hypoxic tumor microenvironment: implications for cancer therapy. Experimental Biology and Medicine 245(13):1073–1086.
[156] Wei, Q., Qian, Y., Yu, J., Wong, C.C., 2020. Metabolic rewiring in the promotion of cancer metastasis: mechanisms and therapeutic implications. Oncogene 39(39):6139–6156.
[157] Abdel-Wahab, A.F., Mahmoud, W., Al-Harizy, R.M., 2019. Targeting glucose metabolism to suppress cancer progression: prospective of anti-glycolytic cancer therapy. Pharmacological Research 150:104511.
[158] Yu, T., Dong, T., Eyvani, H., Fang, Y., Wang, X., Zhang, X., et al., 2020. Metabolic interventions: a new insight into the cancer immunotherapy. Archives of Biochemistry, 108659.
[159] Kapelner, A., Vorsanger, M., 2015. Starvation of cancer via induced ketogenesis and severe hypoglycemia. Medical Hypotheses 84(3):162–168.
[160] Allen, B.G., Bhatia, S.K., Anderson, C.M., Eichenberger-Gilmore, J.M., Sibenaller, Z.A., Mapuskar, K.A., et al., 2014. Ketogenic diets as an adjuvant cancer therapy: history and potential mechanism. Redox Biology 2:963.
[161] Agnihotri, S., Zadeh, G., 2015. Metabolic reprogramming in glioblastoma: the influence of cancer metabolism on epigenetics and unanswered questions. Neuro-Oncology 18(2):160–172.
[162] Katsetos, C.D., Anni, H., Dráber, P., 2013. Mitochondrial dysfunction in gliomas. Seminars in Pediatric Neurology, 216–227. Elsevier.
[163] Sica, V., Bravo-San Pedro, J.M., Stoll, G., Kroemer, G.J.I., 2020. Oxidative phosphorylation as a potential therapeutic target for cancer therapy. International Journal of Cancer 146(1):10–17.
[164] Poteet, E., Choudhury, G.R., Winters, A., Li, W., Ryou, M.-G., Liu, R., et al., 2013. Reversing the Warburg effect as a treatment for glioblastoma. Journal of Biological Chemistry 288(13):9153–9164.
[165] García-Heredia, J.M., Carnero, A., 2020. Role of mitochondria in cancer stem cell resistance. Cells 9(7):1693.
[166] Edmond, J., Robbins, R.A., Bergstrom, J.D., Cole, R.A., De Vellis, J., 1987. Capacity for substrate utilization in oxidative metabolism by neurons, astrocytes, and oligodendrocytes from developing brain in primary culture. Journal of Neuroscience Research 18(4):551.
[167] Chechik, T., Roeder, L.M., Tildon, J.T., Poduslo, S.E., 1987. Ketone body enzyme activities in purified neurons, astrocytes and oligodendroglia. Neurochemistry International 10(1):95.
[168] Chang, H.T., Olson, L.K., Schwartz, K.A., 2013. Ketolytic and glycolytic enzymatic expression profiles in malignant gliomas: implication for ketogenic diet therapy. Nutrition & Metabolism 10(1):1.
[169] Lin, H., Patel, S., Affleck, V.S., Wilson, I., Turnbull, D.M., Joshi, A.R., et al., 2016. Fatty acid oxidation is required for the respiration and proliferation of malignant glioma cells. Neuro-Oncology 19(1):43.
[170] Marin-Valencia, I., Yang, C., Mashimo, T., Cho, S., Baek, H., Yang, X.-L., et al., 2012. Analysis of tumor metabolism reveals mitochondrial glucose oxidation in genetically diverse human glioblastomas in the mouse brain in vivo. Cell Metabolism 15(6):827.
[171] Bailey, P., Chang, D.K., Nones, K., Johns, A.L., Patch, A.-M., Gingras, M.-C., et al., 2016. Genomic analyses identify molecular subtypes of pancreatic cancer. Nature 531(7592):47.
[172] Waddell, N., Pajic, M., Patch, A.M., Chang, D.K., Kassahn, K.S., Bailey, P., et al., 2015. Whole genomes redefine the mutational landscape of pancreatic cancer. Nature 518(7540):495.
[173] Daemen, A., Peterson, D., Sahu, N., McCord, R., Du, X., Liu, B., et al., 2015. Metabolite profiling stratifies pancreatic ductal adenocarcinomas into subtypes with distinct sensitivities to metabolic inhibitors. Proceedings of the National Academy of Sciences of the United States of America 112(32): E4410.
[174] Liang, C., Qin, Y., Zhang, B., Ji, S., Shi, S., Xu, W., et al., 2016. Energy sources identify metabolic phenotypes in pancreatic cancer. Acta Biochimica et Biophysica Sinica 48(11):969.
[175] Vanhove, K., Graulus, G.-J., Mesotten, L., Thomeer, M., Derveaux, E., Noben, J.-P., et al., 2019. The metabolic landscape of lung cancer: new insights in a disturbed glucose metabolism. Frontiers in Oncology 9:1215.
[176] Seyfried, T.N., Mukherjee, P., Iyikesici, M.S., Slocum, A., Kalamian, M., Spinosa, J.-P., et al., 2020. Consideration of ketogenic metabolic therapy as a complementary or alternative approach for managing breast cancer. Frontiers in Oncology 7:21.
[177] Yu, T.-J., Ma, D., Liu, Y.-Y., Xiao, Y., Gong, Y., Jiang, Y.-Z., et al., 2021. Bulk and single-cell transcriptome profiling reveal the metabolic heterogeneity in human breast cancers. Molecular Therapy 29(7):2350–2365.
[178] Baliu-Piqué, M., Pandiella, A., Ocana, A., 2020. Breast cancer heterogeneity and response to novel therapeutics. Cancers 12(11):3271.
[179] Li, H., Ning, S., Ghandi, M., Kryukov, G.V., Gopal, S., Deik, A., et al., 2019. The landscape of cancer cell line metabolism. Nature Medicine 25(5):850–860.
[180] Hensley, C.T., Faubert, B., Yuan, Q., Lev-Cohain, N., Jin, E., Kim, J., et al., 2016. Metabolic heterogeneity in human lung tumors. Cell 164(4):681–694.
[181] Luengo, A., Gui, D.Y., Vander Heiden, M.G., 2017. Targeting metabolism for cancer therapy. Cell Chemical Biology 24(9):1161–1180.
[182] Klement, R.J., Brehm, N., Sweeney, R.A., 2020. Ketogenic diets in medical oncology: a systematic review with focus on clinical outcomes. Medical Oncology 37(2):1–12.
[183] Strickaert, A., Saiselet, M., Dom, G., De Deken, X., Dumont, J.E., Feron, O., et al., 2017. Cancer heterogeneity is not compatible with one unique cancer cell metabolic map. Oncogene 36(19):2637–2642.
[184] Khodabakhshi, A., Akbari, M.E., Mirzaei, H.R., Seyfried, T.N., Kalamian, M., Davoodi, S.H., 2021. Effects of Ketogenic metabolic therapy on patients with breast Cancer: a randomized controlled clinical trial. Clinical Nutrition 40(3): 751–758.
[185] İyikesici, M.S., Slocum, A.K., Winters, N., Kalamian, M., Seyfried, T.N., 2021. Metabolically supported chemotherapy for managing end-stage breast cancer: a complete and durable response. Cureus 13(4).
[186] Elsakka, A., Bary, M.A., Abdelzaher, E., Elnaggar, M., Kalamian, M., Mukherjee, P., et al., 2018. Management of glioblastoma multiforme in a

patient treated with ketogenic metabolic therapy and modified standard of care: a 24-month follow-up. Frontiers in Nutrition 5:20.

[187] Amoedo, N.D., Obre, E., Rossignol, R., 2017. Drug discovery strategies in the field of tumor energy metabolism: limitations by metabolic flexibility and metabolic resistance to chemotherapy. Biochimica et Biophysica Acta (BBA) - Bioenergetics 1858(8):674.

[188] Tsimberidou, A.M., Fountzilas, E., Nikanjam, M., Kurzrock, R., 2020. Review of precision cancer medicine: evolution of the treatment paradigm. Cancer Treatment 86:102019.

[189] Gambardella, V., Tarazona, N., Cejalvo, J.M., Lombardi, P., Huerta, M., Roselló, S., et al., 2020. Personalized medicine: recent progress in cancer therapy. Cancers 12(4):1009.

[190] V Duarte, F., A Amorim, J., M Palmeira, C., P Rolo, A., 2015. Regulation of mitochondrial function and its impact in metabolic stress. Current Medicinal Chemistry 22(20):2468–2479.

[191] Warburg, O., Krippahl, G.J., 1960. Further development of manometric methods. Journal of the National Cancer Institute 24:51–55.

[192] Silva, A.M., Oliveira, P.J., 2018. Evaluation of respiration with clark-type electrode in isolated mitochondria and permeabilized animal cells. Mitochondrial Bioenergetics, 7–29. Springer.

[193] Severinghaus, J.W., 2002. The invention and development of blood gas analysis apparatus. The Journal of the American Society of Anesthesiologists 97(1):253–256.

[194] Hill, B.G., Benavides, G.A., Lancaster, J.R., Ballinger, S., Dell'Italia, L., Zhang, J., et al., 2012. Integration of cellular bioenergetics with mitochondrial quality control and autophagy. Biological Chemistry 393(12):1485–1512.

[195] Ferrick, D.A., Neilson, A., Beeson, C., 2008. Advances in measuring cellular bioenergetics using extracellular flux. Drug Discovery Today 13(5–6):268–274.

[196] Garedew, A., Hütter, E., Haffner, B., Gradl, P., Gradl, L., Jansen-Dürr, P., et al., 2005. High-resolution respirometry for the study of mitochondrial function in health and disease. In: The OROBOROS oxygraph-2k, proceedings of the 11th congress of the European shock society, Vienna, Austria (H Redl, ed) Bologna, Italy: medimond international proceedings. p. 107–11.

[197] Shah, A.T., Diggins, K.E., Walsh, A.J., Irish, J.M., Skala, M.C., 2015. In vivo autofluorescence imaging of tumor heterogeneity in response to treatment. Neoplasia 17(12):862–870.

[198] Walsh, A.J., Cook, R.S., Sanders, M.E., Aurisicchio, L., Ciliberto, G., Arteaga, C.L., et al., 2014. Quantitative optical imaging of primary tumor organoid metabolism predicts drug response in breast cancer. Cancer Research 74(18):5184–5194.

[199] Hou, J., Wright, H.J., Chan, N.S.-K., Tran, R.D., Razorenova, O.V., Potma, E.O., et al., 2016. Correlating two-photon excited fluorescence imaging of breast cancer cellular redox state with seahorse flux analysis of normalized cellular oxygen consumption. Journal of Biomedical Optics 21(6):060503.

[200] TeSlaa, T., Teitell, M.A., 2014. Techniques to monitor glycolysis. Methods in Enzymology, 91. Elsevier.

[201] Schlueter, K., Johnson, J., Warner, C., Miller, W., 2017. Glucose analytical comparability evaluation of the YSI 2300 STAT Plus™ and YSI 2900D biochemistry analyzers. Xylem, Inc.

[202] Mitra, S., Molina, J., Mills, G.B., Dennison, J.B., 2015. Characterization of the role Rab25 in energy metabolism and cancer using extracellular flux analysis and material balance. Rab GTPases: Methods and Protocols 195.

[203] Leippe, D., Sobol, M., Vidugiris, G., Cali, J.J., Vidugiriene, J., 2017. Bioluminescent assays for glucose and glutamine metabolism: high-throughput screening for changes in extracellular and intracellular metabolites. SLAS Discovery: Advancing Life Sciences R&D 22(4):366.

[204] Patergnani, S., Baldassari, F., De Marchi, E., Karkucinska-Wieckowska, A., Wieckowski, M.R., Pinton, P., 2014. Methods to monitor and compare mitochondrial and glycolytic ATP production. Methods in Enzymology, 313. Elsevier.

[205] Acker, M.G., Auld, D.S., 2014. Considerations for the design and reporting of enzyme assays in high-throughput screening applications. Perspectives in Science 1(1–6):56–73.

[206] Gu, X., Ma, Y., Liu, Y., Wan, Q., 2021. Measurement of mitochondrial respiration in adherent cells by seahorse XF96 cell Mito stress test. STAR protocols 2(1):100245.

[207] Zielonka, J., Kalyanaraman, B., 2010. Hydroethidine-and MitoSOX-derived red fluorescence is not a reliable indicator of intracellular superoxide formation: another inconvenient truth. Free Radical Biology and Medicine 48(8):983–1001.

[208] Chen, X., Zhong, Z., Xu, Z., Chen, L., Wang, Y., 2010. 2′, 7′-Dichlorodihydrofluorescein as a fluorescent probe for reactive oxygen species measurement: forty years of application and controversy. Free Radical Research 44(6):587–604.

[209] Zhang, J., Zhang, Q., 2019. Using seahorse machine to measure OCR and ECAR in cancer cells. Cancer & Metabolism, 353–363. Springer.

[210] Krumm, A., Carey, C., 2016. Real-time monitoring of cellular metabolic activity: intracellular oxygen. Nature Methods 13(10):i–ii.

[211] Potter, M., Badder, L., Hoade, Y., Johnston, I.G., Morten, K.J., 2016. Monitoring intracellular oxygen concentration: implications for hypoxia studies and real-time oxygen monitoring. Oxygen Transport to Tissue XXXVII, 257–263. Springer.

[212] Chinopoulos, C., Kiss, G., Kawamata, H., Starkov, A.A., 2014. Measurement of ADP–ATP exchange in relation to mitochondrial transmembrane potential and oxygen consumption. Methods in Enzymology 542:333–348.

[213] Long, Q., Huang, L., Huang, K., Yang, Q., 2019. Assessing mitochondrial bioenergetics in isolated mitochondria from mouse heart tissues using oroboros 2k-oxygraph. Nuclear Receptor, 237–246. Springer.

[214] Salabei, J.K., Gibb, A.A., Hill, B.G., 2014. Comprehensive measurement of respiratory activity in permeabilized cells using extracellular flux analysis. Nature Protocols 9(2):421.

[215] Hall, A., Moghimi, S.M., 2019. Determination of polycation-mediated perturbation of mitochondrial respiration in intact cells by high-resolution respirometry (Oxygraph-2k, OROBOROS). Nanotechnology for Nucleic Acid Delivery, 313–322. Springer.

[216] Cell, A.S.X.H.T., Kit, A.A., 2020. Agilent Seahorse XF Hu T cell activation assay kit.

[217] Winer, L.S.P., Wu, M., 2014. Rapid analysis of glycolytic and oxidative substrate flux of cancer cells in a microplate. PLoS One 9(10):e109916.

[218] Takahashi, E., Yamaoka, Y.J.T., 2017. Simple and inexpensive technique for measuring oxygen consumption rate in adherent cultured cells. The Journal of Physiological Sciences 67(6):731–737.

[219] Yépez, V.A., Kremer, L.S., Iuso, A., Gusic, M., Kopajtich, R., Koňaříková, E., et al., 2018. OCR-Stats: robust estimation and statistical testing of mitochondrial respiration activities using Seahorse XF Analyzer. PLoS One 13(7):e0199938.

[220] Divakaruni, A.S., Paradyse, A., Ferrick, D.A., Murphy, A.N., Jastroch, M., 2014. Analysis and interpretation of microplate-based oxygen consumption and pH data. Methods in Enzymology 547:309–354.

[221] Mookerjee, S.A., Gerencser, A.A., Nicholls, D.G., Brand, M.D.J., 2017. Quantifying intracellular rates of glycolytic and oxidative ATP production and consumption using extracellular flux measurements. Journal of Biological Chemistry 292(17):7189–7207.

[222] Chacko, B.K., Kramer, P.A., Ravi, S., Benavides, G.A., Mitchell, T., Dranka, B.P., et al., 2014. The Bioenergetic Health Index: a new concept in mitochondrial translational research. Clinical Science (London, England : 1979) 127(6):367.

[223] Vayalil, P.K., Landar, A., 2015. Mitochondrial oncobioenergetic index: a potential biomarker to predict progression from indolent to aggressive prostate cancer. Oncotarget 6(40):43065.

[224] Ruas, J.S., Siqueira-Santos, E.S., Amigo, I., Rodrigues-Silva, E., Kowaltowski, A.J., Castilho, R.F., 2016. Underestimation of the maximal capacity of the mitochondrial electron transport system in oligomycin-treated cells. PLoS One 11(3):e0150967.

[225] Demine, S., Renard, P., Arnould, T., 2019. Mitochondrial uncoupling: a key controller of biological processes in physiology and diseases. Cells 8(8):795.

[226] Reynafarje, B.D., Ferreira, J., 2008. Oxidative phosphorylation: kinetic and thermodynamic correlation between electron flow, proton translocation, oxygen consumption and ATP synthesis under close to in vivo concentrations of oxygen. International Journal of Medical Sciences 5(3):143.

[227] Herst, P.M., Berridge, M.V., 2007. Cell surface oxygen consumption: a major contributor to cellular oxygen consumption in glycolytic cancer cell lines. Biochimica et Biophysica Acta (BBA) - Bioenergetics 1767(2):170—177.

[228] Vaupel, P., Mayer, A., 2012. Availability, not respiratory capacity governs oxygen consumption of solid tumors. The International Journal of Biochemistry & Cell Biology 44(9):1477—1481.

[229] Marchetti, P., Fovez, Q., Germain, N., Khamari, R., Kluza, J., 2020. Mitochondrial spare respiratory capacity: mechanisms, regulation, and significance in non-transformed and cancer cells. The FASEB Journal 34(10): 13106—13124.

[230] Solaini, G., Baracca, A., Lenaz, G., Sgarbi, G., 2010. Hypoxia and mitochondrial oxidative metabolism. Biochimica et Biophysica Acta (BBA) - Bioenergetics 1797(6—7):1171—1177.

[231] Schmidt, C.A., Fisher-Wellman, K.H., Neufer, P.D.J., 2021. From OCR and ECAR to energy: perspectives on the design and interpretation of bioenergetics studies. Journal of Biological Chemistry, 101140.

[232] Papkovsky, D.B., Zhdanov, A.V., 2015. Cell energy budget platform for assessment of cell metabolism. Mitochondrial Medicine: Volume II, Manipulating Mitochondrial Function 333.

[233] Bénit, P., Chrétien, D., Porceddu, M., Yanicostas, C., Rak, M., Rustin, P., 2017. An effective, versatile, and inexpensive device for oxygen uptake measurement. Journal of Clinical Medicine 6(6):58.

[234] Sica, V., Bravo-San Pedro, J.M., Pietrocola, F., Izzo, V., Maiuri, M.C., Kroemer, G., et al., 2017. Assessment of glycolytic flux and mitochondrial respiration in the course of autophagic responses. Methods in Enzymology, 155. Elsevier.

[235] Shaw, A.D., Li, Z., Thomas, Z., Stevens, C.W., 2002. Assessment of tissue oxygen tension: comparison of dynamic fluorescence quenching and polarographic electrode technique. Critical Care 6(1):1—5.

[236] Kelbauskas, L., Glenn, H., Anderson, C., Messner, J., Lee, K.B., Song, G., et al., 2017. A platform for high-throughput bioenergy production phenotype characterization in single cells. Scientific Reports 7:45399.

[237] Hai, P., Imai, T., Xu, S., Zhang, R., Aft, R.L., Zou, J., et al., 2019. High-throughput, label-free, single-cell photoacoustic microscopy of intratumoral metabolic heterogeneity. Nature Biomedical Engineering 3(5):381—391.

[238] Heymann, D., Téllez-Gabriel, M., 2018. Circulating tumor cells: the importance of single cell analysis. Single Cell Biomedicine, 45—58.

[239] Tellez-Gabriel, M., Cochonneau, D., Cadé, M., Jubelin, C., Heymann, M.-F., Heymann, D., 2019. Circulating tumor cell-derived pre-clinical models for personalized medicine. Cancers 11(1):19.

[240] Lin, W.N., Tay, M.Z., Lu, R., Liu, Y., Chen, C.-H., Cheow, L.F., 2020. The role of single-cell technology in the study and control of infectious diseases. Cells 9(6):1440.

[241] Vasdekis, A.E., Stephanopoulos, G., 2015. Review of methods to probe single cell metabolism and bioenergetics. Metabolic Engineering 27:115.

[242] Russell, S., Wojtkowiak, J., Neilson, A., Gillies, R.J., 2017. Metabolic Profiling of healthy and cancerous tissues in 2D and 3D. Scientific Reports 7(1):1—11.

[243] Roussakis, E., Li, Z., Nowell, N.H., Nichols, A.J., Evans, C.L., 2015. Bright,"clickable" porphyrins for the visualization of oxygenation under ambient light. Angewandte Chemie 54(49):14728—14731.

[244] Nichols, A.J., Roussakis, E., Klein, O.J., Evans, C.L., 2014. Click-assembled, oxygen-sensing nanoconjugates for depth-resolved, near-infrared imaging in a 3 D cancer model. Angewandte Chemie 126(14):3745—3748.

[245] Ludikhuize, M.C., Meerlo, M., Burgering, B.M., Colman, M.J.R., 2021. Protocol to profile the bioenergetics of organoids using Seahorse. STAR protocols 2(1):100386.

[246] Zhang, X., Yuan, T., Keijer, J., de Boer, V.C.J., 2021. OCRbayes: a Bayesian hierarchical modeling framework for Seahorse extracellular flux oxygen consumption rate data analysis. PLoS One e0253926.

[247] Kam, Y., Rogers, G.W., Jastromb, N., Dranka, B.P., Methods and strategies for normalizing XF metabolic data to cellular parameters.

[248] Guha, M., Srinivasan, S., Raman, P., Jiang, Y., Kaufman, B.A., Taylor, D., et al., 2018. Aggressive triple negative breast cancers have unique molecular signature on the basis of mitochondrial genetic and functional defects. Biochimica et Biophysica Acta (BBA)-Molecular Basis of Disease 1864(4): 1060—1071.

[249] Romero, N., Swain, P.M., Kam, Y., Rogers, G., Dranka, B.P., 2018. Bioenergetic profiling of cancer cell lines: quantifying the impact of glycolysis on cell proliferation. Cancer Research 78(13 Supplement):3487.

[250] Conroy, L.R., Lorkiewicz, P., He, L., Yin, X., Zhang, X., Rai, S.N., et al., 2020. Palbociclib treatment alters nucleotide biosynthesis and glutamine dependency in A549 cells. Cancer Cell International 20(1):1—12.

[251] Lee, D.E., Alhallak, K., Jenkins, S.V., Vargas, I., Greene, N.P., Quinn, K.P., et al., 2018. A radiosensitizing inhibitor of HIF-1 alters the optical redox state of human lung cancer cells in vitro. Scientific Reports 8(1):1—10.

[252] Cytation, B., Normalization of agilent Seahorse XF data by in-situ cell counting using.

[253] Hirsch, C., Schildknecht, S., 2019. In vitro research reproducibility: keeping up high standards. Frontiers in Pharmacology 10:1484.

[254] Place, T.L., Domann, F.E., Case, A.J., 2017. Limitations of oxygen delivery to cells in culture: an underappreciated problem in basic and translational research. Free Radical Biology and Medicine 113:311—322.

[255] Muelas, M.W., Ortega, F., Breitling, R., Bendtsen, C., Westerhoff, H.V., 2018. Rational cell culture optimization enhances experimental reproducibility in cancer cells. Scientific Reports 8(1):1—16.

[256] Diaz-Ruiz, R., Rigoulet, M., Devin, A., 2011. The Warburg and Crabtree effects: on the origin of cancer cell energy metabolism and of yeast glucose repression. Biochimica et Biophysica Acta (BBA) - Bioenergetics 1807(6):568.

[257] Huang, H.-L., Hsing, H.-W., Lai, T.-C., Chen, Y.-W., Lee, T.-R., Chan, H.-T., et al., 2010. Trypsin-induced proteome alteration during cell subculture in mammalian cells. Journal of Biomedical Science 17(1):1—10.

[258] Danhier, P., Copetti, T., De Preter, G., Leveque, P., Feron, O., Jordan, B.F., et al., 2013. Influence of cell detachment on the respiration rate of tumor and endothelial cells. PLoS One 8(1):e53324.

[259] Labuschagne, C.F., Cheung, E.C., Blagih, J., Domart, M.-C., Vousden, K.H., 2019. Cell clustering promotes a metabolic switch that supports metastatic colonization. Cell Metabolism 30(4):720—734 e725.

[260] Sellers, K., Fox, M.P., Bousamra 2nd, M., Slone, S.P., Higashi, R.M., Miller, D.M., et al., 2015. Pyruvate carboxylase is critical for non-small-cell lung cancer proliferation. Journal of Clinical Investigation 125(2):687.

[261] Cheng, T., Sudderth, J., Yang, C., Mullen, A.R., Jin, E.S., Mates, J.M., et al., 2011. Pyruvate carboxylase is required for glutamine-independent growth of tumor cells. Proceedings of the National Academy of Sciences of the United States of America 108(21):8674.

[262] Funes, J.M., Quintero, M., Henderson, S., Martinez, D., Qureshi, U., Westwood, C., et al., 2007. Transformation of human mesenchymal stem cells increases their dependency on oxidative phosphorylation for energy production. Proceedings of the National Academy of Sciences of the United States of America 104(15):6223.

[263] Schaefer, C., Mayer, W.-K., Krüger, W., Vaupel, P.J., 1993. Microregional distributions of glucose, lactate, ATP and tissue pH in experimental tumours

upon local hyperthermia and/or hyperglycaemia. Journal of Cancer Research and Clinical Oncology 119(10):599–608.
[264] Kallinowski, F., Runkel, S., Fortmeyer, H., Förster, H., Vaupel, P.J., 1987. L-glutamine: a major substrate for tumor cells in vivo? Journal of Cancer Research and Clinical Oncology 113(3):209–215.
[265] Haykal, M.M., Nahmias, C., Varon, C., Martin, O.C., 2020. Organotypic modeling of the tumor landscape. Frontiers in Cell and Developmental Biology 8:1406.
[266] Clevers, H., Tuveson, D.A., 2019. Organoid models for cancer research. Annual Review of Cancer Biology 3:223–234.
[267] Fidler, I.J., Kripke, M.L., 1977. Metastasis results from preexisting variant cells within a malignant tumor. Science (New York, N.Y.) 197(4306):893.
[268] Voorde, J.V., Ackermann, T., Pfetzer, N., Sumpton, D., Mackay, G., Kalna, G., et al., 2019. Improving the metabolic fidelity of cancer models with a physiological cell culture medium. Science Advances 5(1):eaau7314.
[269] Sullivan, M.R., Danai, L.V., Lewis, C.A., Chan, S.H., Gui, D.Y., Kunchok, T., et al., 2019. Quantification of microenvironmental metabolites in murine cancers reveals determinants of tumor nutrient availability. Elife 8:e44235.
[270] Cantor, J.R., Abu-Remaileh, M., Kanarek, N., Freinkman, E., Gao, X., Louissaint Jr., A., et al., 2017. Physiologic medium rewires cellular metabolism and reveals uric acid as an endogenous inhibitor of UMP synthase. Cell 169(2):258–272 e217.
[271] Blodgett, T.M., Meltzer, C.C., Townsend, D.W., 2007. PET/CT: form and function. Radiology 242(2):360.
[272] Nahmias, C., Carlson, E.R., Duncan, L.D., Blodgett, T.M., Kennedy, J., Long, M.J., et al., 2007. Positron emission tomography/computerized tomography (PET/CT) scanning for preoperative staging of patients with oral/head and neck cancer. Journal of Oral and Maxillofacial Surgery : Official Journal of the American Association of Oral and Maxillofacial Surgeons 65(12):2524.
[273] Hyder, F., Rothman, D.L., 2017. Advances in imaging brain metabolism. Annual Review of Biomedical Engineering 19:485.
[274] Kinoshita, Y., Yokota, A., 1997. Absolute concentrations of metabolites in the human brain tumors using in vitro proton magnetic resonance spectroscopy. NMR in Biomedicine 10(1):2.
[275] Alexander, A., Murtha, A., Abdulkarim, B., Mehta, V., 2006. Prognostic significance of serial magnetic resonance spectroscopies over the course of radiation therapy for patients with malignant glioma. Clinical and Investigative Medicine 29(5):301.
[276] Coman, D., Graaf, R.A., Rothman, D.L., Hyder, F., 2013. In vivo three-dimensional molecular imaging with Biosensor Imaging of Redundant Deviation in Shifts (BIRDS) at high spatiotemporal resolution. NMR in Biomedicine 26(11):1589.
[277] van Zijl, P., Yadav, N.N., 2011. Chemical exchange saturation transfer (CEST): what is in a name and what isn't? Magnetic Resonance in Medicine 65(4):927.
[278] Paech, D., Schuenke, P., Koehler, C., Windschuh, J., Mundiyanapurath, S., Bickelhaupt, S., et al., 2017. T1ρ-weighted dynamic glucose-enhanced MR imaging in the human brain. Radiology 285(3):914.
[279] Chan, K.W.Y., McMahon, M.T., Kato, Y., Liu, G., Bulte, J.W.M., Bhujwalla, Z.M., et al., 2012. Natural D-glucose as a biodegradable MRI contrast agent for detecting cancer. Magnetic Resonance in Medicine 68(6):1764.
[280] Park, J.M., Spielman, D.M., Josan, S., Jang, T., Merchant, M., Hurd, R.E., et al., 2016. Hyperpolarized 13C-lactate to 13C-bicarbonate ratio as a biomarker for monitoring the acute response of anti-vascular endothelial growth factor (anti-VEGF) treatment. NMR in Biomedicine 29(5):650.
[281] Artzi, M., Liberman, G., Vaisman, N., Bokstein, F., Vitinshtein, F., Aizenstein, O., et al., 2017. Changes in cerebral metabolism during ketogenic diet in patients with primary brain tumors: 1. H-MRS Study 132(2):267–275.
[282] Brindle, K.M.J., 2015. Imaging metabolism with hyperpolarized 13C-labeled cell substrates. Journal of the American Chemical Society 137(20):6418–6427.
[283] Neveu, M.A., De Preter, G., Marchand, V., Bol, A., Brender, J.R., Saito, K., et al., 2016. Multimodality imaging identifies distinct metabolic profiles in vitro and in vivo. Neoplasia (New York, N.Y.) 18(12):742.
[284] Hensley, C.T., Faubert, B., Yuan, Q., Lev-Cohain, N., Jin, E., Kim, J., et al., 2016. Metabolic heterogeneity in human lung tumors. Cell 164(4):681.
[285] Winter, S.F., Loebel, F., Dietrich, J., 2017. Role of ketogenic metabolic therapy in malignant glioma: a systematic review. Critical Reviews in Oncology/hematology 112:41.
[286] Giraudeau, P., 2020. NMR-based metabolomics and fluxomics: developments and future prospects. Analyst 145(7):2457–2472.
[287] Zeki, Ö.C., Eylem, C.C., Reçber, T., Kır, S., Nemutlu, E.J., Analysis, B., 2020. Integration of GC-MS and LC-MS for untargeted metabolomics profiling. Journal of Pharmaceutical and Biomedical Analysis, 113509.
[288] Chen, L., Zhong, F., Zhu, J., 2020. Bridging targeted and untargeted mass spectrometry-based metabolomics via hybrid approaches. Metabolites 10(9):348.
[289] Segers, K., Declerck, S., Mangelings, D., Heyden, Y.V., Eeckhaut, A.V., 2019. Analytical techniques for metabolomic studies: a review. Bioanalysis 11(24):2297–2318.
[290] Buescher, J.M., Antoniewicz, M.R., Boros, L.G., Burgess, S.C., Brunengraber, H., Clish, C.B., et al., 2015. A roadmap for interpreting 13C metabolite labeling patterns from cells. Current Opinion in Biotechnology 34:189–201.
[291] Dong, W., Keibler, M.A., Stephanopoulos, G., 2017. Review of metabolic pathways activated in cancer cells as determined through isotopic labeling and network analysis. Metabolic Engineering 43:113–124.
[292] Lorkiewicz, P.K., Gibb, A.A., Rood, B.R., He, L., Zheng, Y., Clem, B.F., et al., 2019. Integration of flux measurements and pharmacological controls to optimize stable isotope-resolved metabolomics workflows and interpretation. Scientific Reports 9(1):1–17.
[293] Pietzke, M., Kempa, S., 2014. Pulsed stable isotope-resolved metabolomic studies of cancer cells. Methods in Enzymology 543:179–198.
[294] Aggio, R.B.M., Ruggiero, K., Villas-Bôas, S.G., 2010. Pathway Activity Profiling (PAPi): from the metabolite profile to the metabolic pathway activity. Bioinformatics 26(23):2969.
[295] Liesenfeld, D.B., Habermann, N., Owen, R.W., Scalbert, A., Ulrich, C.M., 2013. Review of mass spectrometry–based metabolomics in cancer research. Cancer Epidemiology and Prevention Biomarkers 22(12):2182–2201.
[296] Gkiouli, M., Biechl, P., Eisenreich, W., Otto, A.M., 2019. Diverse roads taken by 13C-Glucose-Derived metabolites in breast cancer cells exposed to limiting glucose and glutamine conditions. Cells 8(10):1113.
[297] Kang, Y.P., Ward, N.P., DeNicola, G.M., 2018. Recent advances in cancer metabolism: a technological perspective. Experimental & Molecular Medicine 50(4):1–16.
[298] Vyas, S., Zaganjor, E., Haigis, M.C., 2016. Mitochondria and cancer. Cell 166(3):555.
[299] Arismendi-Morillo, G., Castellano-Ramírez, A., Seyfried, T.N., 2017. Ultrastructural characterization of the Mitochondria-associated membranes abnormalities in human astrocytomas: functional and therapeutics implications. Ultrastructural Pathology 41(3):234.
[300] Colak, S., Zimberlin, C.D., Fessler, E., Hogdal, L., Prasetyanti, P.R., Grandela, C.M., et al., 2014. Decreased mitochondrial priming determines chemoresistance of colon cancer stem cells. Cell Death and Differentiation 21(7):1170.
[301] Liang, X.J., Finkel, T., Shen, D.W., Yin, J.J., Aszalos, A., Gottesman, M.M., 2008. SIRT1 contributes in part to cisplatin resistance in cancer cells by altering mitochondrial metabolism. Molecular Cancer Research : MCR 6(9):1499.
[302] Cullen, K.J., Yang, Z., Schumaker, L., Guo, Z., 2007. Mitochondria as a critical target of the chemotheraputic agent cisplatin in head and neck cancer. Journal of Bioenergetics and Biomembranes 39(1):43.

[303] Thakur, N., Sharma, A.K., Singh, H., Singh, S., 2020. Role of mitochondrial DNA (mtDNA) variations in cancer development: A Systematic Review. Cancer Investigation 38(7):375—393.

[304] Chen, K., Lu, P., Beeraka, N.M., Sukocheva, O.A., Madhunapantula, S.V., Liu, J., et al., 2020. Mitochondrial mutations and mitoepigenetics: focus on regulation of oxidative stress-induced responses in breast cancers. Seminars in Cancer Biology. S1044-1579X (1020) 30203-30200.

[305] Verschoor, M.L., Ungard, R., Harbottle, A., Jakupciak, J.P., Parr, R.L., Singh, G., 2013. Mitochondria and cancer: past, present, and future. BioMed Research International 2013:612369.

[306] Chatterjee, A., Dasgupta, S., Sidransky, D., 2011. Mitochondrial subversion in cancer. Cancer Prevention Research (Philadelphia, Pa.) 4(5):638.

[307] Popov, L.D.J., 2020. Mitochondrial biogenesis: an update. Journal of Cellular and Molecular Medicine 24(9):4892—4899.

[308] Shin, M.-K., Cheong, J.-H., 2019. Mitochondria-centric bioenergetic characteristics in cancer stem-like cells. Archives of Pharmacal Research 42(2): 113—127.

[309] Lamb, R., Bonuccelli, G., Ozsvári, B., Peiris-Pagès, M., Fiorillo, M., Smith, D.L., et al., 2015. Mitochondrial mass, a new metabolic biomarker for stem-like cancer cells: understanding WNT/FGF-driven anabolic signaling. Oncotarget 6(31):30453.

[310] Yuan, Y., Ju, Y.S., Kim, Y., Li, J., Wang, Y., Yoon, C.J., et al., 2020. Comprehensive molecular characterization of mitochondrial genomes in human cancers. Nature Genetics 52(3):342—352.

[311] Castellana, S., Fusilli, C., Mazzoccoli, G., Biagini, T., Capocefalo, D., Carella, M., et al., 2017. High-confidence assessment of functional impact of human mitochondrial non-synonymous genome variations by APOGEE. PLoS Computational Biology 13(6):e1005628.

[312] Liu, D., Gao, Y., Liu, J., Huang, Y., Yin, J., Feng, Y., et al., 2021. Intercellular mitochondrial transfer as a means of tissue revitalization. Signal Transduction and Targeted Therapy 6(1):1—18.

[313] Ali Pour, P., Kenney, M.C., Kheradvar, A.J., 2020. Bioenergetics consequences of mitochondrial transplantation in cardiomyocytes. Journal of the American Heart Association 9(7):e014501.

[314] Chang, J.-C., Chang, H.-S., Wu, Y.-C., Cheng, W.-L., Lin, T.-T., Chang, H.-J., et al., 2019. Mitochondrial transplantation regulates antitumour activity, chemoresistance and mitochondrial dynamics in breast cancer. Journal of Experimental & Clinical Cancer Research 38(1):1—16.

[315] Elliott, R., Jiang, X., Head, J., 2012. Mitochondria organelle transplantation: introduction of normal epithelial mitochondria into human cancer cells inhibits proliferation and increases drug sensitivity. Breast Cancer Research and Treatment 136(2):347—354.

